HELICOPTER INVERSE SIMULATION FOR WORKLOAD AND HANDLING QUALITIES ESTIMATION

by

GARRY R. LEACOCK, B.Eng.

Thesis submitted to the Faculty of Engineering, University of Glasgow, for the Degree of Doctor of Philosophy.

All aspects of the work contained herein are original in content except where indicated.

This thesis is based on research conducted between February 1996 and January 1999 at the Department of Aerospace Engineering,
University of Glasgow.

Abstract

Helicopter handling qualities are investigated using inverse simulation as the method of providing state and control information for the appropriate quantitative metrics. The main aim of the work was to develop a more comprehensive and versatile method of quantifying handling qualities levels using the available inverse algorithm "Helinv". Subsequently, the assessment of the helicopter model inherent in Helinv, "Helicopter Generic Simulation", (HGS) for its suitability to handling qualities studies was paramount. Since the Helinv inverse algorithm operates by initially defining a mathematical flight test manoeuvre for the vehicle to "fly", considerable time was given to modelling suitable handling qualities assessment manoeuvres. So-called "attitude quickness" values were then calculated thus providing an initial objective insight into handling qualities level of the vehicle under test. Validation of the tasks formed an integral part of successfully fulfilling the flight test manoeuvre development objective.

The influence of the human is captured by the inclusion of a pilot model and the development of a novel method of parameter estimation, supplements the overall objective of modifying Helinv results to achieve potentially more realistic responses and thus correspondingly more realistic handling qualities. A comparative study of two helicopters, one based on the Westland Lynx battlefield/utility type and the other, a hypothetically superior configuration effectively demonstrates the capability of inverse simulation to deliver results adequate for initial handling qualities studies. Several examples are used to illustrate the point. Helinv has been shown to be versatile and efficient and can be used in initial handling qualities studies. The advantages of such a technique are clear when it is seen that actual flight testing, ground based or airborne is extremely costly, as the flight test manoeuvres must be representative of real life, reproducible and of course, as risk free as possible. Many inverse simulation runs and handling qualities calculations have been carried out for different helicopter configurations and manoeuvres thus illustrating the advantages of the technique and fulfilling all the aims mentioned above.

Acknowledgements

I would like to begin by expressing my deepest thanks and gratitude to Dr Douglas Thomson, who has offered great support and guidance throughout the entire research programme and writing of this thesis. I am without doubt indebted to him for the help he has given me in reaching this goal.

The research program was financed by the Engineering and Physical Sciences Research Council (EPSRC) and by the Defence Evaluation and research Agency (DERA). Special thanks must go to the members of the Flight Dynamics and Simulation Department at DERA, Bedford for additional support throughout the duration of the programme. Additionally, I would like to extend my thanks to Professor Roy Bradley and Calum MacDonald, Glasgow Caledonain University for their help and advice.

Now the difficult part. There are so many people I would like to talk about in person that it is an almost impossible task but I'll give it a go. I'll start with 'Xaby' who has been a most excellent friend, buddy and mentor (and not a bad bass player either), keep up the good work, man. To Max, for giving me the courage to keep going and for supporting (starting?) the rumour that there was actually grey matter between my ears, I still doubt it.

The 'guys' in the FD lab., Vassilios, Neil and Sharon, thanks for the chats, and odd (many? I can't remember!) 'sessions' at various locations in and around Byres Rd., I'm sure you all enjoyed them as well in spite of my Irish tendencies to babble on a bit! Special mention for Sharon for proof reading the thesis, I hope you've done a good job! To my (currently absent) Norwegian friend 'Trigger', here's to an excellent future, whatever you do, "Chin-chin". Thanks to Dave and 'Terrie', you both know what for … need I say more? Also to "Mick the German" for just being that little bit too clever, I guess nobody's perfect. There are some other folks, special cases if you like, without whom, Friday nights would have been somewhat more conservative, Allan, Steve, Frank, Brian, Arthur, Quintin and Aileen, always able to say or do something

that little bit different and always completely inappropriate! I like your style! And last but by no means least, my thanks to Ninah, for instilling some life and fun back into me, (rescued from the living-dead). "The T(e)mple" will always be (blue-light) special, but no doubt, still playing the same set. One last mention then, for Paul, the "Sundancer", a guy beyond words that can be safely used in the acknowledgements of a PhD thesis I think, so I'd best leave it at that! Well, I think I have covered most people here but if you feel hard done by, due to the absence of your name, please feel free to pencil it in somewhere.

Jokes aside then…

I'd like to thank Jim and Lisa, and 'Fo' and 'Gordy' for their unending support and encouragement, especially during those times when I was beginning to doubt if I would ever see the light at the end of a long tunnel! Well I finally made it guys! I would like to dedicate the thesis to them and of course my parents, Jim and Isla who somehow managed to get me this far. I know it wasn't easy, but hey, life never is!

Garry R Leacock - January, 2000.

Contents

Nomenclature

Notes :

Except where explicitly stated all parameters are in standard SI units

General

x	variable
$\underline{\boldsymbol{x}}$	vector variable
$[\boldsymbol{X}]$	matrix of variables
$[\mathbf{X}]$	matrix of constants
$\underline{\mathbf{i}}_{\mathbf{sub}}, \underline{\mathbf{j}}_{\mathbf{sub}}, \underline{\mathbf{k}}_{\mathbf{sub}}$	unit vectors describing current axis set (denoted by subscript)
$\underline{\boldsymbol{x}}_{sub/\mathbf{sub}}$	vector where (*sub*) refers to a position/location in an axis set and (**sub**) is the current axis set

Specific

$\underline{\boldsymbol{a}}$	general translation acceleration vector
$\underline{\boldsymbol{a}}_{hub/\mathbf{bl}}$	translation acceleration vector of the main rotor hub referred to blade axes
$\underline{\boldsymbol{a}}_{p/\mathbf{lag}}$	translation acceleration vector of a point p located a distance r_b from the hub, referred to blade element lag axes
a_0	main rotor blade lift curve slope
$a_{0\mathbf{TR}}$	tail rotor blade lift curve slope
A	area of main rotor disc
b	number of blades in main rotor
c	main rotor blade chord
C_l, C_d	lift and drag coefficients of main rotor blade element
C_L, C_M	rolling and pitching moment coefficients

C_Q	general torque coefficient
C_T	main rotor thrust coefficient
C_x, C_y, C_z	general force coefficients
c_ζ	lag damping coefficient
d	drag of blade element per unit span
e	error signal
e	fractional hinge offset
$\underline{\boldsymbol{e}}$	error vector
eR	blade root cut-out
$e^{-\tau s}$	pure time delay
f_y, f_z	components of aerodynamic force/unit span on a blade element
g	acceleration due to gravity
g_{1c0}, g_{1c1}	gains and offsets in the lateral cyclic channel
$g_{1s0}, g_{1s1}, g_{sc0}, g_{sc1}$	gains and offsets in the longitudinal and collective channels
g_{c0}, g_{c1}	gains and offsets in the collective channel
g_{tr0}, g_{tr1}	gearing constants in the yaw channel
$G_H(s), Y_P(s)$	general human operator model
h	Height of obstacle in Pop-up flight test manoeuvre
h_{fin}	height of the fin above fuselage reference point
h_{hub}	distance of rotor hub above a/c centre of gravity
h_{tp}	height of the tailplane above fuselage reference point
H	gradient distance term in 1-Cos Gust Model
$\overline{H}$	non-dimensional rotor height
I_{xx}, I_{yy}, I_{zz}	moments of inertia in body axes
I_{xz}	product of inertia in body axes
I_β	blade flapping inertia
$\underline{\mathbf{i}}, \underline{\mathbf{j}}, \underline{\mathbf{k}}$	unit vectors describing body axis set
$\underline{\mathbf{i}}_{\mathbf{bl}}, \underline{\mathbf{j}}_{\mathbf{bl}}, \underline{\mathbf{k}}_{\mathbf{bl}}$	unit vectors describing blade axis set
$\underline{\mathbf{i}}_{\mathbf{bod}}, \underline{\mathbf{j}}_{\mathbf{bod}}, \underline{\mathbf{k}}_{\mathbf{bod}}$	unit vectors describing body axis set

$\underline{\mathbf{i}}_{\mathbf{hub}}, \underline{\mathbf{j}}_{\mathbf{hub}}, \underline{\mathbf{k}}_{\mathbf{hub}}$	unit vectors describing hub axis set
$\underline{\mathbf{i}}_{\mathbf{lag}}, \underline{\mathbf{j}}_{\mathbf{lag}}, \underline{\mathbf{k}}_{\mathbf{lag}}$	unit vectors describing blade element lag axis set
$\underline{\mathbf{i}}_{\mathbf{sh}}, \underline{\mathbf{j}}_{\mathbf{sh}}, \underline{\mathbf{k}}_{\mathbf{sh}}$	unit vectors describing shaft axis set
K_C	pure gain
K_H, K_P	general gain of human operator
K_β	blade hinge spring stiffness
l	lift of blade element per unit span
l_{fin}	distance from fuselage reference point to fin centre of pressure
l_{tp}	distance of tailplane behind fuselage reference point
$[\mathbf{L}]$	dynamic inflow gains matrix
L, M, N	components of external moment on aircraft
m	aircraft mass
$[\mathbf{M}]$	dynamic inflow mass matrix
m_0	blade mass per unit span
m_b	blade mass
M_β	blade mass moment
n_{ints}	number of discrete intervals that define the manoeuvre
n_β	blade inertia number
p, q, r	general angular rates
$\dot{p}, \dot{q}, \dot{r}$	general angular accelerations
p', q'	normalised hub rotational accelerations ($p' = \dot{p} / \Omega^2$ etc.)
$\overline{p}, \overline{q}, \overline{r}$	normalised angular velocity components ($\overline{p} = p / \Omega$ etc.)
p_{pk}	peak roll rate
q_{pk}	peak pitch rate
Q_E	engine torque
Q_ϕ	roll attitude quickness
Q_θ	pitch attitude quickness
Q_p	general pilot attack

R	main rotor blade radius
$R_{\mathbf{TR}}$	tail rotor blade radius
r_b	distance from main rotor hub to a point on the rotor blade
$\bar{r}_b$	normalised position of blade element
s	main rotor solidity
$s_{\mathbf{TR}}$	tail rotor solidity
s_{fin}	area of fin
s_{tp}	area of tailplane
t	time at any point in any flight test manoeuvre
t_1	some time fraction of a flight test manoeuvre used for modelling the task
t_a	time taken to reach maximum acceleration in Acceleration/deceleration and Rapid Side-step manoeuvres
t_d	time taken to reach maximum deceleration in Acceleration/deceleration and Rapid Side-step manoeuvres
t_m	time taken to complete entire flight test manoeuvre (all tasks)
T_L, T_I	respective lead and lag time constants
T_N	neuro-muscular lag
$\underline{\boldsymbol{u}}$	control vector
U	gust velocity
U_0	gust intensity
U_T, U_P	tangential and normal components of airflow at blade element
$\overline{U}_T, \overline{U}_P$	normalised velocity components ($\overline{U}_T = U_T / \Omega R$ etc.)
u, v, w	general translation velocity components
$\dot{u}, \dot{v}, \dot{w}$	general translation acceleration components
U, V, W	translation velocity components of aircraft centre of gravity
v_0, v_{1s}, v_{1c}	uniform, lateral and longitudinal inflow velocity components
$\underline{\boldsymbol{V}}$	general translation velocity vector
$\underline{\boldsymbol{V}}_{hub/\mathbf{bl}}$	translation velocity vector of the main rotor hub referred to blade axes

$\underline{V}_{p/\mathbf{lag}}$	translation velocity vector of a point *p* located a distance r_b from the hub, referred to blade element lag axes
$[\underline{\mathbf{V}}]$	mass flow parameter matrix
$V(t)$	velocity at any time point *t* in any flight test manoeuvre
V_{gust}	horizontal gust velocity component
$V_{gust/vert}$	vertical gust velocity component
v_i	main rotor induced velocity
$V_{\max}$	maximum velocity attained during flight test manoeuvre
$\dot{V}_{\max}$	maximum acceleration attained during flight test manoeuvre
$\dot{V}_{\min}$	maximum deceleration attained during flight test manoeuvre
x	time taken to reach maximum gust velocity
x_{cg}	distance of rotor hub behind a/c centre of gravity
$\underline{\boldsymbol{x}}$	state vector
x_e, y_e, z_e	components of translation distance in Earth axes
$\dot{x}_e, \dot{y}_e, \dot{z}_e$	components of translation velocity in Earth axes
X, Y, Z	components of external forces on aircraft
$Y_H(s)$	helicopter transfer function
$Y_{\max}$	maximum lateral distance from centreline in Slalom flight test manoeuvres
$\underline{\boldsymbol{y}}$	output vector
z_g	height of main rotor above ground plane

Greek Symbols

α_{bl}	angle of attack of blade element
α_{tp}	tail plane angle of attack
β	aircraft sideslip angle, blade flap angle
$\dot{\beta}$	blade flapping rate, rate of change of sideslip
$\ddot{\beta}$	blade flapping acceleration

β'	derivative of flapping angle w.r.t. blade azimuth position ($d\beta / d\psi$)
β_{fin}	fin sideslip angle
γ_{sh}	shaft tilt angle
δ	blade profile drag coefficient of main rotor
$\delta_{\mathbf{TR}}$	blade profile drag coefficient of tail rotor
$\Delta\phi_{\text{min}}$	coincident minimum roll attitude change
$\Delta\theta_{\text{min}}$	coincident minimum pitch attitude change
$\Delta\phi_{\text{pk}}$	coincident maximum roll attitude change
ζ	blade lag angle
$\dot{\zeta}$	blade lagging rate
$\ddot{\zeta}$	blade lagging acceleration
ζ'	derivative of lag angle w.r.t. blade azimuth position ($d\zeta / d\psi$)
η_{1s}, η_{1c}	longitudinal and lateral stick displacement
η_{1c0}	reference lateral trim position or datum
η_{1s0}	reference longitudinal trim position or datum
η_x, η_y, η_z	normalised rotor hub acceleration ($\eta_x = \underline{\boldsymbol{a}}_{hub/\mathbf{x}} / \Omega^2 R$ etc.)
$\dot{\eta}_{pk}$	peak rate of stick displacement (general)
θ	aircraft pitch attitude, blade pitch angle
θ_0	main rotor collective pitch angle
θ_{1s}, θ_{1c}	main rotor longitudinal and lateral pitch angles respectively
θ_{0tr}	tail rotor collective pitch angle
θ_{tw}	geometric twist of blade
μ	general non-dimensional rotor hub velocity
μ_x, μ_y, μ_z	normalised rotor hub velocities ($\mu_x = u_{\mathbf{hub}} / \Omega R$ etc.)
ρ	density of air (ISA conditions)
$\tau_{c1}, \tau_{c2}, \tau_{c3}, \tau_{c4}$	respective longitudinal, lateral, tail rotor and collective actuator time constants
ψ	aircraft heading angle, blade azimuth angle

ψ_f	cyclic mixing or phasing angle
ψ_{gust}	heading angle at which gust meets aircraft
$\psi_{\mathbf{TR}}$	tail rotor azimuth angle
ψ_{wind}	rotor sideslip angle
$\underline{\omega}$	general rotational velocity vector
ω_{co}	pilot cut-off frequency
Ω	rotational velocity of main rotor
$\Omega_{\mathbf{TR}}$	rotational velocity of tail rotor

Subscripts

aero, **aero**	aerodynamic
bl, *bl*	blade axis set
bod, *bod*	body axis set
e	earth fixed axis set
fin	fin
fus	fuselage
gu	gust
hub, *hub*	hub axis set
lag, *lag*	lag axis set
IGE	in ground effect
OGE	out of ground effect
ROT	main rotor
sh, *sh*	shaft axis set
TR	tail rotor (when mentioned in main rotor model)
TR	tail rotor (when mentioned in tail rotor model)
trbl	tail rotor blade axis set
trh	tail rotor hub axis set
tp	tailplane
vert	vertical

"The allegory of a physical mountain for the spiritual one that stands between each soul and its goal is an easy and natural one to make. Like those in the valley behind us, most people stand in sight of the spiritual mountains all their lives and never enter them, being content to listen to others who have been there and thus avoid the hardships. Some travel into the mountains accompanied by experienced guides who know the best and least dangerous routes by which they arrive at their destination. Still others, inexperienced and untrusting, attempt their own routes. Few of these are successful, but occasionally some, by sheer luck and grace, do make it. Once there they become more aware than any of the others that there's no single or fixed number of routes. There are as many routes as there are individual souls."

"Zen and the Art of Motorcycle Maintenance"
Robert M. Pirsig

Chapter 1

Introduction, Main Aim and Objectives

In considering the design programme of a modern rotorcraft it is inevitable that the majority of the aircraft's *handling qualities* and *mission effectiveness* capabilities, whatever the application, will be imparted to the vehicle in the earliest stages of the project. It is therefore logical to investigate methods to initially aid the design of the aircraft and consequently improve the associated handling qualities. One method of doing so is through the use of computers to model and simulate aircraft. Although the concept of simulation has been in existence for many years the practicalities have become more evident with a corresponding increase in computing power, particularly, inexpensive desktop models.

Aircraft simulation in this context refers to the traditional or conventional method, which generally involves the prediction of the vehicle's open-loop response (output) to a given set of control inputs. An alternative method of simulation has more recently become apparent whereby the output consists of a set of controls required to pilot the aircraft through a prescribed flight test manoeuvre. It is clear that this approach is essentially the opposite of the conventional simulation technique and is thus termed *inverse simulation*. Since the approach is concerned primarily with continuous manoeuvring flight, as opposed to the open-loop response of single control inputs, the technique has found a wealth of alternative applications in both fixed and rotary wing research. *Lane and Stengel (1988)* investigate the uses of inverse simulation in the design and development of automatic flight control systems, while *Whalley (1991)* makes use of the technique to study rotorcraft agility.

Inverse simulation, handling qualities and mission effectiveness are the main points of discussion in this thesis and form the focus of work. As such, the main aim is the development of a simulation technique for the initial assessment of handling qualities and consequently mission effectiveness. The method of assessment is

objective and uses the term *Level* to quantify the associated handling qualities and is directly comparable to the subjective assessment technique detailed by *Cooper and Harper (1969)*. Since the University of Glasgow is at the centre of development of inverse simulation in the UK and *Thomson (1986)* first introduced the concept, as a method of quantifying agility, it is appropriate and timely to extend the research into the handling qualities field. The potential benefits of assessing handling qualities at the conceptual stage are clear in terms of savings on overall cost, flight safety issues and configuration development.

Recall that the aim of the programme of work is concerned with the development of a simulation technique to assess handling qualities with mission effectiveness in mind. The implications of this involve the improvement of the existing helicopter mathematical model and the extension of the existing library of flight test manoeuvres. It follows that a logical and useful starting point would be a general overview of handling qualities and inverse simulation before outlining the remaining thesis objectives and their relevance to the discussion.

1.1 The Subjective Method of Assessing Rotorcraft Handling Qualities

The Cooper-Harper pilot rating scale, *Cooper and Harper, (1969)*, is generally accepted as the most common method of subjectively assessing handling qualities. A handling qualities definition is written using terms such as *ease* and *precision* with which the pilot is able to manoeuvre the vehicle to accomplish the flight test manoeuvre. On the basis of answering a post flight questionnaire a pilot is able to associate a rating with the particular vehicle being assessed. The scale spans three main levels, Figure 1.1, and ranges from an aircraft that is uncontrollable (Handling Qualities Rating (HQR) 10, below Level 3) to one with excellent or highly desirable qualities and warrants little or no compensation from the pilot (HQR 1, Level 1). Rotorcraft are generally required to attain a Level 1 HQR throughout the entire operational flight envelope with Level 2 being associated with emergency situations or poor visual conditions. It can be seen that the pilot arrives at an HQR via several decisions starting from the leftmost side. This is one of a number of rules-of-thumb identified by *Padfield (1996)*, who states that "*pilots should arrive at their ratings by working through the decision tree systematically*". A further fifteen rules are given

and range from, what a final rating means, to effects of pilot fatigue and the required number of pilots required to carry out a valid handling qualities assessment of an aircraft. It would seem that such comments are important in the understanding of the final Cooper-Harper rating and indeed it is recognised that associating an HQR with an aircraft does not present the complete picture. Additional pilot comments must be made available for study, which help explain subjectively the rating given by the pilot. However, in doing so the rating awarded will of course depend on personal opinion which in turn is dependant upon the type of task being flown and/or the visual cues available to the pilot. The ultimate handling qualities rating not only depends on the vehicle and pilot but on many external influences *perceived* by the pilot. As a result, there has been a tendency in recent years to move towards a more detached and impartial means of aircraft appraisal whilst still allowing the pilot to participate. The method used is described in the United States Army, Aeronautical Design Standard (ADS), the most recent version of which is *ADS-33D (Anon., 1994)* and is based upon a more objective approach of aircraft assessment.

1.2 The Objective Method of Assessing Rotorcraft Handling Qualities

ADS-33D is aimed at defining vehicle response types required to achieve Level 1 or 2 handling qualities throughout the normal operational flight envelope of a rotorcraft. The ADS document is mission-orientated and the HQR attributed to any particular aircraft is ultimately associated with the specific task requirements of the Mission Task Elements (MTEs), where an MTE is defined as: "*an element of a mission that can be treated as a handling qualities task*". The required standards are defined for hover, low speed and forward flight regimes of the flight envelope and fall into manoeuvres flown in the Good Visual Environment (GVE) and those in the Degraded Visual Environment (DVE). To further explain the role of the ADS document it is necessary to move into the area of objective criteria for handling qualities assessment. Essentially this means that we are initially dealing with certain flying quality characteristics of the aircraft alone that can be quantified in numerical terms thus yielding a meaningful rating, without subjective opinion. In addition to the Mission Task Elements described uniquely in the ADS document, two other factors are then of primary concern. The Useable Cue Environment (UCE) which is a numerical measure of the quality of the visual cues available to the pilot, is used to

highlight the requirement for different flying qualities especially if the task involves manoeuvring close to the ground. The Response Type (RT) is a measure of how the aircraft responds in the short time after the pilot has made specific control inputs. The combination of these factors is then used to determine the overall handling qualities of the aircraft whilst flying a particular MTE.

The emergence of the aforementioned assessment techniques shows that there is clear emphasis from aircraft operators on the need to establish handling qualities ratings or Levels with any particular machine and flight test manoeuvre. From the manufacturers point of view there is an obvious requirement for simulation to be used during the design process to minimise the risk of developing a vehicle with substandard handling qualities. *Bradley and Thomson (1993)* have shown that inverse simulation provides a method for satisfying these requirements, as it is a technique which provides state and control information for any given manoeuvre thus enabling it to be used for the initial assessment of handling qualities.

1.3 Inverse Simulation at the University of Glasgow

The usefulness of the inverse approach is recognised when applied to rotorcraft where, especially in the military genre, the aircraft often operate in low-level nap-of-the-earth (NOE) flight conditions. In addition, many of the tasks involve precise manoeuvring and positioning of the aircraft and since these tasks lend themselves well to mathematical modelling, the consequential value of inverse simulation is evident. There are two forms of inverse simulation currently available at the University of Glasgow and they utilise entirely different algorithms. The original algorithm (used in this dissertation) is centred on a differentiation based method and is encapsulated in the software package *Helinv* developed by *Thomson and Bradley (1990a)*. Additionally there exists the integration based technique of *Rutherford and Thomson (1996)* which relies on numerical integration as a basis for solving the equations of motion and obtaining the state and control time histories.

Subsequent development of Helinv has found application in offshore manoeuvring simulation *(Thomson and Talbot et al, 1995)*, dynamic analyses of constrained aircraft flight *(Thomson and Bradley, 1990b)* and previous pilot workload

studies, *(Padfield and Jones et al, 1994)*. It has been adopted on the European mainland by the Deutsche Forschungsanstalt für Luft-und Raumfahrt, (DLR), *(Gray and von Grünhagen, 1994)*, the USA by NASA *(Whalley, 1991)* and in China *(Cao and Gao, 1994)*.

Although limitations in the differentiation based algorithm have been identified, (*Rutherford and Thomson 1997*) it is made clear that Helinv, in this instance, is to be utilised primarily as a method for obtaining off-line simulation results for the initial assessment of handling qualities, since state and control information is readily available. Essentially, this means that the data can be used for handling qualities predictions since the objective handling qualities metrics are based on observation of the aircraft's primary attitude angle during the manoeuvre and pilot stick displacement. The work in this context has focused mainly on the suitability of the Helicopter Generic Simulation (HGS) model, inherent in the Helinv algorithm, to yield realistic handling qualities levels from inverse simulation results of flight test manoeuvres.

1.4 Aims of the Research and Thesis Structure

The research is based on the rationalisation that inverse simulation is capable of making an important contribution to the evaluation of helicopter handling qualities. That said, two important implications arise from the statement. The helicopter mathematical model used in the inverse simulation algorithm must have a high enough degree of fidelity so that the conditions encountered in any of the flight test manoeuvres are captured and can be used for handling qualities analysis. Furthermore, the models of the flight test manoeuvres must be representative of the actual task, (usually it is the gross features of the task that are captured in the modelling process). The main aim of the research was introduced on the first page of this chapter and centres on the development of an inverse simulation method for initial assessment of helicopter handling qualities. In order to develop the simulation tool and successfully meet the main aim, several other objectives had to be fulfilled. These objectives and their relevant location within the thesis structure are outlined below.

1.4.1 Research Aims

Main Aim

Development of an Appropriate Simulation Technique for Initial Assessment of Helicopter Handling Qualities

The development of a technique that lends itself well to the study and assessment of rotorcraft handling qualities is fundamental to the research. Upon investigation it was clear that the states and controls of the aircraft would have to be calculated for any given flight test manoeuvre. Since the American Aeronautical Design Standard document, *ADS-33D (Anon., 1994)*, indicates that mathematical modelling of flight test manoeuvres is acceptable for initial assessment of handling qualities, and inverse simulation by its nature encapsulates the precisely defined manoeuvre and mathematical modelling, it seemed appropriate for the situation. Consequently inverse simulation was specifically selected as the method by which the analysis would take place. Inverse algorithms inherently comprise three main components, the helicopter model, manoeuvre models and the inverse algorithm itself. The implications of selecting inverse simulation were then obvious and the research focused on more specific objectives such as the improvement of the existing helicopter mathematical model and the development of flight test manoeuvres suitable for handling qualities assessment.

Additional Objectives

i) Improvement and Analysis of the Helicopter Generic Simulation (HGS) Model for Application to Handling Qualities

It is realised that the validity of results from any rotorcraft inverse simulation algorithm depends not only on the type and method of implementation of the algorithm but also on the underlying mathematical model of the helicopter. Helicopter Generic Simulation (HGS) is a well validated model and numerous results of inverse simulations have been presented illustrating favourable comparisons with flight test data, *Thomson and Bradley (1997)* for example. However, several features

were identified that were absent from the model and consideration was given to the development, modelling and incorporation of these features into the current HGS model, with the aim of improving the fidelity of the simulation and illustrating the effects on the handling qualities. Chapter 4 introduces the concept of rotorcraft modelling in general before approaching HGS, where the assumptions of the model are detailed. The improvements to the mathematical model are presented in three separate sections, each introducing, describing and then detailing the modelling method of that particular topic. In doing so, it was discovered that it was impractical to include one of the suggested improvements in the disc-type model and some limitations are identified and discussed as a result. However, the fidelity of the model is increased with the addition of atmospheric phenomena and the consequential effects on the handling qualities Level are highlighted.

Additionally, an important element of work was the analysis of the suitability of the HGS or indeed any disc-type helicopter model to handling qualities studies. It is shown that certain improvements to the model prove to be too complex to warrant practical implementation especially as little or no improvement in handling qualities Level was expected. The modelling and implementation of HGS improvements are discussed in Chapter 4, while a description of HGS can be found in Appendix C.

ii) Extension of Manoeuvre Library

The aim of Chapter 5 is focused on the improvement of current flight test manoeuvres and the development of additional tasks. These include the Defence Evaluation Research Agency's (DERA) Slalom task and two additional versions of the Slalom as flown by the German rotorcraft flight mechanics research department, Braunschweig. The point is made that, although the ADS document is a regulatory document in the United Sates, it is open for interpretation throughout the rest of the world and has formed the basis of many new flight test manoeuvres.

A final section of Chapter 5 is based on a validation type exercise of the mathematical models of manoeuvres. Confidence testing of mathematical manoeuvre profiles is comparatively novel and in effect shows that inverse simulation is indeed a valid off-line simulation tool for predicting control strategy and vehicle responses for

any of the given manoeuvres.

iii) Extension of Simulation Work to Include a Human Operator Model

The aim of Chapter 6 is to introduce a human operator model to inverse simulation and consequently investigate its effects on handling qualities. Since the inverse algorithm is considered to possess a 'perfect pilot' capable of flying each manoeuvre with precision and exact repeatability, it was postulated that introducing a human element would increase the realism of the results and thus yield a more realistic estimation of the Level of handling qualities. The approach is novel and utilises a unique optimisation method of estimating human equalisation parameters in the pilot model. It is shown that the human equalisation network (based on a form of lead-lag compensation) is variable with manoeuvre type and aggression.

A background to the technique of pilot modelling is presented and the *Precision Pilot Model* is introduced. The main objective is to show that the influence of the pilot model is capable of altering the handling qualities results obtained. A description of the technique and the method of implementation follow a general background section and results are presented from several inverse simulation runs and pilot model parameter optimisations. Additional results are presented illustrating the main differences between handling qualities Levels based on Helinv alone and those results obtained from the pilot model. In this instance a single helicopter model and flight test manoeuvre are used, although it is clear that the technique is applicable to other helicopter and manoeuvre models. This work represents a new application of inverse simulation and the work is ongoing at the University of Glasgow.

iv) Demonstration of the Techniques by Case Study

In an attempt to collate some of the techniques developed in the thesis, Chapter 7 is aimed at collating the individual objective handling qualities topics presented and illustrating the purpose of their development. A parametric study is conducted between two aircraft, one a standard Westland Lynx and the other, a theoretical configuration based on the Lynx but with pilot seating in tandem as opposed to the side-by-side configuration of the Lynx, (reflecting the current trend in

design of battlefield helicopters). By investigating inverse simulation results of the two helicopter models and calculating corresponding handling qualities levels it is shown that one configuration possesses certain handling characteristics that are likely to be more desirable. Thus the usefulness of the technique is demonstrated and the work presented is novel in context.

Furthermore, initial investigative results are presented for each aircraft in different flight states, where the effects of utilising a model of an Automatic Flight Control System, (AFCS) are presented. It is shown that altering the value of the actuator time constants within the model can be advantageous or detrimental to the perceived handling qualities. The value of inverse simulation, coupled with appropriate handling qualities metrics becomes clear and again it is emphasised that the approach is original, with *Charlton and Howell et al (1998)* presenting this type of work in the rotorcraft field for the first time.

Supplementary Information

As a direct result of conducting research in the handling qualities field, two additional sections of general information are given in the thesis.

i) Handling Qualities, Pilot Workload and Mission Effectiveness

In comparison to the period of time that rotorcraft have been in operation the topic of handling qualities is relatively new. That said, the importance of obtaining acceptable handling qualities in general for a new aircraft has been realised since the earliest days of manned flight. In Chapter 2 an overview of handling qualities and its associated topics with reference to rotorcraft is presented. Areas of pilot workload are identified and discussed, whilst some initial metrics are presented as an introduction to the manner in which recent trends have moved towards quantification of parameters associated with desirable rotorcraft handling characteristics. In addition the traditional approach of subjective assessment is discussed and the appropriate metrics presented. The work presented in Chapter 2, together with appropriate references, presents a novel collection of handling qualities topics and discussions and

emphasises the importance of accurate manoeuvre modelling within inverse simulation.

ii) To establish which Analytical Handling Qualities Metrics are suitable for use with Inverse Simulation

There are a number of analytical metrics available for use to assess handling qualities and one of the proposed objectives is to establish which methods can be used with inverse simulation results and if distinct interpretations can be obtained from different metrics. For this reason a number of studies were conducted with different helicopter configurations, manoeuvres and flight conditions. The ability to reliably simulate a rotorcraft performing a flight test manoeuvre, and then yield results based on the likely handling characteristics, is novel in inverse simulation and the potential implications and applications are many. The current disc model represents the first step in a new era of off-line objective handling qualities analysis and will doubtless serve as a basis for future investigations. Chapter 3 outlines the concept of inverse simulation, presenting an example manoeuvre with relevant control time histories. To connect inverse simulation and handling qualities assessment, a further manoeuvre is examined and Attitude Quickness and Pilot Attack parameters calculated and plotted. Chapter 3 is paramount to the understanding of the methods used in the thesis and presents this information in a more general fashion for reference and clarity.

1.4.2 Review of Research Aims

In summary then, the main aim is:

Development of an appropriate simulation technique for initial assessment of helicopter handling qualities

This implies that,

i) The Helicopter Generic Simulation (HGS) model is to be modified.

ii) The number of current flight test manoeuvres is to be extended and current models improved.

iii) The viability of using suitable handling qualities metrics with inverse simulation is to be established.

iv) Demonstration of the technique via a case study comparing the handling qualities Levels of two different helicopter configurations.

1.4.3 Conclusions of the Research Work

Chapter 8 completes the thesis by presenting conclusions drawn from the research. The usefulness of inverse simulation is demonstrated from a handling qualities point of view as it is found that predictions of Levels of handling qualities can be obtained from a combination of inverse simulation and appropriate metrics. The improvements to HGS and manoeuvre library extension are summarised and problems highlighted and it is shown that as it stands the current HGS model is most suitable for handling qualities evaluation studies. HGS model improvements are presented in terms of effect on handling qualities Level. Human operator modelling is coupled successfully with inverse simulation results and the effect of using the human operator model on handling qualites is clearly illustrated. In addition a novel parameter optimisation technique is developed and its implications with manoeuvre type and aggression discussed. A parametric study of two helicopter configurations, one based on the Westland Lynx and the other a conceptually superior aircraft, is used to demonstrate the techniques developed and establishes the feasibility of using current objective handling qualities metrics. This is seen to be successful and is evident from the results obtained.

1.4.4 Thesis Appendices

The thesis is complemented with six appendices, which are aimed at presenting an immediate source of reference. Since the topics discussed are largely based on previous work that has been well documented it was unnecessary to include such text in the main body of the dissertation. The title of each Appendix is listed in the contents pages of the thesis.

Chapter 2

Assessing Handling Qualities

This chapter will address the subject of handling qualities and methods of assessment of rotorcraft. It is intended to provide an overview of the many topics that are contained therein whilst setting the scene for the general perspective of the thesis. It is expected that a large amount of common ground will exist between many of the issues discussed. The approach taken will be to introduce the subject of handling qualities and then investigate the methods of assessment, by looking at current techniques.

2.1 Handling Qualities Applied to Aircraft in General

A modern, general definition of handling qualities of aircraft usually comprises two components. One is concerned with the response of the vehicle after a control input and the other with external influences such as weather conditions, atmospheric turbulence, external/internal load carrying etc. Originally however, handling qualities were associated purely with the static and dynamic stability of the aircraft. Attempts were made to measure these quantities with eventual formal specifications being drawn up to define the limits of acceptable and unacceptable behaviour of the aircraft modes. One such example is *Military Specification 8785 (Anon., 1969)* which set limits for the frequency of the short period mode and was written by the United States Air Force for fixed wing aircraft. The document failed to include atmospheric effects and consequently based itself entirely on the state of the aircraft alone. Modifications to existing documents and entirely new specifications were introduced to deal with atmospheric effects, visibility, and take-off and landing conditions. Many of these observations have been carried forward to the specifications of today and relate to modern fixed or rotary wing handling qualities assessment in a similar manner.

It was clear handling qualities requirements would eventually filter through to V/STOL aircraft. In the mid 1960's a concentrated effort began to improve the status of the handling qualities specifications and it was agreed that the term 'criteria' would serve to outline the desirable characteristics of the aircraft. Previously, requirements had been specified without full understanding or explanation as to why such characteristics would be useful, or detrimental to the pilot. As a consequence some requirements were applied too rigidly thus hindering performance and compromising aircraft utility.

2.1.1 The Cooper-Harper Pilot Rating Scale

At this time the assessment method for aircraft in general, was a subjective or qualitative technique and the handling qualities level was captured through the impression of workload as perceived by the pilot. *Cooper and Harper (1969)* first introduced the method and the subsequent Cooper-Harper scale, Figure 1.1 is generally regarded to be the most developed and universally accepted qualitative method of evaluating aircraft handling qualities ratings. The scale ranges from one to ten and is split into three more basic levels:

- **Level 1: Ratings 1 – 3** Aircraft satisfactory without improvement, minimal workload,

- **Level 2: Ratings 4 - 6** Desired performance requires moderate compensation (Rating 4) OR deficiencies warrant improvement, adequate performance requires considerable to extensive compensation (Ratings 5 and 6) and

- **Level 3: Ratings 7 - 9** Deficiencies require improvement, adequate performance unattainable with tolerable pilot workload. The chart also has a rating of 10, which indicates that the pilot looses control of the aircraft at some point during the manoeuvre.

An aircraft that is associated with a Level 1 rating is seen as attaining the minimum required standard, which is measured in terms of task performance and pilot workload. Level 2 is acceptable in emergency and failed situations only, while Level 3 is unacceptable and describes an aircraft with major deficiencies. Figure 2.1 illustrates the principle that the pilot arrives at the handling qualities rating by initially processing the major categories and making a decision which is succeeded by choosing a rating number based on processing minor decisions.

Although it has been universally accepted that pilots should not give ratings that are non-whole numbers, such as 3.5 etc. there is a suggestion that it is sometimes difficult to determine exactly what the rating is. The best way of illustrating this point is to discuss the boundary between the Level 1 and Level 2 ratings, i.e. the point where the pilot decides on an HQR of 3 or 4. This is clearly an important decision to make and some pilots may feel the aircraft is neither HQR 3 nor HQR 4 hence a rating of 3.5 is returned. Allowing pilots to distinguish between aircraft that demonstrate good handling qualities characteristics but are not exceptional may well lead to a non-whole rating in the Level 1 handling qualities bracket.

The Cooper-Harper rating scale can be used to help the pilot further refine a workload value associated with the task performance and perceived difficulty, hence attributing a handling qualities rating to the aircraft. The method is still seen as an effective way to assess the handling qualities of any aircraft, but obvious needs for elaboration have generated a great deal of interest in developing more modern techniques. The potential to develop a technology that is capable of delivering accurate pilot ratings at the development stage of aircraft using mathematical modelling and flight simulation exposes enormous benefits to the industry and to the aircraft operators. The development of handling qualities metrics and assessment techniques is an on-going process and has special application to rotorcraft because of their unique ability to perform tasks outside of the fixed wing envelope. The problem of applying handling qualities criteria to helicopters is discussed below.

2.2 Handling Qualities Applied to Rotorcraft

The continuing increase in helicopter operational requirements combined with

rigorous demands in commercial and military effectiveness has implied that piloting a helicopter is no longer a simple matter of activating specific controls to manoeuvre the vehicle through a given trajectory. Consequently, good handling qualities play a large role in ensuring the safe and successful execution of any set mission, be it commercial or military. The particular ability of the helicopter to fly nap-of-the-earth (NOE) manoeuvres by its nature demands that the handling qualities be exceptional, as insufficient performance can lead to mission failure and in extreme cases, loss of life.

It would be easy to confuse the terminology used in the literature. For example, *Tischler and Fletcher et al (1991)*, have used the term "flying quality analysis" to describe a more general programme of work that encompasses handling qualities, workload and mission capability. The general consensus though, seems to make a clear distinction between the two, *Padfield (1996)* for example. Here, flying qualities are concerned with the stability and control characteristics of the aircraft, i.e. associated with inherent attributes of the helicopter, whereas handling qualities describe external influences in the task and environment. This is important as it should be appreciated that a handling qualities assessment is not only concerned with individual aircraft features, but also with perceived task difficulty and other flight test manoeuvre conditions. These may include turbulence, or performing the task in a Degraded Visual Environment (DVE), caused by poor weather conditions, night flying or smoke filled battlefield conditions. Henceforth, the term handling qualities is associated with both the vehicle and task dynamics and describes the performance of a particular vehicle and specific flight test manoeuvre.

Clearly the level of handling qualities will only convey the extent to which the aircraft is capable of performing the task in which it is being assessed. If problems are encountered and a low level of handling qualities is assigned, there is no information available as to the exact nature of the difficulties faced during the flight test. Consequently many handling qualities ratings are accompanied with a pilot completed questionnaire which describes the flight test in detail. Appendix A, adapted from *Howell and Charlton (1997)* gives an example of such a questionnaire.

Although the United Kingdom has a set of handling qualities standards, *UK Def Stan 00-970 (Anon. 1984)* for rotorcraft design and airworthiness, the shear magnitude of rotorcraft operated in the United States, has meant that the Aeronautical Design Standard (ADS) document has found greater popularity in the rotorcraft community. Additionally, the most recent version of the document is dated 1994, and it is therefore more applicable to modern helicopter operators. The method of assessing handling qualities as given in the document is addressed below.

2.3 The Aeronautical Design Standard (ADS) Handling Qualities Assessment Technique

Military and civil specifications for rotorcraft have been in existence for many years and were ultimately derived from the specifications from fixed wing aircraft. Increases in technology from ground based simulators to off-line simulation has increased the demand for adequate handling qualities assessment without the need to develop an aircraft to prototype stage. As a result more modern documents have appeared presenting numerous criteria for rotorcraft handling qualities.

The most recent specification for flying and ground handling qualities of rotorcraft is the *Aeronautical Design Standard ADS-33D (1994)* superseding *ADS-33C (1989)*, and it attempts to assure that no limitations on flight safety or mission performance will result from deficiencies in flying qualities. The specification is a US standard and has its origins in a previous document, *MIL-H-8501 (Anon., 1961)*. Since the US military is by far the largest helicopter operator in the world their requirements are bound to receive the most attention. Thus, the ADS document has had a great influence on the assessment techniques adopted elsewhere in the world, particularly Europe.

The document introduces a new method of establishing a handling qualities Level for any given helicopter. It employs the 'Attitude Quickness' parameter as an objective or quantitative means of deriving a rating. This type of quantitative assessment provides the handling qualities engineer with analysis techniques to assess the performance of the aircraft in terms of its open loop response. As well as attitude quickness, in the pitch, roll and yaw axes there are other methods to examine the

behaviour of the aircraft in the vertical axis and for determining cross coupling characteristics. *Ockier and Gollnick (1996)* present a comprehensive quantitative study on the handling qualities of the MBB BO 105 aircraft, based largely on the criteria described in ADS-33D.

2.3.1 Attitude Quickness

The attitude quickness parameters for pitch and roll are defined under the moderate-amplitude attitude changes section of ADS-33D. The parameter for each is calculated in the same manner and plotted on a table, the roll axis example of which is illustrated by Figures 2.2a and b. The parameter is defined as the ratio of peak attitude rate to change of attitude, which for the roll axis would be peak roll rate to corresponding change in roll angle. ADS-33D states that the attitude quickness parameter:

"*shall exceed the limits specified in*" Figures 2.2a and b. "*The required attitude changes shall be made as rapidly as possible from one steady attitude to another without significant reversals in the sign of the cockpit control input relative to the trim position.*"

Figure 2.2a is for *target acquisition* and *tracking* manoeuvres in roll, while Figure 2.2b defines the limits of all other MTEs in the roll axis. The attitude quickness parameter applied to the roll axis is given as,

$$\text{Roll Quickness } (Q_\phi) = \frac{p_{pk}}{\Delta\phi_{\min}} \tag{2.1}$$

where,

p_{pk} is the peak roll rate and

$\Delta\phi_{\min}$ is the coincident change in roll attitude.

The quickness values are calculated and plotted on the associated quickness chart, thus revealing the handling qualities level of that particular aircraft whilst performing a specific flight test manoeuvre.

2.3.2 The Implications on Mission Effectiveness

ADS-33D defines a range of MTEs that can be used as initial assessment exercises for any military helicopter entering service. Adequate descriptions and suggestions have been provided for conducting each test manoeuvre, although provision is made for individual testing authorities to determine how the test manoeuvre will appear to the pilot in terms of visual cues available.

The first classification to be made within the document is to define those manoeuvres which are to be performed in the Good Visual Environment (GVE) and those which fall into the Degraded Visual Environment (DVE) category. A subsequent organisation arranges the manoeuvres into aggressive and precision tasks. Table 2.1 presents an overview of the specified manoeuvres as precision or aggressive tasks and within their respective visual task cue environments.

To complete the Aeronautical Design Standard discussion it is appropriate to describe the basics of flight test experiments designed to examine the flying characteristics of a helicopter. This will include a discussion on the requirement for suitable tasks or Mission Task Elements and how they are designed in real life. ADS-33D will feature considerably in the discussion as many of the requirements have been stated with specific procedures to adopt in order to conduct a valid handling qualities assessment.

2.3.3 The Importance of the Mission Task Element to Flight Testing

The design of a Mission Task Element, although it would initially seem to be uninvolved in handling qualities issues, is perhaps one of the most important elements in the whole handling quality assessment experiment. It has been stated that one of the most influential factors on obtaining a Handling Qualities Rating (HQR) for a particular aircraft is the actual task that the pilot has to perform. In the words of *Padfield (1996)* "*task performance drives workload which drives pilot rating*". Assuming this to be the case, the starting point is to define a suitable flight test procedure that is capable of collecting the handling qualities data.

As stated, ADS-33D suggests possible methods of carrying out specific tasks that will analyse handling characteristics in a particular axis for example. Although the document is regulatory in the United States it is open to interpretation in other countries and in many instances testing authorities have found it beneficial to define tasks based on their own typical flight manoeuvres. In the case of *Howell (1995)* for example, DERA have designed a Slalom task similar to off-line simulation software available for comparison purposes, thus enabling validation of the software and prediction of flight parameters.

One important aspect of conducting flight tests is that the test must be reproducible, that is, the task should be flown by a number of test pilots (at least three) with the same understanding of the desired performance. Obviously with an increased number of pilots the resulting HQRs will have variations. However the variation in the rating no matter how many test pilots are used in the experiment should never be more than two. If the variation is more than two it is likely that the pilots are misunderstanding the exact requirements and the test should be redefined to eliminate any ambiguous possibilities. Equally so, if the ratings are all within two grades of each other then the test is reproducible and an effective HQR can be obtained. *Pausder and von Grünhagen (unknown)* summarise the prerequisites for a successful handling qualities test as the 'R^3' requirements:

- The piloting task must be *representative* of the corresponding operational mission requirement.

- The piloting task must be *reproducible* for different pilots and different vehicle configurations.

- A *low risk,* flight safety procedure must be adopted for the test.

2.3.4 Current Methods of Acquiring Flight Test Data for Handling Qualities Assessment

Advancement in technology has meant that an increasing amount of flight test

data and corresponding HQRs can be obtained from ground based simulators, as opposed to using real aircraft fitted with data gathering equipment. *Howell and Charlton (1997)* give an example of flight testing using an Advanced Flight Simulator (AFS). The objectives of using the AFS were twofold, firstly to investigate the effect of various flight control actuator authorities on the Westland Lynx aircraft and secondly to compare the simulator data with real flight-test data from a Lynx. Results obtained from other off-line simulation techniques were also used for comparison purposes.

The approach taken was to evaluate the aircraft over a number of ADS-33D style tasks followed by a simulated mission sequence taken from an actual combat flight scenario. Three test case aircraft configurations were used, one to compare with the actual Lynx aircraft and two to investigate an unaugmented and full authority case respectively. The ADS flight tasks that were evaluated were typical and examined the behaviour of the aircraft over a range of speeds. Performing manoeuvres that required a completely different primary control strategy allowed the analysis of on and off-axis response and the effects of cross coupling.

The standard description of each manoeuvre as given by ADS-33D in the GVE was taken to be the flight strategy adopted by the pilot. Upon completion of each task the pilots were required to fill out the questionnaire as given in Appendix A, and associate a handling qualites rating. The ratings were compared for each pilot and a final value obtained which in turn could be used for verification purposes in off-line simulation techniques such as inverse simulation.

2.4 Pilot Workload and Further Handling Qualities Assessment Techniques

Aircraft handling qualities have been defined as "*those qualities or characteristics of an aircraft that govern the ease and precision with which a pilot is able to perform the tasks required in support of an aircraft role*", *Cooper and Harper (1969)*. In the assessment of helicopter handling qualities, based on the statement from Cooper and Harper, it is likely that the ultimate rating associated with the aircraft will be determined from the pilot's perception of the words *ease* and *precision*. With a pilot's perceived difficulty in task performance or failure to attain

the degree of precision required for that particular manoeuvre, it is probable that a higher workload rating will be assigned. The importance of using specifically tailored tasks to understand pilot behaviour and handling qualities appraisal is realised by the US Army and is presented in the ADS documents. Before addressing the additional methods of assessing rotorcraft handling qualities it is perhaps useful to understand pilot workload and its sources in a modern battlefield helicopter, for example.

2.4.1 Pilot Workload

Pilot workload has until recently been a phenomenon that has been difficult to define and quantify. Although it is clear that there are specific sources of workload, it was not always understood that workload depended on other factors. ADS-33 was responsible for introducing and discussing outside influences that may have a great deal of effect on the workload rating determined by a pilot. In the same way that fixed wing aircraft were designed to perform different tasks it was accepted that some rotorcraft were clearly more capable than others in specific situations. As ADS-33 is a military specification a large number of the tasks described therein relate to military operations that were likely to be performed in battlefield situations. The Useable Cue Environment (UCE), was introduced as a measure of the visual cues available to a pilot and is defined numerically from 1 to 3. The best possible cues in the Good Visual Environment (GVE) allowing aggressive but precise manoeuvring is defined as a rating of 1, and a rating of 3 is ascribed to cues that allow only gentle manoeuvring without a reasonable degree of precision.

The concept of ‘divided attention’ was also introduced where it was realised that a pilot might have additional cockpit duties to perform or in some cases the workload is divided between two crew members. ADS-33 addresses this problem by defining two levels of attention. One where the pilot is able to give full attention to the guidance and stabilisation of the aircraft and another where attention is diverted elsewhere to other tasks. It is reasonable to assume that the pilot is not able to adopt the same response techniques to those of the fully attended operations. In the case of pilot and co-pilot, situations may arise where specific boundaries have not been set as to who is required to perform which tasks during the mission, resulting in additional workload being placed upon the pilot. Concessions are made for the pilot who is not

able to fly the aircraft with full attention and the handling quality standards are allowed a degree of leniency.

2.4.2 Sources of Pilot Workload

Pilot workload quantifies the amount of effort (physical and mental), expended in flight execution and control. It has been identified as comprising three components, each with its own particular time limitation and demand on the concentration of the pilot, *(Charlton and Jones et al, 1997)*. The workload components of a pilot flying any given task are given below.

i) *Navigation* – it is likely that the navigational exercise will pose the least amount of workload on a pilot as it is composed of piloting control inputs that occur infrequently (up to one hundred seconds between inputs).

ii) *Guidance* – the piloting phenomenon that is particularly suited to NOE flight and is characterised by terrain and obstacle avoidance. In this case the pilot inputs are more frequent, with no more than ten seconds elapsing between control movements.

iii) *Stabilisation* –a compensating workload component to maintain the preferred attitude for that particular manoeuvre. It is possible that this element of workload imposes the greatest demand on pilot attention as control inputs are very frequent (not more than one second between pilot inputs) and involve closed-loop control of the aircraft attitude.

Of course this is not an exhaustive list of pilot workload components but it does encompass all tasks necessary to navigate and fly the vehicle. Additional sources of workload come from subsidiary mission tasks such as maintaining communication, activating threat awareness and deploying weapon systems etc. The net result is that pilot attention becomes divided between these and the primary guidance and control tasks, subsequently jeopardising flight safety and mission effectiveness. The importance of the guidance and stabilisation components of workload will be realised later in the thesis when attitude quickness and an additional parameter called pilot attack are used as handling qualities assessment techniques.

2.4.3 Additional Assessment Techniques

Quantifying handling qualities in some kind of numerical sense has posed a problem for many years. Numerous attempts at potential solutions have been documented including:

1. Observations of pilot control strategy, *Padfield and Charlton et al (1988)*. The approach was to hypothesise that "*pilots generally try to adopt a control strategy that maximises performance and minimises workload*". It was thought that, depending on the mission, a compromise would have to occur and the crux of the work lay in the understanding of concessions made by the pilot during the task.

2. Frequency domain methods such as task bandwidth proposed by *Atencio (1993)*. The method explored here was to look at differences in demands in pilot control for different manoeuvres. In the analysis of pilot stick frequency it was observed that higher frequencies and lower amplitude were generally associated with degraded vehicle handling qualities.

3. Aircraft task frequency ratio as suggested by *Padfield and Jones et al (1994)*, which is the ratio of aircraft to task natural frequencies. For symmetrical Slalom tasks a frequency analysis can produce simple expressions for the natural frequency of the task. The natural frequency of the aircraft for example in roll can be calculated from the rotor moment coefficient. The ratio of these parameters can be used to determine if a pilot will have difficulty in meeting the demands that flying certain manoeuvres will impose on the aircraft.

4. Pilot cut-off frequency as described in *Howell (1995)* is another frequency domain method. Using the process of Fast Fourier Transform (FFT) to analyse pilot control activity and produce a summary of frequency content, a spectrum is obtained which encapsulates an area that is the mean square of the control signal and thus is a measure of its overall energy. The proposed workload metric, "*pilot cut-off frequency ω_{co} is the frequency at which 70.7% of this energy has been accounted for*".

2.4.3.1 Pilot Attack

One approach to quantifying the workload placed upon a pilot in terms of stick displacement is calculation of the 'pilot attack' parameter. The parameter is much the same as the Attitude Quickness defined in ADS-33D, except that the focus is on the pilot stick displacement as opposed to the attitude of the aircraft. Pilot attack is defined mathematically as,

$$\text{Pilot Attack } (Q_p) = \frac{\dot{\eta}_{pk}}{\Delta\eta} \tag{2.2}$$

where,

$\dot{\eta}_{pk}$ is the peak value in the derivative of stick displacement (lateral stick when applied to the roll case) and

$\Delta\eta$ is the corresponding change in net stick displacement.

Performing the task of guidance and stabilisation clearly involves the pilot displacing the stick to some degree, depending on manoeuvre aggression. Each distinct stick displacement is therefore an element of physical workload and can be identified as such by associating an attack parameter to each rate peak with a positive amplitude and each rate trough with a negative amplitude. The pilot attack parameter differs from the attitude quickness in that attitude quickness uses the maximum roll rate peaks occurring between zero crossings to assign corresponding quickness values.

This pilot attack approach to quantifying pilot workload, which is one of the most contemporary objective methods at the time of writing, has been taken by the Defence Evaluation and Research Agency (DERA), Bedford, and is described in more detail in *Charlton and Howell et al (1998)*. Attack parameters calculated in this way can be plotted on an 'attack chart', Figure 2.3 from *Padfied and Jones et al (1994)*, as a function of net stick displacement. The diagram identifies hyperbolic contours of constant effort for the pilot up to the limit of aircraft capability. Calculating pilot attack is an objective or quantitative method of identifying components of workload.

Chapter Summary

The chapter provided a general overview of handling qualities and more specifically considered its application to rotorcraft. The Cooper-Harper scale was discussed and it was shown how that has filtered through to the criteria mentioned in the Aeronautical Design Standard document. Two important handling qualities assessment parameters were introduced. Attitude quickness, given in ADS-33D was shown to be a technique for determining a handling qualities level by applying a simple formula to the aircraft states and their derivatives. Pilot attack on the other hand is entirely different and is concerned with actual stick movement in the cockpit. An attack parameter can be calculated for each distinct stick movement and plotted on a chart that provides information on workload.

Chapter 3

Inverse Simulation as a Handling Qualities Assessment Tool

The purpose of this chapter is to introduce the inverse simulation concept, and further clarify the technique by presenting a typical example with associated results. The handling qualities issue described in the preceding chapter is also included by providing a demonstration of the ADS Attitude Quickness method of assessment using data from a simple linear translation manoeuvre. Initially, inverse simulation in general is discussed followed by the algorithm particular to the software at the University of Glasgow. An example is used to show how the required data for handling qualities assessment is obtained. This essential background to inverse simulation, the algorithm and the example of the analysis tools (used later in the thesis) is presented at this stage to benefit the reader and stress the point that inverse simulation is in effect a simulated flight test tool.

3.1 An Introduction to Helicopter Inverse Simulation

The traditional approach to flight simulation is to formulate a mathematical model of a test vehicle and estimate its response to a predefined input command. This approach can be used in a real time sense with motion and/or visual cues to develop flight simulators for pilot training purposes or the evaluation of potential aircraft configurations in the aerospace industry. It is more often the case however, that off-line or non-real-time simulation is used for the investigation of an aircraft's stability and control characteristics, or to determine short and long term response characteristics from specific control inputs.

This type of work in general, applies to fixed wing aircraft and, although it is valuable for the investigation of rotary wing flight, it does not cover all aspects of

helicopter operational activities. This is made clear when it is recognised that the helicopter has the unique ability to operate close to the ground, tracking a precise flight path at varying speeds. The simulation of this type of behaviour in the conventional sense is virtually impossible since the control inputs required make the aircraft track a predetermined flight path are unknown.

By virtue of this statement alone, the suggestion is made that perhaps a more effective approach would be to invert the problem and use the desired flight path as an input to the problem and recast the mathematics involved to yield the controls required to fly such a manoeuvre. This chapter, together with Appendix B introduces the concept of what has become to be known as inverse simulation, and describes the method applied to a non-linear, flight mechanics model of a conventional battlefield/utility type helicopter. Due to the complex nature of the helicopter the inversion process is significantly more difficult than for a fixed wing aircraft. The technique essentially involves the discretisation of the non-linear differential equations of motion (allowing numerical algebraic solution). The inverse technique described therefore, is not unique to helicopters, and providing the equations of motion are developed in the same form, can be applied to other systems.

3.1.1 Some Elementary Principles of Helicopter Flight Control

Piloting the helicopter is fundamentally about control of the thrust vector produced by the main rotor. In controlling this vector there are two options open to the pilot, magnitude and direction. The magnitude of the thrust vector is altered by adjustment of the *collective* lever, which alters the pitch (and hence lift) of the blades collectively. Main rotor collective pitch is given the symbol, θ_0 and is generally used for altitude and directional-velocity adjustments. The pitch of the rotor blades can also be adjusted in a cyclical fashion, i.e. adjust blade pitch at various points around the rotation of the disc. This is accomplished by use of the *cyclic* stick, which can be used to induce basic rolling or pitching of the aircraft. If for example, the pilot moves the stick to the right, applying *lateral cyclic*, denoted, θ_{1c}, the rotor blades flap up on the left side of the disc and flap down on the right thus generating a rolling moment to the right whilst simultaneously directing the rotor thrust vector and accelerating the

aircraft to starboard.

In a similar manner, to generate a nose down pitching moment, the pilot would push the stick forward (*longitudinal cyclic*, θ_{1s}) causing the blades to flap up at the rear of the disc and flap down at the front thus directing the thrust vector forward and causing the aircraft to accelerate in that direction. In each case, practically speaking, the pilot would also be required to apply collective to maintain altitude, since there would be a loss in the total lift due to the redirection of the thrust vector. In addition the torque transmitted to the main rotor has to be balanced by an equal but opposite moment, the tail rotor, controlled by pedal movement which adjusts the *tail rotor collective*, θ_{0tr}. Consequently, helicopter controls are highly coupled and it is difficult to make single control inputs that do not require adjustment in other channels. In principle the workload placed upon the pilot is kept to an acceptable level by introducing control mixing (mechanical linkages or a Stability and Control Augmentation System, SCAS) and fitting the aircraft with a rotorspeed governor.

3.1.2 Helicopter Inverse Simulation – A General Overview

Inverse simulation, mentioned above, is so-called because it is essentially the opposite of conventional simulation in that it is a predetermined output vector that is used to calculate the control vector of the aircraft. It was seen that this is a particularly appropriate approach for rotorcraft flight since helicopter operations often involve low speed, constrained flight or hovering manoeuvres. For helicopter inverse simulation, the output usually consists of the main and tail rotor blade pitch angles, which can be transformed via an appropriate model to actual pilot stick displacements hence, the actual piloting strategy can be identified. Consequently the input to the simulation consists of a flight path defined in an earth fixed frame of reference. In general then, most inverse simulation techniques require an *input* to the system, a *modelled system* and an *algorithm* to perform the inverse calculations.

Thomson and Bradley (1990a) have discussed one algorithm particular to the University of Glasgow, as used in the helicopter inverse simulation software, Helinv. The method is presented in Appendix B for completeness and immediate reference

and will not be treated here. Instead a more general overview of the technique is given below which illustrates some of the mathematical concepts involved and is intended to give the reader a basic insight into the algorithm, required inputs, outputs and modelling technique.

If it is assumed that the conventional simulation problem can be written in the form,

$$\dot{\underline{x}} = \underline{f}(\underline{x},\underline{u}); \quad \underline{x}(0) = \underline{x}_0 \tag{3.1}$$

$$\underline{y} = \underline{g}(\underline{x}) \tag{3.2}$$

where,

$\underline{x}$ is the state vector of the system and $\underline{u}$ is the control vector, then it can be said that Equation 3.1 is a statement of the modelled system showing the state vector's response to an imposed control vector over some time period. Equation 3.2 simply shows how the output vector, $\underline{y}$ is obtained from the state vector. In inverse simulation, it is a predetermined $\underline{y}$, that is used to produce $\underline{u}$, thus Equations 3.1 and 3.2 are used in an implicit manner. Differentiating and recasting Equations 3.1 and 3.2 can demonstrate the inverse method,

$$\dot{\underline{y}} = \frac{d\underline{g}}{d\underline{x}}\dot{\underline{x}} = \frac{d\underline{g}}{d\underline{x}}\underline{f}(\underline{x},\underline{u}) \tag{3.3}$$

Considering the case where Equation 3.3 can be inverted with respect to $\underline{u}$, it is possible to write,

$$\underline{u} = \underline{h}(\underline{x}, \dot{\underline{y}}) \tag{3.4}$$

Substituting Equation 3.1 gives,

$$\dot{\underline{x}} = \underline{f}(\underline{x}, \underline{h}(\underline{x}, \dot{\underline{y}})) = \underline{F}(\underline{x}, \dot{\underline{y}}) \tag{3.5}$$

Equations 3.4 and 3.5 can be considered to be complete statement of the inverse problem with $\underline{\dot{y}}$ as the input vector and $\underline{\boldsymbol{u}}$ as the output vector. It is worth mentioning that Equation 3.5 is forced by the rate of change of the original output vector and in this form shows a few of the aspects of the practical application of inverse simulation. First, the dynamic characteristics of the system (helicopter) may be significantly different to that described by Equation 3.1, second, if Equation 3.3 cannot be inverted with respect to the control vector, further differentiation of Equation 3.2 will be necessary to provide additional equations for the inversion process. This means that higher order derivatives may appear as forcing functions and care must be taken to ensure smoothness of the required output, $\underline{\boldsymbol{y}}$. If this is not the case it is unlikely that the control vector obtained from inverse simulation will be of any use since discontinuities will produce unrealistic results.

Figures 3.1a and b present flow charts of the Helinv algorithm. It can be seen that the algorithm initiates by defining a manoeuvre in the earth fixed frame of reference and, by differentiation the corresponding velocities and accelerations are found. Heading or side-slip constraints are applied, depending if the manoeuvre involves turning flight, so that a unique output can be defined. The six body equations of motion (Appendix C, Equation C1.1) and the engine equation, (Appendix B, Section B1.2) are solved, the three remaining unknowns being the fuselage pitch and roll attitudes and the engine rotor speed. The solution is cast in a time marching form, and the seven equations of motion are solved at each point in the series, using the flight path information at that point, and elements of the state vector from the previous time point. There are of course many intermediate calculations to be performed that are sequenced in a particular order to facilitate efficient solution times. The reader is referred to Appendix B for the full solution procedure.

The rudimentary diagram presented in Figure 3.1a gives an overview of the entire algorithm, in that the inputs, outputs and the general solution procedure can be easily identified. The user is required to input information pertaining to the particular manoeuvre selected for inverse simulation. The manoeuvre is broken into a number of time points and various positional, velocity and acceleration calculations performed. This information is then used with state information to solve the

equations of motion, Appendix C, Equation C1.1. It is the state information from the previous time point that is used, or in the case where the inverse algorithm has just started (i.e. the first time point), then the information is known from predetermined trim conditions stored within the algorithm.

The more complex task of actually solving the equations for the unknown variables is presented in Figure 3.1b, where the reader is taken through the solution, step-by-step. Here the number and type of intermediate calculations can be seen, with the iteration loop required to for the seven unknown functions which in turn allows calculation of the Jacobian elements and new estimates of the unknown variables to be made. Since there are seven unknown functions and the Jacobian elements are solved by numerical differentiation, the loop iterates a total of fifteen times at each time point within the manoeuvre. When the solution has converged to within a predetermined error tolerance, the algorithm is permitted to move on to the next time point in the manoeuvre, before repeating the procedure. The solution at each time point yields time histories of all the unknown variables, pitch and roll attitudes, the four helicopter controls and the engine rotorspeed, (i.e. state and control information). In this respect the information obtained is ideal for handling qualities studies since the state information can be used for ADS-33D attitude quickness analysis and the control information can potentially be used for pilot attack analysis.

Section 3.1.3 below introduces the concept of manoeuvre modelling and presents inverse simulation results from a simple manoeuvre in longitudinal flight. The use of inverse simulation results to provide initial handling qualities assessments is also introduced. Additional sections are dedicated to further development of manoeuvre models, illustrating the importance of capturing the correct profile.

3.1.3 What Does Inverse Simulation Provide For Handling Qualities Assessment?

Inevitably, the best method of answering the question posed above is by demonstration. Recall that inverse simulation generally comprises three components, Manoeuvre Definition (input), Mathematical Model of Test Vehicle (modelled system) and the Inverse Algorithm (algorithm). In the context of the thesis the

manoeuvre definitions are presented as flight test manoeuvres defined in an earth fixed frame of reference (x_e, y_e, z_e), the test vehicle model (unless otherwise stated) is the Westland Lynx, Figure 3.2, and the inverse algorithm is a differentiation based technique.

The important aspect at this stage lies in the explanation of the reasons why inverse simulation is suitable for handling qualities studies. Put simply, inverse simulation is capable of capturing the specific modelling requirements required for nap-of-the-earth (NOE) or ADS defined flight test manoeuvres and producing the information required for subsequent assessment. The point is made clear by considering the example case of the so-called "Pop-up" manoeuvre, Figure 3.3. The manoeuvre is used to avoid an obstacle by initiating a rapid change in altitude during straight and level flight. The manoeuvre takes place in the longitudinal (x_e, z_e) plane with the lateral displacement (y_e) and the heading angle of the aircraft (ψ_e) set to zero throughout the duration of the task. The altitude changes smoothly from the initial datum of zero to some height, *h* over a time, t_m required completing the task. The horizontal flight speed is typically constant although provision is made for a smooth variation from manoeuvre initiation to termination.

By assigning appropriate boundary conditions the manoeuvre z_e (earth) co-ordinate can be made to vary smoothly from manoeuvre initiation to termination (i.e. from *zero* to some height *–h*). The following polynomial accommodates this smooth transition,

$$z_e(t) = -\left[6\left(\frac{t}{t_m}\right)^5 - 15\left(\frac{t}{t_m}\right)^4 + 10\left(\frac{t}{t_m}\right)^3\right]h \tag{3.6}$$

where,

t_m is the time taken to complete the entire manoeuvre,

t is the time at any point during the manoeuvre and

$0 < t < t_m$.

Figures 3.4a to d illustrate the pilot controls displaced in order to accomplish an 80 knot Pop-up to 20 metres in the Westland Lynx over a distance of 200 metres. They respectively show main rotor collective lever, longitudinal cyclic stick, lateral cyclic stick and tail rotor pedal movement. The control strategy for the manoeuvre can be determined from the plots. It can be seen from Figure 3.4b that an initial pulse of longitudinal stick movement initiates the manoeuvre by making the aircraft adopt a nose up attitude to manoeuvre the aircraft over the obstacle. A gradual forward movement of the stick (to maintain airspeed) follows this to account for increased blade drag, caused by the increase in main rotor collective. Upon reaching the desired altitude the stick is pulled back rapidly to return the aircraft to a straight and level trimmed flight condition. Collective is increased during the climb and is rapidly reduced when the aircraft has completed the climb and returns to a trim position for steady level flight. The increase in main rotor collective results in a similar increase in tail rotor collective, Figure 3.4d hence a greater pedal movement is required to keep the heading angle at zero. Increasing tail rotor collective will clearly generate a slight rolling moment and a counteractive lateral stick movement can be seen in Figure 3.4c.

In addition to the above control information, data is available for all of the states. It follows that the pitch attitude quickness can be calculated from pitch rate peaks, q_{pk} and the corresponding change in pitch attitude, $\Delta\theta_{\min}$. In a similar manner the pilot attack can be obtained from change in longitudinal stick displacement, $\Delta\eta_{1s}$ and derivative of longitudinal stick, $\dot{\eta}_{1s}$.

3.2 The Effect of Manoeuvre Modelling Techniques on Handling Qualities

Inverse simulation can only be applied to the specific MTEs given in the ADS documents if they are mathematically represented in an appropriate manner. Clearly the first task is to convert the manoeuvre descriptions to some kind of flight path depicting the test manoeuvre. There are generally two methods used at the University of Glasgow, both are variations on the development of a polynomial function to model certain main flight parameters which are taken to be the most influential on that particular task. The methods are known as Global and Piecewise Polynomial modelling techniques.

3.2.1. Smooth Global Polynomial

An element of work previously carried out at the University of Glasgow by *Thomson and Bradley (1997)* was the development of a library of basic linear repositioning and turning flight manoeuvres, which were further developed to encompass the more rigorous demands of the test manoeuvres as specified by ADS-33C and ADS-33D. The initial approach taken was to fit polynomial functions to the known profiles of primary aircraft parameters, which, for example in the case of the ADS Rapid Side-step manoeuvre, Figure 3.5 are, aircraft lateral position, velocity and acceleration. The Rapid Side-step is one of the more basic types of manoeuvre found in helicopter flight and is often used to manoeuvre between areas of cover in a "*mask-unmask-mask*" type fashion as shown in Figure 3.6. It can be split into constituent parts, to which specific mathematical boundary conditions can be imposed. The helicopter initiates and terminates the manoeuvre in a trimmed hover state, implying zero velocity and acceleration at these points. Assigning a further boundary condition stipulating that the maximum velocity attained, occurs exactly half way through the manoeuvre, results in seven boundary conditions that when applied mathematically yield a sixth order velocity profile equation of the form,

$$V(t) = \left[-64\left(\frac{t}{t_m}\right)^6 + 192\left(\frac{t}{t_m}\right)^5 - 192\left(\frac{t}{t_m}\right)^4 + 64\left(\frac{t}{t_m}\right)^3 \right] V_{\max} \tag{3.7}$$

where,

t_m is the time taken to complete the entire manoeuvre,

t is the time at any point during the manoeuvre and

$V_{\max}$ is the maximum velocity attained during the manoeuvre.

Figure 3.7 is a graphical representation of the Rapid Side-step velocity profile and illustrates the smooth nature of the global approximation. *Thomson and Bradley (1998)* found that this approximation compared favourably with flight data and that the detail of the profile tended to be of secondary importance, provided the gross features of the manoeuvre were captured.

The smoothness of the profile, although agreeable with flight data was inadequate in capturing the more aggressive approach taken by the ADS-33D document and as a result was unable to produce the required roll attitudes necessary for successful completion and desired performance requirements. It was evident another method would have to be developed to encompass the aggressive features. The method employed was to look at the acceleration profile of the aircraft during the manoeuvre and resolve it into discrete components.

3.2.2. Piecewise Polynomial Function Method

ADS-33D documents the key elements of the Rapid Side-step as follows:

"*Starting from a stabilised hover, ... initiate a rapid and aggressive lateral translation, with a bank angle of at least 25 degrees. ... When the rotorcraft has achieved a lateral velocity within 5 knots of its maximum allowable lateral airspeed or 45 knots, whichever is less, immediately initiate an aggressive deceleration to the hover at constant altitude. The peak bank angle during deceleration should be at least 30 degrees, ...* "

Upon examination of the velocity profile for the global polynomial method, Figure 3.7 and considering the above statement, clearly this is a much more aggressive approach and the polynomial description given by Equation 3.3 would not be satisfactory in achieving all of the requirements. It is possible to identify six separate and distinct sections in the above description and, since they are concerned with the acceleration of the rotorcraft, a logical approach was the development of an acceleration profile for the entire manoeuvre. The manoeuvre was considered as a sequence of individual segments where each segment is representative of the primary acceleration stipulations. The six sections of the acceleration profile consist of:

1. A rapid increase in the lateral acceleration from trimmed hover to a maximum value $\dot{V}_{\max}$ after a time t_1 seconds. These parameters are chosen to ensure that the maximum roll angles achieved are greater than 25 degrees.

2. A constant acceleration section to allow the flight speed to build up to some maximum value V_{max} given as the lesser of the rotorcraft's maximum lateral velocity or 45 knots.

3. Lateral acceleration is decreased rapidly to zero, after the desired flight speed has been attained.

4. A further decrease in lateral acceleration, which is in effect a deceleration, to a maximum negative value of $\dot{V}_{min}$ after a time $2t_1$ seconds to rotate the aircraft in the opposite sense.

5. A constant deceleration phase to allow flight speed to be reduced to zero.

6. A rapid decrease in deceleration to bring the helicopter to a trimmed hover after a full manoeuvre time of t_m seconds.

Figure 3.8 illustrates the acceleration profile of the Rapid Side-step as modelled using the piecewise method. The separate segments are clearly visible and the approach obviously forces the aircraft to attain the required attitudes within the specified times.

For comparison the roll attitudes of the two methods are presented in Figure 3.9. The Lynx aircraft model was used in both inverse simulation runs, with a maximum lateral velocity of 30 knots. The Global method shown by the broken line attains the required attitude but only after the time limit set by the ADS document has expired. Essentially the aircraft over compensates during the periods of maximum roll, but is unable to achieve this as quickly as the Piecewise method. It would seem that the Piecewise method is more effective at capturing the important features of the ADS task description and is therefore more fitting to be used for such applications.

3.3 Calculation of Attitude Quickness for the Two Side-steps

It is useful to present an example of attitude quickness calculations at this stage, first, to introduce the reader to the concept and second, to demonstrate how the parameter is mathematically obtained. Using a combination of an example roll attitude time history (from the piecewise polynomial Rapid Side-step) and the roll attitude quickness equation, sample points will be calculated and presented on the relevant chart. The quickness parameter is used to quantify the fundamental response characteristics of a helicopter and can reveal if the aircraft is capable of achieving Level 1 handling qualities. Usually a simple pulse of cyclic is enough control action to induce the required open loop response for assessment. The maximum roll attitude rate peaks between zero crossings distinguish the open loop responses obtained from Helinv.

3.3.1 Roll Attitude Quickness Calculations

The purpose of this basic exercise is to illustrate the methodology of calculating the roll attitude quickness parameters. Although in this instance, for clarity, the method is presented somewhat simply as hand calculations, the actual technique is performed by Matlab software, developed at Glasgow Caledonian University and the University of Glasgow. Figures 3.10a and b present a general overview of roll attitude quickness calculations and the corresponding attitude quickness chart, obtained from inverse simulation of a piecewise polynomial and a global polynomial Rapid Side-step flight test manoeuvre, Figures 3.5 and 3.6. The Lynx aircraft model was used in the inverse simulation run with a maximum lateral velocity of 30 knots, rolling initially to port. The times taken to reach maximum acceleration and maximum deceleration were 1.5 and 3.0 seconds respectively for the piecewise manoeuvre. Figure 3.10a illustrates the time histories of the roll attitude, ϕ and the roll rate, p. They are annotated to show the calculations of attitude quickness parameters of the main pulses of roll rate (piecewise only). An initial roll into the manoeuvre is succeeded, at approximately the midpoint, by a roll in the opposite direction to bring the rotor into the required position to decelerate the vehicle. Near the end of the task a final roll occurs to position the aircraft in a trimmed hover

position. The quickness parameters corresponding to this data are plotted in Figure 3.10b (ADS-33D Roll Attitude Quickness chart for all other MTEs) and it is clearly seen that they lie in the Level 1 region, thus satisfying the performance requirements.

For the purposes of comparison the nap-of-the-earth Rapid Side-step modelled using the global polynomial method is also plotted on the quickness chart, Figure 3.10b. The points are calculated in exactly the same manner as the piecewise method thus allowing a direct comparison of the two tasks. It can be seen that the attitude quickness points calculated using the global method do not lie in the Level 1 region of the chart and the manoeuvre model is therefore unable to capture the more aggressive features of the task associated with Level 1 handling qualities. Although, in this instance, the attitude quickness parameter is satisfactory for highlighting the differences between two manoeuvres, this is not always the case and later in the thesis it is necessary to introduce the pilot attack parameter for identifying pilot workload.

Chapter Summary

The method of solving the equations of motion using the differentiation based Helinv algorithm was briefly discussed and the reader is referred to Appendix B for further clarification on the algorithm.The question of "what can inverse simulation provide?" was posed and a demonstration using the Pop-up manoeuvre illustrated the point that state and control information from specific manoeuvres can be obtained and used in handling qualities assessment.

Importance was placed upon the manoeuvre models, a number of which have been based on the descriptions given in the ADS-33D document. It was illustrated that the global polynomial method did not always capture the gross features of the flight test manoeuvres, thus a different approach was necessary. The piecewise polynomial modelling method was discussed and the technique applied to the Rapid Side-step Mission Task Element. Using the Westland Lynx model and setting flight velocity at 30 knots, roll attitude quickness parameters were calculated and it was seen that when plotted on the ADS chart, they were in the Level 1 region. Inverse simulation has been demonstrated to work as an effective flight test simulation tool with the ability to initially assess helicopter handling qualities.

Chapter 4

An Improved Helicopter Model for Handling Qualities Research

The current inverse simulation algorithm at Glasgow possesses an intrinsic helicopter model called Helicopter Generic Simulation, (HGS). It is the aim of this chapter to describe the model and assess its suitability for handling qualities studies. The inclusion of lagging dynamics, ground effect and a discrete gust are detailed and it is shown that implementing the lag degree of freedom is impractical in this disc model. In addition it is likely to be of little benefit to handling qualities results. Generally, handling qualities analyses do not take account of ground effect or discrete gusts and since it is postulated that atmospheric effects may play a role in future handling qualities studies, HGS remains the best possible disc-type model for the research. The influence of ground effect and the discrete gust on handling qualities are, however, investigated.

4.1 Fundamental Helicopter Mathematical Model Types

The convoluted flow patterns around the fuselage and empennage of a helicopter in hovering or forward flight dictate that the modelling techniques are either highly involved and complex in nature or comparatively simple calculations involving functions of the aircraft's incidence angles. As the main rotor largely governs the overall system dynamics it is clear why so much emphasis is placed upon modelling it. Table 4.1 illustrates for convenience the three levels of modelling as postulated by *Padfield (1996)*. Level 2 is generally the highest level of sophistication used in flight mechanics work with the model of *Thomson (1992)* being one of a small number of existing Level 1 models for inverse simulation. One modelling approach that is intensive enough to be valid over a wide range of fight states, is very efficient in terms of solution time and still yields comparatively accurate results is the

multiblade or disc method. The multiblade model differs from its counterpart, the individual blade model, by making the assumption that only the steady components of the rotor force/moment calculations are influential on the dynamics of the vehicle. Since the inverse simulation techniques available at the University of Glasgow incorporate both the disc model and the individual blade model, both methods will be discussed and the major discrepancies between the two highlighted.

4.1.1 Major Differences between Disc Model and Individual Blade Model

Although various differences exist between the two, the fundamental concept of both modelling methods is the same in that, each technique is aimed at calculating the forces and moments acting on a rotor blade at any point in time. This approach necessitates the calculation of the airflow velocity relative to the blade. However, since this velocity varies with radial position on the blade span, the blade is divided into a number of elements and the aerodynamic and inertial loads calculated on each one. By integrating along the span from root to tip the loads on the entire blade can be obtained. In addition to radial variation, the elemental airflow velocities are also dependent upon the blade's azimuth position and thus the loads calculated vary in a cyclical manner and are periodic as the blade travels around the rotor disc. In general the technique is known as blade element theory and the most significant difference between disc models and individual blade models is that disc models do not account for the variation in blade loads as the rotor travels around the disc, whilst individual blades models account for this periodicity.

The disc modelling method as used in HGS assumes that only the steady force and moment components influence the dynamics of the vehicle. By assuming simple blade aerodynamic and geometric properties, and calculating blade elemental forces and moments through span-wise integration, the forces transferred to the vehicle by the rotor disc as a whole are obtained. The model is not suited to simulation of severe manoeuvring flight at the edge of the aircraft's flight envelope since non-linear aerodynamic effects are not modelled. Although the method of averaging the total force and moment contributions over the entire disc compromises accuracy, it is computationally efficient and suitable for handling qualities studies as detailed information on rotor dynamics is not required.

Individual blade modelling, *(Rutherford and Thomson, 1997)* on the other hand captures the periodic forcing nature of the rotor by calculating the elemental forces and moments, integrating along the span and summing the contribution of each blade to obtain the total forces and moments transferred to the vehicle instantaneously. This type of forcing is termed unsteady as it is periodic and varies with blade azimuth position. The individual blade modelling approach allows the inclusion of more complex blade geometric and aerodynamic properties and is thus better suited to simulation of areas where the aircraft is likely to operate near the limits of the flight envelope.

Although the inclusion of a higher fidelity model such as the individual blade model effectively expands the simulation envelope, it is postulated that the corresponding effect on handling qualities calculations would be minimal. For example in the case of attitude quickness, in pitch or roll, it is the body modes of the vehicle that are considered for calculation. The attitude rates and attitude angles are required for any particular manoeuvre and are largely independent of the unsteady forcing nature of the rotor. Therefore the HGS model was deemed suitable for handling qualities studies.

4.2 Helicopter Generic Simulation (HGS)

4.2.1 Rudimentary Flight Dynamics Properties of HGS

The full seven degrees of freedom of HGS are described by a system of order eleven, the state vector of which is given by,

$$\underline{\boldsymbol{x}} = \left[u, v, w, p, q, r, \phi, \theta, \psi, \Omega, Q_E\right]^T$$

where,

Ω is the rotorspeed of the main rotor,

Q_E is the torque produced by the engine and all other symbols have their usual meaning. The motion of the helicopter can be described by the homogenous equation,

$$\dot{\underline{x}} - \boldsymbol{A}\underline{x} = 0 \tag{4.1}$$

which has initial conditions, $\underline{x}(0) = \underline{x}_0$. In order to simplify the resulting equations a transformation is introduced so that Equation 4.1 can be rewritten as,

$$\dot{\underline{y}} - \Lambda \underline{y} = 0 \tag{4.2}$$

where,

$\underline{x} = \boldsymbol{W}\,\underline{y}$ and

$\Lambda = \boldsymbol{W}^{-1}\boldsymbol{A}\boldsymbol{W}$

$\boldsymbol{W}$ is a unique transformation matrix that reduces $\boldsymbol{A}$ to a canonical diagonal matrix and permits Equation 4.2 to be written as a series of uncoupled equations.

$$y_i = y_0 e^{\lambda_i t} \tag{4.3}$$

Now, if $\boldsymbol{w_i}$ is a column of $\boldsymbol{W}$ then the pairs $[\boldsymbol{w_i}, \lambda_i]$ are the eigenvectors and eigenvalues of the matrix $\boldsymbol{A}$ respectively. The eigenvalues can be real or complex, positive or negative and for a polynomial of order *n*, there are *n* solutions given by,

$$\det[\lambda I - A = 0] \tag{4.4}$$

Figures 4.1 and 4.2 present the eigenvalues for the Westland Lynx as predicted by HGS and are directly comparable with those values given by *Padfield (1996)* who uses the Helisim model for the same task. The modes are plotted at 10-knot intervals from hover to 140 knots forward flight. One of the most distinguishing features of the plots is the unstable phugoid-type characteristic, which exists throughout the speed range, although it approaches neutral stability at approximately 50 knots. Padfield mentions that in the hover this mode is actually a combination of a longitudinal/lateral oscillation that is coupled with a lateral/longitudinal oscillation, which develops into a Dutch roll as forward speed is increased. Apart from rotorspeed, the other modes are all subsidence modes that have distinct stability characteristics in the hover but

develop into more coupled effects at higher speeds.

HGS is described in detail in Appendix C for completeness and immediate reference and the reader is referred there for a more comprehensive understanding of the modelling techniques used to describe the helicopter system, although as a general overview the modelling assumptions are given below.

4.2.2 Existing Modelling Attributes and Assumptions

1. *Atmospheric Conditions*

In the original HGS model developed by Thomson, calm International Standard Atmosphere conditions were assumed. At a later date, *Thomson and Bradley (1993)* added a basic model for the simulation of a constant steady wind. Typical atmospheric conditions such as air density and temperature are assumed at sea level values.

2. *2-Dimensional Aerodynamics*

No provision is made for the modelling of the flow of air along the blade. The modelled components are two-dimensional with respect to the disc plane and include the lift (normal) component and the drag (parallel) component. It is assumed that the component forces act through the aerodynamic centre of the aerofoil, which according to traditional theory, *Prouty (1990)* is located approximately at the quarter chord point. The simplification that the tangential velocity was assumed to be much greater than the perpendicular velocity was used to reduce lengthy mathematics.

3. *Inertial Forces*

In the original definition of HGS the blade inertial forces were calculated even though it was realised that other than spanwise, the inertial forces are small compared to aerodynamic forces. Later developments though, necessitated the simplification of neglecting these inertial forces and included spanwise only.

4. *Rotor Inflow Modelling*

HGS is equipped with two, user selectable, rotor inflow modelling methods; the momentum theory as developed by *Glauert (1926)* and dynamic inflow model based on the *Peters and HaQuang (1988)* method. Both rotor inflow modelling methods are described in Appendix D.

5. *Rotor Blade Section Aerodynamics*

A constant lift curve slope a_0 is assumed for the span, which permits the application of 2-D aerodynamic theory, described above. Retreating blade and dynamic stall effects are neglected.

6. *Section Geometrical Properties*

The length of the rotor blade span is assumed to have the same aerofoil section and the corresponding properties that go with it, therefore a constant chord can be used in the calculations. To attenuate problems with reversed flow regions and compressibility effects, many rotor blades have a twist incorporated along the length of the blade. HGS assumes a linear variation in the twist of the blade section and this is implemented via a twist slope, θ_{tw}. The blades are assumed to be centrally hinged and include a root cut-out section from the centre of the hub to some distance *eR* along the span *R*.

4.2.3 Initial Limitations of the HGS Model

Examination of the HGS model reveals limitations in two relevant contexts. Initially, like all disc models, the information obtained on the rotor itself is quite limited and the simplifying assumptions are relevant only for normal or moderately aggressive flight conditions. It is unsuitable for examination of highly aggressive manoeuvring flight. For example the use of 2-D aerodynamics, which are not capable of simulating non-linear effects such as compressibility at high rotor tip Mach numbers, or blade stall behaviour, illustrate the point.

Furthermore HGS does not include models of any additional atmospheric effects which may influence the flying characteristics of the vehicle and hence alter the handling qualities. Rotorcraft handling qualities have recognised the need to take account of degraded visual environments, turbulence and other conditions affecting pilot perceived workload. It was intended that the improvements to HGS would increase rotor complexity and inclusion of environmental effects would enhance the suitability of the model to handling qualities studies. The combination of these improvements would leave HGS as one of the most advanced Level 1 helicopter models for inverse simulation, the current validity of the model having been effectively demonstrated by *Thomson and Bradley (1990a)*.

4.2.4 Axes Systems used in the HGS Multiblade Rotor Model

The contribution to the external forces and moments by the rotor requires the calculation of the velocity and acceleration of rotor blade elements, referred to local axes. To formulate such expressions it is assumed that the rotor blade elements are of unit span, the velocities and accelerations are uniform over the entire element and equal to those at the elemental centres. If it is assumed that the velocity and acceleration of the helicopter centre of gravity (c.g.) (aircraft body axis frame) is known then, through a series of axes transformations the velocity and acceleration of the blade elements can be determined in a local axes. Since the velocity and acceleration of the blade element is a function of radial position from the rotor hub and azimuth position around the disc, the sequence of transformations given below was assumed appropriate for relating a multiblade disc element to the helicopter centre of gravity.

Transformation 1: **body** to **hub**

where,

body refers to the body axis set, centred at the helicopter c.g., moving with the aircraft, $\underline{\mathbf{i}}_{\mathbf{bod}}$ axis along the vehicle centreline, $\underline{\mathbf{k}}_{\mathbf{bod}}$ pointing straight down and $\underline{\mathbf{j}}_{\mathbf{bod}}$ completing the right handed set; and

hub refers to the hub axis set, centred at the helicopter rotor hub, moving with the aircraft, orientation obtained by rotation of the rotor shaft tilt angle, γ_{sh} about the $\underline{\mathbf{j}}_{\mathbf{bod}}$ axis.

Transformation 2: **hub** to **shaft**

shaft refers to the shaft axis set, fixed in and rotating with the helicopter rotor shaft, moving with the aircraft, orientation obtained by rotation of the rotor azimuth angle, ψ about the $\underline{\mathbf{k}}_{\mathbf{hub}}$ axis.

Transformation 3: **shaft** to **blade element**

blade element refers to the blade element axis set, placed at blade element aerodynamic centre, moving with the aircraft, orientation obtained by rotation of the rotor flapping angle, β about the $\underline{\mathbf{j}}_{\mathbf{sh}}$ axis.

Further development of the velocity and acceleration of a blade element is detailed below, including a further axis transformation to determine the elemental velocity and acceleration in the blade element lag axis set.

4.3 Mathematical Modelling Improvements to HGS

4.3.1 Modelling Lead-lag Degree of Freedom

Although the HGS model as it stands is considered suitable for handling qualities studies, it is still desirable to increase the fidelity of the model with the aim of improving realism. Since the model includes uncoupled flapping motion the natural progression was to include lead-lag motion and couple the terms with the flapping equations already in place. Recall that attitude quickness is concerned with body rates and attitudes. The logical expectation was that the influence of lead-lag motion on handling qualities levels would be minimal, if at all. However, implementing the lag degree of freedom would leave HGS as one of the most

sophisticated disc models in inverse simulation and permit an increased understanding of blade dynamics in disc models in general.

It is difficult to begin the discussion and deal solely with lead-lag motion as it is very much coupled with rotor flapping motion, currently modelled in HGS. The main rotor blades are allowed to flap to alleviate a rolling moment generated by asymmetrical lift over the whole rotor disc. The blade on the advancing side will experience an increase in lift while the retreating blade will experience a similar loss in lift. The consequence of this is that, theoretically, the advancing blade will flap up to its maximum position at 90^o azimuth and the retreating will have maximum flap down at 270^o azimuth (measured anti-clockwise from the rear of the disc). Figure 4.3 illustrates the effect of flapping motion on the lateral distribution of lift on the rotor disc. However, since the blades will require some time period to flap up or down to their maximum positions some additional travel in azimuth is apparent, corresponding to almost 90^o, depending on rotor type. The resulting effect is that the blades actually flap up at the front of the disc and flap down at the rear of the disc.

Figure 4.4 shows that this flapping motion carries an inherent penalty though, as the upward flapping blade effectively moves its centre of gravity towards the shaft or disc spin axis as does the downward flapping blade. The subsequent reduction in the moment of inertia of each blade causes an increase in rotational velocity, which when opposed by the inertia of the other blades causes in-plane bending as shown by Figure 4.5. This effect is know as Coriolis acceleration and is alleviated by the addition of lead-lag hinges at the rotor hub.

4.3.2 Development of the Lead-lag Equations of Motion

The general approach to the modelling technique within HGS is to calculate the loads on a blade element, which in turn necessitates the calculation of the local velocity at that point (r_b, ψ). A series of relevant transformations relating the translational and rotational velocities of the body axes (located at the aircraft's centre of gravity) to those of the blade element are carried out.

4.3.2.1 Derivation of Blade Element Velocity in Blade Lag Axes

If $\underline{\mathbf{i}}$, $\underline{\mathbf{j}}$ and $\underline{\mathbf{k}}$ are unit vectors in the x, y and z axes respectively then the transformation from body to an intermediate axes set located at the hub and known as the hub axes set (subscript **hub**, *hub*) is given by,

$$\begin{bmatrix} \underline{\mathbf{i}}_{\mathbf{hub}} \\ \underline{\mathbf{j}}_{\mathbf{hub}} \\ \underline{\mathbf{k}}_{\mathbf{hub}} \end{bmatrix} = \begin{bmatrix} \cos\gamma_{sh} & 0 & \sin\gamma_{sh} \\ 0 & 1 & 0 \\ -\sin\gamma_{sh} & 0 & \cos\gamma_{sh} \end{bmatrix} \begin{bmatrix} \underline{\mathbf{i}}_{\mathbf{bod}} \\ \underline{\mathbf{j}}_{\mathbf{bod}} \\ \underline{\mathbf{k}}_{\mathbf{bod}} \end{bmatrix} \tag{4.5}$$

where γ_{sh} is the tilt angle of the main rotor shaft. The next transformation relates the hub axes set to a so-called shaft axes set (subscript **sh**, *sh*) by the transformation,

$$\begin{bmatrix} \underline{\mathbf{i}}_{\mathbf{sh}} \\ \underline{\mathbf{j}}_{\mathbf{sh}} \\ \underline{\mathbf{k}}_{\mathbf{sh}} \end{bmatrix} = \begin{bmatrix} -\cos\psi & \sin\psi & 0 \\ -\sin\psi & -\cos\psi & 0 \\ 0 & 0 & 1 \end{bmatrix} \begin{bmatrix} \underline{\mathbf{i}}_{\mathbf{hub}} \\ \underline{\mathbf{j}}_{\mathbf{hub}} \\ \underline{\mathbf{k}}_{\mathbf{hub}} \end{bmatrix} \tag{4.6}$$

where ψ is the azimuth angle.

A final transformation is made to calculate the blade elemental velocities and accelerations in blade axes (subscript **bl**, *bl*). The transformation angle is the flap angle, β and the corresponding equation is given as,

$$\begin{bmatrix} \underline{\mathbf{i}}_{\mathbf{bl}} \\ \underline{\mathbf{j}}_{\mathbf{bl}} \\ \underline{\mathbf{k}}_{\mathbf{bl}} \end{bmatrix} = \begin{bmatrix} \beta & 0 & \beta \\ 0 & 1 & 0 \\ \beta & 0 & \beta \end{bmatrix} \begin{bmatrix} \underline{\mathbf{i}}_{\mathbf{sh}} \\ \underline{\mathbf{j}}_{\mathbf{sh}} \\ \underline{\mathbf{k}}_{\mathbf{sh}} \end{bmatrix} \tag{4.7}$$

which makes the small angle approximation for the flap angle. The resulting expressions for the velocity and acceleration of the hub in blade axes are given by Equations 4.8 and 4.9 respectively, while 4.10 and 4.11 show the corresponding expressions for angular velocity and acceleration.

$$\begin{aligned}\underline{\boldsymbol{V}}_{hub/\mathbf{bl}} = &\left[(-u_{hub}\cos\psi + v_{hub}\sin\psi - \beta\, w_{hub})\right]\underline{\mathbf{i}}_{\mathbf{bl}} + \\ &\left[(-u_{hub}\sin\psi - v_{hub}\cos\psi)\right]\underline{\mathbf{j}}_{\mathbf{bl}} + \\ &\left[\beta(-u_{hub}\cos\psi + v_{hub}\sin\psi) + w_{hub}\right]\underline{\mathbf{k}}_{\mathbf{bl}}\end{aligned} \tag{4.8}$$

$$\begin{aligned}\underline{\boldsymbol{a}}_{hub/\mathbf{bl}} = &\left[-\underline{\boldsymbol{a}}_{hub/\mathbf{x}}\cos\psi + \underline{\boldsymbol{a}}_{hub/\mathbf{y}}\sin\psi - \beta\underline{\boldsymbol{a}}_{hub/\mathbf{z}}\right]\underline{\mathbf{i}}_{\mathbf{bl}} + \\ &\left[-\underline{\boldsymbol{a}}_{hub/\mathbf{x}}\sin\psi - \underline{\boldsymbol{a}}_{hub/\mathbf{y}}\cos\psi\right]\underline{\mathbf{j}}_{\mathbf{bl}} + \\ &\left[\beta(-\underline{\boldsymbol{a}}_{hub/\mathbf{x}}\cos\psi + \underline{\boldsymbol{a}}_{hub/\mathbf{y}}\sin\psi) + \underline{\boldsymbol{a}}_{hub/\mathbf{z}}\right]\underline{\mathbf{k}}_{\mathbf{bl}}\end{aligned} \tag{4.9}$$

$$\begin{aligned}\underline{\boldsymbol{\omega}}_{hub/\mathbf{bl}} = &\left[(-p_{hub}\cos\psi + q_{hub}\sin\psi - \beta(r_{hub} - \Omega)\right]\underline{\mathbf{i}}_{\mathbf{bl}} + \\ &\left[\dot{\beta} - p_{hub}\sin\psi - q_{hub}\cos\psi\right]\underline{\mathbf{j}}_{\mathbf{bl}} + \\ &\left[\beta(-p_{hub}\cos\psi + q_{hub}\sin\psi) + (r_{hub} - \Omega)\right]\underline{\mathbf{k}}_{\mathbf{bl}}\end{aligned} \tag{4.10}$$

which implies that,

$$\dot{\underline{\boldsymbol{\omega}}}_{hub/\mathbf{bl}} = \dot{\underline{\boldsymbol{\omega}}}_{x}\,\underline{\mathbf{i}}_{\mathbf{bl}} + \dot{\underline{\boldsymbol{\omega}}}_{y}\,\underline{\mathbf{j}}_{\mathbf{bl}} + \dot{\underline{\boldsymbol{\omega}}}_{z}\,\underline{\mathbf{k}}_{\mathbf{bl}} \tag{4.11}$$

Figure 4.6 illustrates diagrammatically a further transformation that must be introduced to include lag motion and enable the above equations to be given in blade lag axes, (subscript **lag**, *lag*). The transformation equation, when making the small angle approximation for the lag angle is given as,

$$\begin{bmatrix}\underline{\mathbf{i}}_{\mathbf{lag}} \\ \underline{\mathbf{j}}_{\mathbf{lag}} \\ \underline{\mathbf{k}}_{\mathbf{lag}}\end{bmatrix} = \begin{bmatrix}1 & \zeta & 0 \\ -\zeta & 1 & 0 \\ 0 & 0 & 1\end{bmatrix}\begin{bmatrix}\underline{\mathbf{i}}_{\mathbf{bl}} \\ \underline{\mathbf{j}}_{\mathbf{bl}} \\ \underline{\mathbf{k}}_{\mathbf{bl}}\end{bmatrix} \tag{4.12}$$

where ζ is the lag angle measured positive clockwise when viewed from above, see Figure 4.7.

Now the absolute velocity and acceleration of a point *p* located some distance r_b from the hub centre along the span of a rotor blade, in local blade axes are given by the respective equations,

$$\underline{\boldsymbol{V}}_{p/\mathbf{bl}} = \underline{\boldsymbol{V}}_{hub/\mathbf{bl}} + (\underline{\boldsymbol{\omega}}_{\mathbf{bl}} \times r_{p/H}) \tag{4.13}$$

where,

$r_{p/H} = r_b\ \underline{\mathbf{i}}_{\mathbf{bl}}$ and

$\underline{\boldsymbol{\omega}}_{\mathbf{bl}}$ is the angular velocity of the blade in blade axis.

and,

$$\underline{\boldsymbol{a}}_{p/\mathbf{bl}} = \underline{\boldsymbol{a}}_{hub/\mathbf{bl}} + (\underline{\boldsymbol{\alpha}}_{\mathbf{bl}} \times r_{p/H}) + \underline{\boldsymbol{\omega}}_{\mathbf{bl}} \times (\underline{\boldsymbol{\omega}}_{\mathbf{bl}} \times r_{p/H}) + 2\underline{\boldsymbol{\omega}}_{\mathbf{bl}} \times \frac{d}{dt} r_{p/H} \tag{4.14}$$

Upon substitution of the above equations derived for the velocity and acceleration, (Equations 4.8 and 4.9) and performing the relevant transformation to blade lag axes, the velocity and acceleration of the blade element in blade lag axes is found from,

$$\begin{aligned}\underline{\boldsymbol{V}}_{p/\mathbf{lag}} = &\left[(-u_{hub}\cos\psi + v_{hub}\sin\psi) - \beta w_{hub} + \zeta(-u_{hub}\sin\psi - v_{hub}\cos\psi)\right]\underline{\mathbf{i}}_{\mathbf{blg}} + \\ &\left[-\zeta(-u_{hub}\cos\psi + v_{hub}\sin\psi - \beta w_{hub}) + (-u_{hub}\sin\psi - v_{hub}\cos\psi) + \right. \\ &r_b\left\{\beta(-p_{hub}\cos\psi + q_{hub}\sin\psi) + (r_{hub} - \Omega) + \dot{\zeta}\right]\underline{\mathbf{j}}_{\mathbf{lag}} + \\ &\left[\beta(-u_{hub}\cos\psi + v_{hub}\sin\psi) + w_{hub} - r_b\left\{-\zeta(-p_{hub}\cos\psi + q_{hub}\sin\psi - \right.\right. \\ &\left.\left.\beta(r_{hub} - \Omega)) + (\dot{\beta} - p_{hub}\sin\psi - q_{hub}\cos\psi)\right\}\right]\underline{\mathbf{k}}_{\mathbf{lag}}\end{aligned} \tag{4.15}$$

which can be written as,

$$\underline{\boldsymbol{V}}_{p/\mathbf{lag}} = \underline{\boldsymbol{V}}_{x/\mathbf{lag}}\ \underline{\mathbf{i}}_{\mathbf{lag}} + \underline{\boldsymbol{V}}_{y/\mathbf{lag}}\ \underline{\mathbf{j}}_{\mathbf{lag}} + \underline{\boldsymbol{V}}_{z/\mathbf{lag}}\ \underline{\mathbf{k}}_{\mathbf{lag}} \tag{4.16}$$

and for the acceleration,

$$\begin{aligned}&\underline{\boldsymbol{a}}_{p/\mathbf{lag}} = \left[-\underline{\boldsymbol{a}}_{hub/\mathbf{x}}\cos\psi + \underline{\boldsymbol{a}}_{hub/\mathbf{y}}\sin\psi - \beta\underline{\boldsymbol{a}}_{hub/\mathbf{z}} + \zeta(-\underline{\boldsymbol{a}}_{hub/\mathbf{x}}\sin\psi - \underline{\boldsymbol{a}}_{hub/\mathbf{y}}\cos\psi) - \right. \\ &\left. r_b(\underline{\boldsymbol{\omega}}^2_{y/\mathbf{lag}} + \underline{\boldsymbol{\omega}}^2_{z/\mathbf{lag}})\right]\underline{\mathbf{i}}_{\mathbf{lag}} + \\ &\left[-\zeta(-\underline{\boldsymbol{a}}_{hub/\mathbf{x}} + \underline{\boldsymbol{a}}_{hub/\mathbf{y}}\sin\psi - \beta\underline{\boldsymbol{a}}_{hub/\mathbf{z}}) + (-\underline{\boldsymbol{a}}_{hub/\mathbf{x}}\sin\psi - \underline{\boldsymbol{a}}_{hub/\mathbf{y}}\cos\psi) + \right. \\ &\left. r_b(\dot{\underline{\boldsymbol{\omega}}}_{z/\mathbf{lag}} + \underline{\boldsymbol{\omega}}_{y/\mathbf{lag}}\underline{\boldsymbol{\omega}}_{x/\mathbf{lag}})\right]\underline{\mathbf{j}}_{\mathbf{lag}} + \\ &\left[\beta(-\underline{\boldsymbol{a}}_{hub/\mathbf{x}}\cos\psi + \underline{\boldsymbol{a}}_{hub/\mathbf{y}}\sin\psi) + \underline{\boldsymbol{a}}_{hub/\mathbf{z}} + r_b(\underline{\boldsymbol{\omega}}_{x/\mathbf{lag}}\underline{\boldsymbol{\omega}}_{z/\mathbf{lag}} - \dot{\underline{\boldsymbol{\omega}}}_{y/\mathbf{lag}})\right]\underline{\mathbf{k}}_{\mathbf{lag}}\end{aligned} \tag{4.17}$$

which, when simplified can be written as,

$$\underline{\boldsymbol{a}}_{p/\mathbf{lag}} = \underline{\boldsymbol{a}}_{x/\mathbf{lag}}\,\underline{\mathbf{i}}_{\mathbf{lag}} + \underline{\boldsymbol{a}}_{y/\mathbf{lag}}\,\underline{\mathbf{j}}_{\mathbf{lag}} + \underline{\boldsymbol{a}}_{z/\mathbf{lag}}\,\underline{\mathbf{k}}_{\mathbf{lag}} \tag{4.18}$$

4.3.2.2 Calculation of Rotor Forces and Moments in Blade Lag Axes

There are two main forces acting on the blade element, aerodynamic and inertial. The coefficient expressions for each were derived and substituted into HGS to test for correctness, before proceeding to evaluate expressions for the blade lagging dynamics.

1. Evaluation of the Aerodynamic Force Coefficients

It is known that the total aerodynamic forces in the *z* and *y* directions of a blade of length *R*, assuming no cut-out section, can be represented by the normalised force coefficient equations,

$$C_{z/\mathbf{lag}} = -\frac{1}{2} s\, a_0 \frac{1}{b} \int_0^1 (\overline{U}_T{}^2 \theta + \overline{U}_P \overline{U}_T) d\overline{r}_b \tag{4.19}$$

$$C_{y/\mathbf{lag}} = \frac{1}{2} s\, a_0 \frac{1}{b} \int_0^1 (\frac{\delta}{a_0} \overline{U}_T{}^2 - \overline{U}_P \overline{U}_T \theta - \overline{U}_P{}^2) d\overline{r}_b \tag{4.20}$$

where,

a_0 is the lift curve slope,

θ is the blade pitch angle,

U_T is the tangential velocity of the airflow over the aerofoil and

U_P is the perpendicular velocity,

the rotor solidity is given as, $s = \dfrac{b\,c}{\pi\,R}$ and

the normalised radial blade position is given by, $\overline{r}_b = \dfrac{r_b - e\,R}{R}$.

To evaluate Equations 4.19 and 4.20 it is clearly necessary to derive

expressions for $\overline{U}_T$ and $\overline{U}_P$. Now,

$$\overline{U}_T = \zeta\left(-\mu_x \cos\psi + \mu_y \sin\psi - \beta\mu_z\right) + \mu_x \sin\psi + \mu_y \sin\psi + \bar{r}_b(1-\dot{\zeta}) \tag{4.21}$$

and

$$\begin{aligned}\overline{U}_P = {} & \beta\left(-\mu_x \cos\psi + \mu_y \sin\psi\right) + \mu_z - \lambda_0 + \bar{r}_b\{\zeta[(-\overline{p}_{hub}\cos\psi + \overline{q}_{hub}\sin\psi) - \\ & \beta(\bar{r}_{hub} - 1)] - \beta_0' + \alpha_{1c}\cos\psi + \alpha_{1s}\sin\psi\}\end{aligned} \tag{4.22}$$

where,

μ_x, μ_y, μ_z are the non-dimensional components of the rotor hub velocity,

β_0' is the derivative with respect the azimuth angle, i.e. $\beta_0' = \dfrac{d\beta_0}{d\psi}$ etc. and

α_{1c} and α_{1s} are expressions used to represent a convenient collection of terms given as,

$$\alpha_{1c} = \overline{q}_{hub} - \lambda_{1c} - \beta_{1c}' - \beta_{1s} \text{ and } \alpha_{1s} = \overline{p}_{hub} - \lambda_{1s} - \beta_{1s}' - \beta_{1c}.$$

The terms $\overline{p}_{hub}$ and $\overline{q}_{hub}$ denote the rotor hub velocities after normalisation by the rotorspeed, Ω.

The main rotor force equations given by 4.19 and 4.20 are evaluated by substituting the normal and parallel force coefficients above, and the blade pitch equation given as,

$$\theta = \theta_0 + \theta_{1s}\sin\psi + \theta_{1c}\cos\psi + \theta_{tw}\frac{r_b}{R} \tag{4.23}$$

Upon integration the final equations can be written as polynomial functions of r_b. The main problem arises in dealing with the extremely lengthy equations, which are initially evaluated in terms of powers of $\cos\psi$ and $\sin\psi$, before being subsequently written in their respective multiple angle format. The most convenient

way of writing the final blade force equations in blade lag axes is given below and for simplicity only shows expressions up to the second harmonic, although Mathematica, *Wolfram (1988)* was used to derive the coefficients up to the fourth harmonic.

$$\begin{aligned} C_{Z_{A/\mathbf{lag}}} &= -\frac{1}{2} s a_0 \frac{1}{b} (C_{Z_{A0}} + C_{Z_{A1c}} \cos\psi + C_{Z_{A1s}} \sin\psi + C_{Z_{A2c}} \cos 2\psi + ...) \\ C_{Y_{A/\mathbf{lag}}} &= \frac{1}{2} s a_0 \frac{1}{b} (C_{Y_{A0}} + C_{Y_{A1c}} \cos\psi + C_{Y_{A1s}} \sin\psi + C_{Y_{A2c}} \cos 2\psi + ...) \end{aligned} \tag{4.24}$$

Since the substituted equations for blade flap and blade cyclic pitch angles were expressed up to the first harmonic only, for consistency the blade force coefficients are expressed to the same degree of accuracy. The coefficients were tested for accuracy by substituting them into the HGS model and setting the lag angle to zero, which yielded identical results to the flap only version of HGS. Figure 4.8 presents a segment of the coefficients.

2. Evaluation of the Inertial Force Coefficients

Due to the large expressions obtained thus far only the inertial component in the spanwise direction will be considered, i.e. the *y* component of the inertial forces.

The equation governing the *y* inertial force acting on a blade element of length dr_b written in blade lag axes format can be given as,

$$dY_{I/\mathbf{lag}} = -m_0 \underline{\boldsymbol{a}}_{y/\mathbf{lag}} dr_b \tag{4.25}$$

The force is normalised, as in the case of the aerodynamic forces, by the term, $\rho(\Omega R)^2 \pi R^2$ to give,

$$C_{Y_I} = \left(\eta_x \sin\psi + \eta_y \cos\psi\right)\overline{m}_b - \frac{\overline{M}_\beta \left(\underline{\dot{\omega}}_z + \underline{\omega}_y \underline{\omega}_x\right)}{\Omega^2} \tag{4.26}$$

where,

$$\eta_x = \frac{\underline{\boldsymbol{a}}_{hub/\mathbf{x}}}{\Omega^2 R}, \eta_y = \frac{\underline{\boldsymbol{a}}_{hub/\mathbf{y}}}{\Omega^2 R}, \overline{m}_b = \frac{m_b}{\rho\pi R^3}, \overline{M}_\beta = \frac{M_\beta}{\rho\pi R^4} \text{ and}$$

$$m_b = \text{blade mass} = \int_0^R m_0 dr_b, M_\beta = \text{blade moment of mass} = \int_0^R m_0 r_b dr_b$$

Clearly the blade element inertial force coefficients can be evaluated using Mathematica, *Wolfram (1988)* and presented in the same way as demonstrated above for the aerodynamic blade force coefficients. Since it was known that the coefficients could be calculated from the expressions derived thus far and the rotor moment could be obtained from Equation 4.27, a more pressing issue concerning the blade lagging dynamics was considered.

$$M_{p/\mathbf{lag}} = -r_b\left(f_{z/\mathbf{lag}} - m_0 \underline{\boldsymbol{a}}_{z/\mathbf{lag}}\right)\mathbf{j}_{\mathbf{lag}} + r_b\left(f_{y/\mathbf{lag}} - m_0 \underline{\boldsymbol{a}}_{y/\mathbf{lag}}\right)\mathbf{k}_{\mathbf{lag}} \tag{4.27}$$

4.3.2.3 Blade Lagging Dynamics

It is assumed that the lagging equation has the general form,

$$\int_0^R \left(f_{y/\mathbf{lag}} - m_0 \underline{\boldsymbol{a}}_{y/\mathbf{lag}}\right) r_b dr_b = Q + c_\zeta \dot{\zeta} \tag{4.28}$$

where,

Q is the torque produced by the main rotor,

$c_\zeta \dot{\zeta}$ is the damping term accounting for the lag dampers and

c_ζ is the damping coefficient.

The calculation of the torque is carried out in the same manner to the aerodynamic and inertial blade force coefficients, given previously to the extent that again the process is split into aerodynamic and inertial torque coefficients given respectively by,

$$\begin{aligned} C_{Q_A} &= C_{Q_{A0}} + C_{Q_{A1c}} \cos\psi + C_{Q_{A1s}} \sin\psi \\ C_{Q_I} &= C_{Q_{I0}} + C_{Q_{I1c}} \cos\psi + C_{Q_{I1s}} \sin\psi \end{aligned} \tag{4.29}$$

The individual blade torque coefficients can be obtained from,

$$C_Q = C_{Q_0} + C_{Q_{1c}} \cos\psi + C_{Q_{1s}} \sin\psi \tag{4.30}$$

where,

$$\begin{aligned} C_{Q_0} &= \frac{sa_0}{2b} C_{Q_{A0}} + C_{Q_{I0}} \qquad C_{Q_{1c}} = \frac{sa_0}{2b} C_{Q_{A1c}} + C_{Q_{I1c}} \\ C_{Q_{1s}} &= \frac{sa_0}{2b} C_{Q_{A1s}} + C_{Q_{I1s}} \end{aligned} \tag{4.31}$$

Subsequent to calculating the aerodynamic terms of the torque coefficient, it was necessary to make the further simplification of neglecting the inertial terms. The reason for this becomes clear when the enormity of algebraic manipulation is appreciated. To this end a component from the final torque coefficient in blade lag axes can be found in Figure 4.9, however due to its shear size all of the material derived using Mathematica, *Wolfram (1988)* is not included.

Assuming the torque is composed entirely of aerodynamic terms and writing it initially as Equation 4.32 then; upon making the relevant substitutions from above, rearranging and then normalising, the lag equation can be written as Equation 4.33.

$$\int_0^R \left(f_{y/\mathbf{lag}} - m_0 \underline{\boldsymbol{a}}_{y/\mathbf{lag}} \right) r_b dr_b - Q - c_\zeta \dot{\zeta} = 0 \tag{4.32}$$

$$\begin{aligned} &\zeta_i'' + \left[\left(\beta_i \overline{q}_{hub} + \beta_i' \overline{p}_{hub} \right) \cos\psi_i + \left(\beta_i \overline{p}_{hub} - \beta_i' \overline{q}_{hub} \right) \sin\psi_i - 2\beta_i \beta_i' \right] \zeta_i^2 + \\ &\frac{\overline{M}_\beta}{I_\beta} \left(\eta_x \cos\psi_i - \eta_y \sin\psi_i + \beta_i \eta_z \right) + \left(2\beta_i \overline{p}_{hub} - 2\beta_i' \overline{q}_{hub} \right) \cos\psi_i - \\ &\left(2\beta_i \overline{q}_{hub} + 2\beta_i' \overline{p}_{hub} \right) \sin\psi_i - 2\beta_i^2 + 2\beta_i'^2 - \lambda_\zeta = \\ &4n_\beta \int_0^1 \left(\frac{\delta}{a_0} \overline{U}_T^2 - \overline{U}_T \overline{U}_P \theta - \overline{U}_P^2 \right) d\overline{r}_b + \frac{\overline{M}_\beta}{I_\beta} \left(\eta_x \sin\psi_i + \eta_y \cos\psi_i \right) - \\ &\left(\beta_i \overline{q}_{hub} + \beta_i' \overline{p}_{hub} \right) \cos\psi_i - \left(\beta_i \overline{p}_{hub} - \beta_i' \overline{q}_{hub} \right) \sin\psi_i + \beta_i \beta_i' - \frac{\overline{Q}}{I_\beta} \end{aligned} \tag{4.33}$$

where,

λ_ζ is the normalised damping coefficient,

I_β is the blade flapping moment of inertia,

n_β is the blade inertia number and

$\overline{Q}$ is the normalised torque. Expressions for these terms are given below.

$$\lambda_\zeta = \frac{C_\zeta}{I_\beta \Omega^2} \qquad I_\beta = \int_0^R m_0 r_b^{\,2} dr_b \qquad n_\beta = \frac{\rho c a_0 R^4}{8 I_\beta} \qquad \overline{Q} = \frac{Q}{\rho(\Omega R)^2 \pi R^3}$$

Referring to the normalised lagging Equation 4.33 it is clear that the integral part of the forcing side of the equation can be evaluated by substitution of $\overline{U}_T, \overline{U}_P$ and θ from Equations 4.21, 4.22 and 4.23 respectively. The derivation was performed as before using symbolic manipulation software and the resulting equation expressed in terms of multiple angles of azimuth. Such is the length of the expression it is not practical to include it in the text.

In order to solve Equation 4.33 a multiblade transformation is applied, which effectively transforms the individual flapping and lagging angles into a multiblade representation. The contribution of external forces and moments acting on the aircraft c.g. can then be found by reversing the sequence of transformations given in Section 4.3.2, i.e.,
blade lag to **blade element**, **blade element** to **shaft**, **shaft** to **hub** and **hub** to **body**.

4.3.3 Further Limitations with Disc Model

On reaching the final stage of deriving the blade lagging equation it is very apparent that the resulting expressions to be substituted into the equation are extremely large although simplifying assumptions have been made. This leads to the inevitable conclusion that the disc model as it stands is the best possible form for handling qualities studies. Inclusion of additional dynamics is unlikely to improve HGS from a handling qualities point of view, indeed it is necessary to remove existing components to facilitate the modelling procedure in the first instance. The evidence to support this is presented below.

- Aerodynamic Force Coefficients

Expressions for the aerodynamic force coefficients containing the lag terms were derived with the assumption that the root cut-out section was negligible. The current version of HGS contains a root cut-out term in the flapping equation.

- Inertial Force Coefficients

It was necessary to assume that the inertial force coefficients could be neglected with the exception of the terms in direction of the blade span. The current version of HGS does not make this assumption and all inertial terms are included.

- Torque Coefficients

Similar assumptions to those described above were made when deriving the torque coefficients with lag terms included. The resulting expressions were too large to include in the thesis and yet represented one component that had to be substituted into the final lag equation.

- Lagging Equation

The lagging equation was derived and presented in Equation 4.33. The forcing part of the equation contains an integral term, as does the corresponding flapping equation. However, upon evaluation, it was found that the final expression was extremely large and unpractical to include in the text. As this was a second component to be substituted into the lag equation, it is clear the final lag expression would constitute several pages of text and reveal no apparent benefit to handling qualities issues.

Inclusion of the lagging dynamics, although unsuccessful, was extremely beneficial from the point of view that the disc model has been shown to have serious limitations when it is taken beyond a certain degree of complexity. That said, a major

conclusion is that the current version HGS contains the best possible disc model for handling qualities studies.

4.3.4 Modelling Ground Effect in Nap-of-the-earth Manoeuvres

Although much of the inverse simulation work is concerned with Aeronautical Design Standard (ADS), Mission Task Elements (MTEs), the original manoeuvres modelled for use within Helinv were assumed to be flight-test manoeuvres flown in the nap-of-the-earth (NOE) area of the flight envelope. The operation of rotorcraft in this region of the flight envelope introduces a variety of characteristics that would not otherwise be found in helicopter flight, two of the most significant being the so-called *ground vortex* anomaly and *ground effect*. Ground effect is well understood, has been under investigation for many years and lends itself readily for inclusion into HGS.

As with fixed wing aircraft, rotorcraft require less power when manoeuvring close to the ground as the induced velocity through the rotor is influenced a great deal by the presence, and indeed type, of surface below it, as mentioned by *Cheeseman and Bennett (1955)*. Such investigations found in the literature largely fall into two categories, namely hovering and forward flight, although exceptions have included take-off and landing performance in ground effect such as that presented by *Cerbe and Reichert (1988)*.

4.3.5 HGS Induced Flow Out of Ground Effect (OGE)

Recall that HGS is equipped with two options to model airflow through the rotor. The original HGS model developed by *Thomson (1992)* included the method as proposed by *Glauert (1926)* which calculates the induced velocity, v_i using momentum theory. The induced velocity is assumed to comprise two components, a uniform component that acts over the entire disc and a component that varies across disc radius and azimuth. Out of ground effect (OGE) the uniform velocity component, v_0 derived by Glauert for the entire rotor disc is given by,

$$v_0 = \frac{T}{2\rho\pi R^2\sqrt{\left(u^2 + v^2 + \left(w - v_0\right)^2\right)}}$$

where,

T is the thrust of the rotor,

u, v and w are the velocity components of the rotor hub and

R is rotor blade span.

Using the terms v_{1s} and v_{1c} to take account of the magnitudes of the lateral and longitudinal variations respectively the induced velocity can be written as a function of azimuth angle, ψ and radial position, r_b and is given as,

$$v_i = v_0 + \frac{r}{R}\left(v_{1s}\sin\psi + v_{1c}\cos\psi\right) \tag{4.34}$$

Glauert's approach however, made several assumptions including, instantaneous acceleration of air across the disc plane and the effects of rolling or pitching moment were neglected.

In order to account for the deficiencies in Glauert's model further inflow development led to the derivation of dynamic inflow models that introduced a mass matrix, $[\mathbf{M}]$ to account for the lag time associated with the build-up of the induced velocity across the disc plane. An additional matrix, the gains matrix, $[\mathbf{L}]$ was included to deal with aerodynamic pitching, M and rolling, L moments. The resulting model is similar in form to Glauert's in that an overall uniform inflow component is included as given by Equation 4.34. The resulting three state expression relating induced velocity build-up, aerodynamic moments and thrust takes the form,

$$[\mathbf{M}]\begin{bmatrix}\dot{v}_0\\ \dot{v}_{1s}\\ \dot{v}_{1c}\end{bmatrix} + [\mathbf{L}]^{-1}\begin{bmatrix}v_0\\ v_{1s}\\ v_{1c}\end{bmatrix} = \begin{bmatrix}T\\ L\\ M\end{bmatrix}$$

Appendix D presents a brief overview of the two methods.

4.3.6 The Ground Effect Model

Figures 4.10a and b illustrate the general effect of hovering OGE and IGE in a helicopter. The induced velocity through the rotor at ground level is clearly reduced to zero with the net thrust effect being transferred upwards to the rotor disc in the form of pressure changes in the wake. The result is a lower induced velocity for any given thrust, which in practical terms increases the gross weight capability of the rotorcraft at a fixed power setting or to decrease the power required at any fixed weight. *Newman (1972)* demonstrated this to good effect where it was reported that, "*... this effect is used operationally by pilots to their advantage, such as the ability of the CH-53A to lift 75% more payload at sea level ...*".

Examining the conditions at a blade element on the main rotor, the observed reduction in power required IGE corresponds to a reduction in the rearward tilt of the lift vector as shown in Figures 4.11a and b. The overall effect is a decrease in the local blade pitch to maintain the same angle of attack and hence the thrust. Thus the presence of the ground forces a pilot to alter the required control inputs to maintain the same desired flight condition that would not otherwise be required OGE.

Cheeseman and Bennett (1955) detail the approach used to model ground effect in HGS. It is based upon the method of images where the ground is modelled as a 'virtual' rotor of equal and opposite strength (in momentum terms) located the same distance below the ground plane, as the real rotor is above it, see Figure 4.12. The mirror image of the rotor was achieved by using, in potential flow theory, a source of strength, $Av_i / 4\pi$ where A is the area of the rotor disc and v_i is the induced velocity. Cheeseman and Bennett then say that the effect is to reduce the induced velocity at the rotor disc by an amount, δv_i, given by,

$$\delta v_i = \frac{A v_i}{16\pi z_g^2}$$

where,

z_g is the height of the rotor above the ground plane.

Since, $v_{i/IGE} = v_i - \delta v_i$, then, assuming constant thrust, and v_i and δv_i to be unchanging over the rotor disc the following induced velocity ratio can be written,

$$\left[\frac{v_{i/IGE}}{v_{i/OGE}}\right]_{T=constant} = \frac{1}{1-\frac{R^2}{16z_g^2}} \tag{4.35}$$

where,

$v_{i/IGE}$ is the induced velocity IGE and

$v_{i/OGE}$ is the induced velocity OGE.

Equation 4.35 can be written in non-dimensional form as,

$$\left[\frac{\lambda_{0/IGE}}{\lambda_{0/OGE}}\right]_{T=constant} = \left[1-\frac{1}{16\overline{H}^2}\right]^{\frac{3}{2}} \tag{4.36}$$

where,

$\lambda_{0/IGE}$ is the uniform component of induced velocity IGE,

$\lambda_{0/OGE}$ is the uniform component of induced velocity OGE and

$\overline{H}$ is the non-dimensional rotor height.

Equation 4.36 enables ground effect calculations to be made whilst in the hover. Although it is recognised that ground effect diminishes rapidly with forward speed it is necessary to obtain expressions predicting the effect of flying close to the ground at some forward airspeed. Cheeseman and Bennett derived a similar expression to that given by Equation 4.36 using the same potential flow theory, but varying the strength of the source to account for the forward velocity. The resulting expression to account for ground effect in forward flight is given in non-dimensional form as,

$$\left[\frac{\lambda_{0/IGE}}{\lambda_{0/OGE}}\right]_{T=constant} = \left[1 - \frac{1}{16\overline{H}^2\left(1+\left(\frac{\mu}{\lambda_{0/OGE}}\right)^2\right)^{\frac{3}{2}}}\right] \tag{4.37}$$

where,

μ is the non-dimensional rotor hub velocity.

4.3.7 Ground Effect and its Influence on HGS Inflow Models

Since HGS contains both the Glauert and Peters-HaQuang inflow models it was necessary to alter both to include the Cheeseman and Bennett ground effect corrections. In Chapter 2 the nap-of-the-earth Pop-up manoeuvre was used as the example to demonstrate the potential of inverse simulation. Chapter 3 used the example of ADS-33D Rapid Side-step to illustrate how roll attitude quickness could be calculated and plotted on a quickness chart. In this Chapter yet another manoeuvre will be used for the example calculations. The effects on inflow velocities will be investigated and the main attitude angle for the manoeuvre calculated using both inflow models, results of which are presented to illustrate why ground effect has little influence on handling qualities.

The nap-of-the-earth Acceleration/deceleration manoeuvre, Figure 4.13 was selected to demonstrate ground effect and is similar to the Rapid Side-step of Chapter 2 as it can be used in a 'mask-unmask-mask' type manner to move between areas of cover. The task begins and terminates in a trimmed hover state and is accomplished by accelerating the aircraft to a predetermined maximum velocity, followed by an immediate deceleration at the manoeuvre halfway point, which brings the aircraft back to the hover. The aircraft being simulated is a battlefield/utility type aircraft based on the Westland Lynx, Figure 3.2, whilst the maximum velocity is 10 knots occurring half way through the manoeuvre, over a distance of 150 metres. The results of inverse simulation runs at 2 metres, 4 metres and 8 metres in ground effect are compared with out of ground effect results for each inflow model, below.

1. Glauert Momentum Inflow Model IGE

Figures 4.14a to c illustrate the Glauert inflow components for the NOE Acceleration/deceleration manoeuvre, OGE and then at various altitudes above ground, IGE. It can be seen that each inflow component is reduced in magnitude by a greater amount as the altitude of the aircraft gets closer to the ground. This would seem to confirm the theory that rotorcraft close to the ground require less thrust than at altitude. The uniform component of inflow velocity shows a decrease in inflow velocity of approximately 2 metres/second that corresponds to a reduction of almost 20 percent. Similar patterns are found in the lateral and longitudinal inflow components, although to a lesser extent. What is also evident is that at the manoeuvre midpoint, where the aircraft reaches the predetermined maximum velocity and initiates an immediate deceleration, the uniform inflow component reduces further still. In addition the lateral component is somewhat less than the longitudinal component, which is expected from a flight test manoeuvre with primarily longitudinal controls.

2. Peters-HaQuang Dynamic Inflow Model IGE

Figures 4.15a to c illustrate the Peters-Haquang inflow components from the NOE Acceleration/deceleration manoeuvre, OGE and then, as before, ground effect modifications are calculated at several altitudes. The main difference is the small lag time required for the ground effect benefit to build up and an increase in the inflow at the manoeuvre halfway point as opposed to a further decrease as predicted by the Glauert case. However, the general pattern is the same and it is the 2 metres altitude case that shows the least required inflow velocity, which is predicted as being even less than the Glauert case. In this instance the uniform component is seen to increase slightly at the manoeuvre midpoint, whilst in ground effect and it is also interesting to note the lateral inflow component that indicates a very small negative flow.

4.3.8 Ground Effect and its Influence on Handling Qualities

Since attitude quickness is determined largely by the nature of the manoeuvre, it was expected that ground effect would have little or no effect. This is confirmed by

observing Figure 4.16 where the pitch attitudes of the Acceleration/deceleration manoeuvres are illustrated. It can be seen that the pitch attitude remains virtually the same for each simulation run, starting at no ground effect and progressing through 2, 4 and 8 metres respectively. In addition, it is unlikely that this task would qualify for Level 1 handling qualities as defined by ADS-33D as the manoeuvre does not attain the desired pitch attitudes specified in the document.

That said, the ADS pitch angle criteria can be approached by increasing manoeuvre velocity, however, ground effect has a negligible influence on aircraft states beyond 30 knots or so. A similar investigation was conducted for the Rapid Side-step manoeuvre, described in Chapter 3 with identical findings. It would seem indeed that attitude quickness is uninfluenced by ground effect. If the helicopter model used is capable of successfully completing the task, and meet the manoeuvre requirements, it will do so regardless of the influence of ground effect.

4.3.9 Atmospheric Disturbance Modelling

HGS was modified to include the '1-cosine', *(Hoblit, 1988)* sharp edged gust. The model of the 1-cos gust is explained below together with the method of implementation within HGS. A result from a manoeuvre experiencing an unfavourable gust condition, determined by ADS-33D, is presented.

4.3.9.1 1-cos Gust

Usually, the effect of a discrete gust or is modelled in two dimensions. In general a vertical or lateral gust will alter the effective local angle of attack of a blade element and thus alter the lift produced. The special case of the head-on gust will alter lift produced, however the local angle of attack remains the same. The 1-cosine pulse represents the most popular idealisation of a singular or discrete gust shape. This approach is a slightly more realistic method of modelling discrete gusts since the wind intensity starts at zero, builds up to a maximum before decreasing back to zero. The resulting gust profile is presented in Figure 4.17 and is given mathematically as,

$$U = \frac{1}{2} U_0 \left(1 - \cos \frac{2\pi x}{2H} \right) \tag{4.38}$$

where,

U_0 is the gust intensity,

H is the gradient distance[1] and

x is taken as the time taken from the start of the gust until maximum gust intensity occurs.

4.3.9.2 Inclusion of 1-cos Gust Equation into HGS

The relative motion of air over a helicopter and through the rotor disc is responsible for the forces and moments acting on the vehicle. If it is assumed that the manoeuvres modelled within Helinv are set in the earth fixed frame of reference and that the air in this frame is taken as possessing calm standard atmospheric conditions, then, clearly the air does not move with reference to the axes. The velocity time histories of the aircraft relative to the ground and to the surrounding air can then be written respectively as,

$$V(t)_{h/gr} = V(t)_{h/a} \tag{4.39}$$

If the effect of the gust is assumed to completely surround the entire aircraft so that the aircraft is considered immersed then, mathematically it can be treated as a point since there are no notable variations in wind speed over the aircraft. Equation 4.39 can then be rewritten to include the gust effect as,

$$V(t)_{h/gr} = V(t)_{h/a} + V(t)_{gu/gr} \tag{4.40}$$

where,

$V(t)_{gu/gr}$ is the time history of the gust velocity vector.

[1] Gradient distance is a term that originated when the gust profile had a clear and definite linear-ramp portion. The term has continued to be used with other gust shapes such as the 1-cos profile.

Since the velocity time history of the gust can be calculated from input information, the velocity of the aircraft can be obtained from,

$$V(t)_{h/a} = V(t)_{h/gr} - V(t)_{gu/gr} \tag{4.41}$$

It is normal for simplification purposes to separate the turbulence into discrete gusts in two dimensions; the horizontal earth *x*-*y* plane and the vertical earth *x*-*z* plane. In the horizontal plane the gust is able to act on the aircraft from any angle, measured clockwise from the earth *x*-axis, see Figure 4.18. Thus the gust velocity component, V_{gust} and the heading angle, at which it meets the helicopter, ψ_{gust} determines the absolute gust velocity. If the vertical gust component, $V_{gust/vert}$ is taken as being positive in a downward direction, then a gust velocity vector in earth axes can be written in the form,

$$\mathbf{V_{gu/gr}} = \begin{bmatrix} -V_{gust}\sin\psi_{gust} \\ -V_{gust}\sin\psi_{gust} \\ V_{gust/vert} \end{bmatrix}_e \tag{4.42}$$

The vector is transformed through the Euler angles, (ϕ, θ and ψ) to determine the velocities of the gust components with respect to the helicopter in body axes. The aerodynamic components of the wind velocity at the aircraft's centre of gravity, u_{aero}, v_{aero} and w_{aero} are then calculated by summing the inertial body velocities of the aircraft, u, v and w, and the gust velocity components in body axes, $u_{aero/\mathbf{gust}}$, $v_{aero/\mathbf{gust}}$ and $w_{aero/\mathbf{gust}}$, giving,

$$\begin{aligned} u_{aero} &= u + u_{aero/\mathbf{gust}} \\ v_{aero} &= v + v_{aero/\mathbf{gust}} \\ w_{aero} &= w + w_{aero/\mathbf{gust}} \end{aligned} \tag{4.43}$$

The resulting fuselage forces and moments calculated within HGS are determined initially from the respective angles of incidence and sideslip given as,

$$\alpha_{fus/\mathbf{aero}} = \tan^{-1}\left(\frac{w_{\mathbf{aero}}}{u_{\mathbf{aero}}}\right) \qquad \beta_{fus/\mathbf{aero}} = \sin^{-1}\left(\frac{v_{\mathbf{aero}}}{V_{f/\mathbf{aero}}}\right)$$

where,

the flight velocity is given as, $V_{f/\mathbf{aero}} = \sqrt{u_{\mathbf{aero}}{}^2 + v_{\mathbf{aero}}{}^2 + w_{\mathbf{aero}}{}^2}$

Indeed similar expressions can be found for the remaining fin and tailplane components of the helicopter. Thus the forces and moments for the entire aircraft may be found.

4.3.9.3 Inverse Simulation of an ADS-33D Manoeuvre with Gust Effect

Although there are four MTEs specified in ADS-33D that have manoeuvre descriptions requiring that the task be performed in a prevailing wind it is adequate to demonstrate the principle using a single flight test manoeuvre. The wind speed is described as "*moderate"* while the direction is assumed to be either the most critical direction or if this has not been determined the direction is "*directly from the rear of the aircraft*". The task that was examined was the precision Hover-turn manoeuvre.

Hover-turn with Direct Tail Gust

The Hover-turn precision flight test manoeuvre, Figure 4.19, is initiated in a trimmed hover condition at an altitude of less than 6.1 metres (20 feet) and terminates in the same trimmed state with a heading change of 180 degrees. The manoeuvre is generally used to accomplish a large heading change in a confined area, or to turn to a target that has been identified near the rear of the aircraft. ADS-33D requires that the task be accomplished to port and starboard and that a gust of 15 knots is blowing from either the most critical position or, if that has not been identified, the rear of the aircraft. In this instance the manoeuvre is conducted to starboard and completed in 10 seconds. The 1-Cos tail gust initiates with the manoeuvre and reaches the maximum amplitude of 15 knots at the manoeuvre midpoint.

Figures 4.20a to d present the pilot control displacement time histories. It can be seen how the gust has an effect on the control movements that the pilot is required to make. Since the gust reaches maximum strength at the manoeuvre midpoint, when the helicopter is at 90 degrees sideslip the main rotor collective required is actually less, Figure 4.20a. This trend is repeated in the other control displacements. It is likely that the effect of the gust actually increases the downwash thus less power is required at that moment. Even so, maximum displacements seem to occur in lateral cyclic, Figure 4.20b and longitudinal cyclic, Figure 4.20c either side of the manoeuvre halfway point. Although these movements are comparatively small, it is likely that a pilot would perceive the task to be more demanding and hence award a lesser handling qualities rating. For example the lateral stick and pedals require approximately 4 to 6 percent of additional control movement during the gust.

ADS-33D does present a moderate-amplitude, heading change, quickness chart for yaw. However as before (ground effect) there is little to be gained from the chart as attitude quickness and thus the handling qualities remain uninfluenced. This can be seen in Figure 4.21, which presents the yaw attitude for the manoeuvre in still air, and with the 15 knot 1-Cos tail gust. The yaw attitudes are very similar and any expected change in attitude quickness is consequently minimal.

Chapter Summary

A brief overview of helicopter mathematical model types at the University of Glasgow University was presented at the start of this chapter followed by a discussion on HGS and the improvements made. Although the current model possesses many features, there were various additional components that were considered advantageous for simulation of different flight conditions that could form part of future handling qualities studies work.

One of the main tasks undertaken was modelling the lead-lag motion. The modelling exercise was complete although it was not implemented. The reasons for this were discussed and it was shown that implementing this feature in a disc model representation of the rotor was impractical and would have led to many simplifications of the current version. It was concluded that HGS as it stands is the

best possible form of disc-type model for handling qualities studies. Additional features such as ground effect and discrete gust modelling were carried out and implemented. The corresponding results were presented and discussed and it was shown how neither of these effects would have had any kind of significant influence on the pitch and yaw attitude quickness for the Acceleration/deceleration and Hover-turn manoeuvre respectively. This further confirms Helinv as a suitable handling qualities assessment tool since attitude quickness is largely independent of external influences and much more dependant on manoeuvre modelling. It is likely however that potential handling qualities metrics such as pilot attack could reveal more information on the actual workload experience by the pilot.

Chapter 5

Modelling Flight Test Manoeuvres for Handling Qualities Studies

The importance of the manoeuvre model has been emphasised throughout the thesis. This chapter will consider the manoeuvre modelling improvements that have been implemented in Helinv to allow the gross features of various manoeuvres to be captured permitting calculation of Level 1 handling qualities. Initially, the Rapid Side-step and Acceleration/deceleration flight test manoeuvres are examined as they are considered to comprise the simple, but important tasks described in ADS-33D. Further consideration is given to Slalom design starting with the ADS-33D variation and moving on to definitions as used by other flight testing authorities. Inverse simulation results are presented in conjunction with attitude quickness calculations and the chapter concludes with a manoeuvre data comparison and confidence testing exercise.

5.1 ADS-33D Linear Translation Manoeuvre Modelling Improvements

5.1.1 Modelling the ADS-33D Rapid Side-step

The first section of this chapter is an elaboration on the piecewise polynomial method (described briefly in Chapter 3), to fully describe how the ADS-33D Rapid Side-step task is modelled. The description of the manoeuvre in ADS-33D, Section 4.2.5 makes it clear that the main parameters controlling the manner in which the task is flown are, the time taken to achieve maximum acceleration, the time taken to reach the maximum deceleration, the bank angles and of course the maximum velocity of the manoeuvre.

"*...Starting from a stabilised hover with the longitudinal axis of the rotorcraft*

orientated 90 degress to a reference line… initiate a rapid aggressive lateral translation with a bank angle of at least 20 degrees… When the rotorcraft has achieved a lateral velocity within 5 knots of its maximum lateral velocity or 45 knots, whichever is less, immediately initiate an aggressive deceleration to hover… The peak bank angle should be at least 30 degrees…"

"*Desired Performance*
... Achieve at least 25 degrees of bank angle within 1.5 seconds of initiating the manoeuvre
... Achieve at least 30 degrees of bank angle within 1.5 seconds of initiating the deceleration…"

Consequently, one method of modelling the manoeuvre is to define these parameters in a mathematical sense, principally the lateral acceleration. This approach has been used successfully and validated by *Thomson and Bradley (1997)*. The basis in describing the manoeuvre trajectory or flight path is to define the acceleration in terms of polynomials, which are in the earth fixed frame of reference, x_e, y_e, z_e. Thomson and Bradley state "*polynomials are attractive as a basis for describing trajectories because of their analytical simplicity and their predictable interpolative properties*".

In considering the ADS-33D lateral Rapid Side-step MTE, there are six segments into which the manoeuvre can be divided to facilitate the modelling process. Recall that each segment has been described in Chapter 3, Section 3.2.2 and the lateral acceleration profile illustrated in Figure 3.8. However, the equations used to model each of the transient piecewise polynomial sections of the manoeuvre, i.e. $0-t_1, 2t_1-4t_1$ and $5t_1-6t_1$ were not presented. Each transient segment can be represented by polynomials in lateral acceleration. The transitions between the values of zero acceleration (i.e. trimmed conditions at the start and end of the manoeuvre), and the maximum values of acceleration / deceleration can be represented by third, fifth or seventh order polynomials. The order of the polynomial can be used to alter the way the vehicle moves from zero acceleration, to full acceleration in the given time, hence controlling the way manoeuvre aggression is applied. For example, the

transition from zero acceleration at time t=0 to a maximum acceleration $\dot{V}_{\max}$ at time $t = t_1$ seconds can be given by the following respective third, fifth and seventh order polynomials,

$$\dot{V}(t) = \left[-2\left(\frac{t}{t_1}\right)^3 + 3\left(\frac{t}{t_1}\right)^2 \right] \dot{V}_{\max} \tag{5.1}$$

$$\dot{V}(t) = \left[6\left(\frac{t}{t_1}\right)^5 - 15\left(\frac{t}{t_1}\right)^4 + 10\left(\frac{t}{t_1}\right)^3 \right] \dot{V}_{\max} \tag{5.2}$$

$$\dot{V}(t) = \left[\frac{10}{3}\left(\frac{t}{t_1}\right)^7 - 14\left(\frac{t}{t_1}\right)^5 + \frac{35}{3}\left(\frac{t}{t_1}\right)^4 \right] \dot{V}_{\max} \tag{5.3}$$

Figure 5.1 shows a graphical representation of each polynomial using the parameters, $\dot{V}_{\max} = 5\,\text{m/s}^2$ and $t = t_1 = 5\,\text{seconds}$. The ADS-33D requirements are precisely met as the aircraft achieves the desired attitude changes within the required times. Of equal importance though is the fact that *Thomson and Bradley (1997)* have shown this modelling approach allows the associated quickness values introduced in Chapter 2 of the thesis to fall within the Level 1 region of the corresponding quickness chart, Figure 2.2b. Clearly this illustrates by inverse simulation that aircraft can be shown to be capable of attaining the desired handling qualities characteristics. The exercise illustrated by Thomson and Bradley will not be repeated here, instead, the Acceleration/deceleration manoeuvre will be addressed and the effect of polynomial order on handling qualities is illustrated.

5.1.2 ADS-33D Manoeuvre Requirements for the Acceleration/deceleration

The Acceleration/deceleration task, Figure 4.13 and its suggested layout, Figure 5.2, is flown in the Good Visual Environment GVE as an aggressive manoeuvring task and is modelled in exactly the same manner as the Rapid Side-step. In fact the same piecewise polynomial equations given by Equations 5.1-5.3 are used to define the flight path although it is obviously the longitudinal acceleration that is modelled. The manoeuvre is described in ADS-33D Section 4.2.4.

"*...Starting from a stabilised hover, rapidly increase power to approximately maximum, and maintain altitude constant with pitch attitude. Hold collective constant during the acceleration to an airspeed of 50 knots. Upon reaching the target airspeed, initiate a deceleration by aggressively reducing the power and holding altitude constant with pitch attitude...*"

"*Desired Performance*
...Achieve a nose-up pitch attitude during the deceleration of at least 30 degrees ..."

The manoeuvre is important in handling qualities analyses as it is relatively simple to perform in a repetitive fashion with several pilots and the visual cueing can be created with ease using flat markers and cones placed on the ground. The influence of the user selectable polynomial aggression parameter is evident from Figure 5.3 where the pitch angle for the first transient section of the manoeuvre is given (i.e. the first 1.5 seconds). The corresponding quickness parameters for the initial transition are presented in Figure 5.4 and it can be seen that general trend is diagonally away from the origin in the direction of increasing task difficulty as postulated by *Padfield (1996)*. Although pitch angle is presented, recall that the pitch rate is also a very significant factor since higher pitch rate peaks will tend to produce higher attitude quickness values thus pushing them farther up the corresponding chart. Figure 5.5 presents a typical inverse simulation result of the pitch angle time history of the entire task. Note the deceleration phase where the aircraft achieves and maintains a nose-up attitude of 30 degrees, thus meeting the desired requirement of ADS-33D mentioned above.

5.2 Modelling the Slalom Flight Test Manoeuvre

Although emphasis was placed on the piecewise modelling method for the ADS-33D linear translation manoeuvres described above, it is not always necessary. *Thomson and Bradley (1998)* have illustrated using flight test data that the global polynomial representation of manoeuvres is capable of capturing the main features of any task for flight dynamics or performance aspects. The aggressive nature of tasks

that require sudden changes in acceleration can be modelled using the piecewise polynomial method. However, since the Slalom is performed in what can essentially be described as a continuous moderately aggressive flight condition, the global representation is more suitable for modelling the manoeuvre whilst ensuring continuity in the profiles of the derivatives of flight parameters. The Slalom has been defined in several ways and in turn has been modelled for use in Helinv and corresponding handling qualities studies. The various Slalom variations and modelling methods are described below.

5.2.1 The ADS-33D Slalom

By assuming complete trimmed conditions at the initiation and termination of the Slalom task, (lateral distance, velocity and acceleration are set to zero), and dividing the manoeuvre into a number of set times where the lateral translation is at a maximum or minimum, fourteen boundary conditions are obtained. Referring to Figure 5.6 then.

Start of manoeuvre $t = 0$

- Lateral distance, velocity and acceleration are zero, i.e.
  $y = \dot{y} = \ddot{y} = 0$.

One-fifth of total manoeuvre time $t = 1/5t_m$

- Lateral distance is at a maximum and lateral velocity is zero, i.e.
  $y = Y_{\max}$, $\dot{y} = 0$.

Two-fifths of total manoeuvre time $t = 2/5t_m$

- Lateral distance is at a negative maximum and lateral velocity is zero, i.e.
  $y = -Y_{\max}$, $\dot{y} = 0$.

Three-fifths of total manoeuvre time $t = 3/5t_m$

- Lateral distance is at a maximum and lateral velocity is zero, i.e.
  $y = Y_{\max}$, $\dot{y} = 0$.

Four-fifths of total manoeuvre time $t = 4/5t_m$

- Lateral distance is at a negative maximum and lateral velocity is zero, i.e. $y = -Y_{\max}$, $\dot{y} = 0$.

End of manoeuvre $t = t_m$

- Lateral distance, velocity and acceleration are zero, i.e. $y = \dot{y} = \ddot{y} = 0$.

The resulting polynomial of order thirteen, has the form,

$$Y(t) = \left[-\frac{1}{13824}\left(\frac{t}{t_1}\right)^{13} + \frac{65}{27648}\left(\frac{t}{t_1}\right)^{12} - \frac{247}{6912}\left(\frac{t}{t_1}\right)^{11} + \frac{9295}{27648}\left(\frac{t}{t_1}\right)^{10} - \frac{29603}{13824}\left(\frac{t}{t_1}\right)^{9} + \frac{86545}{9216}\left(\frac{t}{t_1}\right)^{8} - \frac{95807}{3456}\left(\frac{t}{t_1}\right)^{7} + \frac{1444105}{27648}\left(\frac{t}{t_1}\right)^{6} - \frac{392825}{6912}\left(\frac{t}{t_1}\right)^{5} + \frac{198125}{6912}\left(\frac{t}{t_1}\right)^{4} - \frac{625}{216}\left(\frac{t}{t_1}\right)^{3} \right] Y_{\max}$$

where,

t_1 is the time taken to reach the first maximum lateral translation and is equal to one-fifth of the entire manoeuvre time,

$Y_{\max}$ is the maximum lateral distance traversed, measured from the centreline of the manoeuvre (positive to starboard, negative to port).

In this instance it is appropriate to specify the main flight parameter as the lateral translation, hence the polynomial describing the manoeuvre is in terms of manoeuvre lateral distance. Figure 5.7 illustrates a plot for the Slalom of longitudinal versus lateral displacement for a typical manoeuvre conducted at 60 knots, using the Lynx aircraft and a longitudinal distance of 762 metres. Desired performance for the task is given as maintaining airspeed of at least 60 knots, while adequate performance is specified as maintaining airspeed of at least 40 knots throughout the manoeuvre.

The roll attitude quickness chart, Figure 5.8, shows that the majority of the points actually lie in the Level 2 region suggesting that the handling qualities are degraded for this aircraft and task. The reason for this, is probably that the task is not aggressive enough to generate the roll rates and attitude changes required, to calculate points that lie in the Level 1 region of the chart. In this instance, although the gross features of the manoeuvre are captured by the global polynomial, using the flight parameter criteria specified by ADS-33D does not produce conclusive Level 1 handling qualities.

5.2.2 The DERA Slalom

Although ADS-33D constitutes one of the most important rotorcraft handling qualities specifications it is only a definitive guide as to how the tasks should be designed or flown in the United States. As a consequence, other institutions have developed flight test manoeuvres for further investigation. *Howell (1995)* postulates that the Slalom task is appropriate for exposing "*handling qualities inadequacies that would manifest themselves during rapid NOE manoeuvring to avoid ground obstacles*". Thus the Defence Evaluation and Research Agency (DERA), have developed a variation on the ADS Slalom for such investigations and it has been modelled in Helinv with the aim of providing attitude quickness results.

The DERA Slalom is shown in Figure 5.9. It can be seen to consist of two smaller Slalom tasks, with the initial roll of each in opposing directions. A linear section where the aircraft returns to the manoeuvre centreline and remains in a trimmed straight and level flight condition for a period of time separates these two elements. In terms of simulator visual cues reported by *Howell (1995)*, four pairs of poles represent the ground track with the inner and outer set denoting desired and adequate performance respectively. A white-banded section on the poles provided height cueing.

The method adopted to define the entire DERA Slalom was a combination of the global and piecewise methods mentioned earlier. Global polynomials of order thirteen were developed for each of the smaller Slalom sections, but the complete task was constructed in a piecewise manner. For example the polynomial defining the first

small Slalom section from time = 0 to time = $3t_1$ is given by,

$$Y(t) = \left[\frac{1}{32}\left(\frac{t}{t_1}\right)^{13} - \frac{39}{64}\left(\frac{t}{t_1}\right)^{12} + \frac{83}{16}\left(\frac{t}{t_1}\right)^{11} - \frac{1617}{64}\left(\frac{t}{t_1}\right)^{10} + \frac{2475}{32}\left(\frac{t}{t_1}\right)^{9} - \frac{9801}{64}\left(\frac{t}{t_1}\right)^{8} + \frac{1539}{8}\left(\frac{t}{t_1}\right)^{7} - \frac{8991}{64}\left(\frac{t}{t_1}\right)^{6} + \frac{729}{16}\left(\frac{t}{t_1}\right)^{5} \right] Y_{\max}$$

In the same way the section from time = $4t_1$ to time = $7t_1$ is given by the polynomial with negative coefficients. A typical plot of the DERA Slalom is given in Figure 5.10 conducted at the desired airspeed of 50 knots. To concur with the simulator trials reported by *Howell (1995)*, the task aspect ratio in Helinv can also be varied, that is, the ratio of the maximum lateral distance in the manoeuvre to the length of one Slalom element. A typical appraisal of the handling qualities would probably consist of several pilots flying the manoeuvres at aspect ratios between 0.03 and 0.1, i.e. lateral offsets of 15 to 30 metres and slalom element lengths of 300 to 500 metres.

It is interesting to note that the handling qualities parameters obtained from the DERA Slalom, when plotted on the chart, Figure 5.11, show that the task is almost completely Level 1. However the points seem to be clustered into two groups. The main group in the Level 1 region is representative of the gross features of the manoeuvre and corresponds to the peak roll-rates and minimum attitude changes. Conversely, the group of points on the left outside the boundaries corresponds to the middle section of the task, where the aircraft returns to the centreline in trimmed level flight. The ground track is given in Figure 5.10 and is clearly similar to the ADS-33D task. The modelling method for this Slalom successfully captures the gross features of the task and consequently produces a Level 1 handling qualities rating, the linear portion in the middle of the manoeuvre forcing higher roll rates and corresponding attitude changes.

5.2.3 DLR Slalom Tasks

The Deutsche Forschungsanstalt für Luft und Raumfahrt, (DLR), Braunschweig, Germany have developed two slalom types for handling qualities analysis which are illustrated and discussed in *Blanken and Ockier (1997)*. The reasons for development originate from the realisation that to conduct a handling qualities assessment thoroughly, several expensive processes have to be carried out. This generally involves ground-based and in-flight simulator trials collecting subjective data from the pilot and quantitative data from handling qualities metrics. The process has to be repeated for every single flight test manoeuvre that is investigated. However Blanken and Ockier postulate that by fully understanding the manoeuvre characteristics and the corresponding influences on handling qualities, certain extrapolations can be made on that task in general thus eliminating the need for further testing and cutting costs. By modelling the manoeuvres in Helinv, initial estimates can be made of the handling qualites Level for those tasks consequently adding to the data already available.

The first Slalom is termed the Tracking Slalom, which is divided into two asymmetrical halves each with precise tracking phases through sets of 'gates' marked on the ground. The subsequent Gate Slalom task is a modification of the Tracking Slalom where the tracking phases have been reduced to simple pole type markers that signify the desired performance.

1. Tracking Slalom

The Tracking Slalom was originally designed for, and used in flight tests to assess the effect of time delay and roll attitude bandwidth on handling qualities as reported by *Pausder and Blanken (1992)* and *Blanken and Ockier(1997)*. However later studies by the same authors used the task to analyse handling qualities by looking at piloting tasks and manoeuvre metrics. The desired performance for the Tracking Slalom is given as,

"*Successfully tracking the 3 metre wide gates (± 1.5 metres from the centreline), with height and speed within the tolerances (± 10 feet and ± 5 knots) ...*"

Adequate performance was defined as performing the manoeuvre with error margins double those of the desired requirements. Flying the manoeuvre without a clear tracking phase was not considered adequate for the manoeuvre.

Clearly the task of modelling such a manoeuvre would not be as straightforward as previous flight test manoeuvres and the method of developing a global polynomial that described the entire manoeuvre was unlikely. The approach taken was to divide the manoeuvre into a number of transient segments and a number of linear portions as shown in Figure 5.12. Ensuring continuity in lateral acceleration when piecing each of the segments together, required that each transient be defined up to, and including the jerk[1] term. Although each half of the manoeuvre is asymmetrical, the entire Tracking Slalom is symmetrical. It was therefore not necessary to calculate polynomial coefficients for all of the transient phases. The coefficients obtained for one half of the manoeuvre could be used to describe the shape of the other half. For example, the section given as time = 0 to time = t_1 with eight associated boundary conditions yielded the following seventh order polynomial,

$$Y(t) = \left[-20\left(\frac{t}{t_1}\right)^7 + 70\left(\frac{t}{t_1}\right)^6 - 84\left(\frac{t}{t_1}\right)^5 + 35\left(\frac{t}{t_1}\right)^4 \right] Y_{\max}$$

where $Y_{\max}$ is the maximum lateral distance from the centreline.

In a similar way the polynomials were calculated for time = $1.5t_1$ to time = $2t_1$ and time = $2.25t_1$ to time = $2.75t_1$ are given respectively as,

$$Y(t) = \left[1280\left(\frac{t}{t_1}\right)^7 - 2240\left(\frac{t}{t_1}\right)^6 + 1344\left(\frac{t}{t_1}\right)^5 - 280\left(\frac{t}{t_1}\right)^4 + 1 \right] Y_{\max}$$

and

$$Y(t) = \left[1280\left(\frac{t}{t_1}\right)^7 - 2240\left(\frac{t}{t_1}\right)^6 + 1344\left(\frac{t}{t_1}\right)^5 - 280\left(\frac{t}{t_1}\right)^4 + \frac{1}{2} \right] Y_{\max}$$

[1] "Jerk" is defined as being the derivative of acceleration, in this instance, lateral acceleration.

Clearly, reversing the sign of the respective polynomial coefficients will result in suitable equations to define the second half of the Tracking Slalom. Figure 5.13 illustrates the inverse simulation results of the lateral translation for the Tracking Slalom task, while the corresponding attitude quickness is seen in Figure 5.14. The manoeuvre was simulated at 60 knots using the Lynx aircraft, over a longitudinal distance of 1546 metres as suggested by *Blanken and Ockier(1997)*. Although quite a few points lie in the Level 1 region it is clear that the task is far from being completely Level 1 since a considerable number of points are plotted in the Level 2 and Level 3 regions. Again this is largely due to small peak roll rates since the manoeuvre is very long and does not seem to require aggressive handling. The small roll attitude changes are also symptomatic of a manoeuvre that is non-aggressive and requires a lesser degree of net attitude change.

2. Gate Slalom

The Gate Slalom, Figure 5.15 removes the tracking elements from the manoeuvre and presents the pilot only with a set of gates or poles, which have to be rounded successfully in order to meet the performance limits of the task. To conform to manoeuvres developed thus far the Gate Slalom was developed with an overall manoeuvre symmetry about the mid-point, although the task illustrated in *Blanken and Ockier (1997)* has an overall asymmetry. The modelling approach used was to divide the manoeuvre into three elements, an initial section with three gates, a middle linear section and a final section opposite in direction to the first element. Blanken and Ockier specify that when passing the gates the aircraft's flight path must be parallel with the longitudinal axis of the manoeuvre (i.e. perpendicular to the gates). Desired performance for the task is quoted as as,

"*Passing through the 3 metre wide gates parallel to the longitudinal axis of the course with height and speed within the tolerances (± 10 feet and ± 5 knots) ...*"

Task performance to an adequate level was defined as passing within 3 metres from the centre gate parallel to the longitudinal axis of the course and with error margins double those of the desired requirements. Flying through the gates without trying to keep the aircraft parallel to the course was not considered adequate for the

manoeuvre.

Global polynomials with boundary conditions defined in jerk were used to describe the initial and final elements of the course, i.e. from time = 0 to time = $3t_1$ and time = $4t_1$ to time = $7t_1$. The following polynomial of order ten was found to be adequate to describe the Gate Slalom task when conjoined to the intermediate linear section of zero lateral translation (final phase having sign reversed coefficients).

$$Y(t) = \left[\frac{3}{32}\left(\frac{t}{t_1}\right)^{10} - \frac{23}{16}\left(\frac{t}{t_1}\right)^{9} + \frac{291}{32}\left(\frac{t}{t_1}\right)^{8} - \frac{243}{8}\left(\frac{t}{t_1}\right)^{7} + \frac{1809}{32}\left(\frac{t}{t_1}\right)^{6} - \frac{891}{16}\left(\frac{t}{t_1}\right)^{5} + \frac{729}{32}\left(\frac{t}{t_1}\right)^{4} \right] Y_{\max}$$

where,

$Y_{\max}$ is the maximum lateral translation in the overall manoeuvre.

Figure 5.16 illustrates the lateral and longitudinal translations from Helinv using the Lynx aircraft simulated at 60 knots and a longitudinal distance of 1546 metres. The attitude quickness is plotted on Figure 5.17 and it can be seen that at no point are Level 1 handling qualities realised. This is not surprising since the manoeuvre is similar to the Tracking Slalom except that the pilot is no longer required to manoeuvre aggressively to achieve the linear portions of flight in the Tracking Slalom, but can simply fly over the gates marked on the ground. This would seem to require smaller roll rates and net roll attitude changes, the results being in the Level 2 and Level 3 regions.

5.3 Manoeuvre Confidence Testing

An important aspect of developing mathematical models of flight test manoeuvres is comparison with data available from actual flight tests, either ground-based or airborne. The following sections aim to show that at the very least, components of inverse simulation results are compatible with real data and as such are satisfactory for use in ADS-33D handling qualities studies. The manoeuvres

investigated are the DERA Slalom, and two ADS-33D linear translation manoeuvres, the Rapid Side-step and the Acceleration/deceleration. The flight data used for comparison was made available by DERA, Bedford from the flight simulator trials reported by *Howell and Charlton (1997)*. Note that the emphasis of the exercise is on testing the confidence of the accuracy of the manoeuvre profile, i.e. ensuring the main or gross features of the task are captured by the particular modelling method used. Validation of the helicopter mathematical model is not an issue in this instance, as previous studies, *Thomson (1992)* for example, has shown that the helicopter model is capable of adequately capturing the main flight dynamics features of the Westland Lynx.

5.3.1 The Basis for Manoeuvre Data Comparison and Confidence Testing

In an attempt to test the manoeuvre modelling techniques developed, inverse simulation results from three manoeuvres were compared with data from the DERA large motion simulator. Clearly the two systems (off-line inverse simulation and real time visual/motion simulation) are substantially different so care must be taken when comparing data. However, there are several reasons that allow such comparisons and consequently permit a certain degree of satisfaction in the methods used to model the flight test manoeuvres, summarised below.

- Helicopter Model

The helicopter model used in the DERA real time simulations is a variation on the model which forms the core aircraft model of Helinv, i.e. Helicopter Generic Simulation, HGS. It is a generic engineering model with the same principal features and modelling methods for the main rotor, tail rotor, fuselage and empenage aerodynamics. In the same way as HGS it can be configured to represent a specific aircraft type, for example, the Westland Lynx, by using a data set specific to that aircraft. The data set is the same as that used in HGS.

- Manoeuvre Models

The manoeuvre modelling techniques for the large motion simulator have been based on descriptions given in ADS-33D, as have those developed for use with Helinv. The visual cues developed for the pilots to act upon are specifically located to represent those detailed in the ADS document, in terms of spatial location. The modelling process in Helinv was designed to attempt to capture the same spatial representation of the manoeuvre.

- Piloting Strategy

Since the pilots fly the ADS flight test manoeuvres in the large motion simulator based on low level, visual cueing system they are in essence acting in a closed loop fashion. This is very similar to inverse simulation, in that the process is manoeuvre driven and the pilot is attempting to follow a tightly constrained flight path. The main difference is that Helinv can be thought of as possessing the perfect pilot, whereas, in the real time situation, there will always be some degree of human error.

Considering the points made above it is fair to say that to some degree manoeuvre data from the large motion simulator at DERA, Bedford can be used for testing the confidence of the manoeuvre modelling techniques developed at the University of Glasgow. The final sections of the chapter, below are aimed at doing just that.

5.3.2 DERA Slalom

Figure 5.18 illustrates a plot of ground-based flight simulator, roll angle data against inverse simulation, roll angle data of the same manoeuvre from Helinv. Between the times of 10 and 25 seconds approximately the inverse simulation data fits the flight data quite closely and it is clear that the piloting strategy is very similar. Examination of the gradients of several of the port or starboard roll attitudes confirms this. The likely reason that such a good match was achieved in this instance lies in the

fact that inverse simulation is a form of constrained simulation. The visual cueing system and manoeuvre layout for the ground based simulator DERA Slalom also forced the pilot to fly a constrained flight path thus operating in a similar manner to the inverse algorithm and generating roll angles with very similar characteristics to the inverse simulation results.

Note that the actual initial pulse of lateral cyclic to port could be made to match with the inverse data by removing the start portion, where the pilot is stabilising the aircraft before initiating the manoeuvre. Additionally, the gross features of the task are clearly modelled adequately with Helinv producing roll angles of similar amplitude to the simulator data.

For completeness (this manoeuvre only), Figure 5.19 presents the attitude quickness chart of Helinv and the flight data. It can be seen that the inverse simulation data yields a few points in the Level 1 region, while the flight data has the majority in the Level 2 region. The points do form in clusters suggesting similarities in the roll attitudes and rates, which of course is correct. Flight data in general tends to produce an increased number of points due to the greater number of zero crossing roll attitude movements, which are characteristic of stabilisation control movements. Recall Helinv can be thought of as possessing the perfect pilot and is thus required to make lass stabilising corrections.

5.3.3 ADS-33D Acceleration/Deceleration

Upon initial examination of Figure 5.20, one would be forgiven for thinking that the two pitch angles are unrelated. However, closer examination reveals some interesting comparisons that are clearly similar characteristics. For example, the gradients of the slopes of initial nose-down pitch into the manoeuvre, the nose-up pitch at the manoeuvre mid-point and the final nose-down pitch angles are very similar indeed, suggesting a similar piloting strategy. Possible reasons for not attaining greater consistency include, poorer tracking ability caused by inadequate visual cues, thus the pilot is unaware if the ADS-33D criteria have been fulfilled whilst piloting the manoeuvre. Hence the reason for not attaining the required nose-down/nose-up pitch attitudes. In addition, the final stabilisation to hover produces a

considerable amount of data, superfluous to the pitch angle data required for calculating handling qualities. There is little point in producing an attitude quickness chart since, in this respect the data are incompatible.

5.3.4 ADS-33D Rapid Side-step

The final manoeuvre validation, Figure 5.21 is perhaps the least convincing of all, however, like the previous task, there are elements available for comparison. The port roll into the task and the starboard roll to decelerate the aircraft again have similar gradients, suggesting at least that the pilot is flying the task in a similar manner. Poor visual cueing is perhaps responsible for the pilots awareness of roll attitude thus the angles of bank required for Level 1 handling qualities are not achieved. Like the Acceleration/deceleration, the pilot has to spend some time before manoeuvre initiation and at the end stabilising the aircraft into a trimmed hover condition, hence affecting the output data. Plotting the attitude quickness would yield little useful information since the flight data does not meet ADS requirements and contains a considerable amount of zero crossing stabilising inputs.

Chapter Summary

Initially the chapter considered the modelling of ADS-33D linear translation flight test manoeuvres, the Rapid Side-step and the Acceleration/deceleration. The methods of modelling and improvements were detailed in accordance with the descriptions given in the ADS document. The second manoeuvre development concentrated on the Slalom and its interpretations as found at two leading rotorcraft institutions. The modelling methods were described, and presented with plots of the manoeuvres and corresponding attitude quickness results. It was seen that some tasks conform to the ADS Level 1 criteria better than others do and reasons for this were offered.

The final section of the chapter was dedicated to the testing the confidence of the manoeuvre modelling techniques of three manoeuvres. The DERA Slalom flight data compared favourably with Helinv and an explanation was given. Conversely the ADS-33D Rapid Side-step and Acceleration/deceleration did not do as well and

possible explanations were postulated. However, the point is emphasised that the manoeuvre modelling method can be considered satisfactory if it is capable of reproducing in general, the actual piloting strategy for that particular task, which seems to be the case for the manoeuvres considered at the end of the chapter.

Chapter 6

Pilot Modelling and the Effect on Analytic Handling Qualities Estimation

The concept of modelling the human operator in a single-axis closed loop system is introduced. A conventional forward simulation system is constructed using a pilot model as the controller of a transfer function representation of the Westland Lynx helicopter in single-axis flight. A method is given whereby inverse simulation results can be used in conjunction with the helicopter model to derive a set of parameters specific to the pilot model for any particular simulation run. It will be shown that the pilot model parameters differ according to the manoeuvre type and aggression level. The effect of pilot modelling is to introduce an element of human limitation to the subsequent inverse results and thus alter the corresponding handling qualities level. This technique represents a novel approach to pilot modelling investigations and to the author's knowledge the method of calculating the pilot model parameters is unique in the field.

6.1 Human Operator Models Applied to Aircraft - The Pilot Model

Humans have shown great versatility and resourcefulness in the face of changing technology throughout all aspects of development in human-machine systems. *Sutton (1990)* describes the human controller as an element that is "*time varying, has variable gain, and is non-linear"*, while *Tustin (1947)* was one of the first people to develop any kind of theory that enabled humans to be described in a mathematical sense. The approach was to use a servomechanism hypothesis. It was from this that human operator modelling originated and, as a multitude of applications started to emerge the modelling methods increased in complexity. The basic generic human-machine system can be represented in block diagram form given by Figure 6.1. This type of system is pertinent to the chapter as the human operator is

performing a single-axis continuous tracking task, and is clearly an integral element of the closed loop system illustrated.

The desire to model the human operator in the aircraft environment, i.e. as a pilot has largely arisen from another area of massive development within the aircraft industry. Flight Control System (FCS) technology has given aircraft designers the power to shape the response desired from any given aircraft. Techniques such as Fly-by-Wire (FBW) allow high precision handling and manoeuvring whilst making full use of available aerodynamic performance and minimising the risk of loss of control. Fundamentally though, it is the human pilot that is required in the cockpit to initiate control inputs and respond to changing situations. In essence the pilot acts as the outer loop of the entire aircraft control system. As a result, the need to model the human pilot is more important to the successful development of aircraft flight control systems and indeed an ideal situation would certainly involve dual simulation of FCS and pilot models to investigate aircraft handling qualities, performance and dynamics.

6.2 The Precision Pilot Model

On reviewing the literature, *McRuer and Jex (1967), McRuer and Krendel (1974), Gerlach (1977)* and *Pausder and Jordan (1976),* it seemed the most appropriate starting point for pilot model investigation, was with the basic compensatory tracking control model type. This does not however undermine the importance or relevance of the work, as in the vast majority of aircraft the most important class of manoeuvre in a closed-loop control situation is compensatory control. Of the basic types of human operator models that were readily available in the literature one of the most appropriate was the "*Precision Model*". It is a quasi-linear model and operates by nullifying an input error signal. The approach taken to model a pilot is to set up the system in a compensatory tracking mode as shown in Figure 6.2a. Figure 6.2b merely illustrates the point that modelling the human operator requires a display with a fixed reference and a follower, which in turn generates the error. A compensatory tracking task presents the operator with only this error, calculated from the difference between the reference input and the actual output (follower) of the system. The operator is unaware of the actual state of the system, as no information is available regarding input or output. For this reason the operator is

unsure if the error is a cause of poor performance, target movement or a combination of both. However, compensatory tracking displays are favoured in many tasks as it is the only method that allows human input/output characteristics to be directly measured and the corresponding analysis is much easier. The following section presents an analysis of the model.

The original method employed to develop the model for piloting applications was to monitor and model the response of a pilot carrying out a single-axis stabilisation task in compensatory control. This type of approach involved fitting a describing function to the operator's response, thus, the precision model when given as a transfer function is,

$$Y_P(s) = K_P \frac{(1 + T_L s)}{(1 + T_I s)} \left\{ \frac{e^{-\tau s}}{1 + T_N s} \right\} \tag{6.1}$$

where,

K_P is the 'Pilot Gain' which gives an indication of the pilot's ability to respond to an error in the magnitude of a controlled variable within the system.

T_L is the 'Lead Time Constant' which characterises a pilot's ability to foresee or predict a particular control action. In simple terms it can be thought of as a counter measure to the limitations described below.

$e^{-\tau s}$ represents a 'Pure Time Delay' factor, sometimes known as transport lag, where τ is the latency or pure time delay constant. It is one component of the limitations inherent in all humans, and can be summarised as the time taken for decision making and implementation. Representative values of pure time delay are between one tenth and one quarter of a second.

T_I is the 'Lag Time Constant', which can be utilised to attenuate an oscillatory response from the dynamics of a controlled element by allowing the pilot to input smoother control actions. This may help achieve a closed-loop compensatory tracking task especially if the controlled element is characterised by unstable

dynamics.

T_N represents the muscular dynamics of the operator and is called the 'Neuromuscular Lag Time Constant'. It is concerned with the time taken to actuate the muscles after a signal from the brain has travelled to a specific limb. The model given in Equation 6.1 is split into two components, the bracketed expression on the right hand side of the equation being responsible for human limitations, while the rest of the parameters represent the equalisation network.

In the following sections two novel theories are proposed. Initially an alternative method is suggested for calculating the pilot model equalisation parameters using a constrained optimisation technique. Furthermore it is then seen that numerically optimum parameters exist for any particular flight test manoeuvre and level of flight aggression (aggression controlled by manoeuvre velocity in this instance), exercised in the task. The effect is to influence the inverse simulation results (produced by a "perfect pilot") by the presence of a pilot model implemented in a conventional simulation sense thus yielding what could be considered as more realistic results and handling qualities levels.

6.3 Pilot Model Equalisation Parameter Estimation

It is proposed that numerically optimum parameters for any given input signal to the pilot model are those parameters that minimise the resulting error between the input signal and the actual output of the system. In the initial study a simple function for the controlled element (system transfer function) is used to introduce the methods adopted and illustrate the role of the optimisation technique in obtaining parameter values. Section 6.2 showed that the precision model is constructed of five main parameters characterising the human limitations and a counterbalancing equalisation network. The method proposed allows the calculation of three of these parameters, (equalisation network parameters), therefore it is assumed that in any one particular study the human limitations will be fixed at specific values determined from the literature, *Pausder and Jordan (1976)* for example. A constrained optimisation technique was then applied to determine the values of the remaining three equalisation

parameters.

6.3.1 Equalisation Network Parameter Estimation

It is assumed that the generated error between reference input and system output is determined by a cost function given as,

$$F_{err}(K_P, T_L, T_I) = \int_0^1 \left(r_{in}(t) - r_{out}(K_P, T_L, T_I)\right)^2 dt^* \tag{6.2}$$

where,

$t^* = \frac{t}{t_m}$,

t is a general time at any point in the input signal and

t_m is the terminating time for the input signal.

The cost function is unrelated to handling qualities in general, although is given as a standard "Integral of the Square of Error (ISE)" in *Jacobs (1993)*. It is generally used for measuring control errors, compromising between steady state and transient behaviour and was assumed to be appropriate for the initial numerical optimisation process, as it is a non-weighted function. Effectively, the pilot model tries to minimise the cost function by obtaining suitable values for the gain, lead and lag time constants respectively. In this way the numerically optimum parameters for the pilot model can be found for any given input. The approach taken to minimise the cost function and hence optimise the equalisation network constants in the pilot model, is a form of constrained optimisation, discussed below.

6.3.2 Constrained Optimisation

The form of constrained optimisation utilised is known as Sequential Quadratic Programming (SQP) and is comprehensively discussed by *Grace (1992)*. It is a technique that transforms the original problem into one that can be solved using an iterative solution process. The Quadratic Programming (QP) sub-problem is

solved at each major iteration point of the calculation, so the solution technique can be viewed as it is in progress.

Essentially the process can be described as a method whereby the establishment of a feasible solution point initiates the algorithm. Consequently the solution proceeds by solving the QP sub-problem at each major iteration and uses a line search technique to identify the most likely direction of the final solution and generates a new iterate. This whole action continues until a satisfactory convergence has been reached, or, in some circumstances a solution cannot be found.

6.3.3 Initial Study with Basic Fixed Wing Aircraft Transfer Function

The dynamic system simulation software SIMULINK was used to model the system illustrated in Figure 6.2a. The method permitted each element of the system to be entered as a gain or transfer function of lead, lag etc. The initial study incorporated the following transfer function as given by *O'Hara (1967)* to represent an acceptable handling qualities transfer function for the short-period pitch motion of a fixed wing aircraft.

$$\frac{\dot{\theta}}{\delta}(s) = \frac{-K_C(s+\alpha)}{s^2 + 2\zeta\omega_{ns}s + \omega_n^2} \tag{6.3}$$

where,

ζ is the damping ratio,

ω_{ns} is the undamped natural pulsatance

$\dot{\theta}$ is the pitch rate and

δ is the stick deflection.

By varying the parameters it can represent an aircraft with satisfactory, acceptable or poor handling qualities. For the actual study, O'Hara defines the acceptable handling qualities transfer function as having the form,

Acceptable: $$\frac{\dot{\theta}}{\delta} = \frac{-10(s+5)}{s^2+4.5s+9} \tag{6.4}$$

Also for the initial study a simple sine wave function with different frequencies was used as the input reference signal. Since the algorithm used is a form of constrained optimisation, boundary limits were set for the equalisation network parameters and of course, numerical values were given to the limitations which were assumed to remain constant for any given individual throughout the task. The following limits and numerical values were assigned to each pilot model parameter and were obtained from observations of *McRuer and Krendel (1974)* and *Pausder and Jordan (1976)*,

$$[0.1 \le K_C \le 1.1], [0.2 \le T_L \le 1.0] \text{ and } [0.1 \le T_I \le 1.2]$$

The values selected for the pure time delay constant, τ and the neuromuscular lag constant T_N were 0.25 and 0.1 seconds respectively. A generic algorithm was devised and programmed to minimise the cost function.

The input frequencies of the sine waves investigated for the plant varied from 0.01 to 2 Hertz and a summary of results can be found in Table 6.1 – Part 1. The table presents the optimum values for individual equalisation parameters for the satisfactory handling qualities transfer function and the tracking ability of the pilot model can be seen from Figures 6.3a to 6.3d.

A number of other basic transfer functions representing idealised aircraft dynamics were also considered and the results can be found in Table 6.1 – Part 2. It would seem in most cases that the error increases as the frequency decreases, with the gain following the opposite pattern. The lead and lag equalisation terms operate in a manner of lead/lag compensation to achieve a cost function, minimum error value. The point of including this section is to illustrate the fact that a minimum error can be achieved and it follows that the corresponding equalisation characteristics are at numerically optimum values. Recall that the method used to obtain estimates for the equalisation parameters is a form of constrained optimisation and operates by

reducing the input error to the pilot model to its smallest numerical value. The corresponding pilot model parameters are then used as the best parameters for that particular system.

Results have been presented, Figures 6.3a to 6.3d and discussed for cases where the human operator model is required to control basic plant dynamics. The purpose of the exercise was to introduce the concept of human operator modelling and the technique by which it may be accomplished. In addition a novel technique was introduced whereby constrained optimisation was used to calculate values for the equalisation network parameters.

The technique was applied to inverse simulation results, for the purposes of parameter identification and investigation of handling qualities, in terms of human influence on inverse time histories resulting in a change in attitude quickness. Before a start can be made on obtaining results however, the correct dynamics must be identified for the system under consideration, i.e. an appropriate transfer function of the Westland Lynx HGS model, captured at some trim condition. The following section outlines the method.

6.4 Helicopter Model and Mission Task Element Selection

The Lynx model that was linearised was based on the forward simulation version of HGS and takes account of the fuselage and rotor degrees of freedom, i.e. the same model as that inherent in the inverse simulation algorithm. The resulting seven degree of freedom state vector has the form,

$$\underline{\boldsymbol{x}} = [u, v, w, p, q, r, \phi, \theta, \psi, \Omega, Q_E]^T \tag{6.5}$$

The corresponding control vector is of the form,

$$\underline{\boldsymbol{u}} = [\theta_0, \theta_{1s}, \theta_{1c}, \theta_{0tr}]^T \tag{6.6}$$

where, the first three elements correspond to main rotor collective, longitudinal cyclic and lateral cyclic pitch angles respectively, while the final element is representative of the tail rotor collective pitch angle.

The forward simulation version of HGS is capable of delivering state and control matrices in the above form based on any one of a large number of appropriate trim conditions selected by the user. The system is linearised about the trim condition using the familiar method of computing the partial derivatives with respect to the state and control variables given by Equations 6.5 and 6.6. Having obtained the matrices based on a selected trim condition the system can be written in the following well-known form,

$$\dot{\underline{x}} = \boldsymbol{A}\underline{x} + \boldsymbol{B}\underline{u} \tag{6.7}$$

and transformed via the Laplace variable (assuming zero initial conditions) to,

$$\frac{\underline{X}(s)}{\underline{U}(s)} = \left(s\boldsymbol{I} - \boldsymbol{A}\right)^{-1}\boldsymbol{B} \tag{6.8}$$

In effect this basic generic formula can be used to define transfer functions illustrating the relationships between many system variables. However, to remain in keeping with similar studies, *Pausder and Jordan (1976)*, the transfer functions were derived to relate the Euler angles, (i.e. ϕ, θ, ψ) to the particular pilot control that is most influential, for example pitch angle (θ) to longitudinal cyclic (θ_{1s}). In addition a rudimentary model of the helicopter actuator dynamics was included. For the Westland Lynx, *Padfield (1981)* defines an appropriate transfer function for the actuator dynamics in the longitudinal and lateral cyclic pitch channels to be,

$$Y_A(s) = \frac{1}{1 + 0.125s} \tag{6.9}$$

The entire system was then modelled as shown in Figure 6.4.

To demonstrate the point, the longitudinal Acceleration/deceleration task, Figures 4.13 and 5.2 was selected from the ADS type flight test manoeuvres developed in Chapter 5, section 5.1. It is assumed that the manoeuvre is flown primarily with one control in a single-axis fashion. This may seem to be an over simplification, but there are several reasons that permit this assumption. The Acceleration/deceleration does to large extent use one control to fly the manoeuvre, (longitudinal cyclic). Additionally though, Helinv can be thought of as inherently containing the perfect pilot as in essence perfect manoeuvres are flown, thus implying perfect control inputs. Such a piloting strategy will undoubtedly reduce the amount of off-axis control inputs, again making the manoeuvre a more single-axis case.

A further requirement is to define various levels of manoeuvre aggression (based on flight speed and ADS-33D required pitch attitude) for the Acceleration/deceleration manoeuvre. Table 6.2 illustrates the target levels of aggression set for the task, and the corresponding parameter that was adjusted to alter the aggression level of the manoeuvre. The levels are similar to those aggression levels used in flight trials at DERA, Bedford and documented in *Howell and Charlton (1997)*. The ADS document requires that the specific pitch attitude of 30 degrees nose-up should be attained just before coming to the final hover in the Acceleration/deceleration manoeuvre. It was found that this could be achieved by using only the velocity of the vehicle as the aggression parameter. In effect the time taken to achieve maximum Acceleration/deceleration as well as the value of the maximum Acceleration/deceleration can be specified as aggression parameters. The trim condition selected for the simulation was based on the higher aggression case, i.e. 40 knots steady level flight. Upon converting the state-space formulation to transfer function format the equation relating pitch attitude to longitudinal cyclic was found to be approximately,

$$\frac{\theta(s)}{\theta_{1s}(s)} = \frac{s^{10} + 26s^9 + 576s^8 + 4657s^7 + 17989s^6 + 30501s^5 + 39279s^4 + 22775s^3 + 3545s^2 + 168s + 2}{s^{11} + 24s^{10} + 226s^9 + 1067s^8 + 2572s^7 + 3763s^6 + 3879s^5 + 1877s^4 + 543s^3 + 175s^2 + 19s + 0.0005} \quad (6.10)$$

The above equation is relevant in the context that it presents an approximation of the Lynx aircraft in steady level flight at 40 knots. The relevant Eigen Values of the characteristic equation and the corresponding modes (see Figures 4.1 and 4.2) as

identified by *Padfield (1996)* are presented below,

$s = -10.24$	Roll Subsidence
$s = -5.04 \pm 3.37\,i$	Rotorspeed
$s = -2.37$	Heave Subsidence
$s = -0.43 \pm 1.39\,i$	Dutch Roll
$s = -0.57$	Pitch Subsidence
$s = 0.01 \pm 0.33\,i$	Phugoid
$s = -0.12$	Spiral Subsidence

It can be seen that there is only one pair of positive unstable roots (Phugoid) which is not of a large enough value to seriously influence the stability of the vehicle over a short time period. The transfer function is therefore adequately stable for the pilot model to track the input pitch angles from the three Acceleration/deceleration manoeuvres, since they can be completed within this time frame.

In this instance the tracking ability of the pilot model is not hindered by the Lynx transfer function relating pitch angle to longitudinal cyclic, since it is stable enough over the required time period (time taken to complete the Acceleration/deceleration manoeuvre). By choosing not to reduce the model into longitudinal and lateral components, there will clearly be some aspect of cross-coupling involved hence making the task of compensatory tracking more difficult for the pilot model. However, it was assumed that leaving the model in its current form (providing a relatively stable flight condition could be found) would provide a more accurate representation of the real aircraft, and consequently the parameters obtained from the optimisation algorithm may be more realistic. That said it is difficult to speculate whether or not a real pilot would operate in order to numerically optimise gain, lead and lag time associated with the task at hand.

6.5 Optimisation of Pilot Model Parameters Using Helicopter Transfer Function

The helicopter transfer function developed above, Equation 6.10 was used in

the optimising algorithm with pitch attitude data from the Acceleration/deceleration flight test manoeuvre as input functions (3 levels of aggression with 3 corresponding pitch angle time histories). After inputting the time history of each pitch angle time history and comparing it with the system response (output) an error vector was generated. Minimisation of this error vector resulted in the calculation of numerically optimum pilot model parameters (equalisation network) for the manoeuvre and each level of aggression. The system was set up and the optimisation process run, in an identical manner to that described in section 6.2.3.

The results obtained can be seen in Table 6.3 - Part 1. The lag times are seen to take on the value of the lower limit set in the optimising algorithm boundary conditions, and this seems to support previous studies. It is possible to conclude that the lag contributes to a numerically optimum solution or minimum error by approaching zero. The gain and lead time adopt the pattern also seen previously where the high aggression (high velocity manoeuvre) and low aggression (low velocity manoeuvre) cases have very similar optimum values. It is the gain and lead time constant of the medium aggression (mid velocity manoeuvre) case that varies from the similar values of the other two.

Additional studies were conducted using a number of other flight test manoeuvres based both on ADS descriptions and nap-of-the-earth type manoeuvres, see Table 6.3 - Part 2. The lag results are the same in all cases and remain at the lower limit of 0.1 seconds while the gain and lead time results tend to form one of two patterns. The first follows a diminishing gain and increasing lead pattern whilst the other confirms the trend of the above medium aggression manoeuvre case where the gain and lead time constants seem to vary in an almost random fashion when compared to the low and high aggression tasks.

It terms of handling qualities, some consideration was given to the possibility of determining if there was some correlation between the HQ levels and the associated pilot model parameters that were numerically optimised for each manoeuvre. Although it is possible to determine a relationship, *Pausder and Jordan (1976)*, the worth of doing so was not thought to be significant in this instance, since this method generally requires the introduction of a new technique for estimating

handling qualities levels; (i.e. there is no direct correlation between pilot model parameters and ADS HQ Levels). It was postulated that this might confuse the issue of the handling metrics already discussed, and would ultimately have little substantiated worth, when compared to those already developed by ADS. Consequently the conclusion was drawn that the parameters calculated via the SQP optimisation process, were optimum only in a numerical sense and do not necessarily relate to the actual performance of a real pilot operating under similar circumstances. That said, it is more than likely that there is some kind of connection between the pilot model equalisation network and handling qualities levels, the problem lies in making the association in the first instance and having some method of testing and evaluation.

Figures 6.5a to c illustrate the input reference time histories (solid line) of pitch angle and the subsequent system output (broken line). The medium aggression case is seen to be the more oscillatory and produces overshoots at the pitch angle extremities. The lag offset is clear in all three figures and it is reasonable to assume that if this value were zero the tracking accuracy would be increased. It would seem that using the 40 knot trim condition transfer function (obtained from the conventional simulation version of HGS) relating pitch angle to longitudinal cyclic is more favourable and yields better tracking solutions for the low and high aggression tasks (i.e. the pitch angles obtained from the low and high velocity Acceleration/deceleration manoeuvres). The medium aggression manoeuvre, pitch angle, when passed through the system produces a poorer response and a lesser degree of tracking accuracy.

6.6 Pilot Modelling and the Effect on Handling Qualities Level

Although the pilot model is supplied with numerically optimum parameters calculated from the optimisation algorithm, it is assumed that a well-trained, motivated pilot will operate in a near optimum manner thus permitting the use of numerically optimum values for the equalisation network parameters. In essence, it is the effect of the human limitations that influence the final pitch attitude output in the case of the Acceleration/deceleration flight test manoeuvre and this is clearly seen in Figures 6.5a to c. Using the pilot model influenced time histories of pitch attitude

(broken line Figures 6.5a to c) and the time histories from Helinv (solid line Figures 6.5a to c) with an appropriate objective handling qualities metric (pitch attitude quickness), the effect of the pilot model on the handling qualities level can be seen.

6.6.1 Pitch Attitude Quickness Calculations for Pilot Model Influenced Time History of Acceleration/deceleration Flight Test Manoeuvre

The time histories from Figures 6.5a to c were used to obtain pitch attitude quickness parameters. For the purpose of comparison both Helinv and the pilot model influenced time histories are used. The results are plotted on attitude quickness charts, Figures 6.6a to c, representing the Low, Medium and High aggression cases respectively. There are two important conclusions that can be immediately drawn from the charts. Initially the quickness values based on the pilot model pitch attitude do not fall into pairs as readily as those points calculated from Helinv. Since pairs of points are a direct result of symmetrical manoeuvre mathematical modelling, it can be said that the effect of the pilot model is to make the manoeuvre response more realistic as, even in a symmetrical task, the pilot will not make identical control inputs. Furthermore there are less attitude quickness parameters in the Level 2 region of the charts, Figures 6.6b and c. The explanation for this resides in the fact that there are actually fewer small-scale changes in the pitch rate resulting from small oscillations observed in nap-of-the earth flight. One final observation is that the pilot model adopts a slightly different piloting strategy since there are more quickness points in the Level 1 region. This effectively corresponds to a greater number of larger control inputs (most likely to be guidance) in the task 'flown' by the pilot model.

If the task were subjectively rated it is possible that a lower work rating would be returned for the pilot model influenced pitch attitude. Reasons for this include the relative absence of Level 2 handling qualites level points and the evidence for larger control inputs. *Jones and Padfield et al (1996)* postulate that the higher value parameters are related to aircraft guidance (lower frequency control inputs), while the lower value quickness parameters are related to vehicle stabilisation and have shorter periods of input between them, thus implying a higher degree of workload. They do however admit that there is a large degree of overlap and it is difficult to speculate on

such matters using objective methods alone. The method does show promise for pilot modelling and its application to inverse simulation and corresponding quantitative handling qualities analyses.

Chapter Summary

The results from inverse simulations were used to develop a novel approach of estimating the equalisation parameters within the precision pilot model. The method is generic and could effectively be applied to other forms of model. It was shown that the parameters varied considerably depending on the manoeuvre and the level of aggression exercised (where aggression in this instance was controlled by manoeuvre velocity). The approach offers an alternative method of estimating these parameters which, until now, relied on the method of using verbal adjustment rules.

It has been shown that using the pilot modelling technique with inverse simulation results, it is possible to create potentially more realistic influences on the corresponding handling qualities. This is extremely important since the objective or quantitative method of assessment using inverse simulation, although effective, is clearly lacking in any form of human influence. By using more sophisticated pilot models, adapted to optimum flight, it is possible to obtain a more accurate representation of piloted helicopter flight.

Chapter 7

A Case Study of Two Different Helicopter Configurations

It is the intent of this chapter to assemble several of the components that have been discussed thus far in the dissertation and present them as a demonstration of the usefulness of Helinv with particular reference to the potential of inverse simulation and handling qualites metrics. The standard aircraft model for use in Helinv is based on the Westland Lynx. By making several theoretical improvements it is possible to simulate an altogether different type of aircraft. The aim of the chapter is to illustrate the effects of such enhancements and present the results in the form of standard quickness charts illustrated in the previous chapter and the so-called pilot attack chart, introduced in this chapter. In this way it will be shown that initial conclusions can be drawn as to aircraft handling qualities and subsequently on mission effectiveness.

7.1 The Pilot Attack Handling Qualities Metric

Chapter 2 provided an overview of handling qualities and the associated objective and subjective metrics. The attitude quickness parameter was used to good effect in subsequent chapters where it was shown that it is possible to discriminate between the quickness values obtained from inverse simulation, flight data and a pilot/helicopter system response. The intention of this chapter initially is to introduce the pilot attack parameter discussed briefly in Chapter 2 and illustrate how it differs from attitude quickness. In general the term “quickness” is reserved for the assessment of the manoeuvre whereas “attack” or “aggression” pertains to pilot behaviour. In effect the metrics are computed in a mathematically similar manner although the information gleaned from them is substantially different. To demonstrate the potential of the metric, as in Chapter 6 the pitch axis (longitudinal cyclic stick) will again be given more serious consideration, while an example

calculation will be shown using the roll axis control inputs (lateral cyclic stick).

Pilot attack is calculated from the actual control displaced in order to accomplish the manoeuvre. For example, in the case of lateral manoeuvres it is mainly lateral cyclic that is applied to achieve the roll angle necessary before using collective to translate the aircraft. Thus the lateral cyclic attack parameter is calculated from,

$$\text{Pilot Attack } (Q_{p_{1c}}) = \frac{\dot{\eta}_{1c_{pk}}}{\Delta\eta_{1c}} \tag{7.1}$$

where,

$\dot{\eta}_{1c_{pk}}$ is the peak value in the derivative of stick displacement (lateral stick when applied to the roll case) and

$\Delta\eta_{1c}$ is the corresponding change in net stick displacement.

7.1.1 Example Pilot Attack (Lateral Cyclic) Calculations

At the time of writing there is no single method of identifying levels of workload from the pilot attack chart, as it is still a novel approach. However there are several interesting approaches in the literature that warrant further discussion. The typical form of the standard attack chart is illustrated in Figure 7.1 where each attack parameter is calculated from Equation 7.1. Upon analysis of a typical stick displacement time history for any manoeuvre, it is evident that the control activity can be divided into a number of discrete demands or inputs from the pilot. Each individual control action is characterised by a maximum stick rate and corresponding change in stick displacement, hence calculation of attack parameters or worklets. The attack parameters are calculated in a similar manner to the attitude quickness parameters, although they are plotted on an attack chart.

Figure 7.2a illustrates plots of lateral cyclic stick displacement and its derivative obtained from inverse simulation of a Rapid Side-step MTE, Figures 3.5 and 3.6 at medium aggression level (see Table 6.3). The pilot attack parameters are

calculated for the first three peaks on the time history and plotted on the corresponding attack chart, Figure 7.2b. It has been identified by *Padfield and Jones et al (1994)* that the points on the chart corresponding to the higher stick displacement values are associated with vehicle guidance, while those appearing in the region of low net stick displacement tend to be associated with vehicle stabilisation. Therefore those values plotted up and to the right of the chart are probably related to control inputs for accomplishing vehicle guidance. Lower values plotted at the bottom of the chart and near to the origin are more likely to be associated with manoeuvre stabilisation.

A problem that has been identified and analysed by *MacDonald and Bradley (1997)* is the method of partitioning of the attack chart into relevant areas of guidance and stabilisation. Several approaches have been looked at, including lines of constant attack, rectangular areas, hyperbolic lines and combinations of the aforementioned. It would seem that, based on experiment, the most suitable and effective method of chart partition enabling calculation of more realistic handling qualities ratings, is using horizontal bands of constant attack as illustrated on Figure 7.1.

A method has been identified and used to determine the pilot HQRs that is complex and beyond the scope of this dissertation, however a general overview is presented in Appendix F (Rule Induction). Using the methods of attitude quickness and pilot attack it is possible to present case studies, investigating manoeuvre aggression and helicopter configuration in relation to handling qualities. However, to do so, it was necessary to develop an appropriate representation of an aircraft that was hypothetically superior to the current model of the Westland Lynx.

7.2 Modification and Enhancement of the Westland Lynx Model

As stated in the chapter introduction, the aim is to develop a theoretically superior aircraft to the Westland Lynx and conduct a basic parametric study in terms of attitude quickness and pilot attack. The term superior in this context is meant to reflect the trend is modern combat helicopter design, a typical example being the Boeing-Sikorsky RAH-66, Comanche. This particular helicopter was designed to have low pilot workload by initially fitting the aircraft with a sophisticated flight

control system. In addition however, the external features of the aircraft were redesigned to enhance performance and agility. Specifically, the aircraft is fitted with a five bladed rotor, has a tandem crew seating arrangement, (as opposed to the side-by-side arrangement of the Lynx) and has a comparatively low mass due to the utilisation of composite materials. Advantages of the tandem arrangement, five bladed, lower mass aircraft, from an agility point of view are obvious, and include less frontal drag, lower roll inertia, enabling a higher roll attitude bandwidth, which should endow the aircraft with a more responsive performance. The Lynx data file in Helinv was altered to reflect the major modern features present in aircraft such as the Comanche, in order to generate some kind of representation of the helicopter. By conducting off-line inverse simulations of various manoeuvres and plotting attitude quickness and pilot attack charts the advantages of identifying possible advantageous or detrimental characteristics in either aircraft are clear.

Table 7.1 presents a full summary of the modifications made to the current Lynx model in order to endow the conceptual aircraft with supposedly better flying qualities. It can be seen that other parameters such as all-up-mass and main rotor, equivalent spring stiffness were altered with the aim of improving performance characteristics. The Westland Lynx data presented in Table 7.1 is based on data from *Padfield (1996)* and the modified data, although not representative of existing operational aircraft, is consistent with recent helicopter design trends as mentioned above. The parameters that were modified (with relevant explanations) were, starting with the main rotor:

- Number of main rotor blades increased from 4 to 5. It was assumed that an increase in the number of rotor blades would provide greater lift and hence performance in terms of achieving the required thrust as quickly as possible. In this case there is no significant weight penalty since the blades are comparatively low in mass.

- Blade chord increased to complement above, i.e. larger chord generates an additional increase in lift.

- Height of main rotor above fuselage reference point / rotor radius increased to add to the rolling moment which in turn should give the aircraft a higher roll rate capability, hence improving the chances of meeting Level 1 handling qualities in roll axis tasks. Furthermore high roll rate capability is a desirable feature in battlefield aircraft for threat avoidance, and/or quick concealment.

- Equivalent stiffness for centre-spring blade flapping model increased to represent next generation hingeless rotors. It is a fair assumption that aircraft such as the Comanche will possess a higher degree of equivalent spring stiffness thus increasing the value to improve overall rotor responsiveness is a valid development.

- Aircraft mass was decreased to reflect the use of modern composite materials in the fuselage and empenage. Coupled with increased rotor performance, the real aircraft should have a more responsive nature, and indeed previous inverse simulation studies, (*Thomson and Bradley, 1998*) have shown that a reduction in mass can lead to an aircraft with improved handling characteristics; i.e. attitude quickness points moved further into the Level 1 area of the ADS attitude quickness chart.

- Moment of inertia about the aircraft x-axis. The idea behind changing this parameter was a coupling effect of altering the vehicle's fundamental configuration from one of, side-by-side seating arrangement to tandem. It was assumed that such a change would make the aircraft considerably narrower, hence the aircraft would have a decreased plan drag area and lower roll inertia.

- Tail rotor solidity was increased to counteract the likelihood of increased torque produced by the main rotor.

- The fuselage X-force coefficient was halved in value to give a representation of the tandem seating arrangement, i.e. the aircraft is assumed to be half the width of the Lynx. Since the X-force coefficient is directly proportional to the fuselage plan area, (according to this modelling method) the assumption was made that halving the fuselage X-force coefficient would be in some way representative of an aircraft having a tandem seating arrangement. In effect the equations used by *Padfield (1996)*

(and of course HGS) are based on simple functions of fuselage incidence, sideslip, area, flight velocity and atmospheric conditions. It is realised that this is a crude approximation but nevertheless, for a first estimate, is in keeping with assumptions made so far. The point of the exercise is to conduct a parametric study of two helicopters with fundamental configuration differences thus highlighting the usefulness of inverse simulation and handling qualities metrics. There is no requirement at this stage to develop a high fidelity next generation rotorcraft model since relevant handling metrics are not fully in place and details about such aircraft are generally limited to basic configuration and aerodynamic properties.

7.3 Assessed Mission Task Elements

It was assumed that an adequate demonstration of the method could be achieved by examining a single flight test manoeuvre. In keeping with Chapter 6 primarily, and assessing the main flight test manoeuvres developed in Chapter 5, the longitudinal translation Acceleration/deceleration (Figures 4.13 and 5.2) task was selected for pilot attack analysis. The manoeuvre is defined in spatial terms, (earth based frame of reference), and in temporal terms, (each point in space is also defined as a point in time). The inverse simulation procedure can be repeated as many times as is desired with exactly the same results, since in effect, inverse simulation can be thought to possess the perfect pilot capable of flying a manoeuvre in an optimum fashion.

7.3.1 Flight Test Manoeuvre Aggression Levels and Other Flight Conditions

Table 6.3 is a summary of aggression levels specified for the pilot modelling work discussed in Chapter 5. The same aggression levels are adopted for this chapter and are merely target levels of aggression (mostly determined by speed and/or a required pitch/roll attitude angle). It was possible to achieve at least the required levels of aggression by altering manoeuvre velocity and it is evident from the results that this is the case. In addition to altering the level of aggression (velocity) for each manoeuvre, two further parametric studies were conducted. The first involved the use of a Stability and Control Augmentation System (SCAS). Only the mid-level aggression Acceleration/deceleration manoeuvre was flown with the SCAS activated,

the model of which is presented in *Padfield (1981)* and is based on an approximation of the standard Westland configuration. The SCAS is one half of the Automatic Flight Control System (AFCS), the remaining component being the Autopilot. In general the SCAS functions are realised through series actuators from pilot stick deflection to main rotor actuation. The autopilot, on the other hand, makes use of parallel actuators to apply the necessary functions. For completeness and immediate reference, a description of the SCAS system used in Helinv is given in Appendix E although in essence it comprises pilot controls, mechanical linkages, an actuation system and control rods.

An additional study was carried out, again featuring the medium aggression manoeuvre. Here the SCAS lateral and longitudinal cyclic actuator time constants, (τ_{c2} and τ_{c1} respectively) were altered in value. Two examples were simulated. The actuator time was set to provide instantaneous control deflection at the rotor, (i.e. $\tau_{c1} = \tau_{c2} = 0$ seconds) and finally, actuation lag time was defined as being double the standard value, (i.e. $\tau_{c1} = \tau_{c2} = 2\tau_{c1} = 2\tau_{c2}$ seconds). In this way the effect of simple enhancement or degradation of system performance could be examined and the results plotted on both attitude quickness and pilot attack charts.

7.4 Effect of Manoeuvre Aggression Level on Attitude Quickness and Pilot Attack

Importance is placed upon the fact that the overall Handling Qualities Rating (HQR) in aggressive manoeuvring tasks is based upon a pre-specified performance requirement (ADS-33D Level 1 attitude quickness) associated with the principal axis of the manoeuvre. For this reason inverse simulation is suited to such analysis as the objective component of the HQR can be predicted. It is the aim of this section to investigate the effects of manoeuvre aggression (or flight speed) on the attitude quickness and pilot attack.

Since ADS criteria define that attitude quickness should lie in the Level 1 region of the attitude quickness charts, it should be seen that this is the case and remains largely independent of the aggression level. Assuming the aggression levels

suggested by DERA, *Howell and Charlton (1997)* are within current, Lynx operational standards and should therefore yield handling qualities around the Level 1 region. This has a beneficial spin-off in that the manoeuvre models used in Helinv are validated from a handling qualities viewpoint. Indeed the aggression levels are representative of Advanced Flight Simulator (AFS) trials conducted at DERA, Bedford. Figures 7.3a and b respectively illustrate the attitude quickness and pilot attack chart for the Lynx configuration helicopter based on data obtained from the Acceleration/deceleration flight test manoeuvre. It is evident that the main quickness parameters associated with the gross features of the manoeuvre lie in the Level 1 region of the chart. Furthermore, the three aggression levels are plotted quite close together suggesting aggression level in this instance has little bearing on attitude quickness. This is not unexpected however as the three aggression levels are quite similar and in effect the aircraft will perform similar attitude changes in order to accomplish the task. The level of aggression exercised in this instance is therefore not responsible for altering the required attitude changes for this particular example of a flight test manoeuvre.

Examination of pilot stick displacement behaviour, Figure 7.3b is likely to reveal similar results to the attitude quickness chart, since in effect the aircraft attitude is being displaced to approximately the same degree at each aggression level (thus meeting ADS criteria). However, the aggression level is also dependent upon manoeuvre velocity and it is likely that the pilot will subjectively provide comments of increasing task difficulty as manoeuvre velocity is increased, since pilot gain is higher and manoeuvre forethought is less. Inverse simulation data is unlikely to reveal the effect of increasing velocity on pilot workload, since the aircraft will attain target levels of aggression independently of manoeuvre velocity (up to a point) and for a standard configuration aircraft model it is likely that the control stops will be reached beforehand. Therefore Helinv is recognised in this instance as a facility for the investigation of the main workload features inherently present in pilot stick activity. That said, the point is to illustrate that the objective component of workload can be determined from inverse simulation data and corresponding attack charts, which in turn provide valuable information about task performance, not obtainable from attitude quickness alone.

The Lynx Acceleration/deceleration pilot attack chart, Figure 7.3b, shows that for all three levels of aggression, the one hundred percent-per-second line is almost reached for one particular gross control input, suggesting that the Lynx configuration demands considerable pilot control inputs during execution of the manoeuvre. Additionally the highest values of pilot attack occur during the medium aggression manoeuvre. The attack chart though yields much more information about the stabilisation of the vehicle, seen as the lower attack values near the chart origin since attack parameters are assigned for stick rate peaks of positive amplitude and troughs of negative amplitude. Recall that the attitude quickness parameters are calculated from maximum attitude rate peaks between zero crossings and therefore will not show up this type of behaviour.

The greater number of attack parameters in the high aggression case are a consequence of a greater number of oscillations in the stick rate which in turn is a result of increasing manoeuvre velocity and task difficulty. Therefore it is likely that a greater number of attack parameters in the stabilisation region of the chart will lead to a higher workload rating being assigned by a pilot, thus the handling qualities rating will deteriorate.

In actual flight test conditions the effect of increasing flight speed (hence task difficulty) becomes ever more present in the form of so-called ‘constraint oscillations’ resulting from a modification of the dynamic characteristics of the aircraft due to the fact that the pilot is forced to follow a tightly defined flight path. In effect the pilot may find that some control actions required to perform the manoeuvre have to be input at frequencies higher than the reaction time (natural frequency) of the aircraft and higher workload results from the pilot’s attempts to improve ride quality. The phenomenon has been investigated using a linear version of HGS and a technique was developed for predicting the nature of the oscillations. The investigation is well documented in *Thomson and Bradley (1990b)* and will not be treated here. Clearly then, perceived aggression and associated workload (of this nature) are measures of aircraft agility in nap-of-the-earth flight[1] and discrepancies between vehicles of different configurations should present themselves in a handling qualities analysis. In

[1] It is assumed that the visual cues available to the pilot conform to ADS-33D UCE 1 conditions.

keeping with this statement, the following investigation aims to highlight the variations between two helicopter configurations, one with a hypothetically superior configuration.

7.5 Pitch Attitude Quickness

The initial approach was to examine the attitude quickness of each aircraft from inverse simulations of the Acceleration/deceleration flight test manoeuvre. An important point to raise is that ADS-33D defines the extent of the boundaries separating the various requirement levels for moderate amplitude pitching tasks such as the manoeuvre in question. However, in most cases it was necessary to extrapolate the boundaries to accommodate all attitude quickness parameters. Although no mention is made of the viability of doing so, it was assumed that such a step was necessary and appropriate.

Since much work has been published elsewhere regarding the calculation of attitude quickness of the Slalom family of manoeuvres, for example, *Howell (1995)*, the Acceleration/deceleration was selected to present similar studies from a different prospective, i.e. the longitudinal axis. The associated figures in the following sections are representative of ADS requirements and are shown at approximately the same scale to allow further comparisons. Additionally the plots are obtained from all levels of aggression for each aircraft and it is hoped that any particular configuration will generate a trend, distinguishable from alternative configurations. Since the effect of aggression level has been treated already it is assumed that further discussion is not warranted.

Figure 7.4a illustrates the quickness chart associated with the Acceleration/deceleration MTE for each of the two aircraft models. It is expected (as in the effect of manoeuvre aggression above) that the points lie in the same locale, as attitude quickness is largely independent of configuration since each aircraft is making similar pitch attitude changes to conform to manoeuvre requirements. However it is interesting to note that the Lynx configuration has a higher average in attitude quickness and more gross control input features, suggesting higher maximum peaks in the attitude rate time history. Furthermore, an increased number of the Lynx

points lie closer to the Level 1 region, suggesting that, although the conceptual aircraft performs a lesser number of attitude changes, the Lynx in this instance represents an aircraft with arguably better handling characteristics.

It is perhaps appropriate to include further discussion on the pitch attitude quickness chart given in Figure 7.4a, since confusion may arise from that fact that the attitude quickness points for each aircraft are not clearly separated as might be expected for two aircraft with quite different physical characteristics. There are several points that can be made about the closeness of the points in Figure 7.4a.

The first is of course that the results used to calculate and plot the attitude quickness chart are from off-line inverse simulations. In effect, the inverse simulation method forces the aircraft's centre of gravity to fly the prescribed trajectory no matter what the physical configuration of the aircraft. This of course is true up until some cut-off point where the physical control limits of the aircraft are reached and the manoeuvre no longer becomes physically possible. Since in this case both aircraft are clearly capable of performing the manoeuvre and attaining Level 1 handling qualities the fundamental difference is likely to be small, which indeed is the case.

Further, the manoeuvre model and input parameters for each helicopter case are obviously identical for each aircraft, i.e. required speed, time to maximum and minimum accelerations etc. are the same. This will in effect force each helicopter to fly manoeuvres that are identical, resulting in output time histories that are naturally going to be very similar. The differences in state time histories result from the fact that one aircraft is able to reach the required pitch angles (for Level 1 handling qualities) more quickly (Comanche type aircraft) and will also tend to return to a steady flight state more quickly resulting in less pitch attitude zero line crossings. Consequently the gross inputs of the Lynx are likely to be greater in number and amplitude. This indeed is the case, and can be seen from careful examination of Figure 7.4a.

A final point can be made in that, the pitch inertia of the advanced helicopter was not altered and is therefor not going to be a great deal different to that of the Lynx. Since the manoeuvre is flown entirely in the longitudinal plane, it is expected

that the pitch response of each aircraft is going to be similar. However, several other inverse simulation runs were conducted in the lateral plane (Rapid Side-step and Slalom manoeuvres) and it was seen that the advanced aircraft did indeed have a greater attitude quickness response. Results from the pitch manoeuvre have been presented to initially emphasise the point that attitude quickness is generally independent of configuration, except for gross configuration changes. In addition this leads to the fact that new additional metrics are required that are independent of vehicle configuration, manoeuvre type and are capable of analysing handling qualities characteristics in a way more directly related to the pilot. Thus the pilot attack analysis is carried out in Section 7.6, where the usefulness of the technique is more fully appreciated.

Before moving on however, it is interesting to note that the mathematical model of the Acceleration/deceleration flight test manoeuvre is excellent for capturing the gross features of the task. This is evident by the presence attitude quickness parameters in the Level 1 region of the chart, Figure 7.4a. The points lying in the Level 2 region will certainly degrade the perceived handling qualities level, even if they are associated with small scale inputs made over a very short period of time and are largely independent of manoeuvre guidance. Some of the attitude quickness values are very close to zero suggesting a very low peak in pitch rate, thus implying that the aircraft is merely 'settling' into a new flight state and it is likely that the pilot is required to make additional small control inputs.

7.6 Longitudinal Pilot Attack

In keeping with the previous study, the pilot attack investigation will concentrate mainly on differences that can be highlighted between the two aircraft using data from each manoeuvre at three aggression levels. Consequently, the effect of aggression level will not form the focus of the results since attaining the ADS Level 1 requirements force the aircraft to attain very similar pitch attitude displacements for each case, which in turn fixes the gross control displacements to similar values also.

It will be seen that pilot attack, although calculated in a similar manner to the

attitude quickness, reveals information that is considerably different. For example, many studies show the attitude quickness for different aircraft configurations in the ADS Level 1 region of the quickness chart, suggesting that the aircraft satisfies the requirements. An examination of the aircraft using pilot attack charts may present an alternative picture. The aircraft that requires greater pilot activity and hence workload will be evident from the pilot attack study, which could be advantageous in studies conducted in the early design stages of helicopters. Although the attitude quickness chart revealed the two aircraft to be quite similar, the pilot attack chart presents a considerably different story, since one aircraft is seen to require more pilot control inputs in order to accomplish the same manoeuvre.

Upon examination of Figure 7.4b the obvious difference with the attitude quickness chart is that there are many more points. Recall that attitude quickness is calculated from zero crossing peaks/troughs in the relevant time histories, whereas pilot attack is calculated from peaks/troughs whether the datum is crossed or not. A line representing one hundred percent of stick movement per second is plotted the attack chart and it is evident that the Lynx aircraft attack parameters approach this line more so than the conceptual configuration. This would suggest greater stick activity and it is a fair to assume the pilot workload is increased as a consequence. It would seem that the conceptual configuration allows the pilot to make less control inputs and those that are made, are not as large in magnitude when compared to the Lynx. From a mission effectiveness point of view logic would dictate that the chance of mission success would be higher for this aircraft.

7.7 Westland Lynx Studies

The Westland Lynx configuration will be used solely in the study of utilising the SCAS and altering the value of the cyclic actuator time constants. Only the medium level aggression manoeuvre is plotted on the charts in order to generate enough points to allow recognition of any trends that appear in piloting behaviour for each aircraft configuration. This is the first time an investigation of this nature has been carried out hence the investigation is quite straightforward, and the results obtained were not unexpected. It is perhaps useful to clarify the situation of using a SCAS, since it is not immediately obvious that all previous studies in thesis were

conducted without the use of the SCAS.

7.7.1 Effect of Utilising SCAS in Lynx Model

Recall from Section 7.5 where the pitch attitude quickness study was conducted, that the difference between the conceptual aircraft and the Lynx was not immediately obvious and thus the requirement for a further handling qualities metric was emphasised. In this instance the pilot attack parameter was used to highlight the differences between the two aircraft and in addition, explanations were put forward as to why the attitude quickness for each aircraft was very similar, especially in the longitudinal axis. The situation encountered in this section of the chapter is likely to be very similar in that, utilising the SCAS and altering the longitudinal or lateral actuator time constants is not likely to have a significant effect on the pitch attitude quickness. Again, this points out the need for an additional handling qualities metric that is associated with the pilot as opposed to the aircraft. Before presenting results from the study however, it is worth reiterating the reasons why this effect occurs.

Recall that this study involves the Lynx aircraft alone and inverse simulation results are presented from one manoeuvre. It is clear therefore that we are dealing with one model of the aircraft and one model of the manoeuvre. Since the very nature of inverse simulation is to force the aircraft's centre of gravity to follow a specific, tightly constrained flight path (defined by the manoeuvre model), it follows that the aircraft will do this no matter what additional conditions are present (including the effect of the SCAS). It is appreciated that in real life, or indeed conventional simulation there would be a requirement for some kind of stability augmentation system since the aircraft is free to respond to control inputs and of course the Lynx is naturally unstable. This is not the case with inverse simulation however, and the effect of the SCAS will really only serve to reduce the amount of workload (in terms of pilot stick movement) in the cockpit and this can be seen from the pilot attack results.

Appendix E presents an overview of the SCAS model used in Helinv. It can be seen that each cyclic channel includes a first order time delay to model the actuators at the rotor hub. It was postulated that altering the value of the actuator time

constants would considerably alter the piloting behaviour required to achieve the same manoeuvre. Initially though, the effect of actually utilising the SCAS throughout the manoeuvre was analysed to provide an insight into the possible usefulness of flight control augmentation systems. This has potentially important implications for the future of flight control system design. In effect the aircraft can be forced to fly the same manoeuvre with or without stability augmentation, and achieve Level 1 handling qualities in terms of attitude quickness, since this is largely dependant on the manoeuvre model that is used to drive the inverse simulation. However if the pilot attack metric is used and utilising a flight control system presents a significant advantage in terms of required control activity then the potential worth of such a system can be easily identified. Thus in this sense inverse simulation results and appropriate handling qualities metrics are again seen to be extremely useful in initial investigation of aircraft configuration and/or flight control system performance.

Figure 7.5a confirms the expectation that utilising a SCAS has absolutely no effect on the attitude quickness of the aircraft since attitude quickness is based on achieving the required ADS-33D standards (i.e. the manoeuvre), regardless of the method used (explained above). However, the diagram is useful for identifying individual points of attitude quickness. It is clear that each manoeuvre has seven points, three Level 1 points associated with the larger attitude displacements required to accomplish the manoeuvre and four associated with smaller zero crossing transients that are likely to be stabilising inputs. They are found in the Level 2 region, as the peak pitch rates are small in comparison to the associated change in pitch attitude.

Figure 7.5b presents the pilot attack chart for the same manoeuvre and at the medium level of aggression. This is where the usefulness of the pilot attack approach is realised. Now, although the longitudinal pilot attack chart shows that the SCAS has little effect on the required command inputs, since the points occur in close pairs, at least it does show some difference and it is not difficult to envisage a scenario where the effect of the SCAS is much greater (full authority system) and will therefor have an amplified effect on piloting commands. In this instance the rudimentary SCAS model coupled with the pitch inertia of the vehicle has a role to play in reducing the effect on pilot attack parameter calculations. In pitch the aircraft will still demand a lot of control input as the aircraft has a much higher inertia value. It is possible that in

roll the SCAS may be more advantageous since the roll inertia is less. Since the SCAS offers additional control movement in roll, it is likely that the aircraft can achieve a higher degree of agility for the same workload with the SCAS activated. However the net effect in pitch seems to be a very small reduction in the amount of longitudinal stick required flying the manoeuvre with the SCAS activated.

7.7.2 Effect of Altering Value of Cyclic Actuator Time Constants in Lynx Model

Altering the longitudinal cyclic actuator time constant during SCAS activation had no effect on the pitch attitude quickness for the reasons explained above and Figure 7.6a is testimony to this, which in effect is identical to the normal SCAS figure already illustrated.

However, examination of the longitudinal pilot attack chart, Figure 7.6b again allows the effects to be shown from a piloting point of view. Although it has been established that the main piloting components of flying each task lie in the Level 1 region of the attitude quickness chart, the point here is that more favourable conditions can be identified. The instantaneous actuation of the rotor blades (i.e. longitudinal actuator lag time constant set to zero) seemed most favourable as the corresponding attack parameters are the furthermost from the one hundred percent per second line and have a much lower net value of attack. The effect of doubling the longitudinal actuator time constant to 0.25 seconds has the general effect of initially moving the points further up the attack chart and further towards the one hundred percent per second line. This general diagonal trend has been recognised as the direction of increasing task difficulty and pilot workload, *Padfield and Jones et al (1994)*. Hence the pilot attack chart is seen to be extremely useful in identifying potentially advantageous configurations. Since this investigation is a simple one, the results serve to support logical reasoning; that said, the worth of the technique should not be underestimated.

It is appreciated that a common sense approach would most likely lead to similar conclusions being drawn from the above study. However, recall that the issue at hand is concerned with the demonstration of a technique which, even without the

aid of metrics to calculate specific pilot awarded workload ratings, is nevertheless very capable of illustrating desirable handling characteristics in different rotorcraft configurations. Furthermore the method is clearly capable of identifying desirable characteristics in any specific configuration.

7.8 Review of Results and Chapter Summary

The aim of this chapter was to present a parametric case study of two different helicopter configurations. One was based on data from the Westland Lynx and the other was assumed to be an initial representation of next generation rotorcraft. The studies initially highlighted the effect of manoeuvre aggression (in terms of increasing velocity), before directly comparing the aircraft using data from inverse simulations of the Acceleration/deceleration flight test manoeuvre.

It was not explicitly clear from the pitch attitude quickness charts that the conceptual aircraft was in any way superior and reasons for this were presented. The point was made that there was a requirement for an additional handling qualities parameter that could perhaps give a clearer distinction between the two aircraft. The pilot attack parameter was then used to identify possible advantages in either configuration. This proved to be a greater success and it was seen that at certain points in the Acceleration/deceleration manoeuvre, the Lynx required an increased amount of pilot control activity. The assumption was made that increased pilot activity mean a higher workload and hence it is possible that mission performance could be degraded.

To fully make clear the potential of the inverse simulation and the associated handling qualities metrics presented in the thesis, a large number of case studies considering different manoeuvres and aircraft configurations would have to be undertaken. For the purposes of this dissertation though, the number of manoeuvres that have been considered are representative of typical flight test manoeuvres conducted by military aircraft. By considering two aircraft configurations, handling qualities differences can be highlighted (although this was seen in this instance to be largely dependent upon the pilot attack parameter).

It is worth mentioning that the pilot attack handling qualities metric used in this chapter is not the only metric outside of attitude quickness. *Thomson and Bradley (1993)* for example have developed an alternative method. The technique analyses rotor blade, control deflections at the hub, after the pilot has input stick commands. The metric is calculated in much the same way as pilot attack. However, since recent trends (*MacDonald and Bradley, 1997* and *Charlton and Jones et al, 1997*) have focused on actual pilot behaviour and the development of associated attack charts with partitioning methods the emphasis currently resides with methods of obtaining physical pilot workload. The usefulness of Helinv and the developed workload metrics are only really seen when a study such as that described in this chapter is conducted. Helinv is seen to be versatile since a number of ADS, DERA and DLR flight test tasks are available in the manoeuvre library and there is an ability to inverse simulate up to four helicopter configurations at any one time. The handling qualities software offers a novel approach at tackling the pilot workload problem since it is purely objective and does not depend on subjective pilot opinion.

The chapter concluded with a study (using the Lynx helicopter alone) into the effects of initially switching on the SCAS model and then investigating the effect of altering the longitudinal actuator time constants in the model. It was shown that the attitude quickness parameter was incapable of distinguishing between the SCAS switched on and switched off modes. Again, reasons for this were put forward and explanations offered. However, the pilot attack parameter showed more promise at identifying which flight mode (SCAS on or off) could potentially offer advantages in terms of required stick movement.

Chapter 8

Conclusions

This final chapter presents a synopsis on the achievements of the research, with particular relevance to the aims and objectives set out in Chapter 1. Additionally, where relevant, particular problems that hindered the successful completion of the work are also mentioned. However, it is appropriate as well as important to focus on the overall objective of the thesis, which is rooted in inverse simulation and rotorcraft handling qualities. The development of a methodology whereby helicopter handling qualities can be assessed, at least in part, by a combination of inverse simulation and appropriate metrics is pertinent to the research undertaken at the University of Glasgow. The following text presents a general overview of the achievements of the thesis with particular relevance to each initial aim set out in Chapter 1.

8.1 List of Achievements, Conclusions and Additional Remarks

- Successful development of an inverse simulation technique that produces state and control information for initial assessment of handling qualities.

- HGS seen to be in the best possible form for handling qualities studies. It is unlikely that modelling additional higher frequency rotor states will have a significant effect on handling qualities.

- Development of new manoeuvres, not previously available in Helinv. The Slalom tasks were of particular relevance since they were based tasks used to assess the Westland Lynx in the large motion simulator, DERA, Bedford.

- Lag degree of freedom modelled but not implemented. It was postulated that such a modification would lead to large-scale simplification of HGS. Ground

Effect and discrete gust modelling was undertaken and completed.

- A novel technique for estimating the parameters within the Precision Pilot Model was developed. To date the author is aware of no other method of doing so. Initial study of human influence on handling qualities.

- Demonstration of the techniques developed by a parametric case study of two helicopters. The study illustrated that changes in configuration could potentially be recognised as advantageous or detrimental to handling qualites.

- An intensive review of current and previous work in the field of rotorcraft handling qualities was completed and presented. The work is pertinent to the entire thesis as well as timely, since rotorcraft handling qualities have become increasingly important and will undoubtedly extend into civil areas.

- The combination of work presented in this thesis and elsewhere within collaborating institutions is novel and represents a significant step towards the prediction of workload ratings.

8.2 Suggestions for Future Research

- Although comprehensive descriptions of flight test manoeuvres are given in ADS-33D, there is still room for additional support from a mathematical modelling point of view. In addition, the availability of flight test data is limited to certain sources, thus making manoeuvre confidence testing difficult.

- At present Helinv is practically the only inverse simulation software associated with the handling qualities side of rotorcraft. More sophisticated models (for example individual blade rotor models) are available for use and a comparative study would prove interesting.

- Assuming that the workload of any pilot from a flying point of view comprises guidance and stabilisation tasks, it would be desirable to implement a pilot

model within the inverse algorithm that would yield state and control time histories representing the pilot more accurately.

- This dissertation has, in part, explained the usefulness of inverse simulation. Perhaps the technology can be applied to investigate a wider variety of problems, relating not only to rotorcraft but many other vehicles and/or dynamic systems.

- The development of inverse tools and associated handling qualities assessment metrics permits investigation of advanced or indeed radical helicopter configurations. This may lead to the opening of new ideas and possibilities within the rotorcraft industry and reach fruition in next generation helicopters.

Concluding Remarks

The research presented in this dissertation has effectively shown one component of an on-going large-scale research project aimed at developing techniques to accurately predict pilot workload ratings for different vehicle configurations and manoeuvres. A significant breakthrough has come in the form of the pilot attack chart and correct implementation of workload metrics. Inverse simulation has shown promise in that it is a cheap and effective method to reproduce piloting strategies, which in turn reveal the locations of workload components. Continuing development of inverse techniques aimed at developing a more authentic pilot response is very much at the forefront of current research and will undoubtedly play a major role in future versions of the workload methodology.

This research has served to partially validate existing manoeuvre models as well as illustrate the usefulness of attitude quickness and pilot attack assessment techniques. It is clear that advantageous vehicle configuration alterations can be recognised very quickly. In short, much groundwork has been laid for the development of software tools having the potential to uniquely shape the future of rotorcraft handling qualities assessment.

Tables

Good Visual Environment		Degraded Visual Environment	
Precision Tasks	Aggressive Tasks	Precision Tasks	Aggressive Tasks
Hover	Turn to Target	Hover	Bob-up/Bob-down
Hovering Turn	Bob-up/Bob-down	Hovering Turn	Acceleration/ Deceleration
Landing	Vertical Remask	Landing	Rapid Side-step
Pirouette	Acceleration/ Deceleration	Pirouette	Slalom
Slope Landing	Rapid Sidestep		
	Slalom		
	Deceleration to Dash		
	Transient Turn		
	Pullup/Pushover		
	Roll Reversal at Reduced and Elevated Load Factors		
	High Yo-Yo		
	Low Yo-Yo		

Table 2.1 ADS-33D Mission Task Elements, ***ADS-33D (1994)***

	Level 1	**Level 2**	**Level 3**
Aerodynamics	linear 2-D dynamic inflow/local momentum theory analytically integrated loads	non-linear (limited 3-D) dynamic inflow/local momentum theory local effects of blade vortex interaction unsteady 2-D compressibility numerically integrated loads	non-linear 3-D full wake analysis (free or prescribed) unsteady 2-D compressibility numerically integrated loads
Dynamics	rigid blades (1) quasi-steady motion (2) 3 DoF Flap (3) 6 DoF Flap + lag (4) 6 DoF Flap + lag + quasi-steady torsion	(1) rigid blades with options as in Level 1 (2) limited number of blade elastic mdes	detailed structural representation as elastic modes or finite elements
Applications	parametric trends for flying qualities and performance studies well within operational flight envelope low bandwidth control	parametric trends for flying qualities and performance studies up to operational flight envelope medium bandwidth appropriate to high gain active flight control	rotor design rotor limit loads prediction vibration analysis rotor stability analysis up to safe flight envelope

Table 4.1 Levels of Rotor Mathematical Modelling, *Padfield (1996)*

Case 1: Acceptable HQ Transfer Function for Pitch Rate Motion of Fixed Wing Aircraft				
Period (s)	**Error**	**Gain**	**Lead (s)**	**Lag (s)**
100	1.2260	1.8000	0.1833	2.0907
20	1.7000	1.5000	0.3303	1.9562
1	2.7491	0.1000	0.1000	2.1000

Table 6.1 - Part 1 Pilot Equalisation Results for Acceptable HQ Transfer Function for Pitch Rate Motion of a Fixed Wing Aircraft

Pure Gain Transfer Function					Pure Gain and Integrator Transfer Function				
Period (s)	Error	Gain	Lead (s)	Lag (s)	Period (s)	Error	Gain	Lead (s)	Lag (s)
100	1.0989	1.2000	0.1584	1.5000	**100**	1.0110	1.0355	0.6000	1.7604
20	1.1121	1.2000	0.1183	1.4400	**20**	1.0763	0.6000	0.5000	0.7831
1	2.0940	0.1735	0.5000	0.5000	**1**	2.7492	0.1000	0.1000	2.1000
0.5	2.7806	0.1000	0.1000	2.1000	**0.5**	2.4938	0.4517	0.3000	0.1595
Pure Gain and Double Integrator Transfer Function					**Unnacceptable HQ Transfer Function**				
Period (s)	Error	Gain	Lead (s)	Lag (s)	Period (s)	Error	Gain	Lead (s)	Lag (s)
100	1.0396	0.1882	0.6000	0.1000	**100**	1.1963	0.1000	0.5000	0.3000
20	1.2230	0.1901	0.6000	0.1000	**20**	1.2138	0.1000	0.3000	0.1000
1	2.8141	0.1000	0.6000	0.1634	**1**	3.6491	0.1000	0.3312	0.1348
0.5	2.6869	0.2092	0.6000	0.1000	**0.5**	2.6562	0.1000	0.4000	0.1000

Table 6.1 - Part 2 Pilot Equalisation Results for Other Basic Dynamics

MTE	Aggression Parameter	Level of Aggression		
		Low	Medium	High
ADS-33D Slalom	Speed	40 kn	50 kn	60 kn
DERA Slalom	Speed	40 kn	50 kn	60 kn
ADS-33D R. S/step	Speed	25 kn	30 kn	35 kn
	Roll Attitude	8 - 12^o	18 - 22^o	28 - 32^o
ADS-33D Acc. / dec.	Speed	20 kn	30 kn	40 kn
	Pitch Attitude	8 - 12^o	18 - 22^o	28 - 32^o
NOE Acc. / dec.	Speed	20 kn	30 kn	40 kn
	Pitch Attitude	8 - 12^o	18 - 22^o	28 - 32^o

where,

Acc. / dec refers to the Acceleration / deceleration MTE

R. S/step refers to the Rapid Side-step MTE

Table 6.2 Target Levels of Aggression for Flight Test Manoeuvres

ADS-33D Acceleration / Deceleration				
Aggression	**Error**	**Gain**	**Lead (s)**	**Lag (s)**
Low	8.4873	0.1927	0.6000	0.1000
Med	8.8495	0.2074	0.1135	0.1000
High	9.4182	0.1906	0.6000	0.1000

Table 6.3 - Part 1 Pilot Equalisation Results for Helicopter Transfer Function and ADS Acceleration/deceleration Manoeuvre

ADS-33D Slalom				
Aggression	**Error**	**Gain**	**Lead (s)**	**Lag (s)**
Low	6.2244	0.2392	0.2250	0.1000
Med	15.6648	0.2293	0.2740	0.1000
High	40.6102	0.2183	0.2925	0.1000

Nap-of-the-earth Acceleration / Deceleration				
Aggression	**Error**	**Gain**	**Lead (s)**	**Lag (s)**
Low	5.1976	0.2072	0.4888	0.1000
Med	4.6473	0.1850	0.5995	0.1000
High	9.3557	0.1930	0.6000	0.1000

DERA Slalom				
Aggression	**Error**	**Gain**	**Lead (s)**	**Lag (s)**
Low	26.6468	0.2396	0.2000	0.1057
Med	88.0090	0.2170	0.3750	0.1000
High	-	-	-	-

Table 6.3 - Part 2 Pilot Equalisation Results for Helicopter Transfer Function and Other Flight Test Manoeuvres

Symbol	Description	Units	Lynx Value	Concept Rotorcraft Value
m	Aircraft Mass	kg	4313.74	3500.00
I_{xx}	Moment of inertia about the aircraft x-axis	kgm^2	2767.09	1383.54
c	Main rotor chord	m	0.391	0.45
b	Number of main rotor blades	-	4	5
K_β	Equivalent stiffness for centre-spring blade flapping model	Nm/rad	166352.33	332704.66
h_R	Height of main rotor above fuselage reference point / rotor radius	-	0.1986	0.25
TR_{Sol}	Tail rotor solidity	-	0.208	0.250
-	Fuselage X-force Coefficients from look-up tables halved in value	-	-	-

Table 7.1 Comparison of Westland Lynx and Conceptual Aircraft Parameters

Chapter 1 Figures

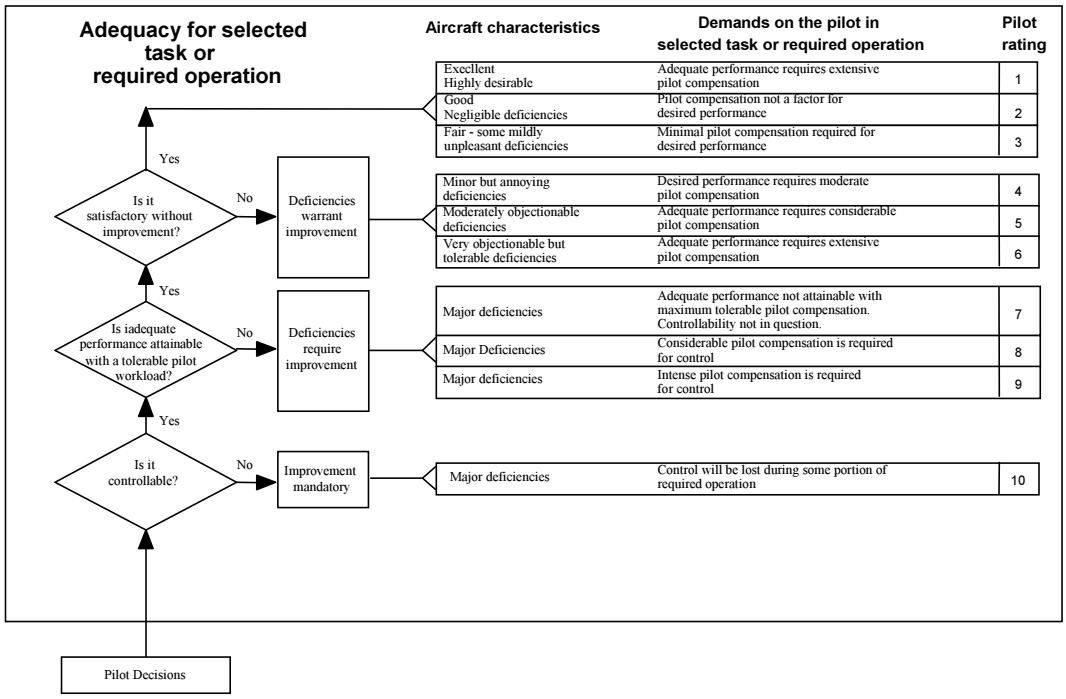

Figure 1.1 Cooper-Harper Pilot Rating Scale, *Cooper and Harper (1969)*

Chapter 2 Figures

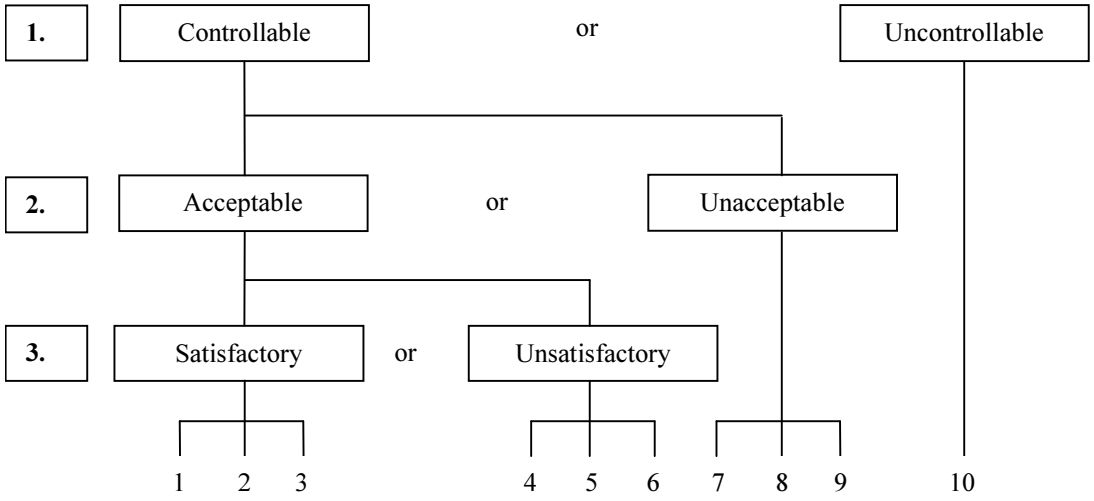

Figure 2.1 Major Pilot Decisions in Handling Qualities Assessment

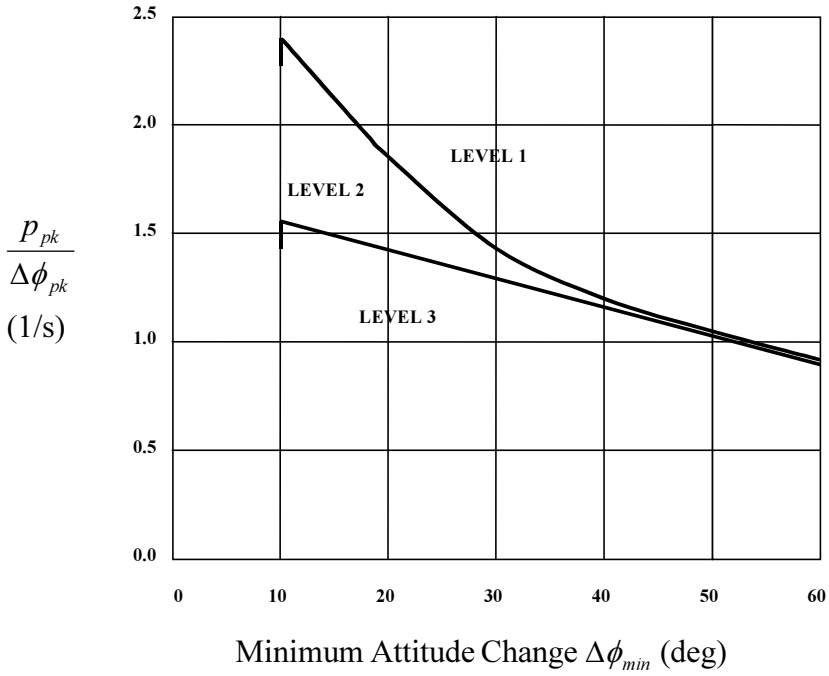

Figure 2.2a Roll Attitude Quickness, Target Acquisition and Tracking

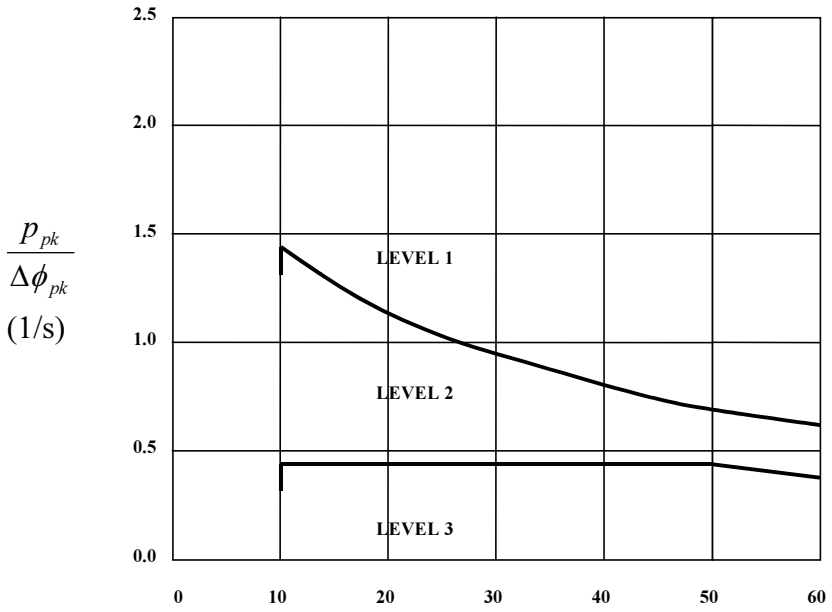

Figure 2.2b Roll Attitude Quickness, All other MTEs

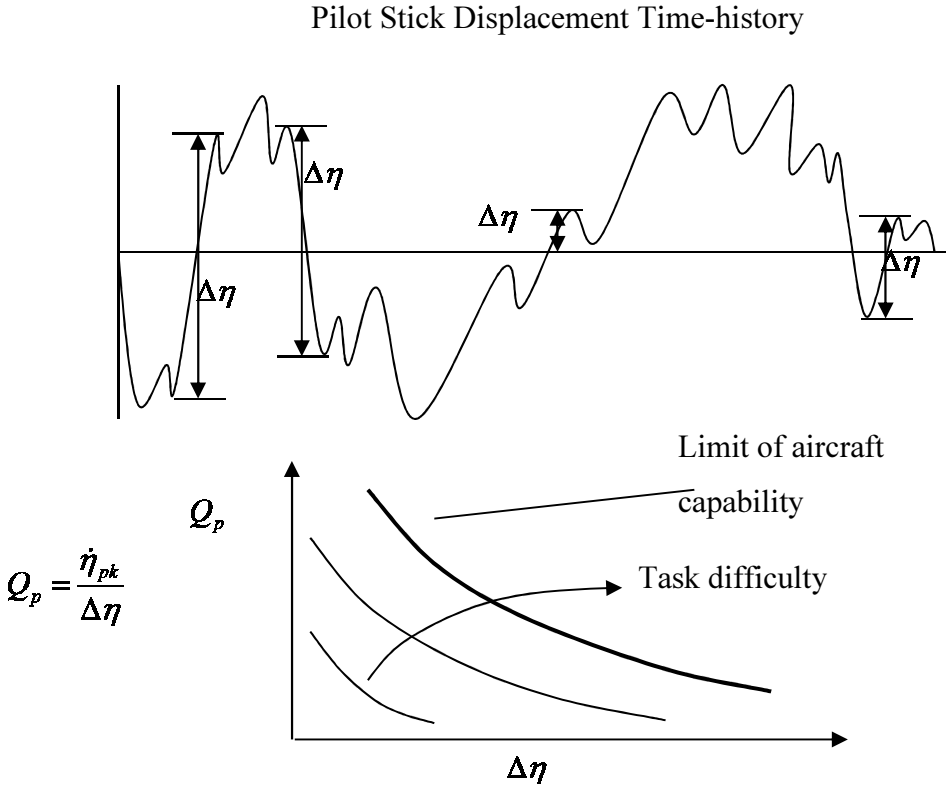

Figure 2.3 Conceptual Relationship between Pilot Attack and Task Difficulty

Chapter 3 Figures

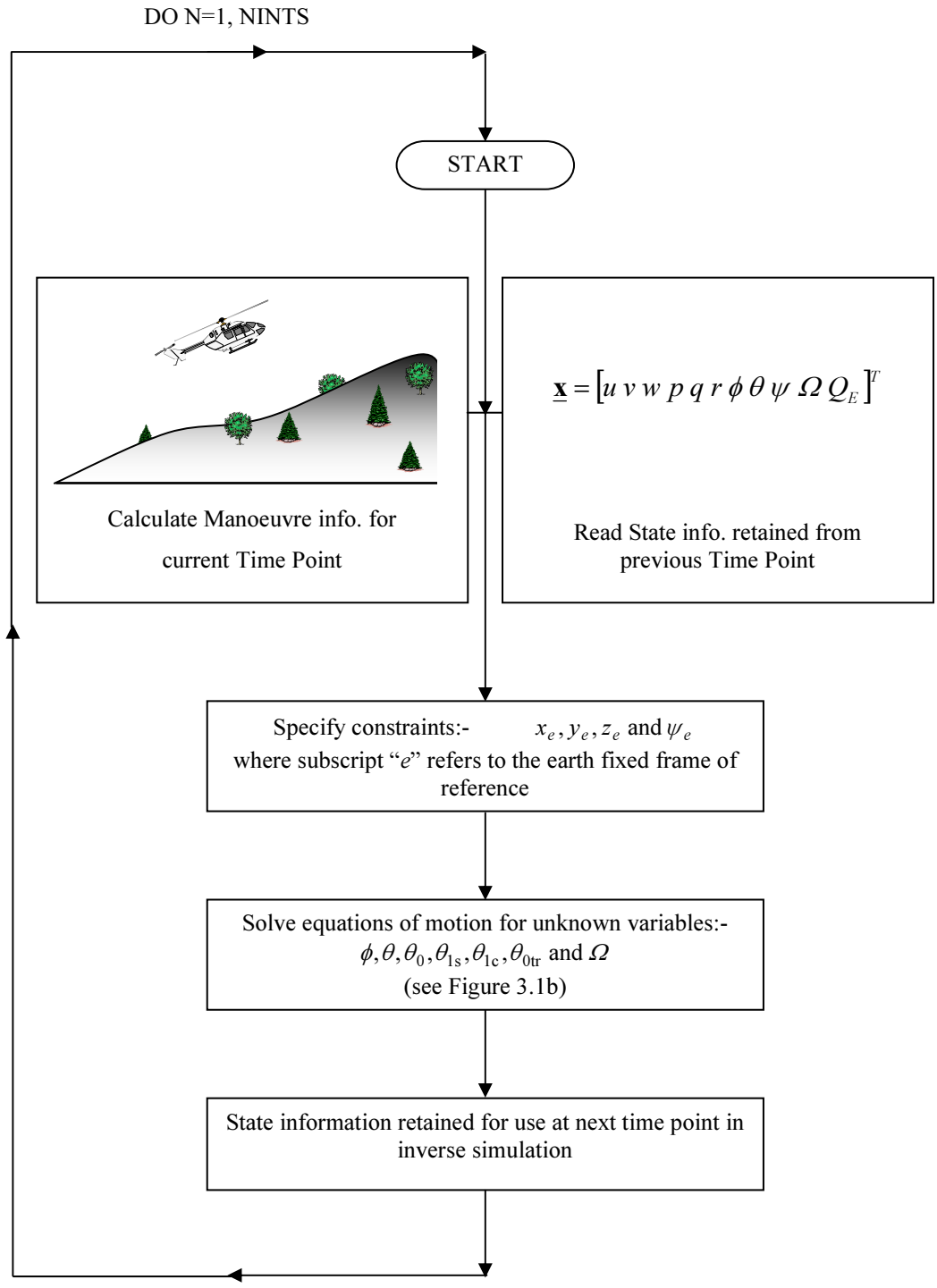

Figure 3.1a Basic Flow Chart of Inverse Simulation Technique

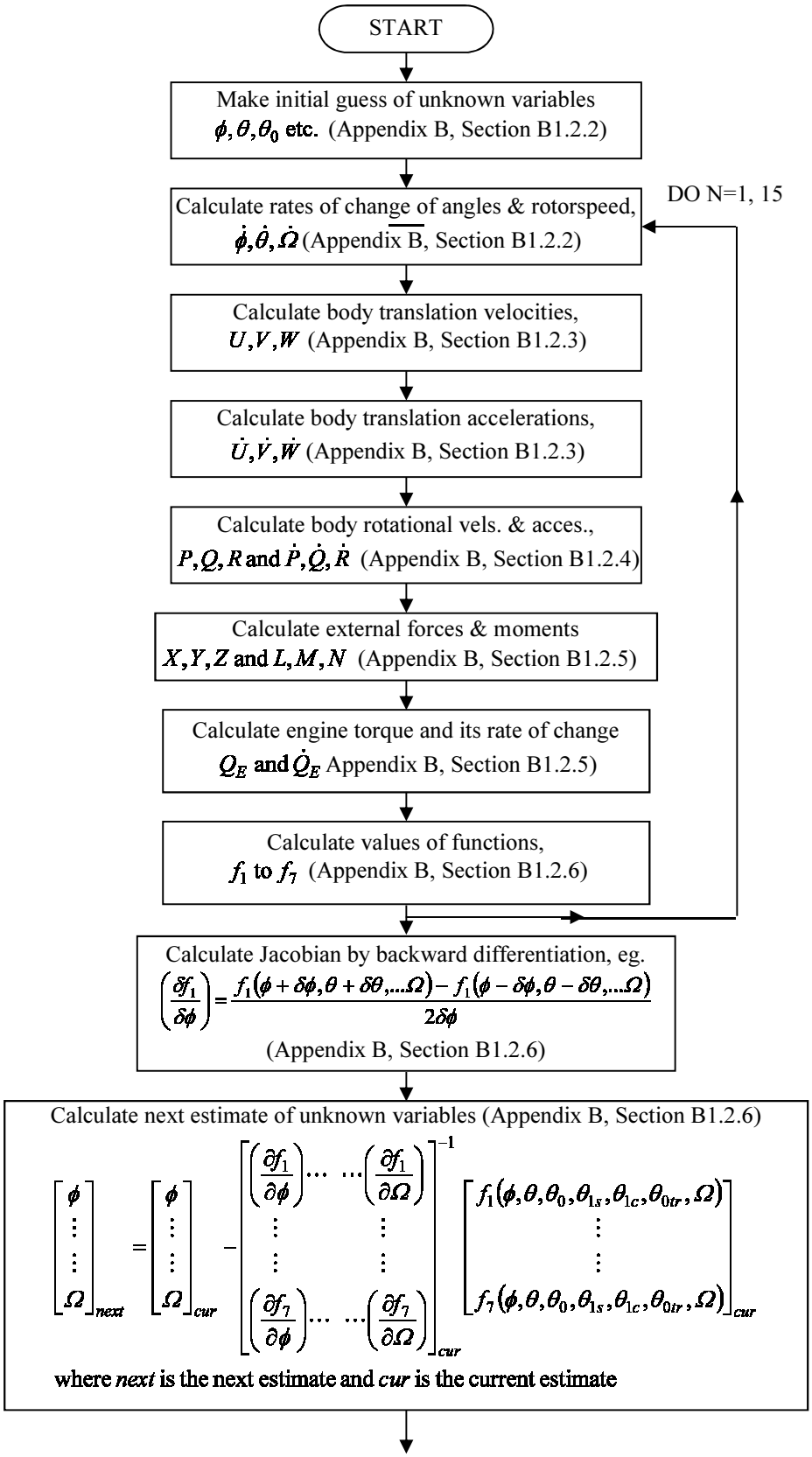

Figure 3.1b Flow Chart of Inverse Algorithm for Solving the Equations of Motion at each Time Point in the Manoeuvre

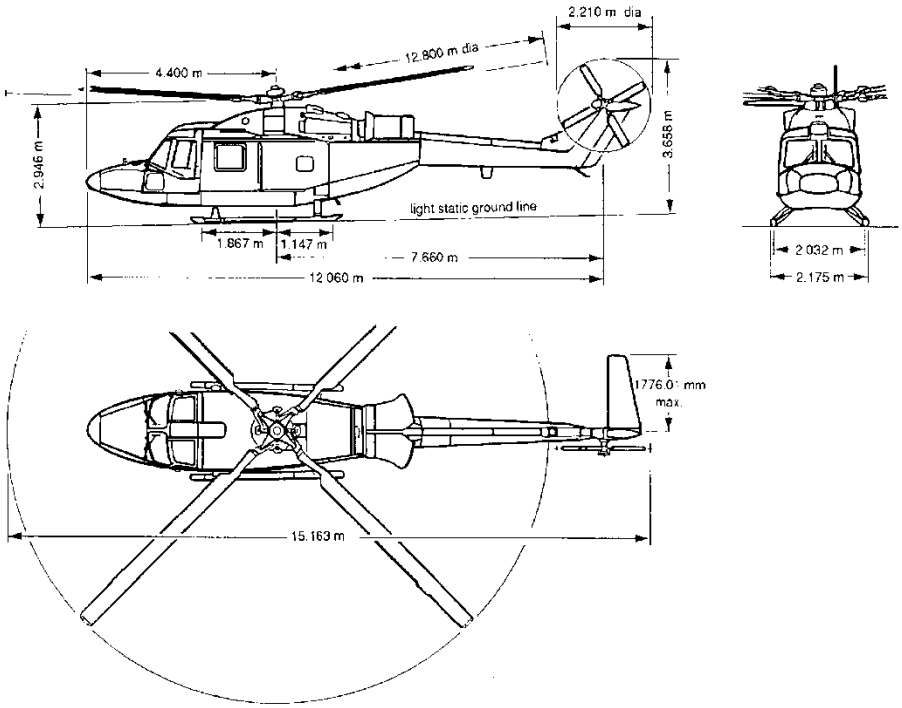

Figure 3.2 Westland Lynx, Mk. 7

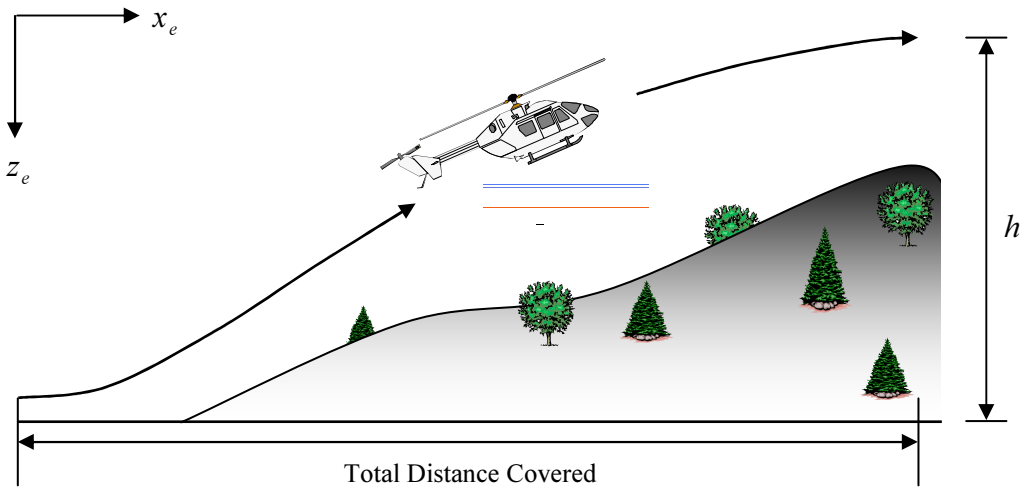

Figure 3.3 The Pop-up manoeuvre

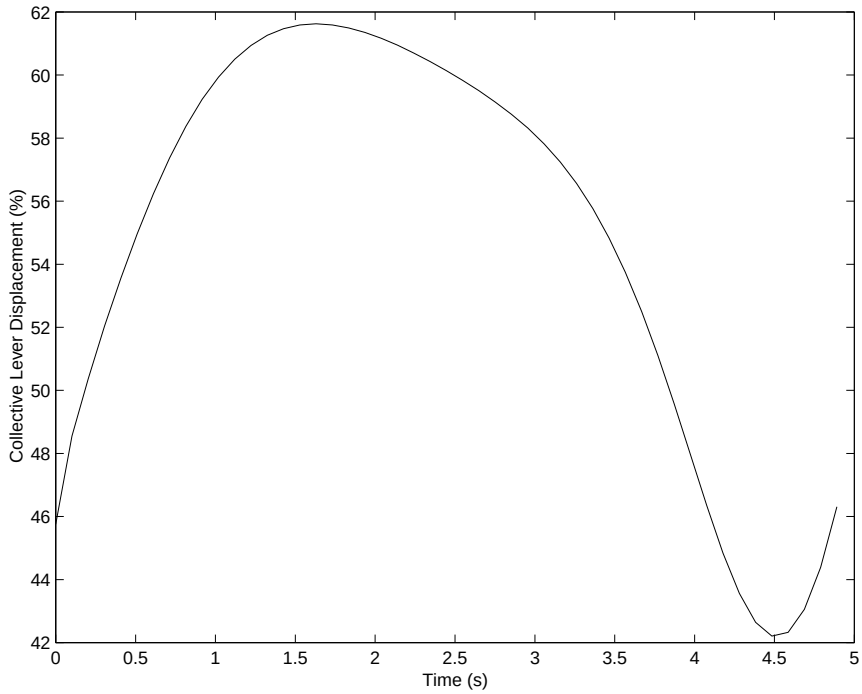

Figure 3.4a Main Rotor Collective Lever Displacement for Pop-up Manoeuvre

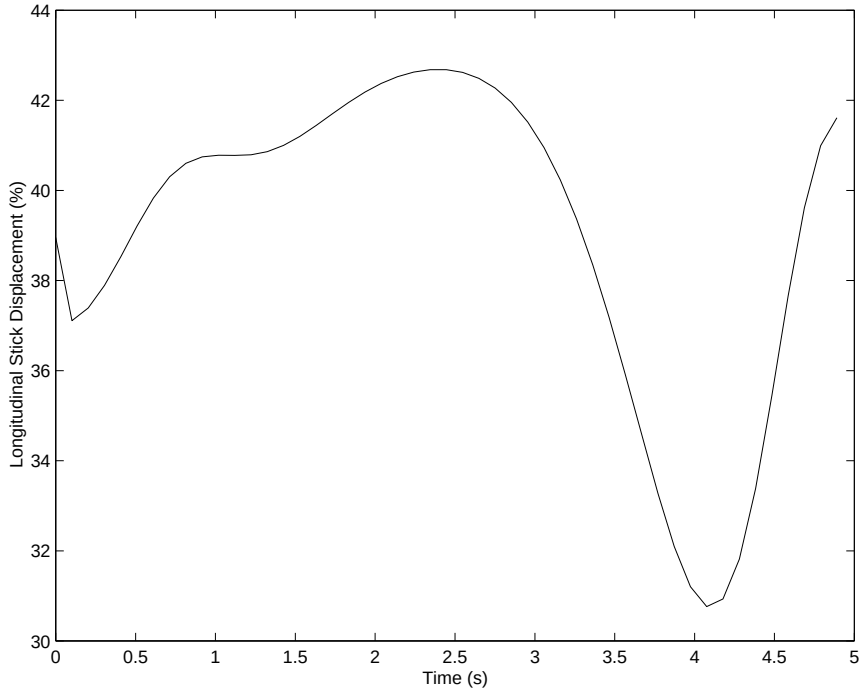

Figure 3.4b Longitudinal Cyclic Stick Displacement for Pop-up Manoeuvre

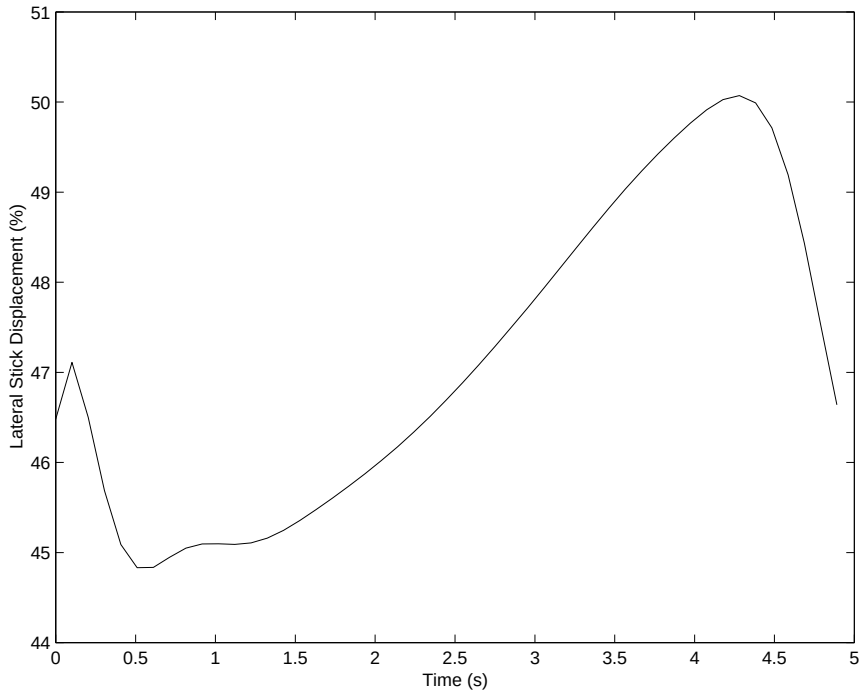

Figure 3.4c Lateral Cyclic Stick Displacement for Pop-up Manoeuvre

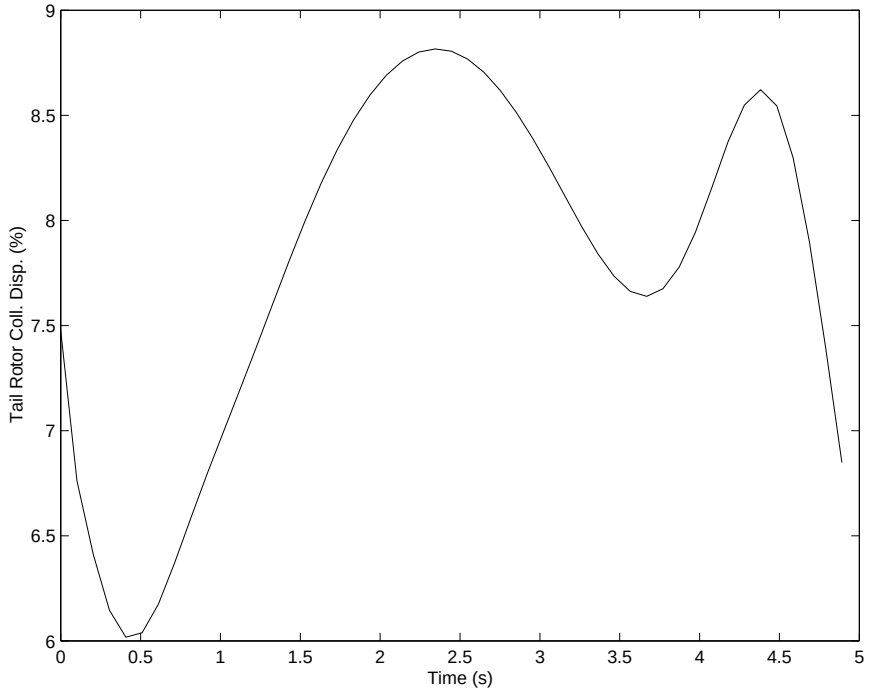

Figure 3.4d Tail Rotor Collective Pedal Displacement for Pop-up Manoeuvre

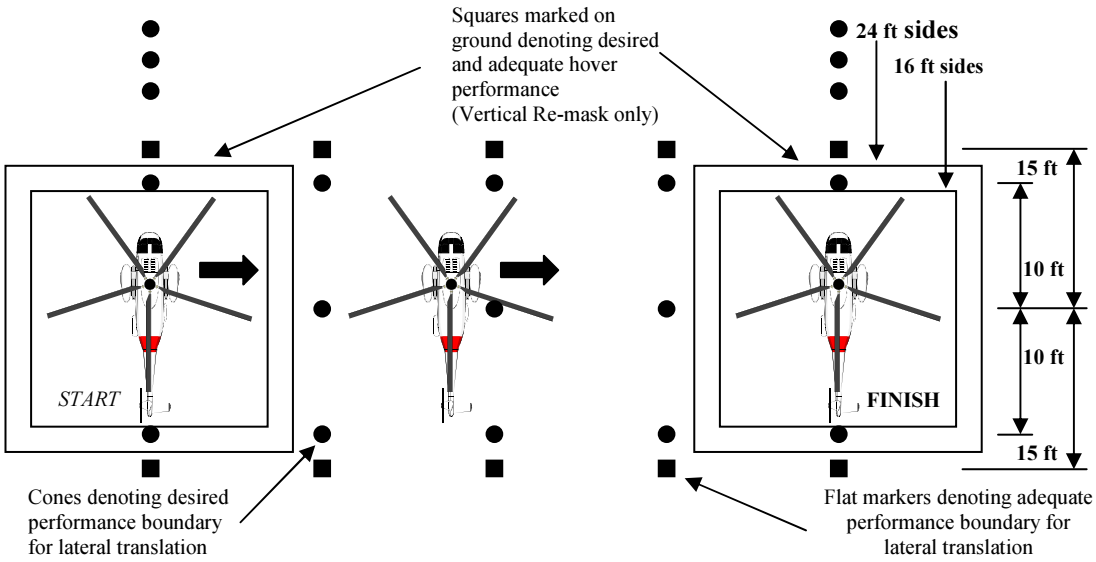

Figure 3.5 ADS-33D Course for Rapid Side-step

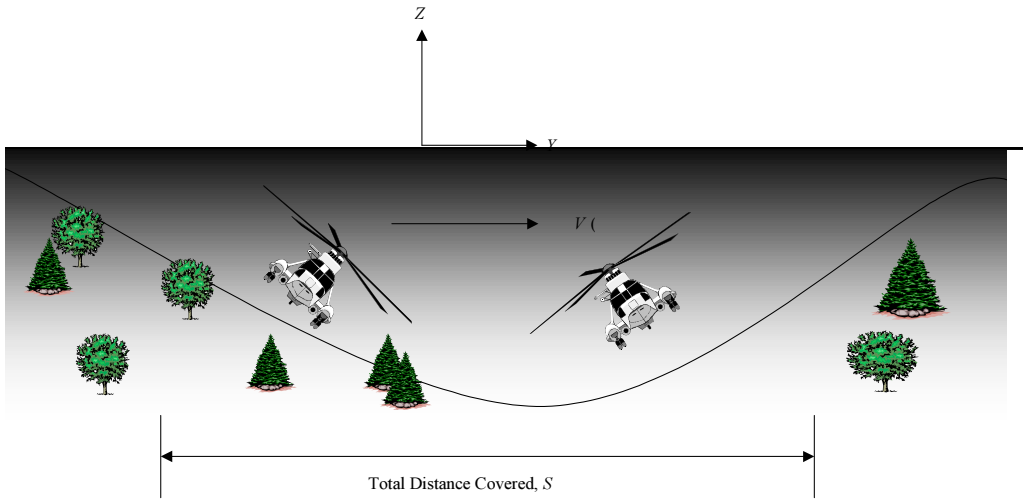

Figure 3.6 "*Mask-Unmask-Mask*" Application of Rapid Side-step Flight Test Manoeuvre

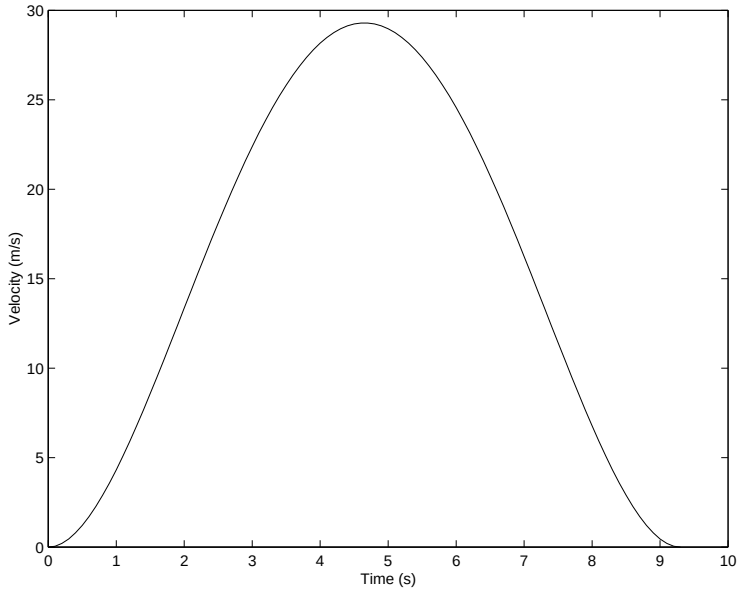

Figure 3.7 Plot of Lateral Velocity Profile of NOE Rapid Side-step

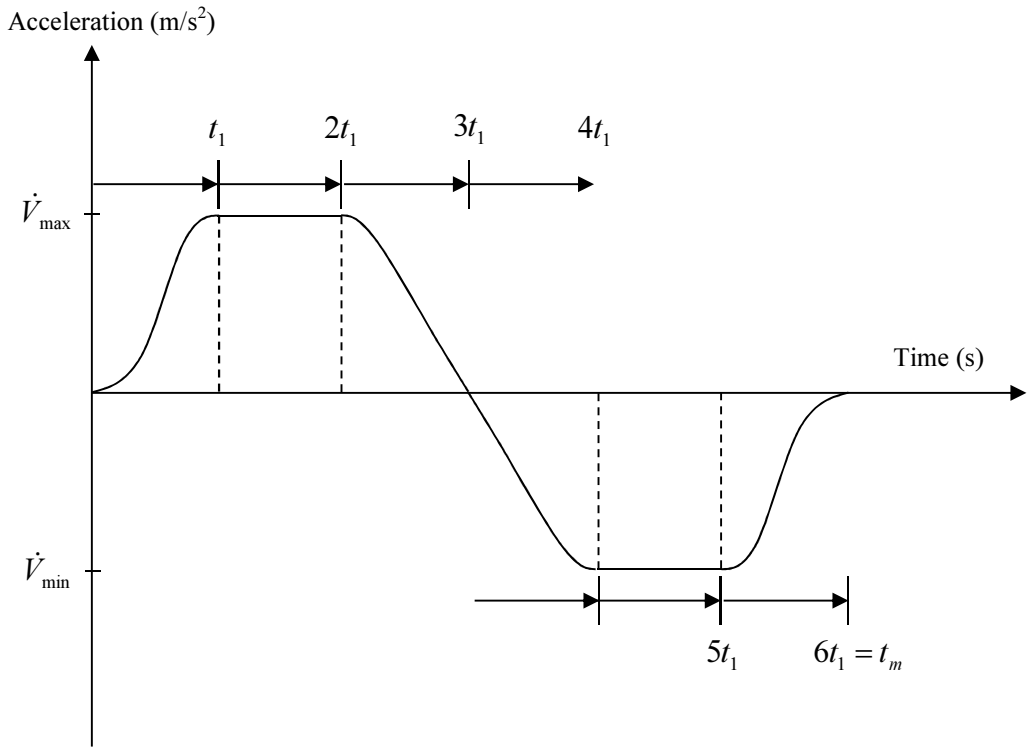

Figure 3.8 Lateral Acceleration Profile of ADS-33D Rapid Side-step MTE

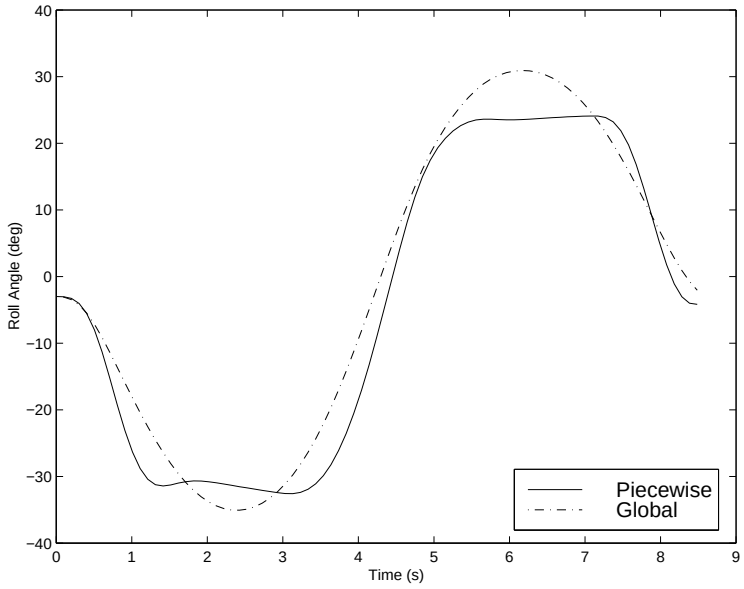

Figure 3.9 Comparison of Roll Angles from Rapid Side-steps Modelled Using Global and Piecewise Polynomial Methods

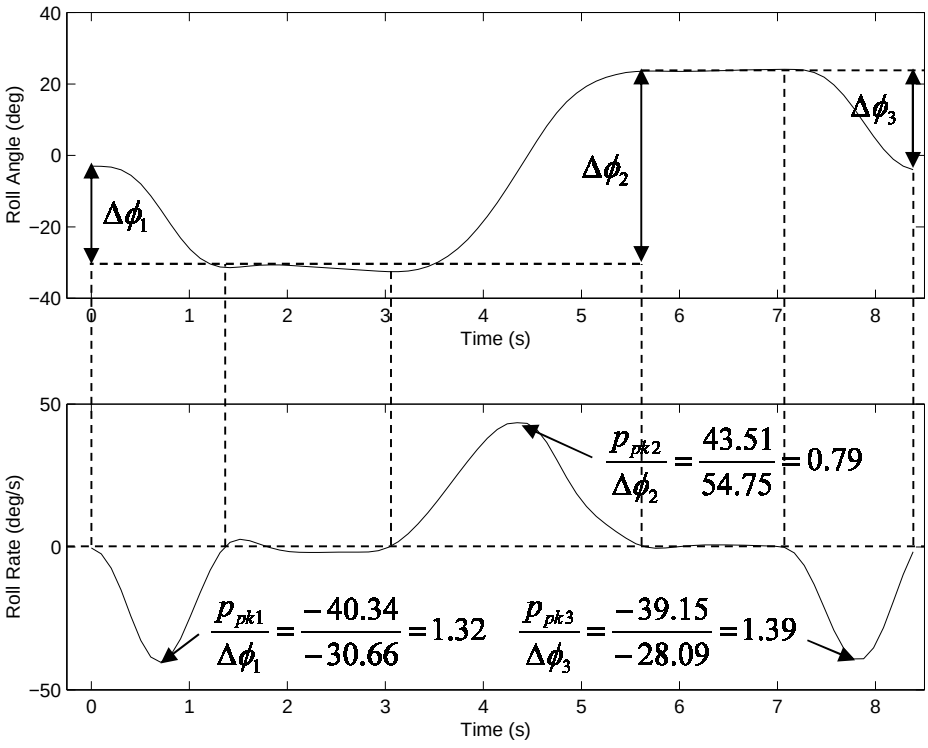

Figure 3.10a Calculation of Roll Attitude Quickness Parameters from ADS Rapid Side-step (Westland Lynx, 30 knots, Initial Roll to Port)

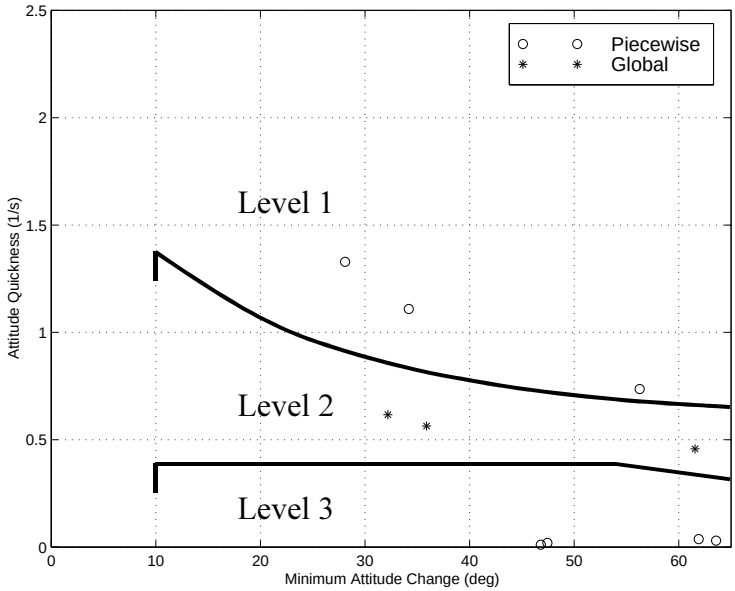

Figure 3.10b Corresponding Roll Attitude Quickness Chart

Chapter 4 Figures

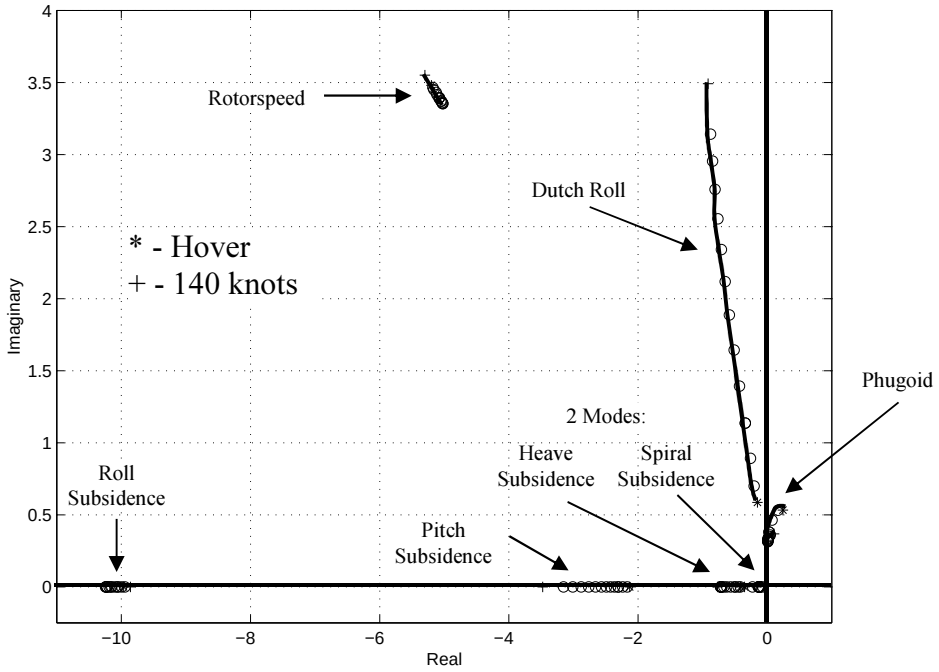

Figure 4.1 Loci of all Westland Lynx Eigenvalues

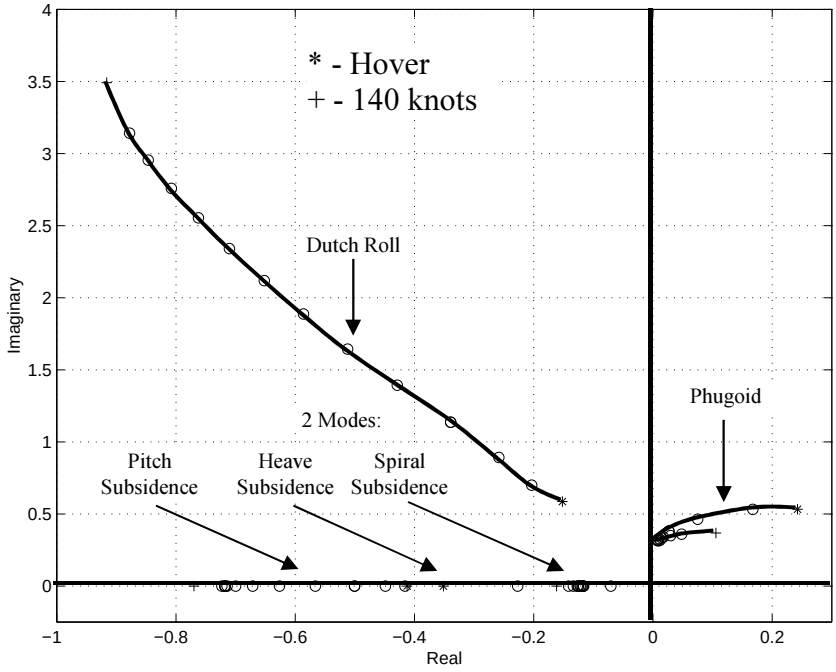

Figure 4.2 Loci of Westland Lynx Eigenvalues less than Unity on the Real Axis

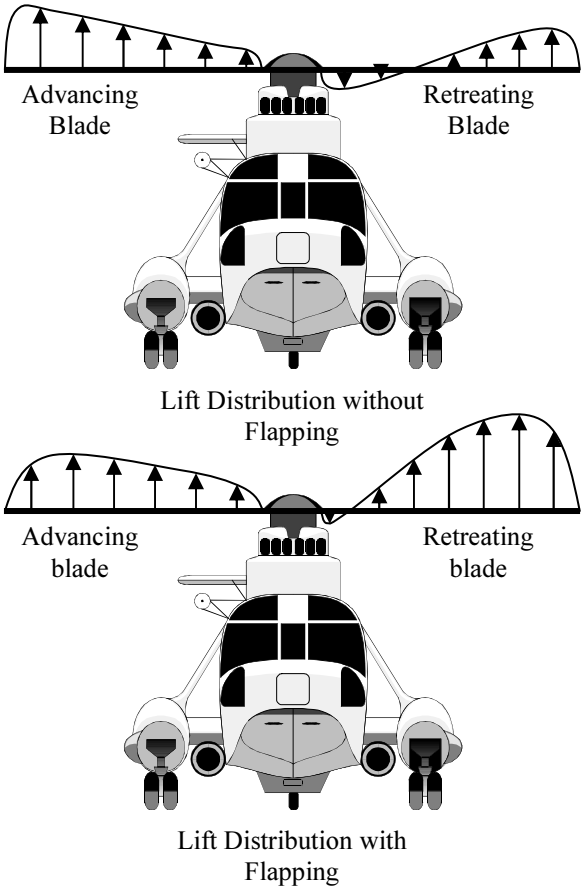

Figure 4.3 Effect of Blade Flapping on Rotor Disc Lateral Lift Distribution

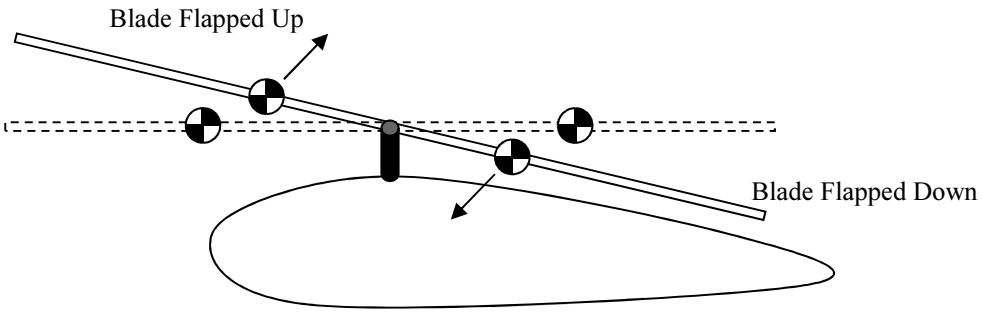

Figure 4.4 Blade CG Movement Due to Blade Flapping

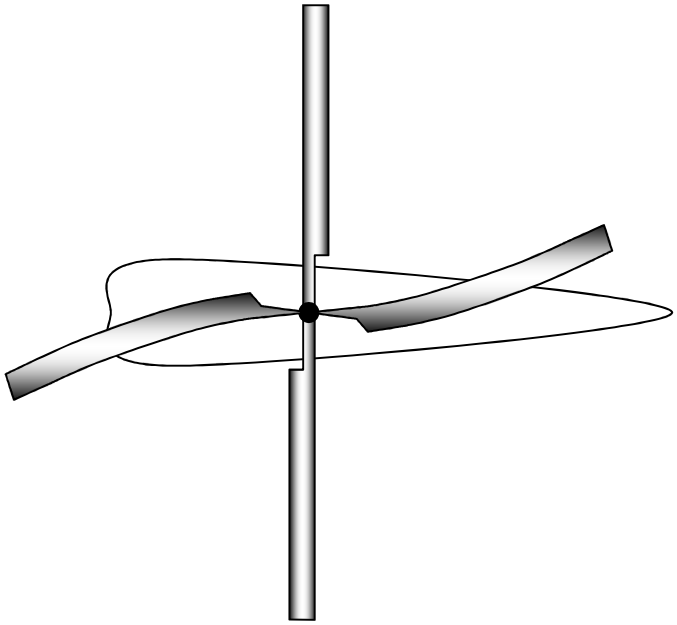

Figure 4.5 Blade Bending Due to CG Movement

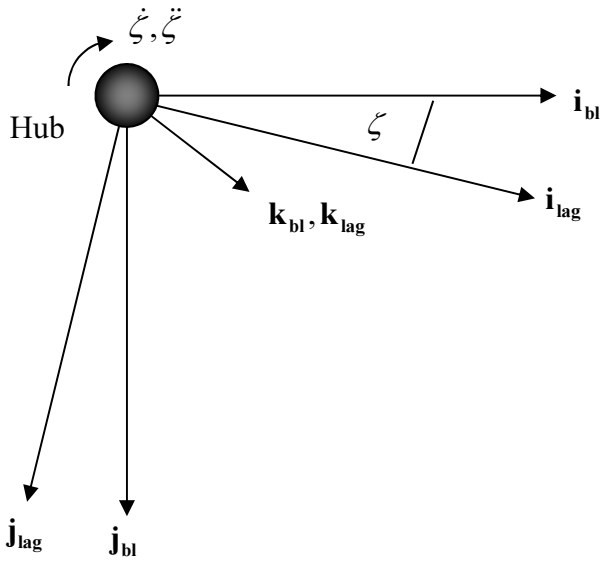

Figure 4.6 Blade to Lag Axes Transformation

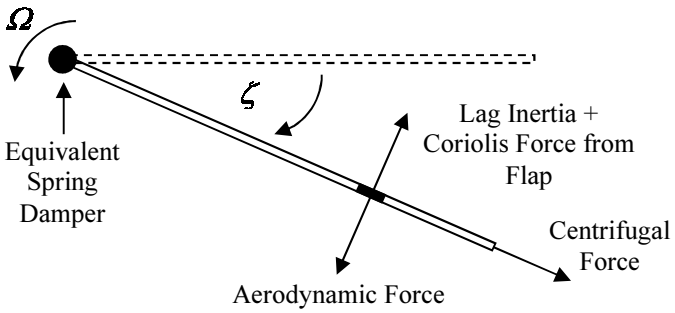

Figure 4.7 Rotor Blade Lag Motion

$$C_{z/\mathbf{lag}} = \left[\; ... - ... \; \right]\cos\psi + \left[\; ... - ... \; \right]\sin\psi +$$

$$\theta_0\left[\zeta'^2\left(\frac{1}{3}\right)+\zeta'\zeta\left(\beta_0\mu_z\right)+\zeta'\left(-\frac{2}{3}\right)+\zeta^2\left(\beta_0^2\mu_z^2+\frac{1}{2}\beta_{1s}^2\mu_z^2+\frac{1}{2}\beta_{1c}^2\mu_z^2-\beta_{1s}\mu_y\mu_z+\right.\right.$$

$$\left.\left.\beta_{1c}\mu_x\mu_z+\frac{1}{2}\mu_y^2+\frac{1}{2}\mu_x^2\right)+\zeta\left(-\beta_{1c}\mu_y\mu_z-\beta_{1s}\mu_x\mu_z-\beta_0\mu_z\right)+\frac{1}{2}\mu_x^2+\frac{1}{2}\mu_y^2+\frac{1}{3}\right]+$$

$$\theta_{1c}\left[\zeta'\zeta\left(\frac{1}{2}\beta_{1c}\mu_z+\frac{1}{2}\mu_y\right)+\zeta'\left(-\frac{1}{2}\mu_y\right)+\zeta^2\left(\beta_{1c}\beta_0\mu_z^2+\beta_0\mu_x\mu_z\right)+\right.$$

$$\left.\zeta\left(-\beta_0\mu_y\mu_z-\frac{1}{2}\beta_{1c}\mu_z-\frac{1}{2}\mu_x\right)+\frac{1}{2}\mu_y\right]+$$

$$\theta_{1s}\left[\zeta'\zeta\left(\frac{1}{2}\beta_{1s}\mu_z-\frac{1}{2}\mu_y\right)+\zeta'\left(-\frac{1}{2}\mu_x\right)+\zeta^2\left(\beta_{1s}\beta_0\mu_z^2+\beta_0\mu_y\mu_z\right)+\right.$$

$$\left.\zeta\left(-\beta_0\mu_x\mu_z-\frac{1}{2}\beta_{1s}\mu_z-\frac{1}{2}\mu_y\right)+\frac{1}{2}\mu_y\right]+\zeta'^2\left(\frac{1}{4}\right)+\zeta'\zeta\left(\frac{2}{3}\beta_0\mu_z\right)+\zeta'\left(-\frac{1}{2}\right)+$$

$$\zeta^2\left(\frac{1}{2}\beta_0^2\mu_z^2+\frac{1}{4}\beta_{1s}^2\mu_z^2+\frac{1}{4}\beta_{1c}^2\mu_z^2-\frac{1}{2}\beta_{1s}\mu_y\mu_z+\frac{1}{2}\beta_{1c}\mu_x\mu_z+\frac{1}{4}\mu_y^2+\frac{1}{4}\mu_x^2\right)+$$

$$\zeta\left(-\frac{1}{2}\beta_{1c}\mu_y\mu_z-\frac{1}{2}\beta_{1s}\mu_x\mu_z-\frac{2}{3}\beta_0\mu_z\right)+\frac{1}{4}\mu_y^2+\frac{1}{4}\mu_x^2+\frac{1}{4}+$$

$$\beta_0'\left[\; ... - ... \; \right]+\beta_0\left[\; ... - ... \; \right]+\beta_0^2\left[\; ... - ... \; \right]+\beta_{1s}\left[\; ... - ... \; \right]+\beta_{1c}\left[\; ... - ... \; \right]+$$

$$\alpha_{1s}\left[\; ... - ... \; \right]+\alpha_{1c}\left[\; ... - ... \; \right]+ \text{ other terms that are not functions of the above.}$$

Figure 4.8 $C_{z/\mathbf{lag}}$ Aerodynamic Force Coefficient with Lag Terms

$$C_{QA0} = \left[\; ... - ... \; \right] \cos\psi + \left[\; ... - ... \; \right] \sin\psi +$$

$$\theta_{1c}\left[\zeta'\zeta\left(-\frac{1}{8}\beta_{1c}\bar{r}_{hub} - \frac{1}{8}\bar{p}_{hub} + \frac{1}{8}\beta_{1c} \right) + \zeta'\left(-\frac{1}{6}\beta_0\mu_x + \frac{1}{8}\alpha_{1c} \right) + \right.$$

$$\zeta^2\left(-\frac{1}{3}\beta_{1c}\beta_0\mu_z\bar{r}_{hub} - \frac{1}{6}\beta_0\mu_x\bar{r}_{hub} - \frac{1}{6}\beta_0\mu_z\bar{p}_{hub} + \frac{1}{3}\beta_{1c}\beta_0\mu_z + \frac{1}{6}\beta_0\mu_x \right) +$$

$$\zeta\left(\frac{1}{6}\beta_0\mu_y\bar{r}_{hub} + \frac{1}{8}\beta_{1c}\bar{r}_{hub} + \frac{1}{8}\bar{p}_{hub} + \frac{1}{4}\beta_{1c}\mu_z^2 + \frac{1}{8}\beta_{1c}\beta_{1s}\mu_y\mu_z - \frac{1}{4}\beta_0^2\mu_x\mu_z - \right.$$

$$\frac{1}{16}\beta_{1s}{}^2\mu_x\mu_z - \frac{3}{16}\beta_{1c}{}^2\mu_x\mu_z + \frac{1}{4}\mu_x\mu_z - \frac{1}{4}\beta_{1c}\lambda_0\mu_z - \frac{1}{6}\beta_{1c}\beta_0'\mu_z + \frac{1}{6}\alpha_{1c}\beta_0\mu_z -$$

$$\left. \frac{1}{16}\beta_{1c}\mu_y^2 + \frac{1}{8}\beta_{1s}\mu_x\mu_y - \frac{1}{6}\beta_0\mu_y - \frac{3}{16}\beta_{1c}\mu_x^2 - \frac{1}{4}\lambda_0\mu_x - \frac{1}{6}\alpha_{1c}\beta_0'\mu_x \right) -$$

$$\frac{1}{4}\mu_y\mu_z - \frac{1}{16}\beta_{1s}\mu_y^2 + \frac{1}{8}\beta_{1c}\mu_x\mu_y + \frac{1}{4}\lambda_0\mu_y + \frac{1}{6}\beta_0'\mu_y + \frac{1}{16}\beta_{1s}\mu_x^2 +$$

$$\left. \frac{1}{6}\beta_0\mu_x - \frac{1}{8}\alpha_{1c} \right] + \theta_{1s}\left[\zeta\zeta'\left(-\frac{1}{8}\beta_{1s}\bar{r}_{hub} + \frac{1}{8}\bar{q}_{hub} + \frac{1}{8}\beta_{1s} \right) + \zeta'\left(\frac{1}{6}\beta_0\mu_y + \frac{1}{8}\alpha_{1s} \right) + \right.$$

$$\zeta^2\left(-\frac{1}{3}\beta_{1s}\beta_0\mu_z\bar{r}_{hub} + \frac{1}{6}\beta_0\mu_y\bar{r}_{hub} + \frac{1}{6}\beta_0\mu_z\bar{q}_{hub} + \frac{1}{3}\beta_{1s}\beta_0\mu_z + \frac{1}{6}\beta_0\mu_y \right) +$$

$$\zeta\left(\; ... - ... \; \right) + \text{ Remainder of terms that are not functions of the lag angle.}$$

Figure 4.9 C_{QA0} Coefficient of Torque Equation

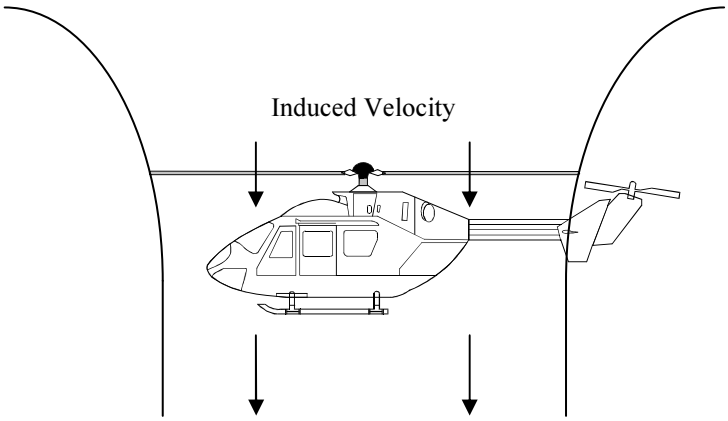

Figure 4.10a Induced Velocity Pattern Out of Ground Effect (OGE)

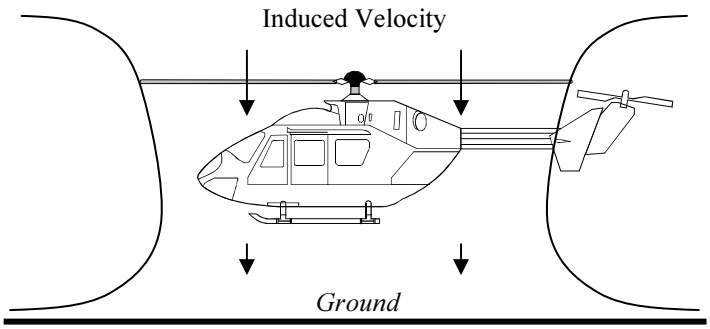

Figure 4.10b Induced Velocity Pattern In Ground Effect (IGE)

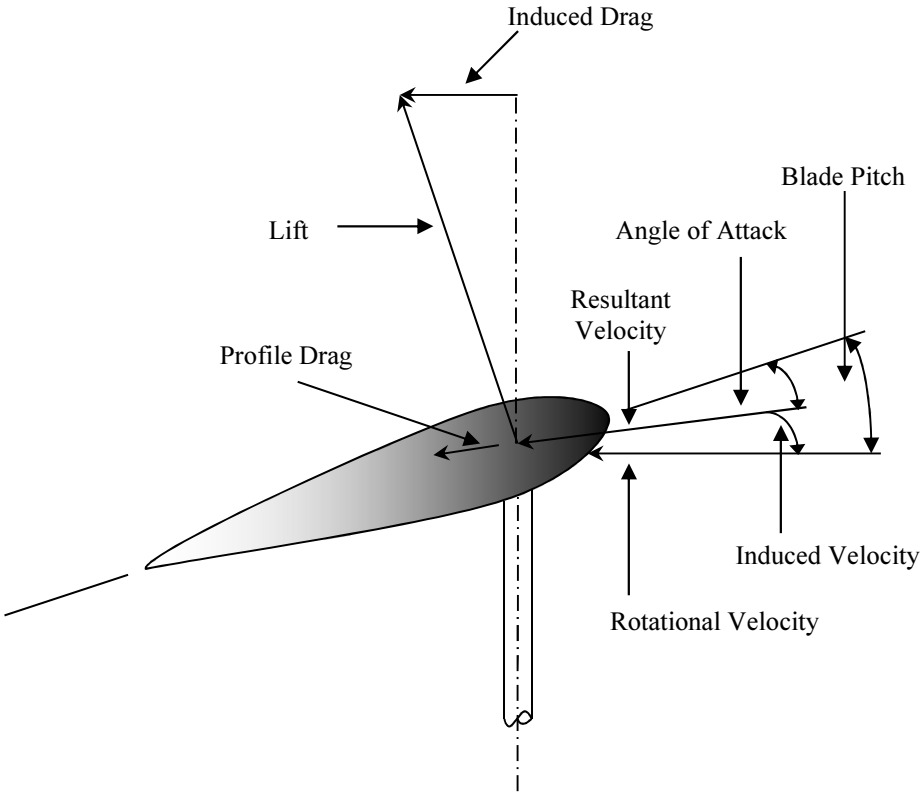

Figure 4.11a Conditions at Blade Element Out of Ground Effect (OGE)

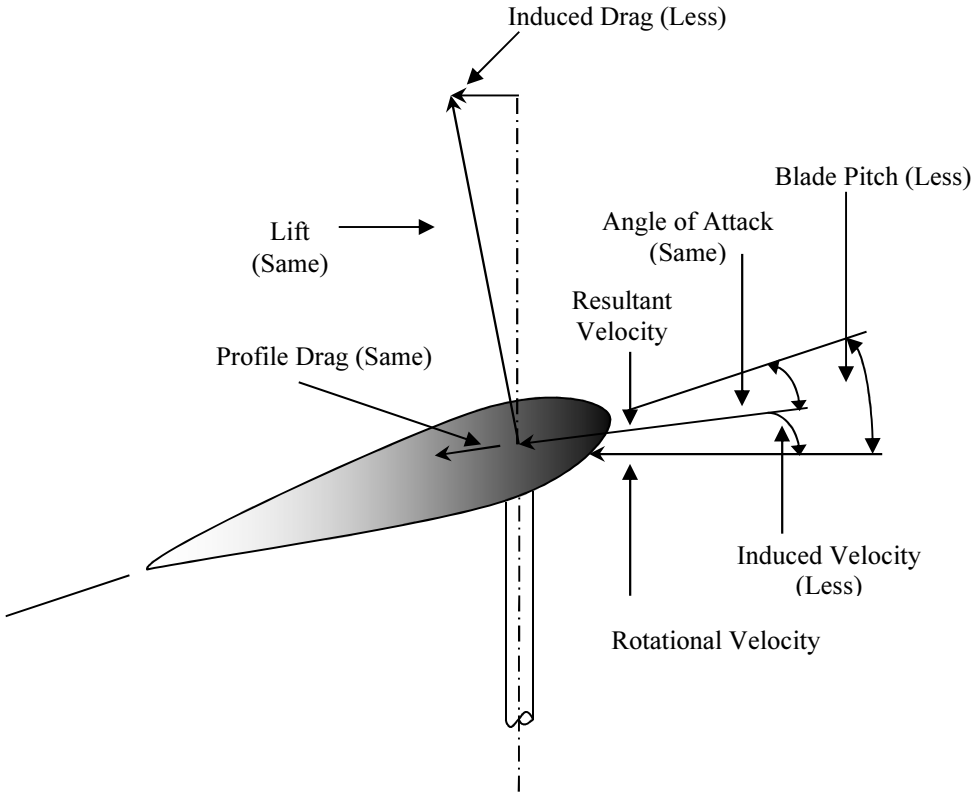

Figure 4.11b Conditions at Blade Element In Ground Effect (IGE)

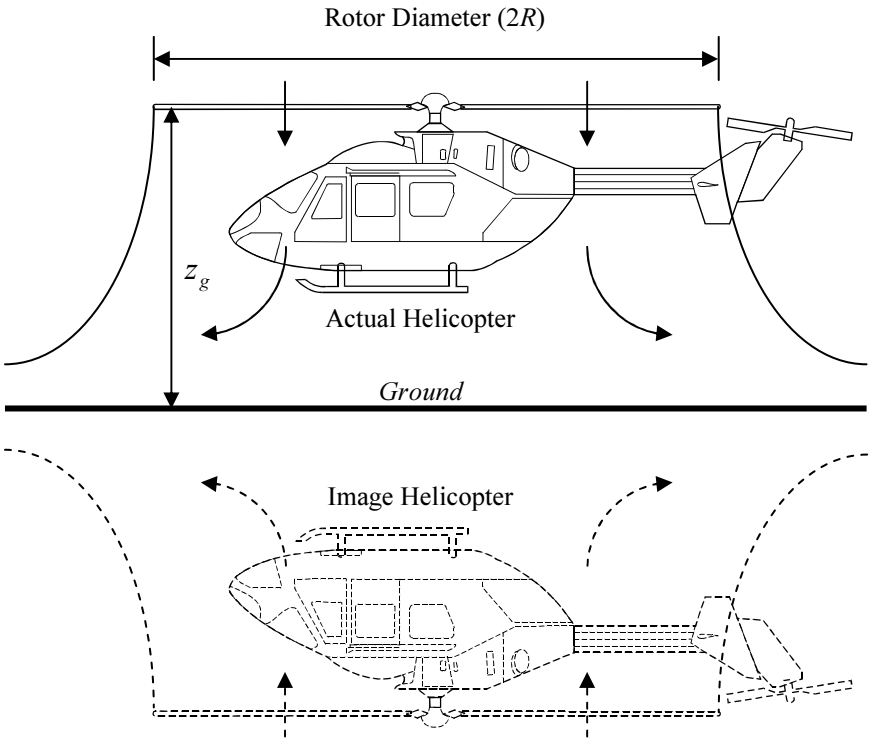

Figure 4.12 Image Helicopter Concept for Modelling Ground Effect

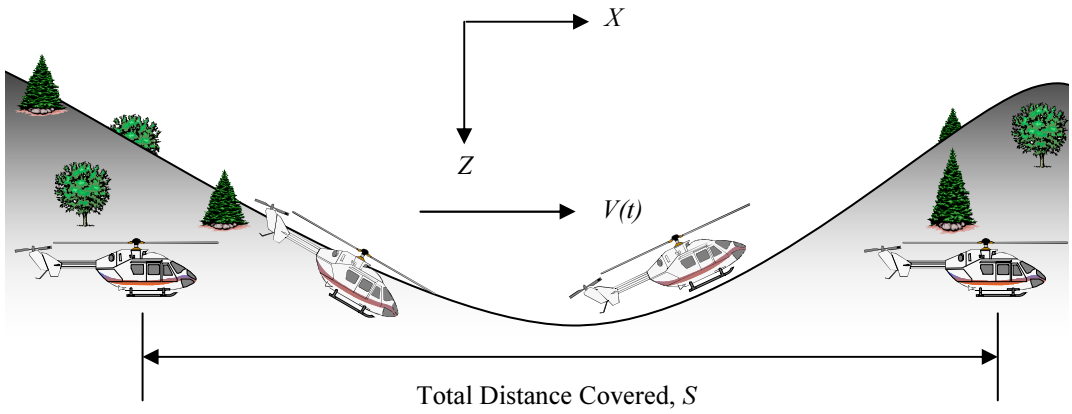

Figure 4.13 Nap-of-the-earth Acceleration/deceleration Flight Test Manoeuvre

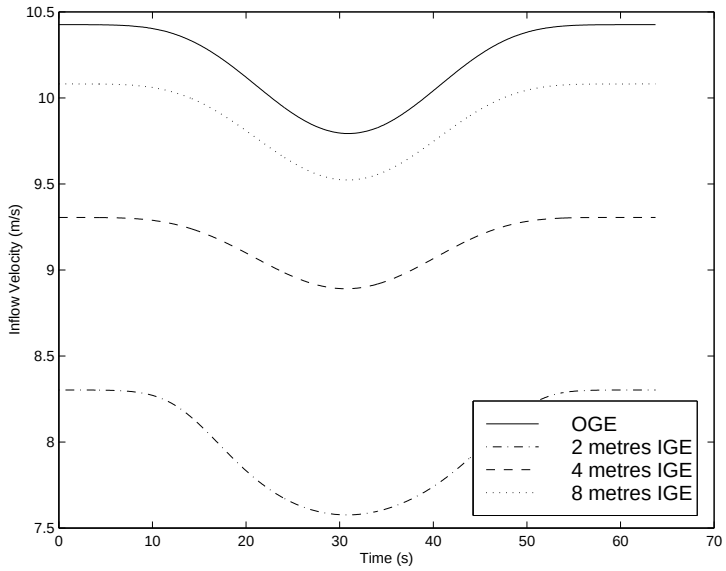

Figure 4.14a Uniform Component of Inflow Velocity OGE and at Several Altitudes IGE

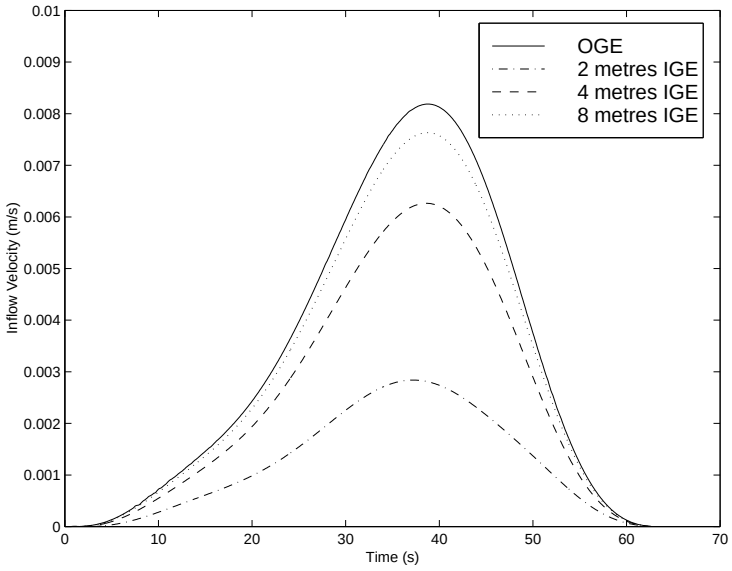

Figure 4.14b Lateral Component of Inflow Velocity OGE and at Several Altitudes IGE

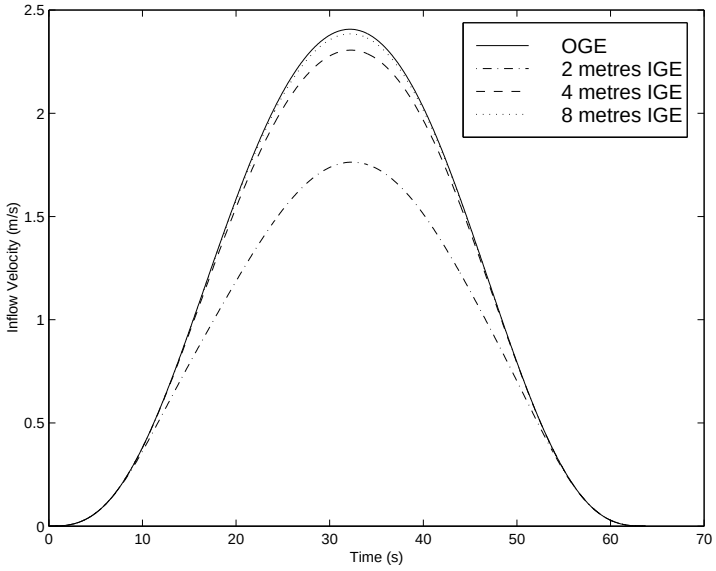

Figure 4.14c Longitudinal Component of Inflow Velocity OGE and at Several Altitudes IGE

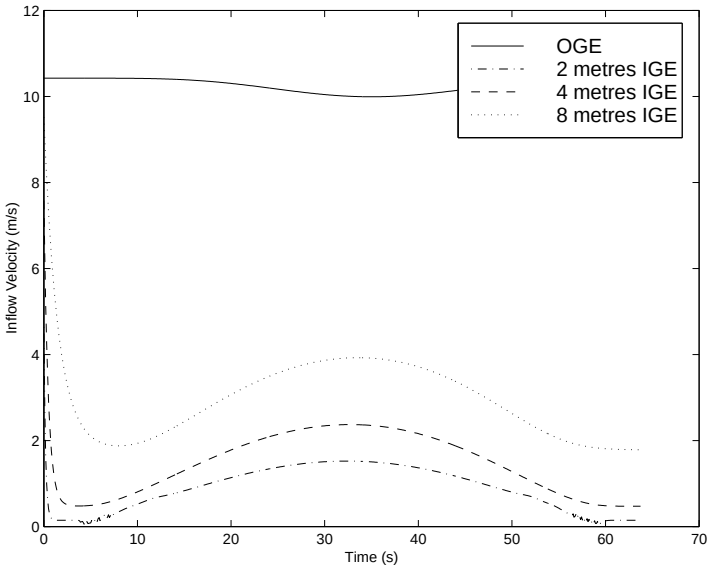

Figure 4.15a Peters-Haquang Uniform Component of Inflow Velocity OGE and at Several Altitudes IGE

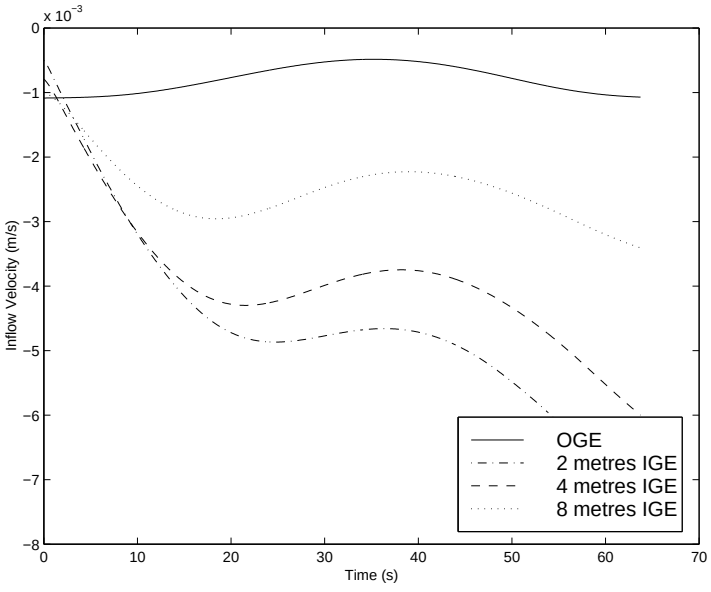

Figure 4.15b Peters-Haquang Lateral Component of Inflow Velocity OGE and at Several Altitudes IGE

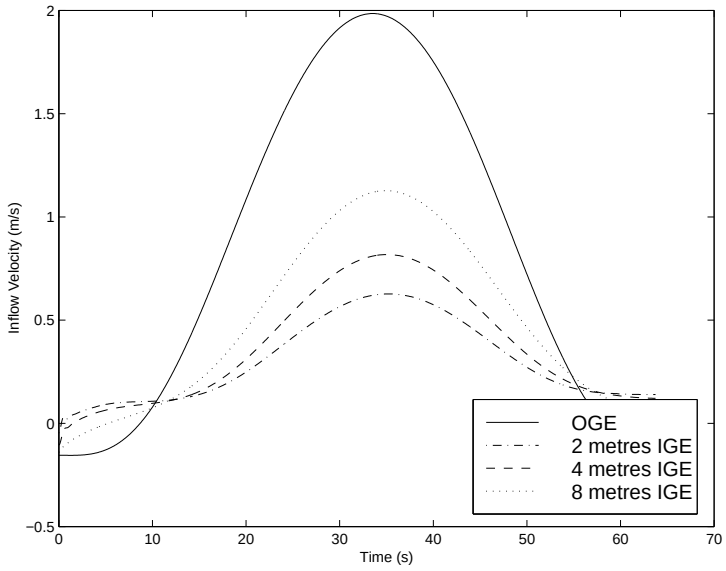

Figure 4.15c Peters-Haquang Longitudinal Component of Inflow Velocity OGE and at Several Altitudes IGE

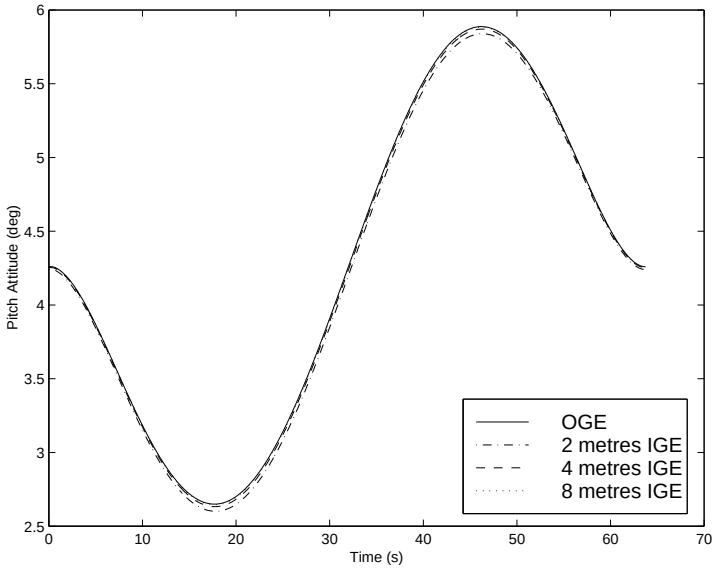

Figure 4.16 Influence of Ground Effect on Acceleration/deceleration Flight test Manoeuvre

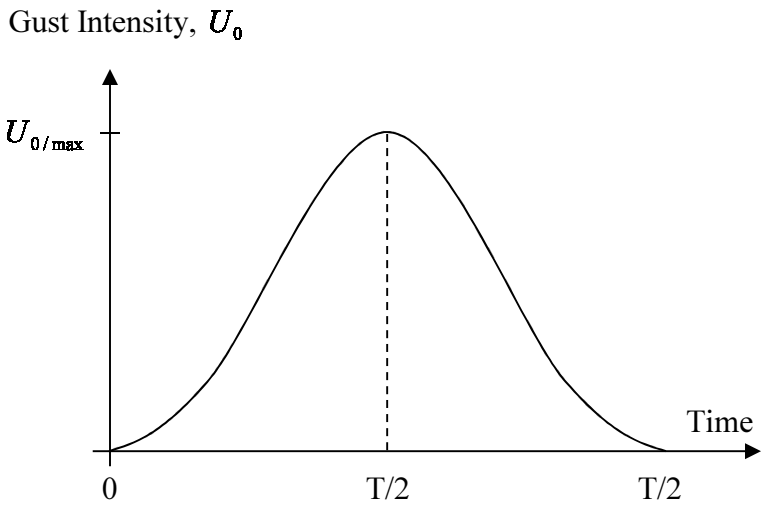

Figure 4.17 One-minus Cosine Gust Profile

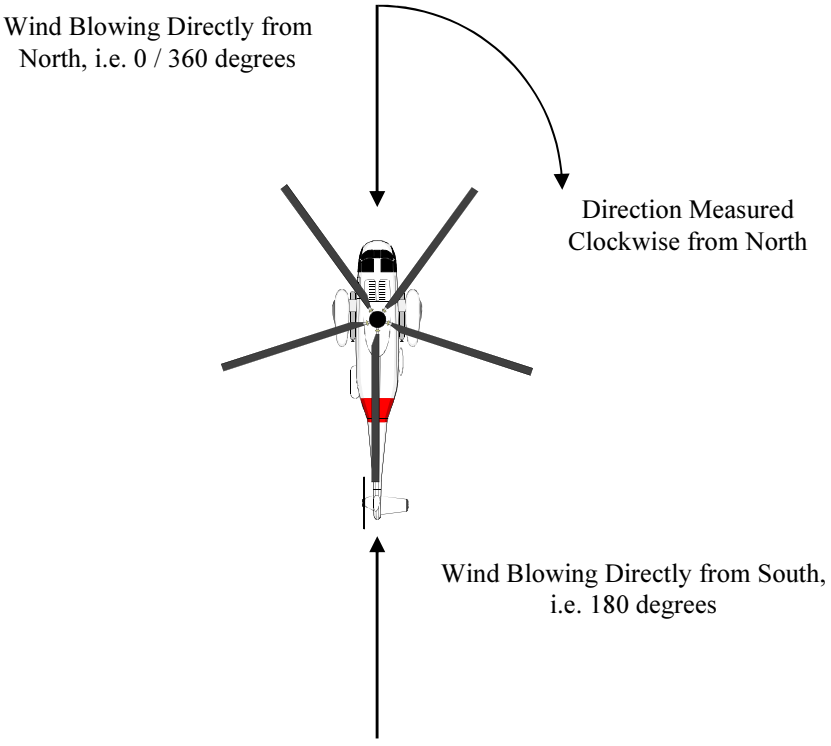

Figure 4.18 Gust Direction Measurement

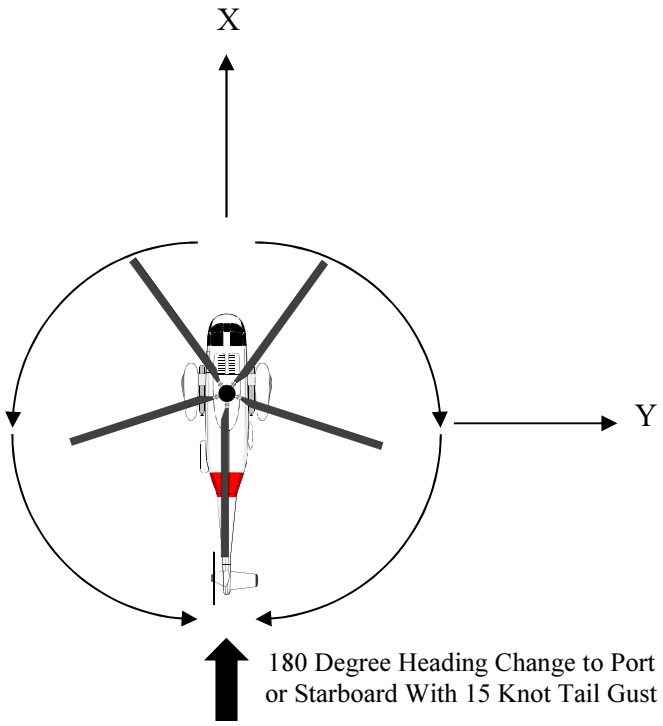

Figure 4.19 Hover-turn Precision Flight Test Manoeuvre

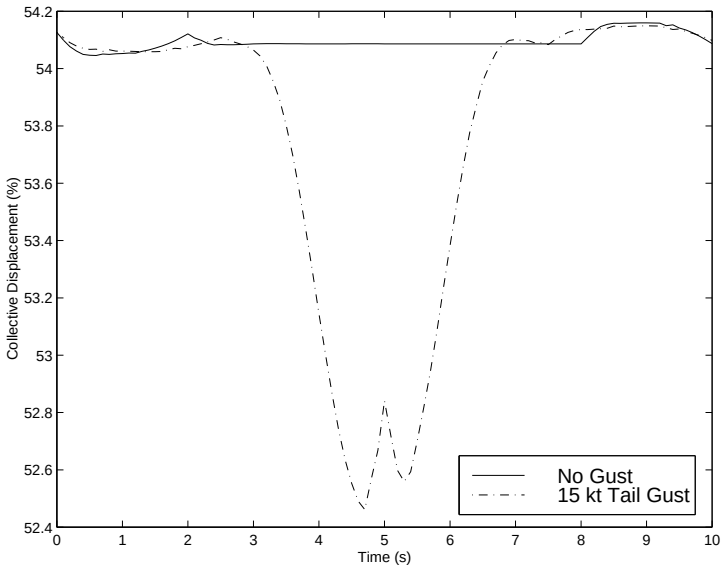

Figure 4.20a Hover-turn Collective Lever Displacement

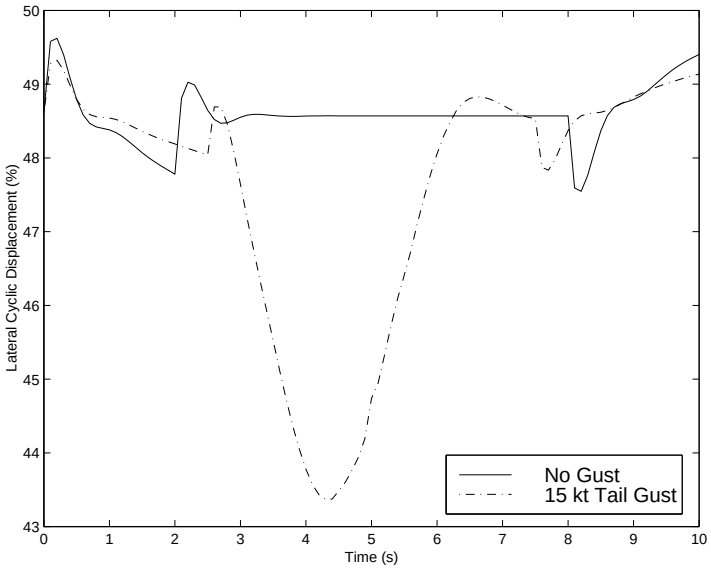

Figure 4.20b Hover-turn Lateral Cyclic Stick Displacement

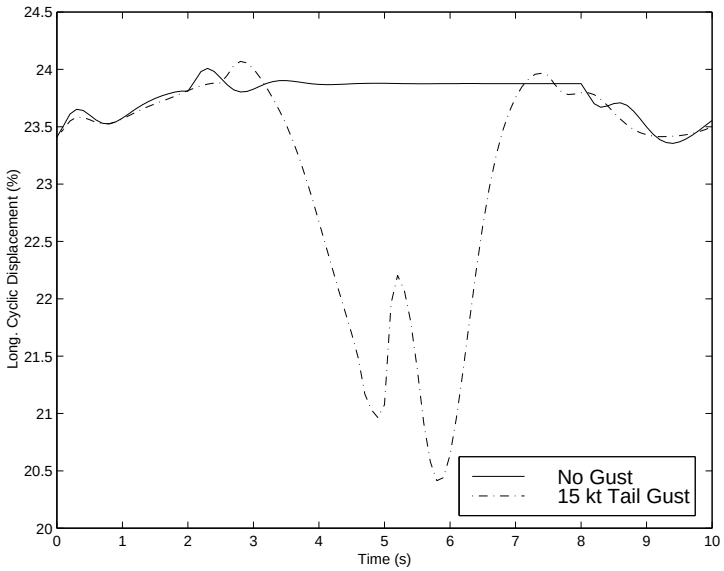

Figure 4.20c Hover-turn Longitudinal Cyclic Stick Displacement

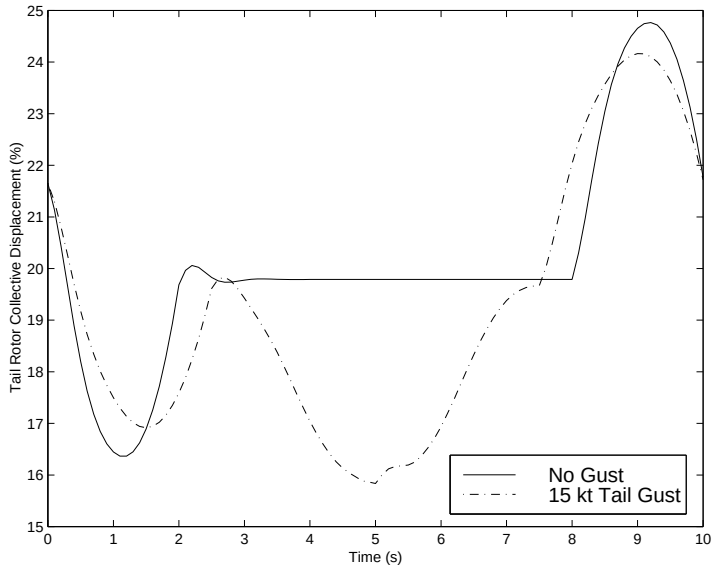

Figure 4.20d Hover-turn Tail Rotor Pedal Displacement

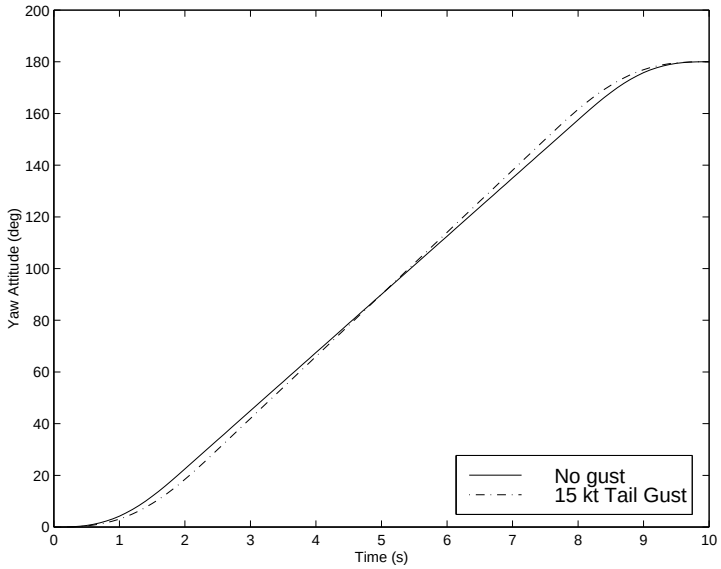

Figure 4.21 Yaw Attitude for Precision Hover-turn Manoeuvre in Still Air and with a 15 Knot 1-Cos Tail Gust

Chapter 5 Figures

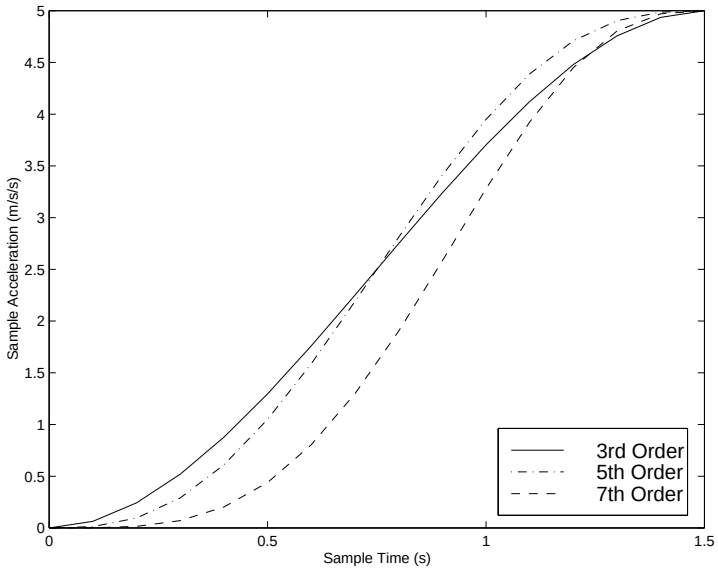

Figure 5.1 Example Illustrating 3rd, 5th and 7th Order Polynomials

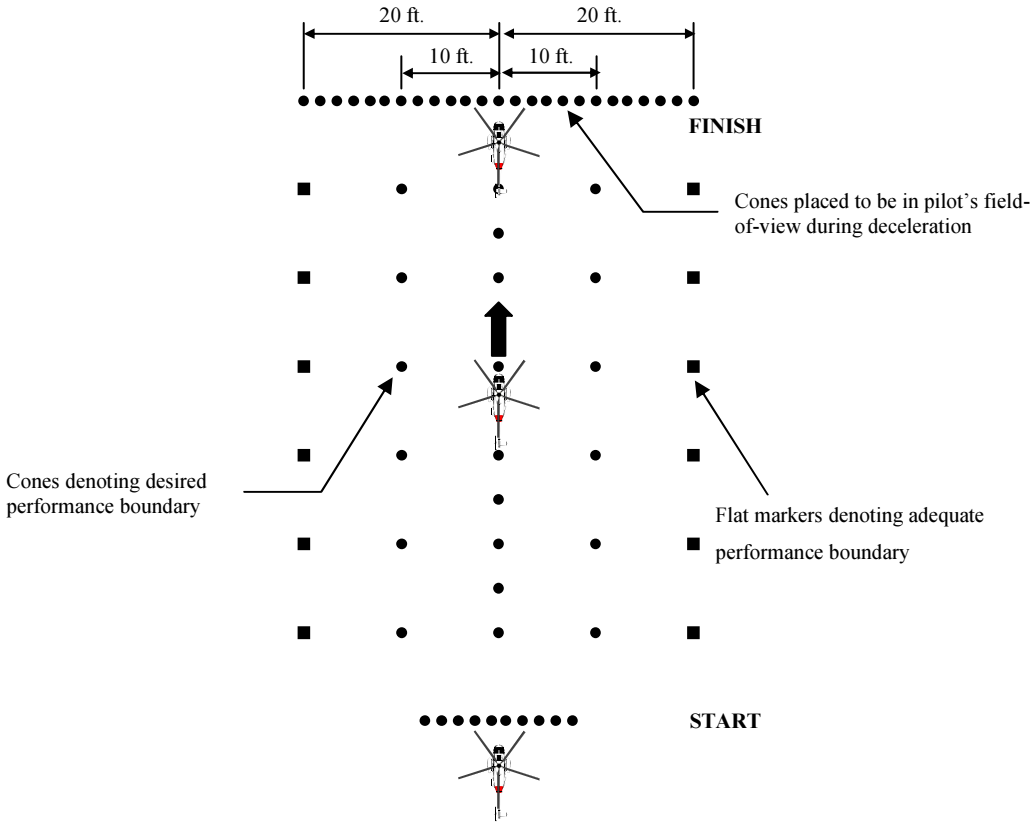

Figure 5.2 ADS-33D Course for Acceleration/deceleration

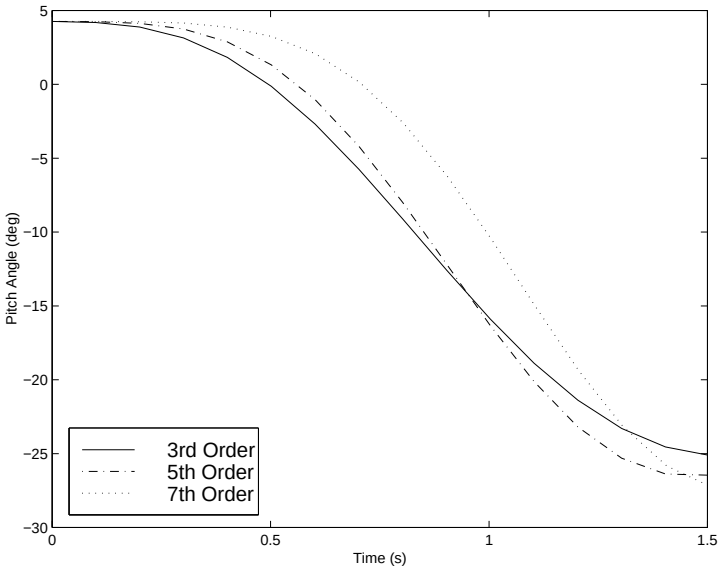

Figure 5.3 Effect of 3rd, 5th and 7th Order Polynomials on Pitch Angle for Acceleration/deceleration MTE

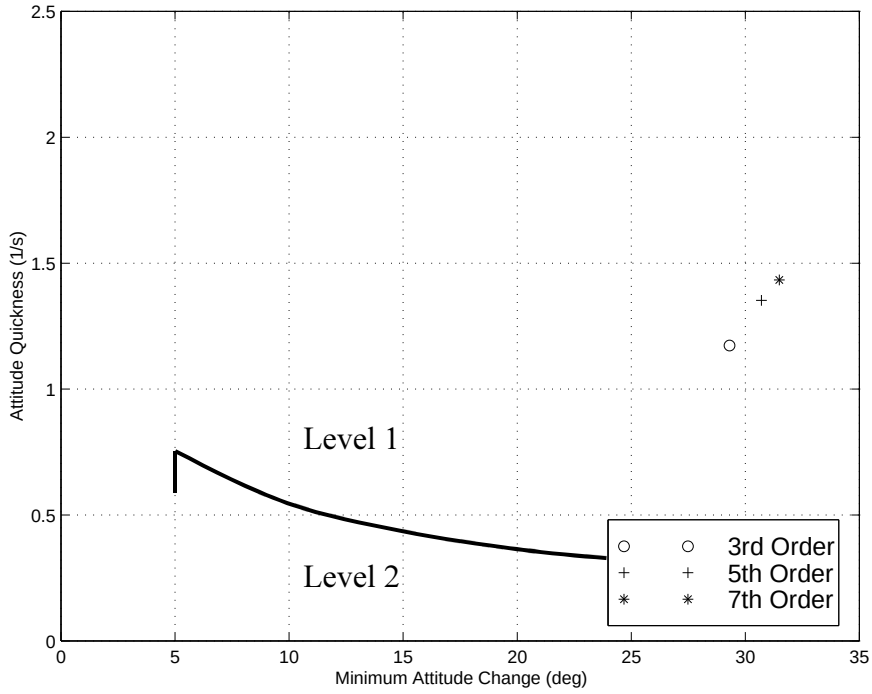

Figure 5.4 Effect of 3rd, 5th and 7th Order Polynomials on Pitch Attitude Quickness for Acceleration/deceleration MTE

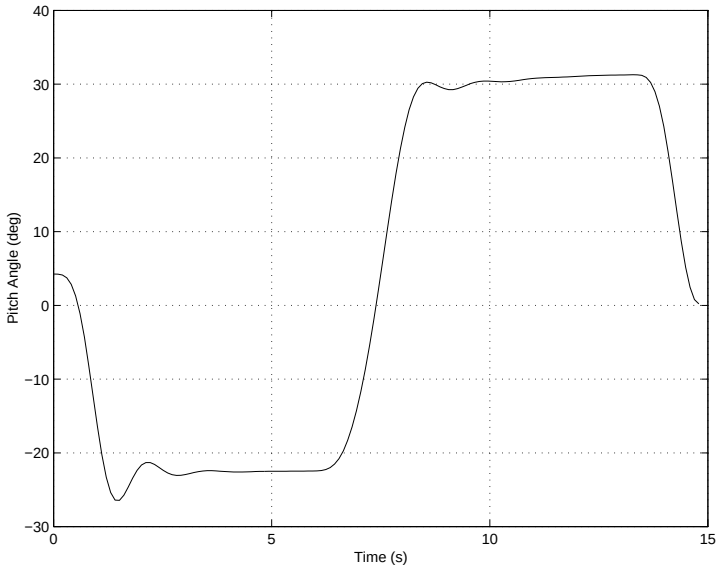

Figure 5.5 Example Pitch Angle Plot from Inverse Simulation of the Acceleration/deceleration Flight test manoeuvre

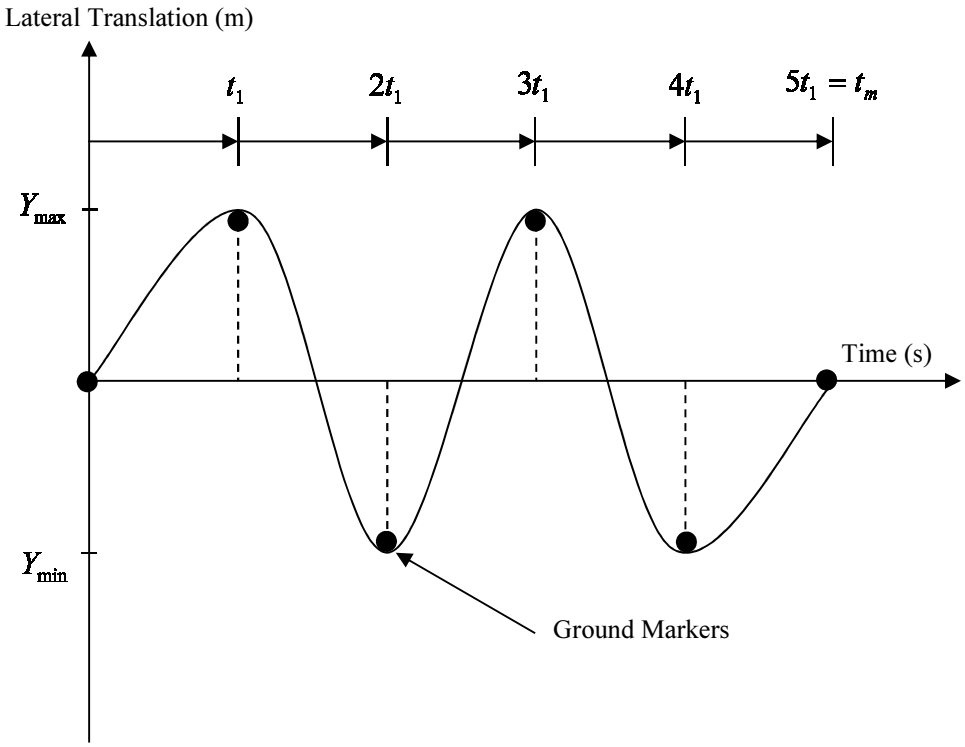

Figure 5.6 Ideal Lateral Translation Profile of ADS-33D Slalom MTE

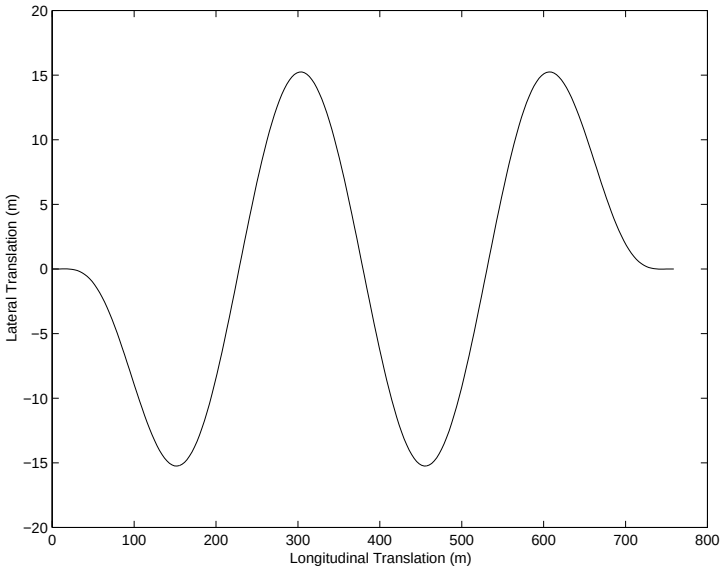

Figure 5.7 Helinv Manoeuvre Profile of ADS-33D Slalom MTE

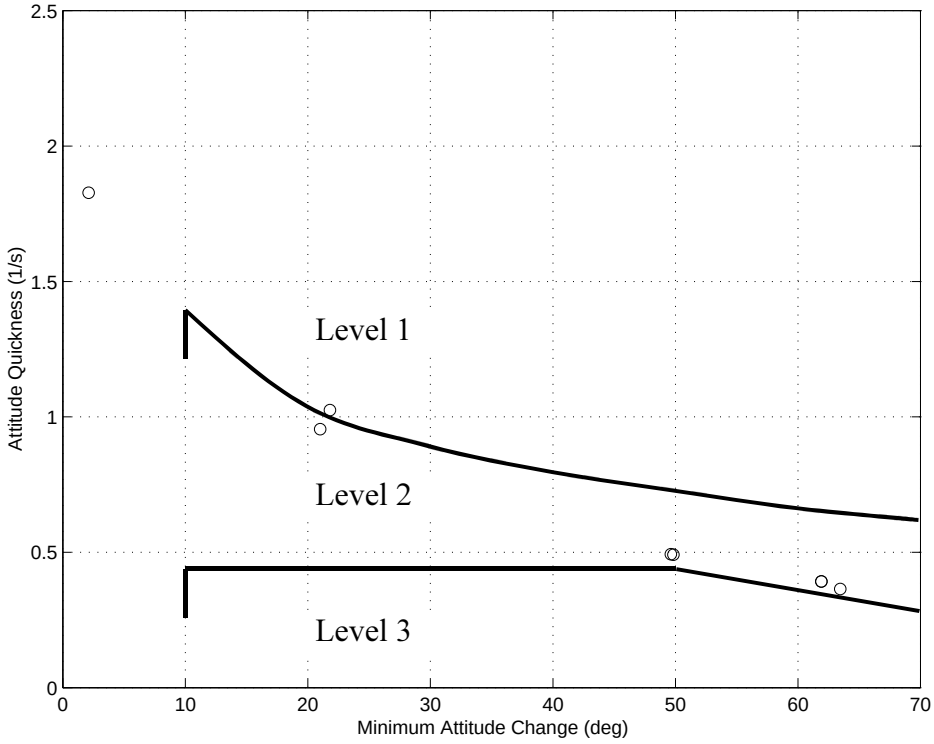

Figure 5.8 Roll Attitude Quickness for ADS-33D Slalom MTE

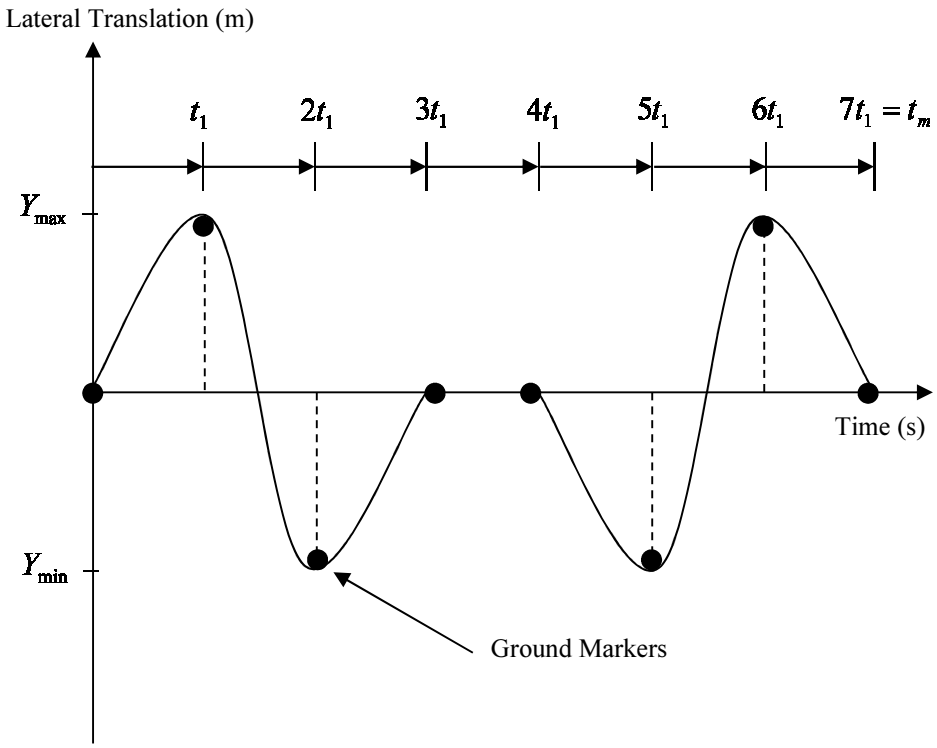

Figure 5.9 Ideal Lateral Translation Profile of DERA Slalom

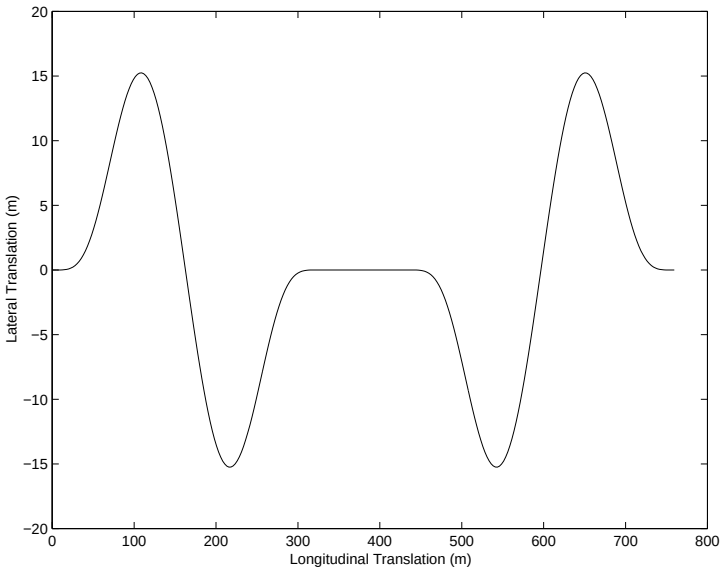

Figure 5.10 Helinv Manoeuvre Profile of DERA Slalom

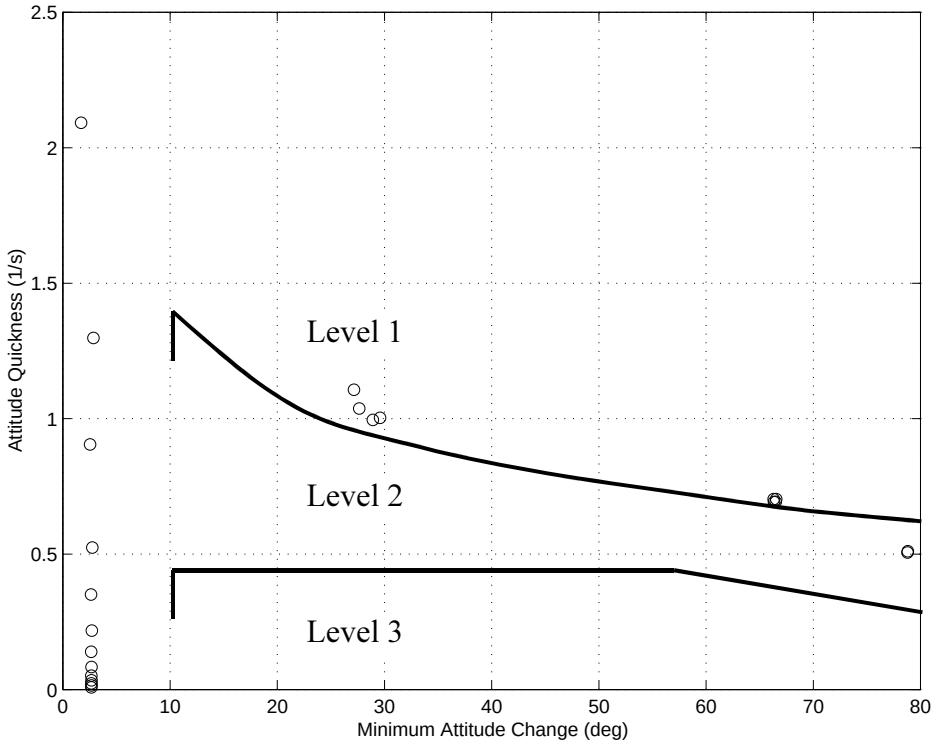

Figure 5.11 Roll Attitude Quickness for DERA Slalom

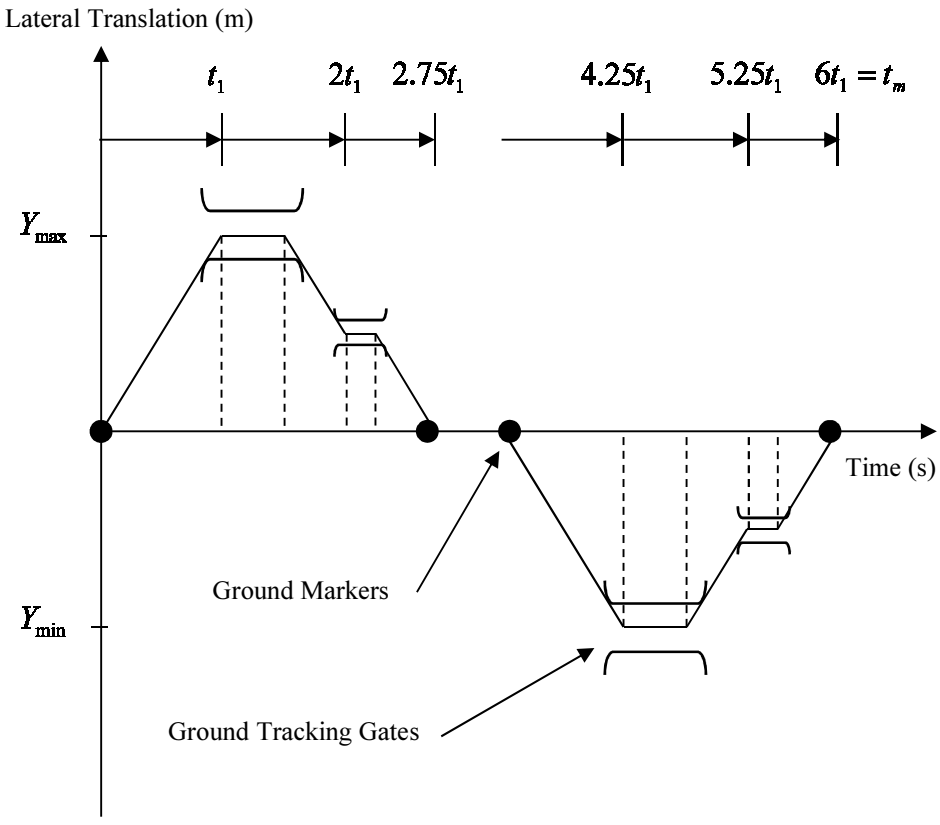

Figure 5.12 Ideal Lateral Translation Profile of DLR Tracking Slalom

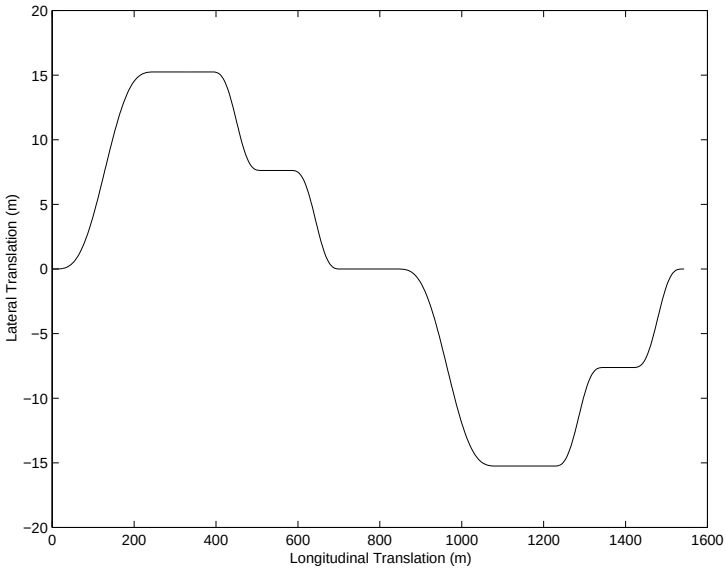

Figure 5.13 Helinv Manoeuvre Profile of DLR Tracking Slalom

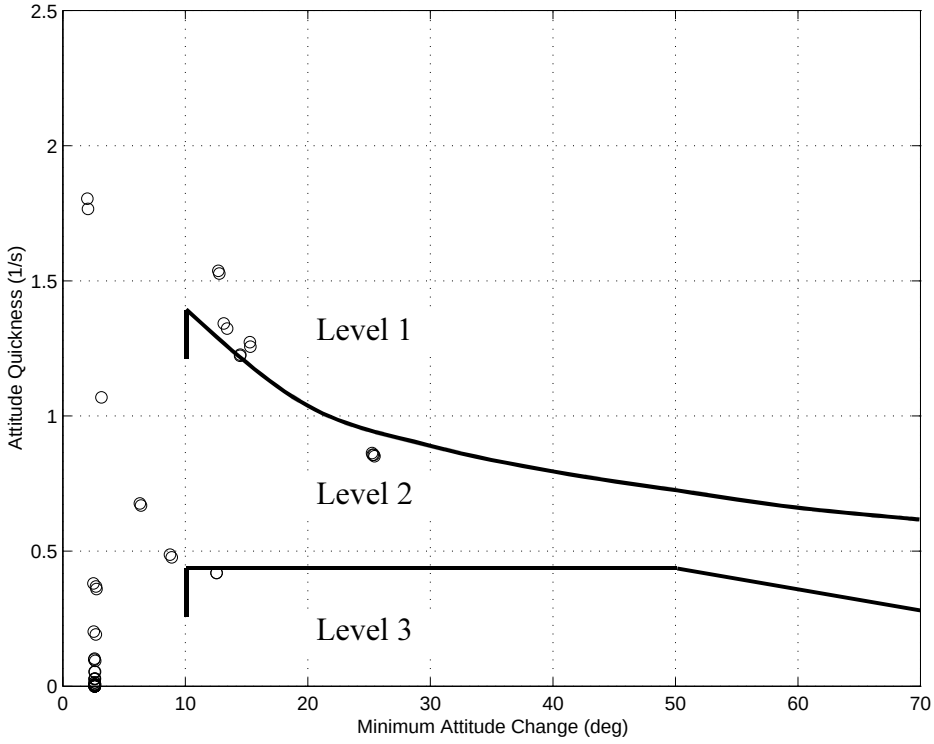

Figure 5.14 Roll Attitude Quickness for DLR Tracking Slalom MTE

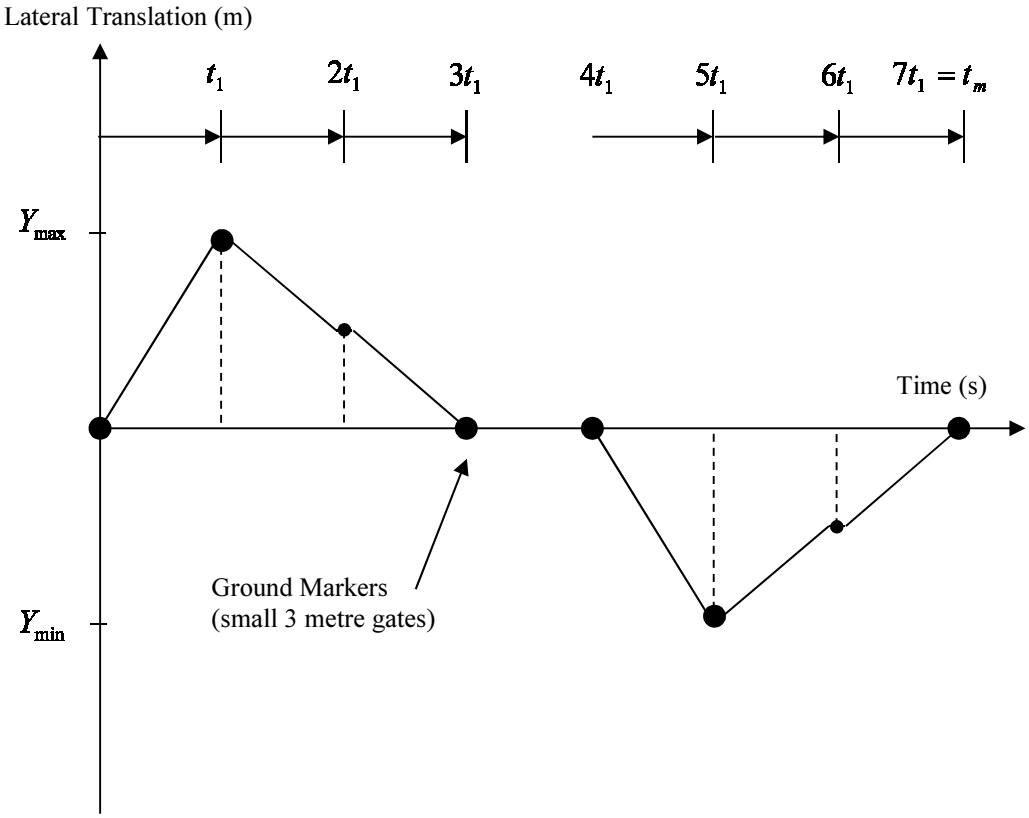

Figure 5.15 Ideal Lateral Translation Profile of DLR Gate Slalom

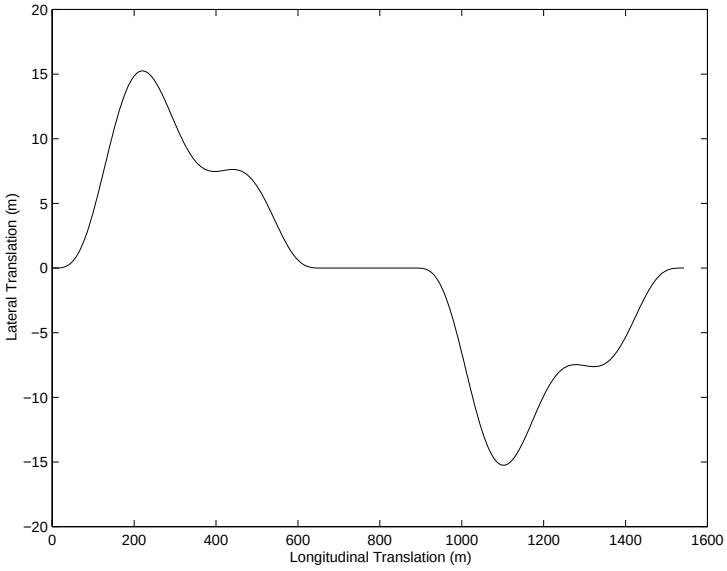

Figure 5.16 Helinv Manoeuvre Profile of DLR Gate Slalom

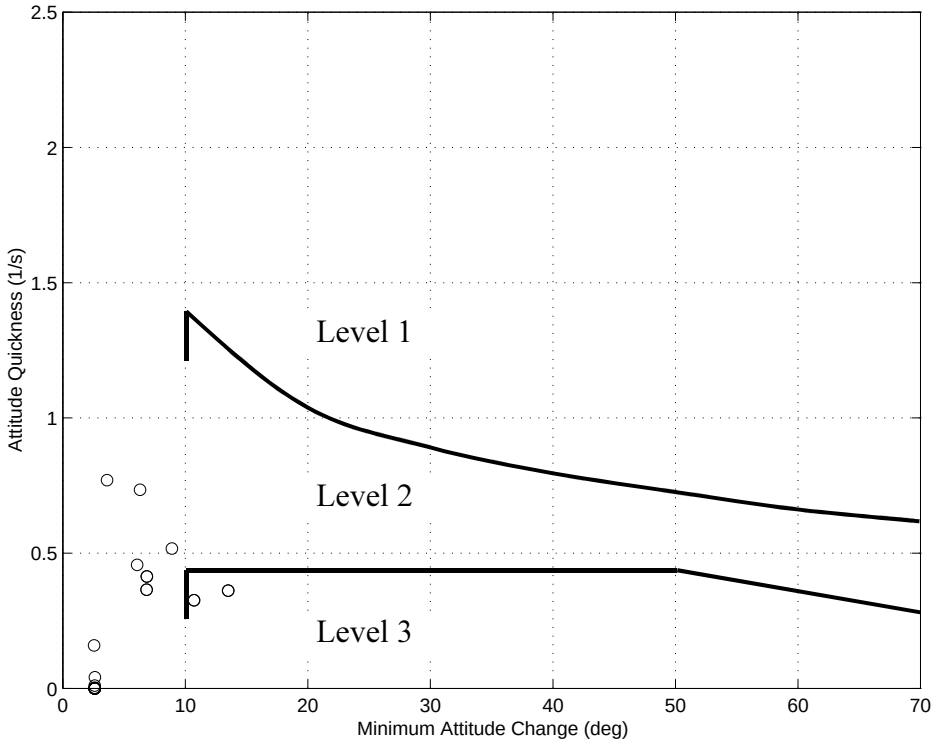

Figure 5.17 Roll Attitude Quickness for DLR Gate Slalom

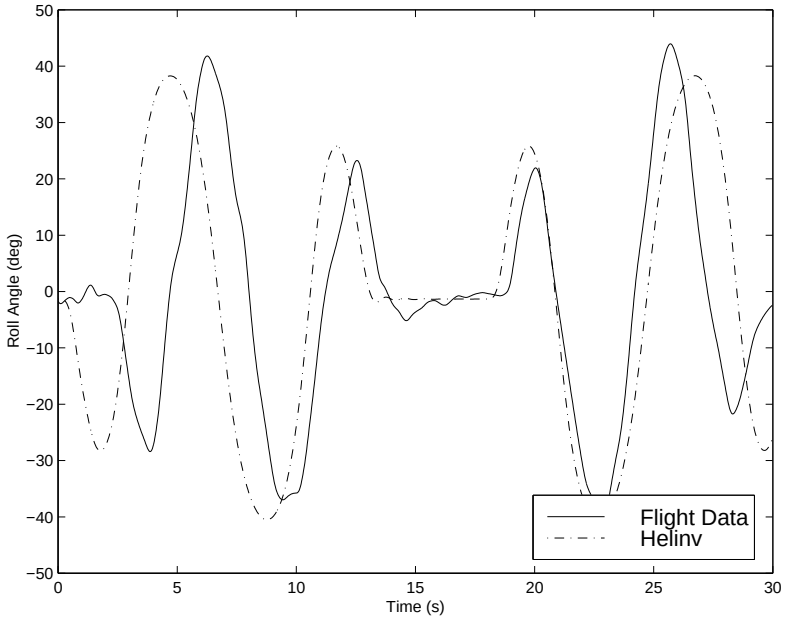

Figure 5.18 Comparison of Flight Data and Helinv Results for a DERA Slalom Manoeuvre

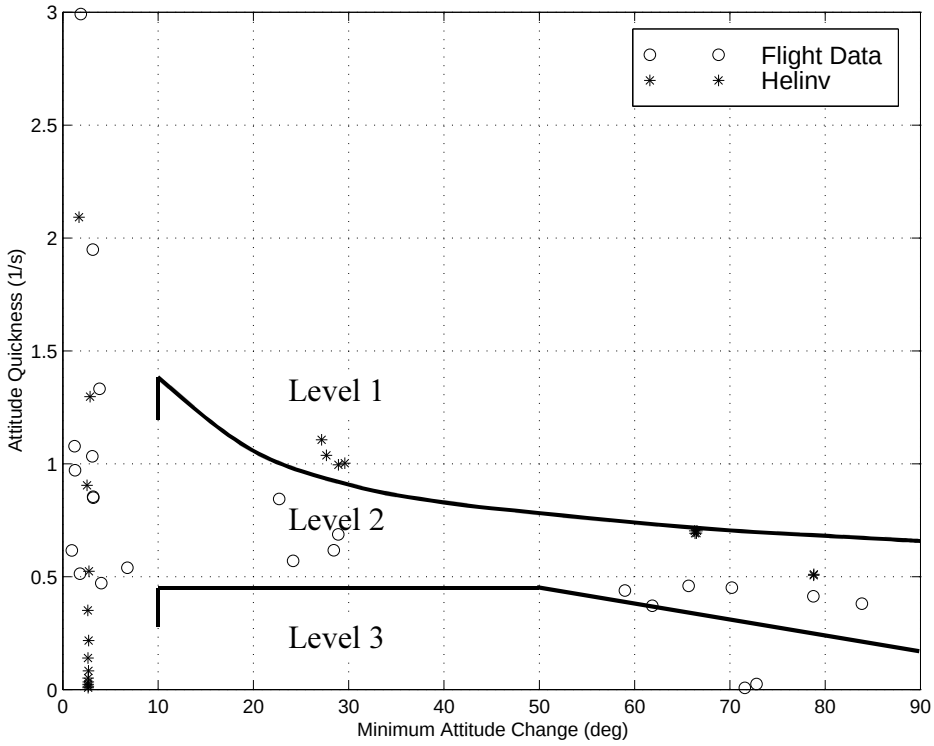

Figure 5.19 Comparison of Flight Data and Helinv Roll Attitude Quickness for DERA Slalom Manoeuvre

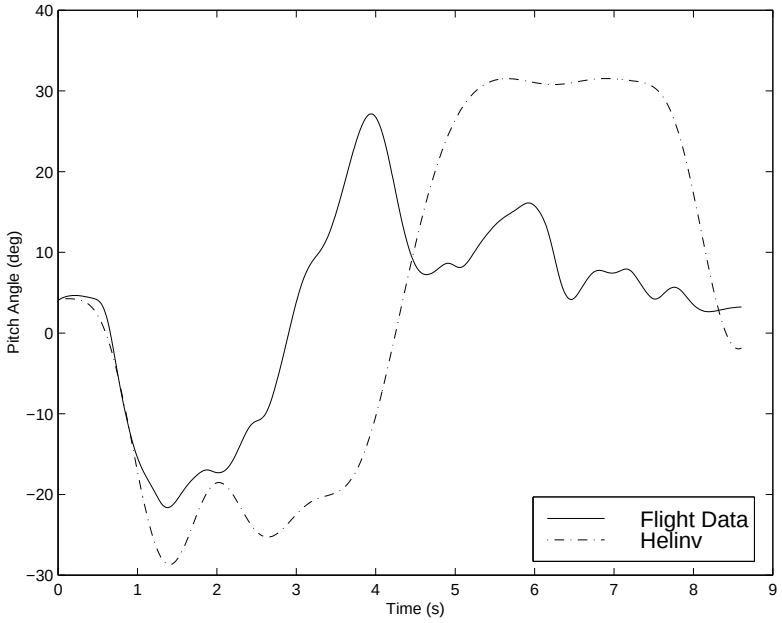

Figure 5.20 Comparison of Flight Data and Helinv Results for a ADS-33D Acceleration/deceleration Manoeuvre

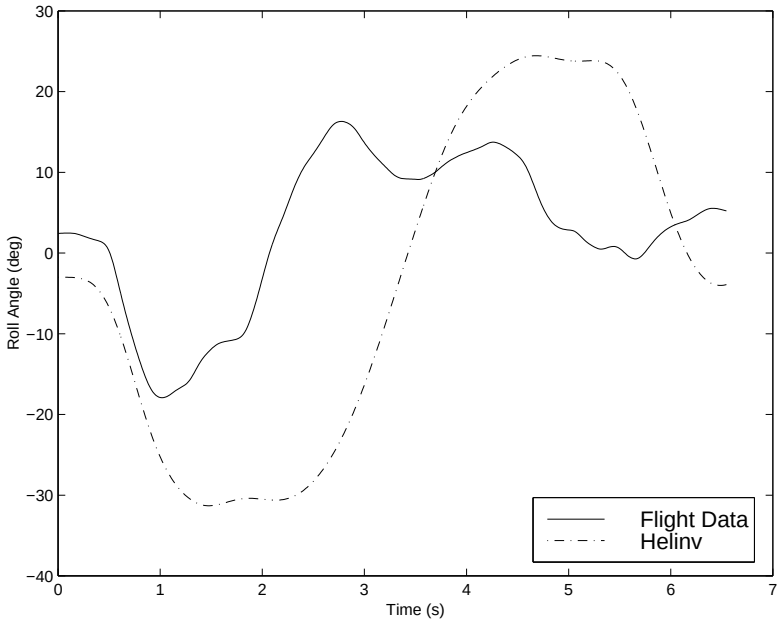

Figure 5.21 Comparison of Flight Data and Helinv Results for a ADS-33D Rapid Side-step Manoeuvre

Chapter 6 Figures

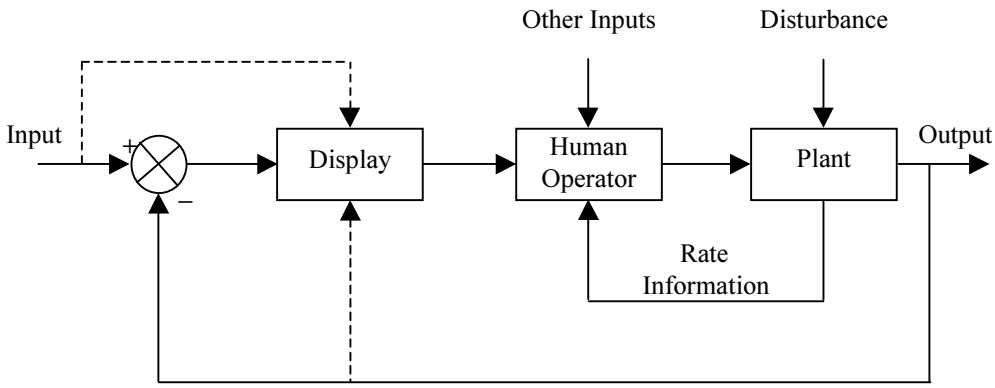

Figure 6.1 Block Diagram Layout Of Basic Human-machine System

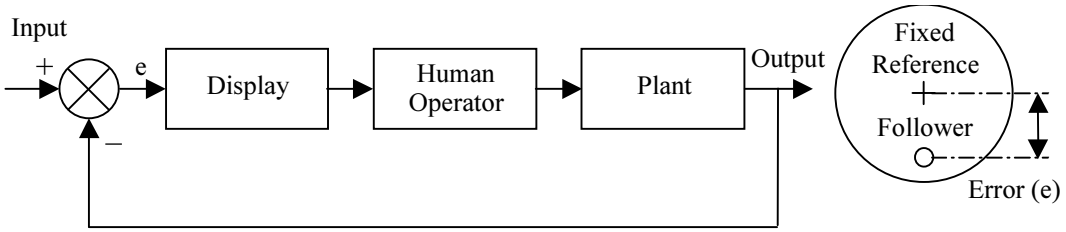

Figure 6.2a Continuous Compensatory Tracking

Figure 6.2b Compensatory Display

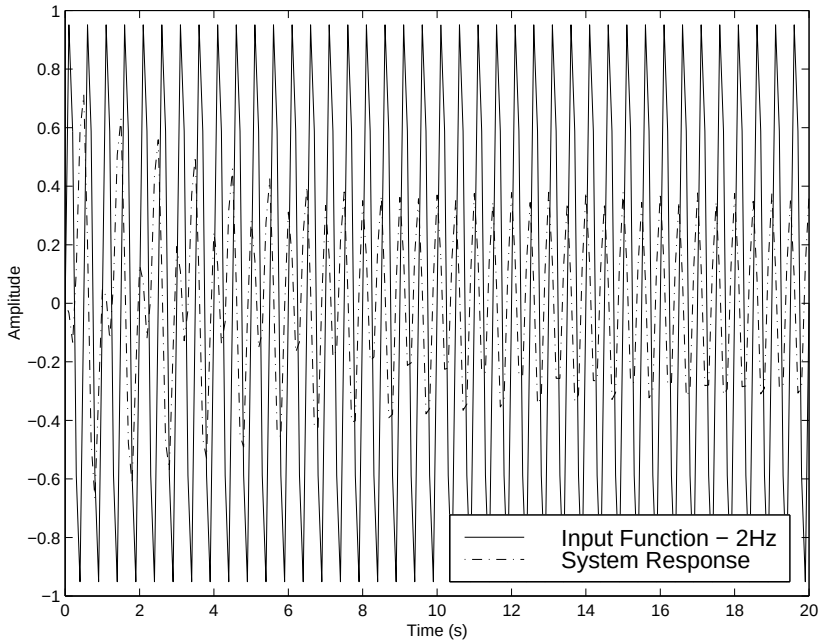

Figure 6.3a Plant Dynamics – Satisfactory HQ Transfer Function

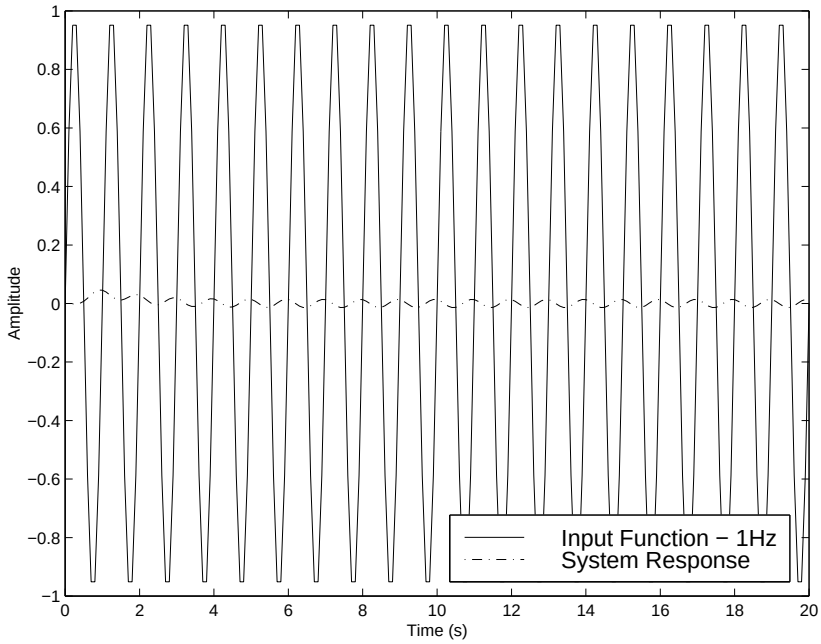

Figure 6.3b Plant Dynamics – Satisfactory HQ Transfer Function

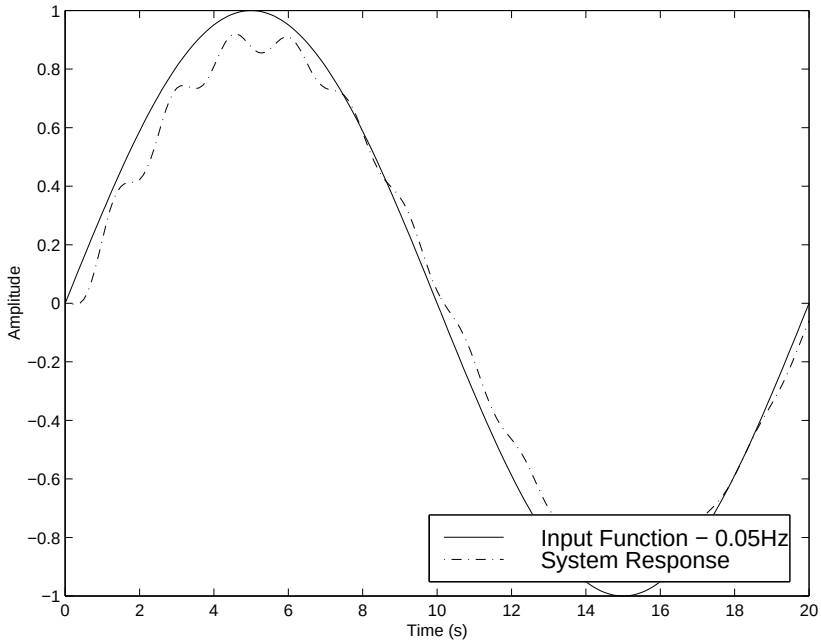

Figure 6.3c Plant Dynamics – Satisfactory HQ Transfer Function

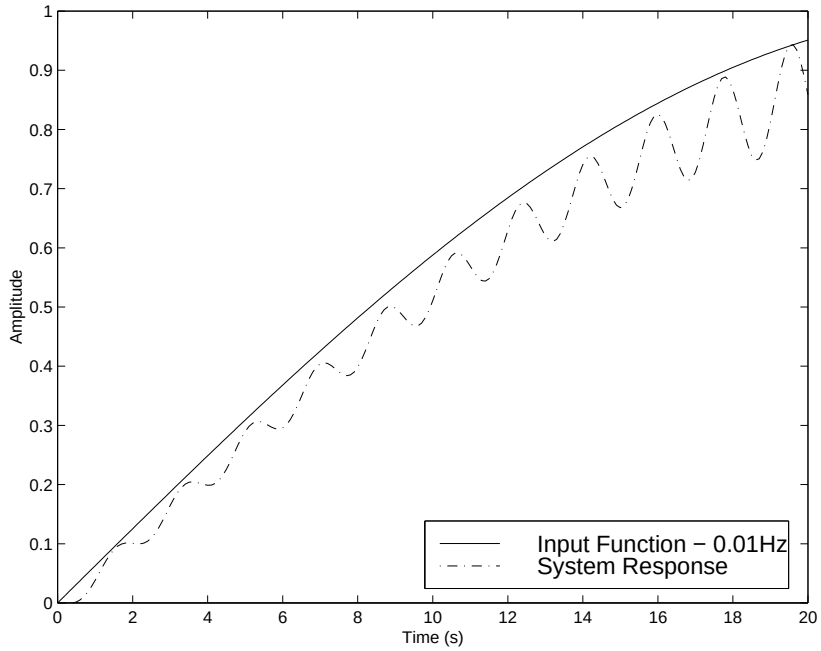

Figure 6.3d Plant Dynamics – Satisfactory HQ Transfer Function

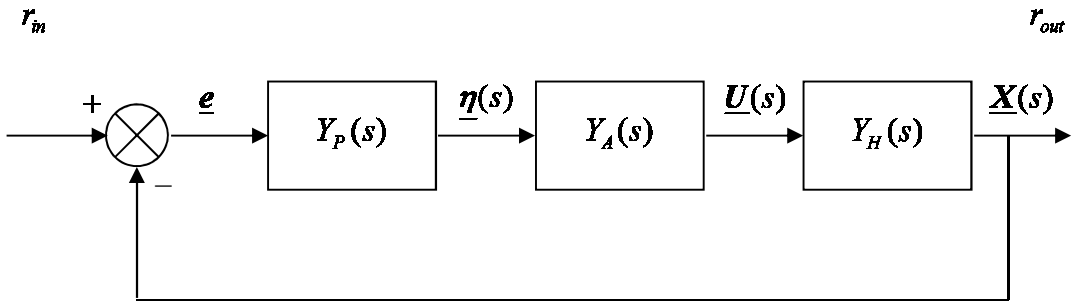

Figure 6.4 Single Axis Compensatory Tracking Using Optimum Pilot Model Parameters

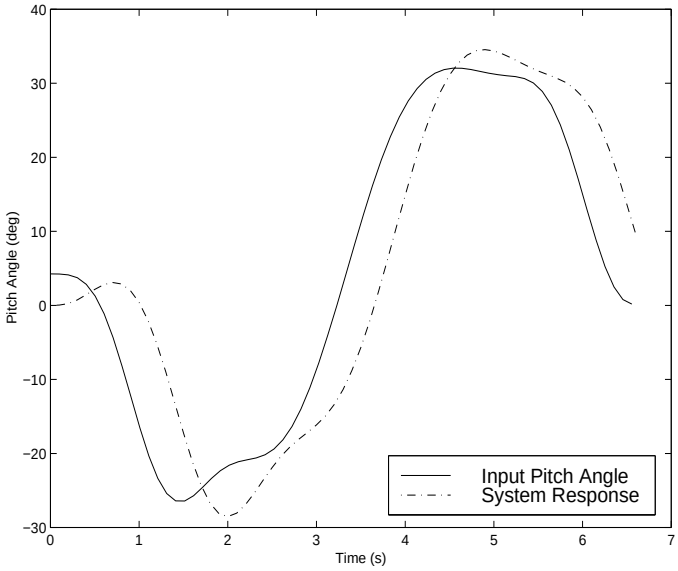

Figure 6.5a Low Aggression Acceleration/deceleration

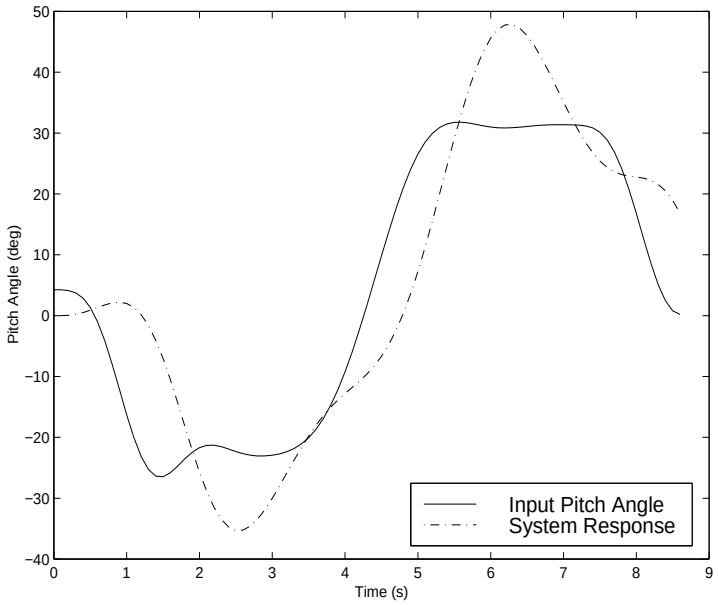

Figure 6.5b Medium Aggression Acceleration/deceleration

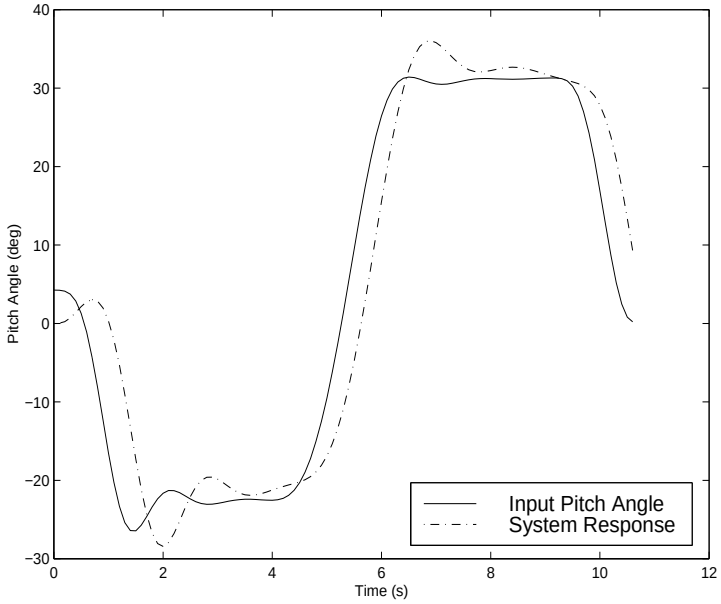

Figure 6.5c High Aggression Acceleration/deceleration

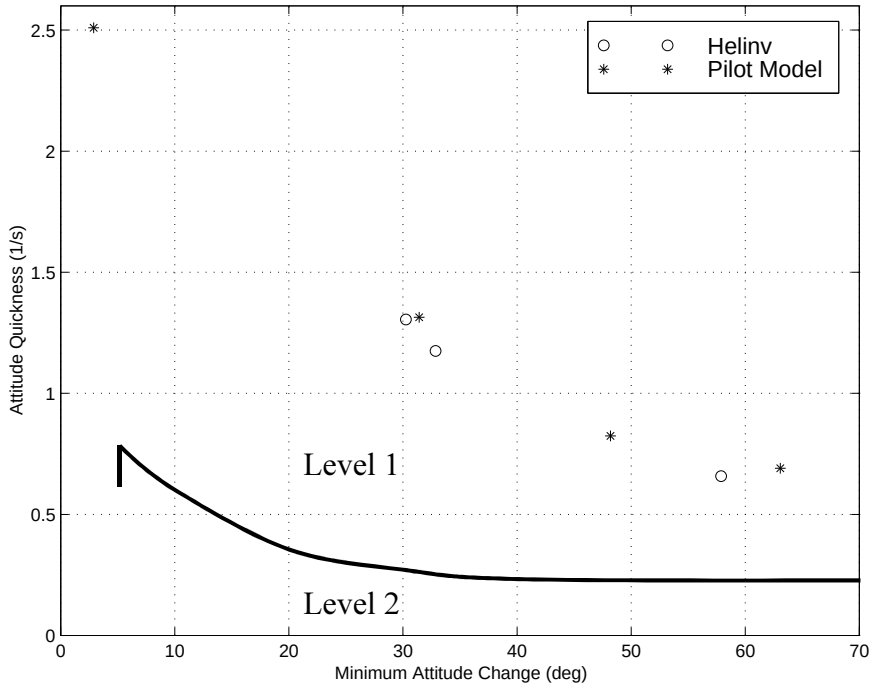

Figure 6.6a Low Aggression Accel./decel. From Helinv and Pilot Model

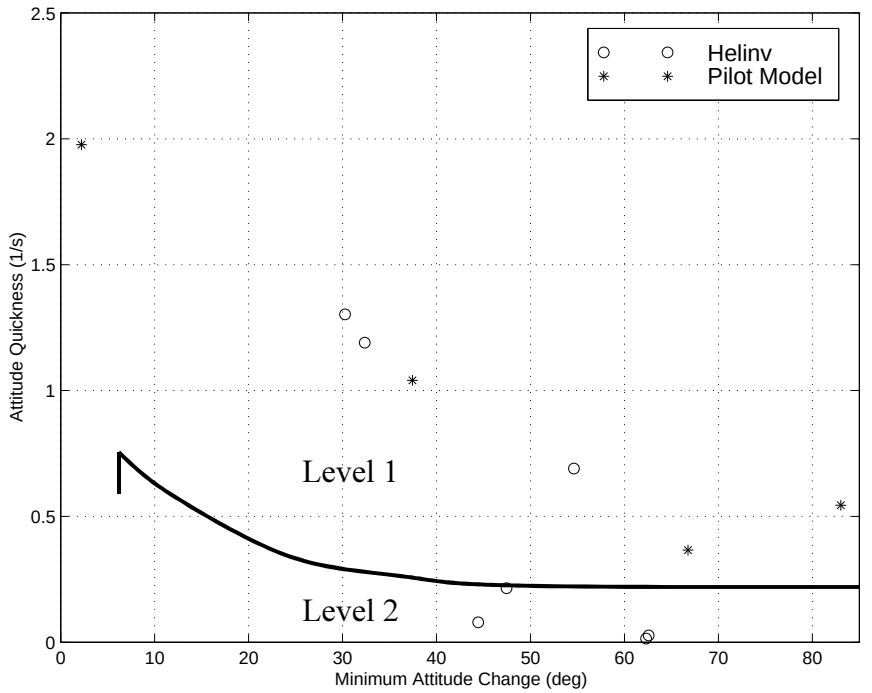

Figure 6.6b Med. Aggression Accel./decel. From Helinv and Pilot Model

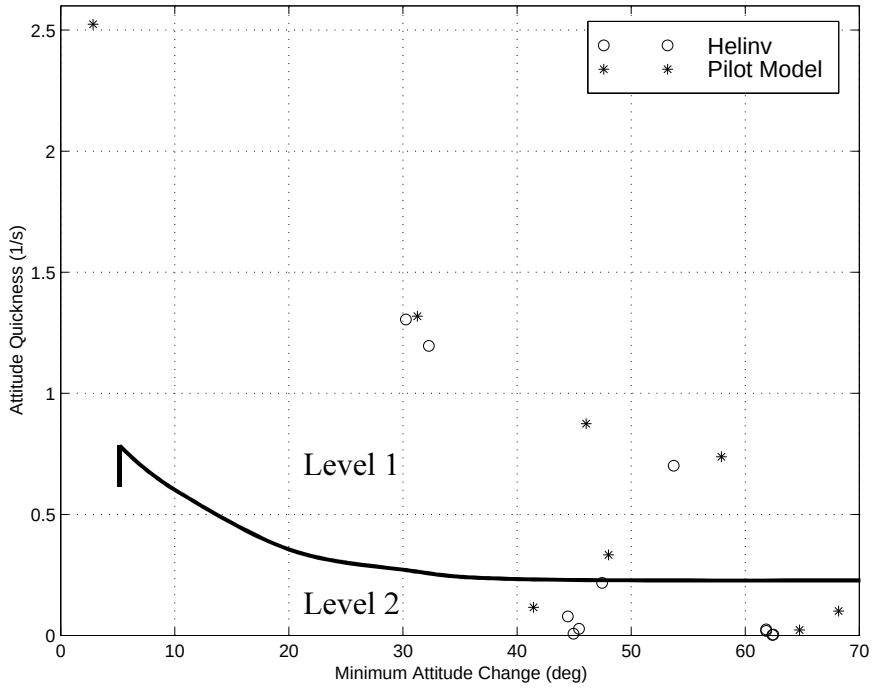

Figure 6.6c High Aggression Accel./decel. From Helinv and Pilot Model

Chapter 7 Figures

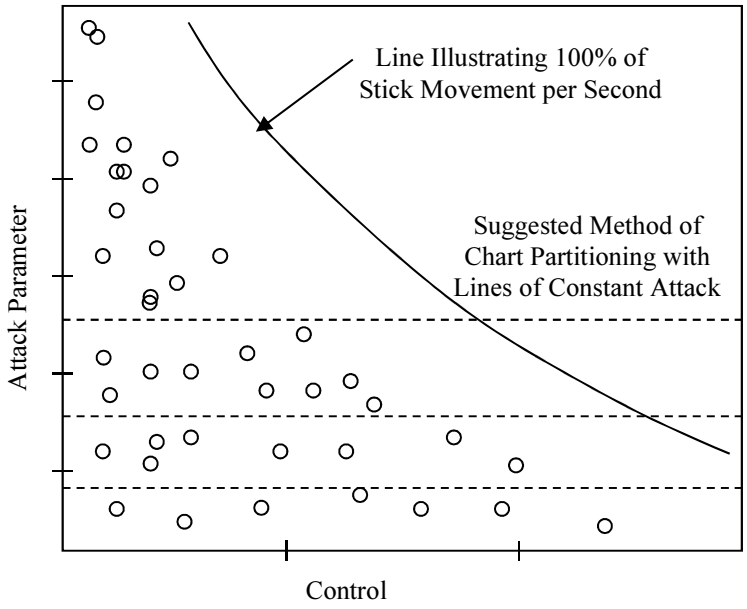

Figure 7.1 General Form of the Pilot Attack Chart with Suggested Partitions

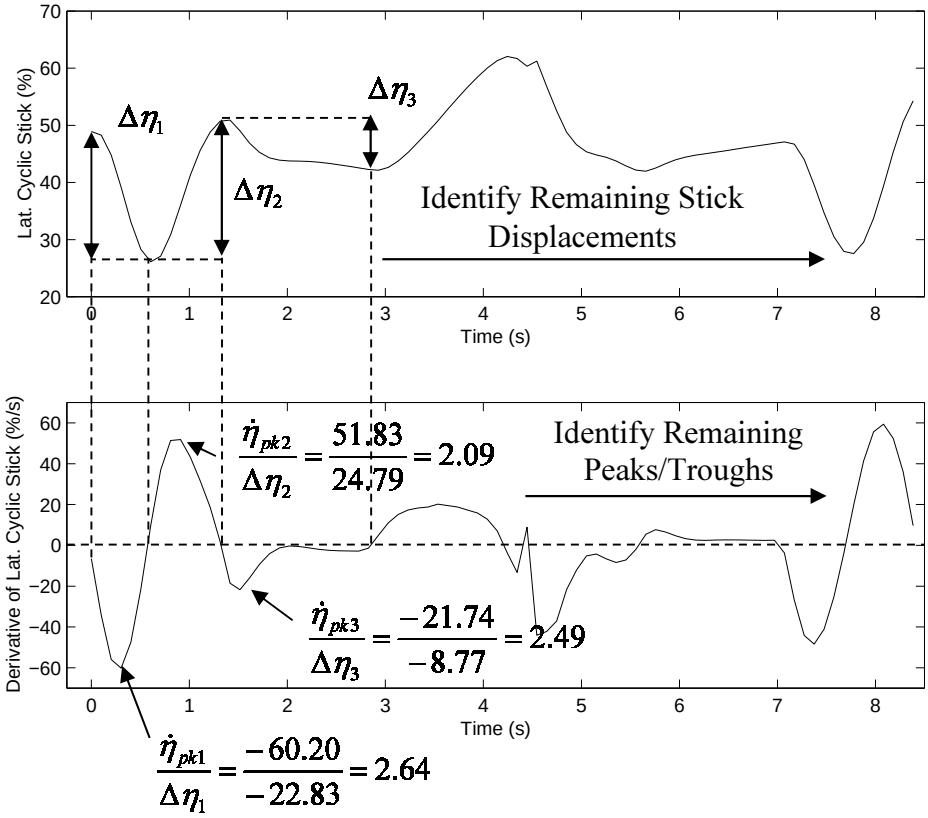

Figure 7.2a Calculation of Pilot Attack Parameters

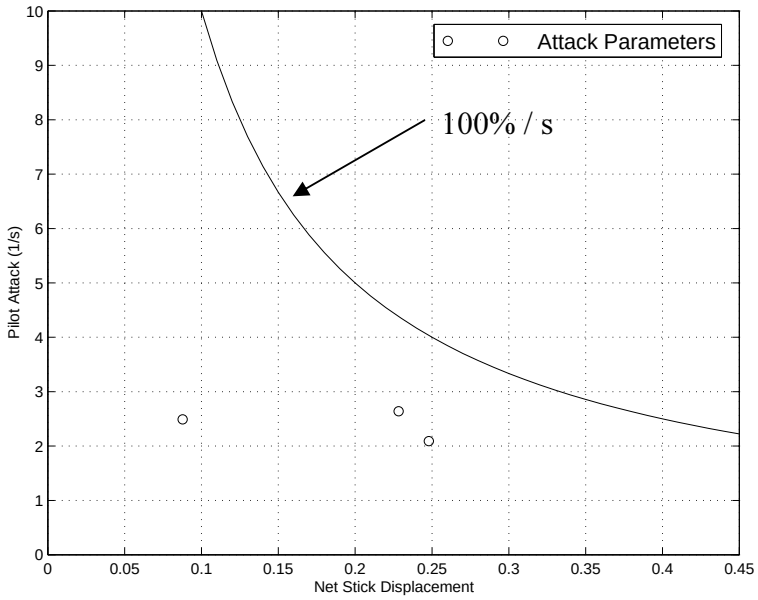

Figure 7.2b Corresponding Pilot Attack Chart

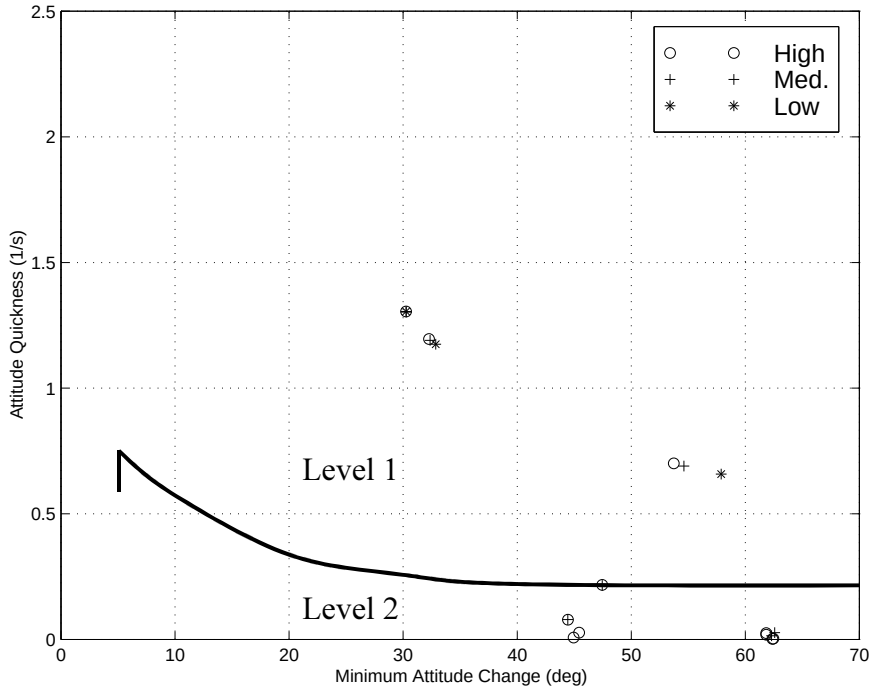

Figure 7.3a Pitch Quickness for Lynx and Acceleration/deceleration

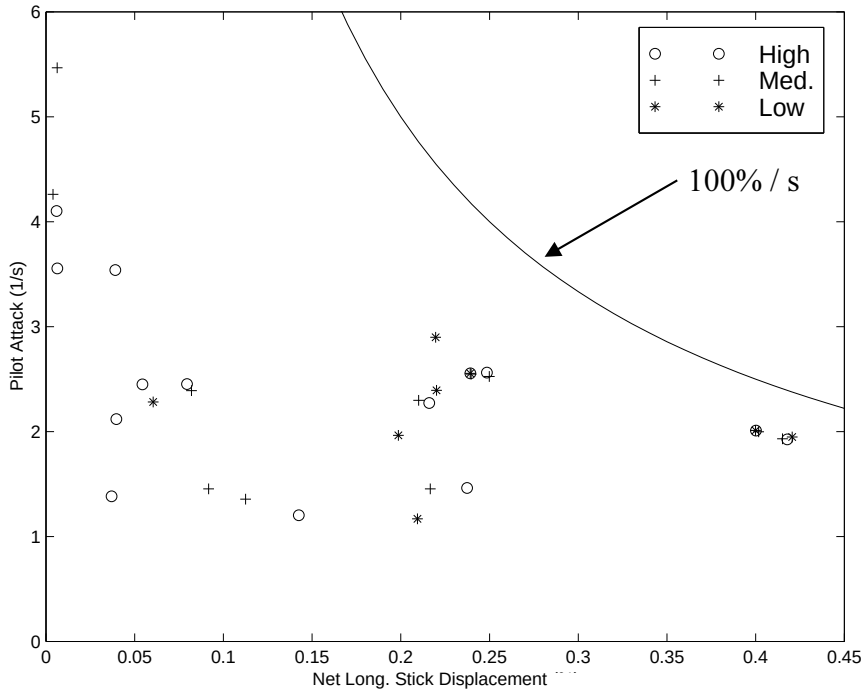

Figure 7.3b Longitudinal Pilot Attack for Lynx and Acceleration/deceleration

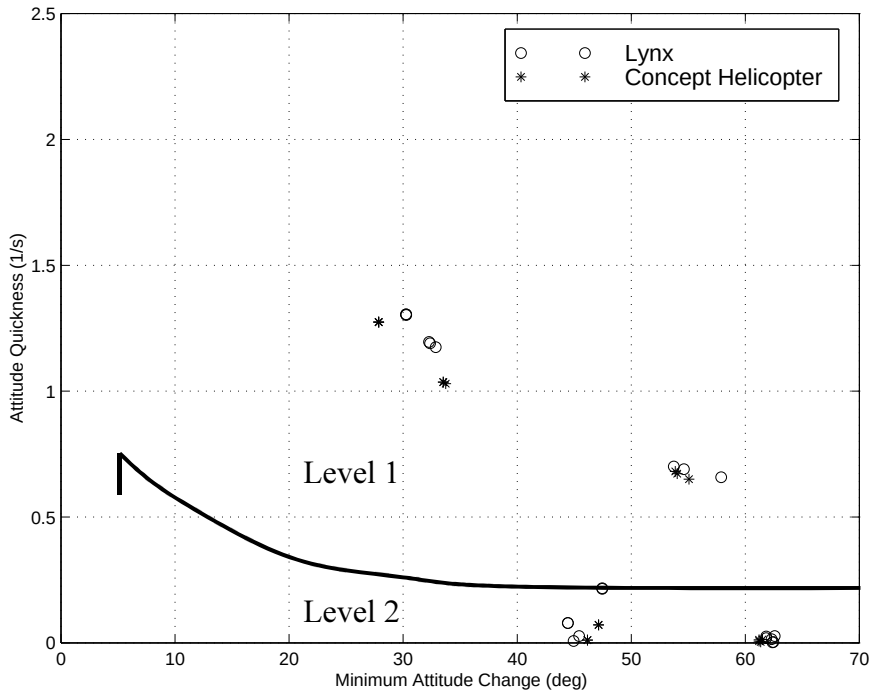

Figure 7.4a Pitch Quickness for Lynx and Concept Helicopter and Accel./decel.

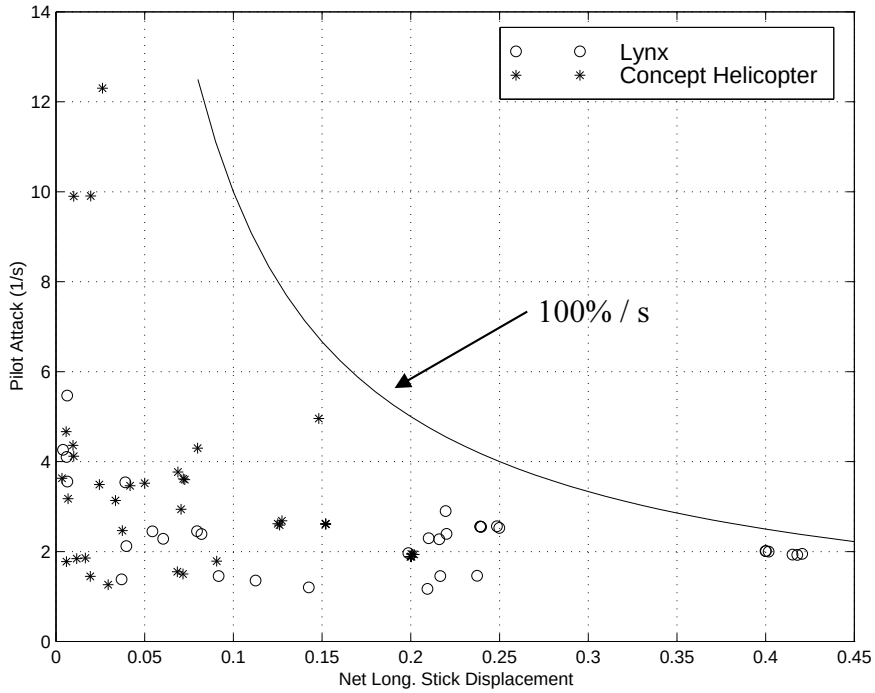

Figure 7.4b Long. Attack for Lynx and Concept Helicopter and Accel./decel.

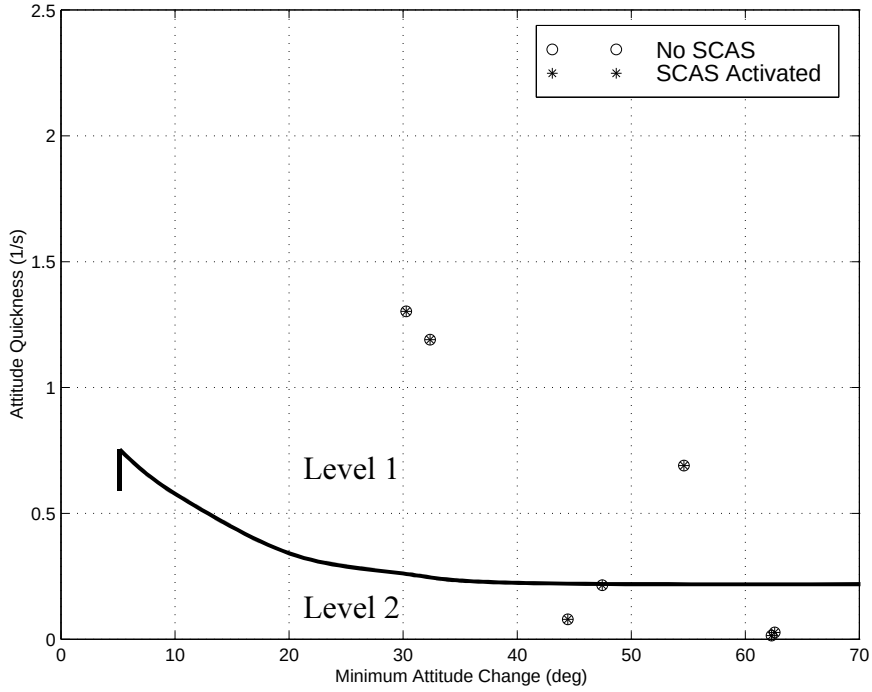

Figure 7.5a Pitch Quickness for Lynx and Acceleration/deceleration

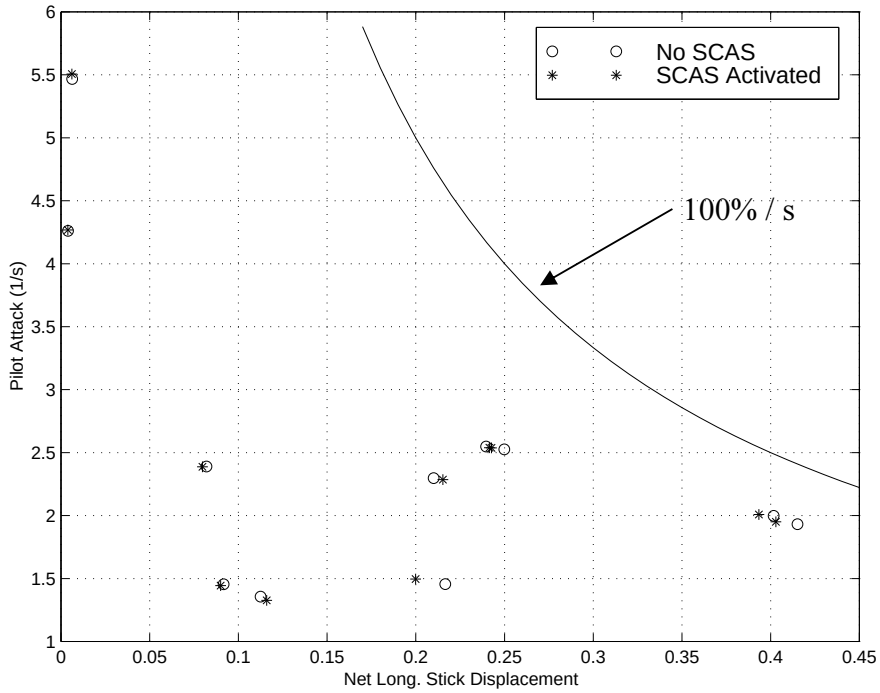

Figure 7.5b Longitudinal Attack for Lynx and Acceleration/deceleration

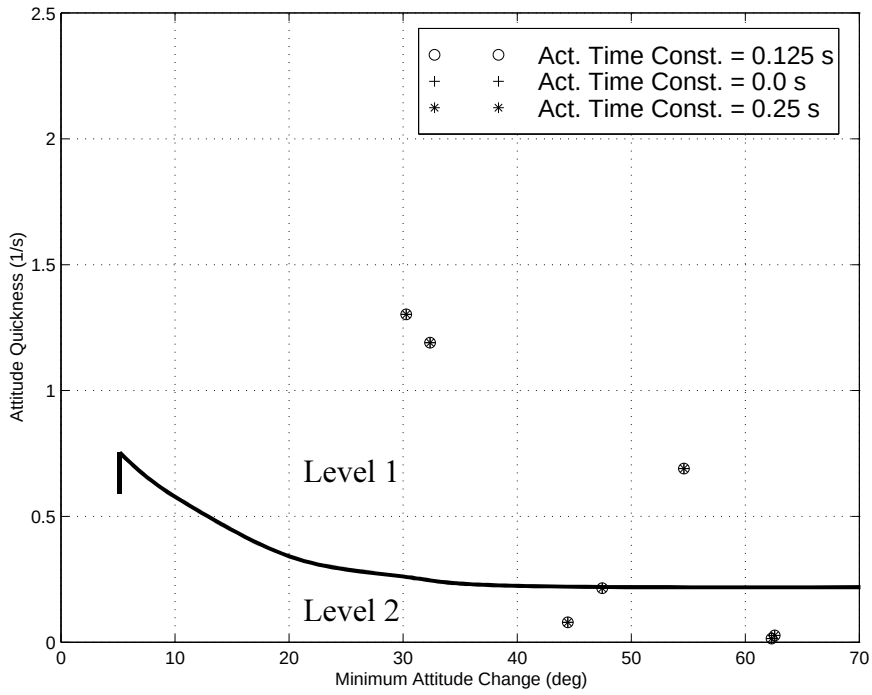

Figure 7.6a Pitch Quickness for Lynx and Acceleration/deceleration

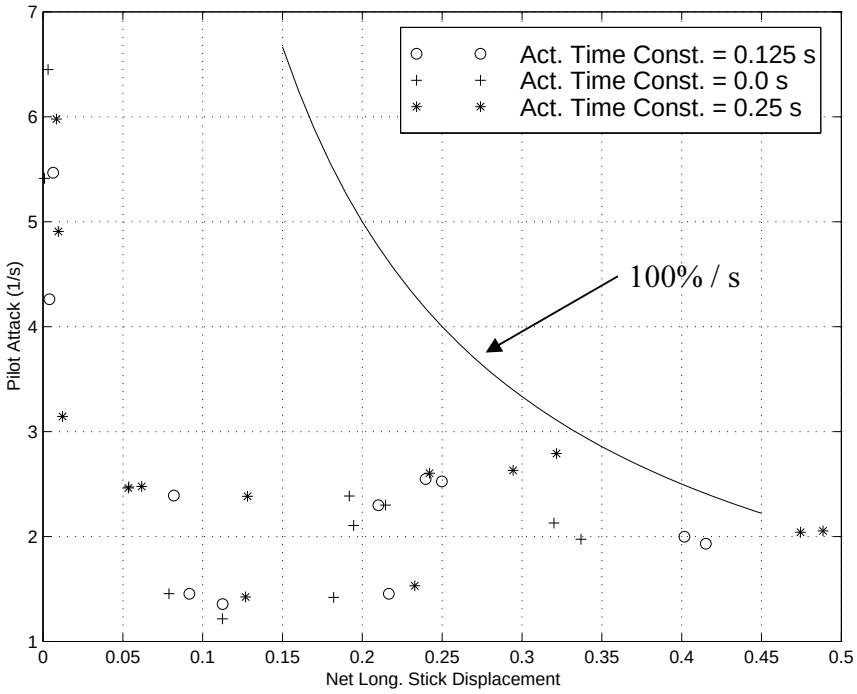

Figure 7.6b Longitudinal Attack for Lynx and Acceleration/deceleration

Appendix A

Pilot Questionnaire

In cockpit Questionnaire

Pilot:……	MTE:……	Configurations……

A) **TASK CUES**	Excellent	Good	Fair	Poor	Inadequate
Rating	← 1	2	3	4	5 →

B) **AGGRESSION**	Minimal	Low	Moderate	High	Maximum
Rating	← 1	2	3	4	5 →

C) **TASK PERFORMANCE**	Clearly within desired performance limits	Desired performance marginally	Clearly within adequate performance limits	Adequate performance marginally	Adequate performance not achievable
Rating	← 1	2	3	4	5 →

D) **TASK WORKLOAD**	Low	Moderate	Considerable	Extensive	Intolerable
Rating	← 1	2	3	4	5 →

E) **SYSTEM CHARACTERISTICS**	Satisfactory or better	Minor but annoying deficiencies	Moderately objectionable deficiencies	Very objectionable but tolerable deficiencies	Major deficiencies but controllable
Heli + Control Law	← 1	2	3	4	5 →
Inceptor	← 1	2	3	4	5 →

HQR		1	2	3	4	5	6	7	8	9
HQR/Subphases	Transition/Acquisition				Tracking					
Influencing Factors			--		-		o		+	++
VEHICLE + CONTROL LAW	Primary response Stability Coupling effects due to inceptor or H/C Vehicle limits									
INCEPTOR	Ergonomics Mech. Char. (Breakout, friction, freeplay) Control Char. (Shaping, force feel, harmony) Sensitivity (Response/displacement)									
CUES	Outside visual cues Instruments (HUD, HDD…) Acceleration cues (missed > negative)									
Comments:										

Appendix B

The Helinv Numerical Algorithm

The reason that inverse simulation has found application in handling qualities investigations is of course that it is possible to make an initial estimate of the Level of handling qualities of any modelled vehicle and trajectory, when coupled with the numerical techniques such as attitude quickness or pilot attack described in Chapter 2. *Bradley and Thomson (1992)* have shown that less agile aircraft can be identified from inverse simulation runs of the same manoeuvre using aircraft with different handling qualities characteristics. The advantages of inverse simulation in effect, conform agreeably to the three suggested stipulations made by *Pausder and von Grünhagen (unknown)*, in that, the modelled test manoeuvres are *representative* of real life test cases, the method is easily *reproducible* and since no aircraft or simulators are involved is completely *without risk.* An overview of the inverse simulation technique and in particular, Helinv is appropriate at this point.

The conventional approach to simulation i.e. simulation in a forward sense is a well-understood problem and involves calculating the response of the vehicle to a particular, well defined sequence of inputs. The problem can be expressed conveniently as,

$$\dot{\underline{x}} = \underline{f}(\underline{x},\underline{u}); \qquad \underline{x}(0) = \underline{x}_0 \tag{B1.1}$$

$$\underline{y} = \underline{g}(\underline{x}) \tag{B1.2}$$

where,

$\underline{x}$ is the state vector of the system and $\underline{u}$ is the control vector.

Equation B1.1 effectively shows how the state vector changes with time and in response to the imposition of the control vector, while Equation B1.2 illustrates how

the resultant output vector $\underline{\boldsymbol{y}}$ is obtained from the state vector. Unlike the system described above, where emphasis is placed upon careful selection of the control vector to produce the required result, the inverse problem places importance on the output vector and calculates the various control time-histories required achieving the desired output.

The helicopter model employed in Helinv is known as Helicopter Generic Simulation which employs a seven degree of freedom state vector $(\underline{\boldsymbol{x}})$ consisting of three translation velocities (U,V,W), three rotational velocities (P,Q,R), three attitude angles (ϕ,θ,ψ), the engine rotorspeed (Ω) and engine torque (Q_E). The control vector $(\underline{\boldsymbol{u}})$ comprises the four helicopter controls, main rotor collective (θ_0), longitudinal and lateral cyclic $(\theta_{1s},\theta_{1c})$, and tail rotor collective (θ_{0tr}). Since inverse simulation requires emphasis to be placed upon defining the output vector correctly, careful consideration must be given to the methods whereby the flight test manoeuvres are described, as they will uniquely define the nature of the output vector.

Chapter 3 remarks on the inverse problem in a general sense and subsequently presents a brief introduction to the differentiation based method of the Helinv algorithm, *Thomson and Bradley (1990a)*. The method adopted by Thomson and Bradley uses numerical differentiation to form the equations of in an algebraic form, hence allowing solution in a closed loop manner. This involves forming a number of equations, n_x in the same number of unknowns whilst introducing a new unknown variable for each equation of motion, hence the inverse solution algorithm is specific to the particular model being used. Appendix C presents an overview of the Helicopter Generic Simulation (HGS) model used in Helinv whilst *Cheney and Kincaid (1985)* discuss the Newton-Raphson iterative solution scheme used to solve the equations of motion.

B1.1. Defining the Flight Path

Helinv contains a number of pre-defined manoeuvres in the form of ADS type Mission Task Elements (MTEs) or manoeuvres defined to be typical piloting tasks in

the nap-of-the-earth (NOE) region of the flight envelope. Each manoeuvre defines in terms of earth fixed axes the required trajectory for the aircraft's centre of gravity to track. With an additional constraint (discussed below) this output vector is used as the input to the inverse simulation algorithm and has the initial form,

$$\underline{\boldsymbol{y}} = \left[x_e \;\; y_e \;\; z_e\right]^T$$

This output vector is defined at equally spaced intervals or time points throughout the manoeuvre. For example if a certain task takes a total time, t_m to complete and it is divided into a series of consecutive time points, n_{ints}, then a general time point in the solution, t_k can be written as, $0 < t_k < t_m$ where $1 < k \leq (n_{ints} + 1)$. The input vector to the inverse simulation algorithm at this time is given by, $\underline{\boldsymbol{y}} = \left[x_e(\mathrm{t_k}) \;\; y_e(\mathrm{t_k}) \;\; z_e(\mathrm{t_k})\right]^T$, which can be differentiated to yield the respective velocities and accelerations,

$$\dot{\underline{\boldsymbol{y}}} = \left[\dot{x}_e(\mathrm{t_k}) \;\; \dot{y}_e(\mathrm{t_k}) \;\; \dot{z}_e(\mathrm{t_k})\right]^T \text{ and } \ddot{\underline{\boldsymbol{y}}} = \left[\ddot{x}_e(\mathrm{t_k}) \;\; \ddot{y}_e(\mathrm{t_k}) \;\; \ddot{z}_e(\mathrm{t_k})\right]^T$$

However, specifying only these three components of the flight path is insufficient to define the motion of the aircraft exactly since it is only determining the position of the centre of gravity of the aircraft, and it is subsequently free to point in any direction. Looking at the four available controls in the vehicle it is clear that the main rotor collective will be most influential on controlling displacements in heave, or in the *z* direction. The *x* and *y* directions are essentially controlled by use of longitudinal and lateral cyclic respectively. This leaves the yaw control, or tail rotor collective as the remaining control and it follows that the heading angle (ψ), of the aircraft will be a suitable constraint. Thus the output vector from Helinv defining the manoeuvre for inverse solution at any general time point is,

$$\underline{\boldsymbol{y}} = \left[x_e(\mathrm{t_k}) \;\; y_e(\mathrm{t_k}) \;\; z_e(\mathrm{t_k}) \;\; \psi(\mathrm{t_k})\right]^T$$

This is most suitable when the manoeuvre concerned is to be flown at a constant heading, for example the Pop-up flight test manoeuvre introduced in Chapter 3, Figure 3.3. However, if the manoeuvre involves turning flight, such as a Slalom task where the heading is constantly changing, it is more convenient to define the sideslip angle $(\beta(t_k))$ of the aircraft. The corresponding sideslip velocity and acceleration can be found from,

$$V = V_f \sin\beta(t_k) \text{ and } \dot{V} = \dot{V}_f \sin\beta(t_k) + \dot{\beta}(t_k)\dot{V}_f \cos\beta(t_k)$$

where,

V_f is the flight path velocity and

$\dot{\beta}(t_k)$ is the rate of change of sideslip.

The sideslip velocity can also be determined from the transformation of the velocity components in earth axes, $(\dot{x}_e, \dot{y}_e, \dot{z}_e)$ to the aircraft body axes given by,

$$V = \left[m_1\dot{x}_e + m_2\dot{y}_e + m_3\dot{z}_e\right]^T \tag{B1.1}$$

where,

m_1, m_2 and m_3 are given in Chapter 4, Equation 4.3.

Upon substitution of m_1, m_2 and m_3 into Equation B1.1, with further rearrangement it can be presented in the form,

$$a\cos\psi + b\sin\psi + c = 0 \tag{B1.2}$$

where,

$a = \dot{x}_e \sin\phi \sin\theta + \dot{y}_e \cos\phi,$
$b = -\dot{x}_e \cos\phi + \dot{y}_e \sin\phi \sin\theta$ and
$c = \dot{z}_e \sin\phi \cos\theta - V$

Clearly, Equation B1.2 can be solved for ψ using the Newton-Raphson method provided values of ϕ and θ and known. When all the required flight parameters have been calculated from the input manoeuvre data the inverse solution procedure can proceed.

B1.2 Helinv Inverse Simulation Algorithm

The basic problem of the Helinv algorithm is the solution of the seven equations of motion, (above) for seven unknowns given by,

$$\underline{\boldsymbol{u}} = \left[\phi, \theta, \theta_0, \theta_{1s}, \theta_{1c}, \theta_{0tr}, \Omega\right]$$

Considering the basic model the seven equations of motion are initially rearranged to give,

$$f_1\left(\phi, \theta, \theta_0, \theta_{1s}, \theta_{1c}, \theta_{0tr}, \Omega\right) = -m\left(\dot{U} + WQ - VR\right) + X - mg\sin\theta = 0$$

$$\vdots$$

$$f_7\left(\phi, \theta, \theta_0, \theta_{1s}, \theta_{1c}, \theta_{0tr}, \Omega\right) = \ddot{Q}_E \tau_{e1}\tau_{e2} + \left(\tau_{e1} + \tau_{e3}\right)\dot{Q}_E + Q_E - K_3\left(\Omega - \Omega_{idle} + \tau_{e2}\dot{\Omega}\right) = 0$$

The inverse algorithm starts the solution process by providing an initial guess of the vector $\underline{\boldsymbol{u}}$. It then proceeds to calculate the rates of the unknown attitudes, $\dot{\phi}$ and $\dot{\theta}$ by numerical differentiation. This allows the unsteady terms in the equations of motion to be calculated thus converting the vehicle equations of motion into a set of non-linear algebraic expressions. The Newton-Raphson iterative scheme is used to provide a better estimate of the unknown vector, $\underline{\boldsymbol{u}}$. As the output vector $\underline{\boldsymbol{y}}$, expresses the desired flight path in the form of a manoeuvre time history, the inverse algorithm is cast in a "time marching" form and solves the equations of motion at each point in the flight trajectory. The complex nature of the expressions that form the body velocities, vehicle forces and moments etc. determines that the calculation sequence of the inverse algorithm must be undertaken in a specific order as briefly mentioned in Chapter 3.

B1.2.1 Earth Fixed Velocities and Heading Angle

At any general time point in the manoeuvre, t_k the earth fixed velocities, $\dot{x}_e(\mathrm{t_k}), \dot{y}_e(\mathrm{t_k})$ and $\dot{z}_e(\mathrm{t_k})$ are known from differentiation of the manoeuvre model definitions in earth axes. Since many of the manoeuvres are given by simple polynomial functions of time this generally involves elementary calculations. The heading angle is calculated from the method described above in section B1.1. and is therefore also known at any general time point in the manoeuvre.

B1.2.2 Determination of Body Attitude Angles and Rates

An estimate of the roll and pitch attitude is made at the start of each iteration, *m*, of the Newton-Raphson scheme. Considering only the pitch attitude at time point $t_k, \theta(t_k)$ the initial guess is given by,

$$\theta(t_k)_m = \begin{cases} \theta(0) & \text{for } m = 1, k = 1 \\ \theta(t_{k-1}) & \text{for } m = 1 \\ \theta(t_k)_{m-1} & \text{for } m > 1 \end{cases}$$

It is evident from the above expressions that the value from the previous time point, $k-1$, is used as an initial estimate for the first iteration at each time point. Additionally, for the first iteration at time point, $t = 0$, the estimate of pitch attitude assumes a value that is available from a predetermined trim condition available at the start of the simulation of the manoeuvre. The roll attitude, ϕ is treated in the same manner. Using numerical differentiation it is possible to evaluate the first, $\dot{\theta}(t_k)_m$ and second, $\ddot{\theta}(t_k)_m$ derivatives with respect to time, of the pitch attitude angle as follows,

$$\dot{\theta}(t_k)_m = \frac{\theta(t_k)_m - \theta(t_{k-1})}{t_k - t_{k-1}}$$

and

$$\ddot{\theta}(t_k)_m = \frac{\dot{\theta}(t_k)_m - 2\dot{\theta}(t_{k-1}) - \dot{\theta}(t_{k-2})}{(t_k - t_{k-1})^2}$$

The roll attitude and rotorspeed rates can be determined in the same way.

B1.2.3 Determination of Body Translation Velocities and Accelerations

The body axes translation velocities are evaluated by a series of transformations of the earth fixed velocities $\dot{x}_e, \dot{y}_e$ and $\dot{z}_e$ via the Euler attitude angles, $(\phi, \theta \text{ and } \psi)$. This transformation is the transpose of that implied in Chapter 4, Equation 4.3 where the output vector, $\underline{\boldsymbol{y}}$ is related to the system state, $\underline{\boldsymbol{x}}$ and attitude vector, $\underline{\boldsymbol{\chi}}$, through the function, $\underline{\boldsymbol{h}}$. Therefore the vehicle translation velocities for the m^{th} iteration of time point k can be found from,

$$\begin{bmatrix} U \\ V \\ W \end{bmatrix}_{(t_k)_m} = \begin{bmatrix} l_1 & l_2 & l_3 \\ m_1 & m_2 & m_3 \\ n_1 & n_2 & n_3 \end{bmatrix} \begin{bmatrix} \dot{x}_e \\ \dot{y}_e \\ \dot{z}_e \end{bmatrix}_{(t_k)} \tag{B1.3}$$

where,

$l_1, l_2, \ldots n_3$ are the direction cosines given in Chapter 4, Equation 3.3.

The rotorcraft body axes accelerations can be found by differentiating Equation B1.3 to give,

$$\begin{bmatrix} \dot{U} \\ \dot{V} \\ \dot{W} \end{bmatrix}_{(t_k)_m} = \begin{bmatrix} l_1 & l_2 & l_3 \\ m_1 & m_2 & m_3 \\ n_1 & n_2 & n_3 \end{bmatrix} \begin{bmatrix} \ddot{x}_e \\ \ddot{y}_e \\ \ddot{z}_e \end{bmatrix}_{(t_k)} + \begin{bmatrix} \dot{l}_1 & \dot{l}_2 & \dot{l}_3 \\ \dot{m}_1 & \dot{m}_2 & \dot{m}_3 \\ \dot{n}_1 & \dot{n}_2 & \dot{n}_3 \end{bmatrix} \begin{bmatrix} \dot{x}_e \\ \dot{y}_e \\ \dot{z}_e \end{bmatrix}_{(t_k)}$$

where,

$\dot{l}_1, \dot{l}_2, \ldots \dot{n}_3$ are the derivatives with respect to time of the direct cosines and can be written as,

$$\dot{l}_1 = -\dot{\theta}(t_k)_m \sin\theta(t_k)_m \cos\psi(t_k) - \dot{\psi}(t_k)\cos\theta(t_k)_m \sin\psi(t_k) \text{ etc.}$$

B1.2.4 Determination of Body Rotational Velocities and Accelerations

The rotational velocities of the vehicle about the body fixed axes set for the k^{th} time point and the m^{th} iteration of the Newton-Raphson scheme can be evaluated by rearranging the Euler angle rates, Chapter 4, Equation 4.2. Considering only the roll rate P the following expressions are used to determine the respective rotational velocity and acceleration.

$$P(t_k)_m = \dot{\phi}(t_k)_m - \dot{\psi}(t_k)\sin\theta(t_k)_m$$

$$\dot{P}(t_k)_m = \ddot{\phi}(t_k)_m - \ddot{\psi}(t_k)\sin\theta(t_k)_m - \dot{\psi}(t_k)\dot{\theta}(t_k)_m\cos\theta(t_k)_m$$

The same process is used to find expressions for, $Q(t_k)_m, \dot{Q}(t_k)_m, R(t_k)_m$ and $\dot{R}(t_k)_m$.

B1.2.5 Determination of Vehicle External Forces and Moments

With estimates of all the states it is possible to evaluate the external forces and moments as described in Appendix C. Once the net contribution of individual forces and moments generated by the constituent components of the helicopter is determined, all the information is present to permit the calculation of the latest error vector, $\underline{\boldsymbol{e}}$.

B1.2.6 Updating the Current Control Estimate

The Newton-Raphson iterative scheme employed in the Helinv algorithm has the following structure,

$$\begin{bmatrix} \phi \\ \vdots \\ \vdots \\ \Omega \end{bmatrix}_{(t_k)_{m+1}} = \begin{bmatrix} \phi \\ \vdots \\ \vdots \\ \Omega \end{bmatrix}_{(t_k)_m} - \begin{bmatrix} \left(\frac{\partial f_1}{\partial \phi}\right) \cdots & \cdots \left(\frac{\partial f_1}{\partial \Omega}\right) \\ \vdots & \vdots \\ \vdots & \vdots \\ \left(\frac{\partial f_7}{\partial \phi}\right) \cdots & \cdots \left(\frac{\partial f_7}{\partial \Omega}\right) \end{bmatrix}^{-1}_{(t_k)_m} \begin{bmatrix} f_1(\phi,\theta,\theta_0,\theta_{1s},\theta_{1c},\theta_{0tr},\Omega) \\ \vdots \\ \vdots \\ f_7(\phi,\theta,\theta_0,\theta_{1s},\theta_{1c},\theta_{0tr},\Omega) \end{bmatrix}_{(t_k)_m}$$

This allows new estimates of the unknown variables to be made. The Helinv algorithm iterates until the error functions are within a prescribed tolerance. The Jacobian elements are calculated by numerical differentiation, so that, for example,

$$\left(\frac{\delta f_1}{\delta \phi}\right) = \frac{f_1(\phi + \delta\phi, \theta + \delta\theta, ...\Omega) - f_1(\phi - \delta\phi, \theta - \delta\theta, ...\Omega)}{2\delta\phi}$$

for a small perturbation in $\phi, \delta\phi$.

The calculation sequence can be summarised by the following six steps.

1. The three earth fixed velocities and heading angle, $(\dot{x}_e, \dot{y}_e, \dot{z}_e$ and $\psi)$ are known from the flight trajectory definition (flight test manoeuvre model). Since each manoeuvre is defined in spatial and temporal terms and these component velocities and the heading angle are known at each time point in the manoeuvre.

2. Initial estimates are made of the unknown roll and pitch attitudes, $(\phi$ and $\theta)$ and the control vector, $\underline{\boldsymbol{u}}$. At the start of the flight test manoeuvre the initial estimates are calculated from a trim position defined for that particular task.

3. Transformations through the attitude or Euler angles allow determination of the body referenced translation velocities, U, V and W and accelerations $\dot{U}, \dot{V}$ and $\dot{\mathrm{W}}$ by differentiation.

4. The angular velocities, P, Q and R and accelerations, $\dot{P}, \dot{Q}$ and $\dot{\mathrm{R}}$ are obtained by differentiation of the attitudes.

5. Having established estimates for all of the vehicle's states and controls, the external forces and moments, X, Y, Z, L, M and N can be calculated. This section of the calculation is best seen in Appendix C where the HGS model is described further.

6. Values for the seven functions, $f_1 \ldots f_7$, Equation B1.3 below, and the error vector $\underline{\boldsymbol{e}}$ can be obtained, hence allowing, through the Newton-Raphson scheme *Cheney and Kincaid (1985)*, new estimates of the control vector $\underline{\boldsymbol{u}}$.

Appendix C

Helicopter Generic Simulation (HGS)

C1.1 Overview of Model

HGS was developed originally to investigate nap-of-the-earth (NOE) flight and the approach taken was to calculate the forces and moments generated by each of the components comprising the vehicle. The fuselage degrees of freedom are described using the familiar Euler rigid body equations of motion, Equations C1.1 and the dynamics are expressed in terms of the body velocities and accelerations, corresponding derivatives and the total external forces and moments. The method adopted is to calculate individual force/moment contributions of each component and summate them to obtain the overall external forces and moments influencing the dynamics of the vehicle.

$$
\begin{aligned}
\dot{U} &= -(WQ - VR) + \frac{X}{m} - g\sin\theta \\
\dot{V} &= -(UR - WP) + \frac{Y}{m} + g\cos\theta\sin\theta \\
\dot{W} &= -(VP - UQ + \frac{Z}{m} - g\cos\theta\cos\theta \\
I_{xx}\dot{P} &= (I_{yy} - I_{zz})QR + I_{xz}(\dot{R} + PQ) + L \\
I_{yy}\dot{Q} &= (I_{zz} - I_{xx})RP + I_{xz}(R^2 - P^2) + M \\
I_{zz}\dot{R} &= (I_{xx} - I_{yy})PQ + I_{xz}(\dot{P} - QR) + N
\end{aligned}
\qquad \text{(C1.1)}
$$

where,

U, V, W are the velocities of vehicle translation referred to generalised body axes ($x_{\mathbf{bod}}$, $y_{\mathbf{bod}}$ and $z_{\mathbf{bod}}$) and are positive in the directions of the unit vectors $\underline{\mathbf{i}}_{\mathbf{bod}}$, $\underline{\mathbf{j}}_{\mathbf{bod}}$ and $\underline{\mathbf{k}}_{\mathbf{bod}}$ respectively,

P, Q, R are the rotational velocities about the same body axes and are positive in the direction consistent with those determined by the right-hand rule,

m is the all-up-mass of the vehicle,

I_{xx}, I_{yy}, I_{zz} are the moments of inertia of the vehicle referred to the body axes,

I_{xz} is the product of inertia of the vehicle,

X, Y, Z are the external forces acting upon the vehicle at its centre of gravity and are positive in the directions of the unit vectors $\underline{\mathbf{i}}_{\mathbf{bod}}$, $\underline{\mathbf{j}}_{\mathbf{bod}}$ and $\underline{\mathbf{k}}_{\mathbf{bod}}$ respectively and

L, M, N are the external moments acting about the centre of gravity of the vehicle.

The rates of change of the Euler attitude angles $(\dot{\phi}, \dot{\theta}$ and $\dot{\psi})$ are related to the body axes rotational velocities P, Q and R by the kinematic expressions,

$$\begin{aligned} \dot{\phi} &= P + Q\sin\phi\tan\theta + R\cos\phi\tan\theta \\ \dot{\theta} &= Q\cos\phi - R\sin\phi \\ \dot{\psi} &= Q\sin\phi\sec\theta + R\cos\phi\sec\theta \end{aligned} \qquad \text{(C1.2)}$$

where,

ϕ, θ and ψ are the respective roll, pitch and yaw attitude angles of the fuselage.

Using the body fixed translation velocities U, V and W from Equation C1.1 and the Euler attitude angles ϕ, θ and ψ from Equation C1.2, the vehicle velocities referred to the earth fixed axes set $\dot{x}_e, \dot{y}_e$ and $\dot{z}_e$ can be calculated from the following Euler transformation equations.

$$\begin{bmatrix} \dot{x}_e \\ \dot{y}_e \\ \dot{z}_e \end{bmatrix} = \begin{Bmatrix} l_1 & m_1 & n_1 \\ l_2 & m_2 & n_2 \\ l_3 & m_3 & n_3 \end{Bmatrix} \begin{bmatrix} U \\ V \\ W \end{bmatrix} \tag{C1.3}$$

where,

$l_1 = \cos\theta\cos\psi,\ m_1 = \sin\phi\sin\theta\cos\psi - \cos\phi\sin\psi,\ n_1 = \cos\phi\sin\theta\cos\psi + \cos\phi\sin\psi,$
$l_2 = \cos\theta\sin\psi,\ m_2 = \sin\phi\sin\theta\sin\psi + \cos\phi\cos\psi,\ n_2 = \cos\phi\sin\theta\sin\psi - \cos\phi\cos\psi,$
$l_3 = -\sin\theta,\quad m_3 = \sin\phi\cos\theta,\quad n_3 = \cos\phi\cos\theta.$

Now, a single main and single tail rotor helicopter will typically comprise the following components:

i) Main rotor (subscript *ROT*),
ii) Tail rotor (*TR*),
iii) Fuselage (*fus*),
iv) Tailplane (*tp*) and
v) Fin (*fin*).

The expressions for calculation of the total forces and moments are formulated as follows,

$$\begin{aligned} X &= X_{ROT} + X_{TR} + X_{fus} + X_{tp} + X_{fin} \\ Y &= Y_{ROT} + Y_{TR} + Y_{fus} + Y_{tp} + Y_{fin} \\ Z &= Z_{ROT} + Z_{TR} + Z_{fus} + Z_{tp} + Z_{fin} \\ L &= L_{ROT} + L_{TR} + L_{fus} + L_{tp} + L_{fin} \\ M &= M_{ROT} + M_{TR} + M_{fus} + M_{tp} + M_{fin} \\ N &= N_{ROT} + N_{TR} + N_{fus} + N_{tp} + N_{fin} \end{aligned} \tag{C1.4}$$

C1.2 The Rotor Model

Typically, mathematical models of helicopter rotor blades have a common starting point to calculating the forces and moments. This initial step usually starts with the calculation of the aerodynamic and inertial loads on an individual blade element and then integrating the elemental loads along the blade span. Since HGS is a multiblade or disc model the assumption is made that only the steady components

calculated affect the dynamics of the vehicle. Although the individual blade modelling technique permits calculations of a higher fidelity to be made, the multiblade approach does allow the rotor forces and moments to be calculated over the entire rotor disc, while producing a comparatively fast analytical tool.

C1.2.1 Kinematics of a Blade Element

The axes system of the helicopter is assumed to be fixed at the aircraft's centre of gravity, (itself assumed fixed in the aircraft). The action of the external forces and moments applied to the aircraft cause the axes system to move with varying translation (u, v and w) and rotational (p, q and r) component velocities. If we assume that $\underline{\mathbf{i}}, \underline{\mathbf{j}}$ and $\underline{\mathbf{k}}$ are unit vectors along the x, y and z axes respectively then, for any general flight state it can be shown that the linear translation velocity and acceleration of the centre of mass of the helicopter in body axes, (subscripts **bod**, *bod*) is given by,

$$V_{cm} = u\,\underline{\mathbf{i}}_{\mathbf{bod}} + v\,\underline{\mathbf{j}}_{\mathbf{bod}} + w\,\underline{\mathbf{k}}_{\mathbf{bod}} \text{ and } \quad a_{cm} = \dot{u}\,\underline{\mathbf{i}}_{\mathbf{bod}} + \dot{v}\,\underline{\mathbf{j}}_{\mathbf{bod}} + \dot{w}\,\underline{\mathbf{k}}_{\mathbf{bod}} \qquad \text{(C1.5)}$$

The corresponding rotational velocity and acceleration in body axes are expressed in the form,

$$\underline{\omega}_{\mathbf{bod}} = p\,\underline{\mathbf{i}}_{\mathbf{bod}} + q\,\underline{\mathbf{j}}_{\mathbf{bod}} + r\,\underline{\mathbf{k}}_{\mathbf{bod}} \text{ and } \quad \underline{\alpha}_{\mathbf{bod}} = \frac{\partial \underline{\omega}_{\mathbf{bod}}}{\partial t} = \dot{p}\,\underline{\mathbf{i}}_{\mathbf{bod}} + \dot{q}\,\underline{\mathbf{j}}_{\mathbf{bod}} + \dot{r}\,\underline{\mathbf{k}}_{\mathbf{bod}} \qquad \text{(C1.6)}$$

C1.2.1.1 Velocity and Acceleration of the Main Rotor Hub

Since the ultimate aim is to find expressions for the velocity and acceleration of a blade element (in blade element axes) the formulation for the same rotor parameters must first be found for the rotor hub and subsequently transformed to the blade element. The relevant transformations are,

i) body to hub axes (transformation through shaft angle),
ii) hub to shaft axes (transformation through azimuth angle) and
iii) shaft to blade element axes (transformation through flap angle).

The respective velocity, acceleration and angular velocity in blade axes are given by,

$$\begin{aligned}\underline{\boldsymbol{V}}_{hub/\mathbf{bl}} = &\left[(-u_{hub}\cos\psi + v_{hub}\sin\psi - \beta\, w_{hub})\right]\underline{\mathbf{i}}_{\mathbf{bl}} + \\ &\left[(-u_{hub}\sin\psi - v_{hub}\cos\psi)\right]\underline{\mathbf{j}}_{\mathbf{bl}} + \\ &\left[\beta(-u_{hub}\cos\psi + v_{hub}\sin\psi) + w_{hub}\right]\underline{\mathbf{k}}_{\mathbf{bl}}\end{aligned} \tag{C1.7}$$

$$\begin{aligned}\underline{\boldsymbol{a}}_{hub/\mathbf{bl}} = &\left[-\underline{\boldsymbol{a}}_{hub/\mathbf{x}}\cos\psi + \underline{\boldsymbol{a}}_{hub/\mathbf{y}}\sin\psi - \beta\underline{\boldsymbol{a}}_{hub/\mathbf{z}}\right]\underline{\mathbf{i}}_{\mathbf{bl}} + \\ &\left[-\underline{\boldsymbol{a}}_{hub/\mathbf{x}}\sin\psi - \underline{\boldsymbol{a}}_{hub/\mathbf{y}}\cos\psi\right]\underline{\mathbf{j}}_{\mathbf{bl}} + \\ &\left[\beta(-\underline{\boldsymbol{a}}_{hub/\mathbf{x}}\cos\psi + \underline{\boldsymbol{a}}_{hub/\mathbf{y}}\sin\psi) + \underline{\boldsymbol{a}}_{hub/\mathbf{z}}\right]\underline{\mathbf{k}}_{\mathbf{bl}}\end{aligned} \tag{C1.8}$$

$$\begin{aligned}\underline{\boldsymbol{\omega}}_{hub/\mathbf{bl}} = &\left[(-p_{hub}\cos\psi + q_{hub}\sin\psi - \beta(r_{hub} - \Omega)\right]\underline{\mathbf{i}}_{\mathbf{bl}} + \\ &\left[\dot{\beta} - p_{hub}\sin\psi - q_{hub}\cos\psi\right]\underline{\mathbf{j}}_{\mathbf{bl}} + \\ &\left[\beta(-p_{hub}\cos\psi + q_{hub}\sin\psi) + (r_{hub} - \Omega)\right]\underline{\mathbf{k}}_{\mathbf{bl}}\end{aligned} \tag{C1.9}$$

Now, assuming the absolute velocity of some point, *p* a distance r_b from the centre of rotation on a rotor blade, assuming a rigid system, can be written in blade axes as,

$$\underline{\boldsymbol{V}}_{p/\mathbf{bl}} = V_{hub/\mathbf{bl}} + (\underline{\boldsymbol{\omega}}_{\mathbf{bl}} \times r_{p/H}) \tag{C1.10}$$

where,

$r_{p/H} = r_b\, \underline{\mathbf{i}}_{\mathbf{bl}}$ and

$\underline{\boldsymbol{\omega}}_{\mathbf{bl}}$ is the angular velocity of the blade in blade axis.

Substituting Equation C1.7 into the above expression and reducing to a simpler format yields the expression for the velocity at a point on the blade as,

$$\underline{\boldsymbol{V}}_{p/\mathbf{bl}} = \underline{\boldsymbol{V}}_{x/\mathbf{bl}}\, \underline{\mathbf{i}}_{\mathbf{bl}} + \underline{\boldsymbol{V}}_{y/\mathbf{bl}}\, \underline{\mathbf{j}}_{\mathbf{bl}} + \underline{\boldsymbol{V}}_{z/\mathbf{bl}}\, \underline{\mathbf{k}}_{\mathbf{bl}} \tag{C1.11}$$

In a similar manner the absolute acceleration of a point *p* in local blade axes, assuming a fully rigid system can be written as,

$$\underline{\boldsymbol{a}}_{p/\mathbf{bl}} = \underline{\boldsymbol{a}}_{hub/\mathbf{bl}} + (\underline{\boldsymbol{\alpha}}_{\mathbf{bl}} \times r_{p/H}) + \underline{\boldsymbol{\omega}}_{\mathbf{bl}} \times (\underline{\boldsymbol{\omega}}_{\mathbf{bl}} \times r_{p/H}) + 2\underline{\boldsymbol{\omega}}_{\mathbf{bl}} \times \frac{d}{dt} r_{p/H} \qquad \text{(C1.12)}$$

With the substitution of Equation C1.7 Equation C1.12 can be expressed conveniently as,

$$\underline{\boldsymbol{a}}_{p/\mathbf{bl}} = \underline{\boldsymbol{a}}_{x/\mathbf{bl}}\, \underline{\mathbf{i}}_{\mathbf{bl}} + \underline{\boldsymbol{a}}_{y/\mathbf{bl}}\, \underline{\mathbf{j}}_{\mathbf{bl}} + \underline{\boldsymbol{a}}_{z/\mathbf{bl}}\, \underline{\mathbf{k}}_{\mathbf{bl}} \qquad \text{(C1.13)}$$

The derivation of Equations C1.10 and C1.13 prove fundamental to the rotor model. It is now possible to determine the expressions for the blade loads.

C1.2.2 Rotor Forces and Moments

The HGS model assumes that there are two forces acting on a blade element, namely aerodynamic and inertial force components.

C1.2.2.1 Rotor Aerodynamic Forces

In simple terms, the lift and drag force components are calculated for a blade element. These normal and tangential components can be given by the equations,

$$f_{z/\mathbf{bl}} = -l\cos\phi - d\sin\phi \qquad \text{(C1.14)}$$

$$f_{y/\mathbf{bl}} = d\cos\phi - l\sin\phi \qquad \text{(C1.15)}$$

where,

l denotes the lift per unit span,

d is the drag per unit span and

ϕ is the angle of incidence of the blade element.

Using the simplifying assumptions that the tangential velocity of the airflow over the blade element, U_T is very much greater that the normal or perpendicular velocity U_P, the angle of attack of the blade element in assumed small so that $l\cos\phi >> d\sin\phi$ and from 2-D aerodynamic theory the lift and drag force coefficients are given by,

$$f_{z/\mathbf{bl}} = -\frac{1}{2}\rho\, c\, a_0 (U_T{}^2\theta + U_P U_T) dr_b \tag{C1.16}$$

$$f_{y/\mathbf{bl}} = \frac{1}{2}\rho\, c\, a_0 (\frac{\delta}{a_0} U_T{}^2 - U_P U_T\theta - U_P{}^2) dr_b \tag{C1.17}$$

The total forces acting on the blade are then found by integrating the elemental forces along the blade span. Recalling that a root cut out term of length *eR* has been included assuming a rotor span of *R* and *e* is some fraction of the total span, then the rotor forces and moments can be calculated from the following normalised rotor force coefficients,

$$C_{z/\mathbf{bl}} = -\frac{1}{2} s\, a_0 \frac{1}{b}\int_0^{1-e} (\overline{U}_T{}^2\theta + \overline{U}_P\overline{U}_T) d\overline{r}_b \tag{C1.18}$$

$$C_{y/\mathbf{bl}} = \frac{1}{2} s\, a_0 \frac{1}{b}\int_0^{1-e} (\frac{\delta}{a_0}\overline{U}_T{}^2 - \overline{U}_P\overline{U}_T\theta - \overline{U}_P{}^2) d\overline{r}_b \tag{C1.19}$$

where,

the rotor solidity is given as, $s = \dfrac{b\, c}{\pi\, R}$ and

the normalised radial blade position is given by, $\overline{r}_b = \dfrac{r_b - e\, R}{R}$.

The rotor force coefficients, Equations C1.18 and C1.19 can be obtained by substituting, firstly, an expression for blade flap and then substituting two non-dimensional perpendicular and tangential components. An additional substitution of the blade pitch equation is made to complete the rotor force coefficient expressions. The integration of the resulting expressions with respect to $\overline{r}_b$ is relatively straightforward as the equations can be arranged into simple polynomial functions of

$\bar{r}_b$. The problem encountered after integration was the manipulation of the lengthy terms in $\cos\psi$ and $\sin\psi$ which resulted from the substitutions mentioned above. The algebraic manipulation was performed using the *Wolfram Mathematica (1990)* symbolic manipulation package. The resulting expressions were large and obtained in powers of $\cos\psi$ and $\sin\psi$ which were expressed in terms of their multiple angles, giving the following expressions for the total blade force coefficients.

$$\begin{aligned} C_{Z_A} &= -\frac{1}{2} s a_0 \frac{1}{b}(C_{Z_{A0}} + C_{Z_{A1c}} \cos\psi + C_{Z_{A1s}} \sin\psi + C_{Z_{A2c}} \cos 2\psi + ...) \\ C_{Y_A} &= \frac{1}{2} s a_0 \frac{1}{b}(C_{Y_{A0}} + C_{Y_{A1c}} \cos\psi + C_{Y_{A1s}} \sin\psi + C_{Y_{A2c}} \cos 2\psi + ...) \end{aligned} \quad \text{(C1.20)}$$

C1.2.2.2 Rotor Inertial Forces

The inertial forces acting on the blade element of length dr_b can be given by,

$$dX_{I/\mathbf{bl}} = -m_0 \underline{\boldsymbol{a}}_{x/\mathbf{bl}} dr_b \quad dY_{I/\mathbf{bl}} = -m_0 \underline{\boldsymbol{a}}_{y/\mathbf{bl}} dr_b \quad dZ_{I/\mathbf{bl}} = m_0 \underline{\boldsymbol{a}}_{z/\mathbf{bl}} dr_b \quad \text{(C1.21)}$$

where,

$\underline{\boldsymbol{a}}_{x/\mathbf{bl}}, \underline{\boldsymbol{a}}_{y/\mathbf{bl}}, \underline{\boldsymbol{a}}_{z/\mathbf{bl}}$ are the components of blade accelerations in blade axes,

$X_{I/\mathbf{bl}}, Y_{I/\mathbf{bl}}, Z_{I/\mathbf{bl}}$ are the inertial components of the blade element forces in blade axes

m_0 is the mass per unit length of the blade element.

Making the relevant substitutions from the blade accelerations, Equation C1.13 yields the following expressions for the blade inertial forces,

$$\begin{aligned} X_{I/\mathbf{bl}} &= (\underline{\boldsymbol{a}}_{hub/\mathbf{x}} \cos\psi - \underline{\boldsymbol{a}}_{hub/\mathbf{y}} \sin\psi + \beta \underline{\boldsymbol{a}}_{hub/\mathbf{z}}) m_b + (\underline{\omega}_{\mathbf{y}}{}^2 + \underline{\omega}_{\mathbf{z}}{}^2) M_\beta \\ Y_{I/\mathbf{bl}} &= (\underline{\boldsymbol{a}}_{hub/\mathbf{x}} \sin\psi + \underline{\boldsymbol{a}}_{hub/\mathbf{y}} \cos\psi) m_b - (\dot{\underline{\omega}}_{\mathbf{z}} + \underline{\omega}_{\mathbf{y}} \underline{\omega}_{\mathbf{z}}) M_\beta \\ Z_{I/\mathbf{bl}} &= \left[\beta(\underline{\boldsymbol{a}}_{hub/\mathbf{x}} \cos\psi - \underline{\boldsymbol{a}}_{hub/\mathbf{y}} \sin\psi) - \underline{\boldsymbol{a}}_{hub/\mathbf{z}})\right] m_b - (\underline{\omega}_{\mathbf{x}} \underline{\omega}_{\mathbf{z}} - \dot{\underline{\omega}}_{\mathbf{y}}) M_\beta \end{aligned} \quad \text{(C1.22)}$$

where,

the blade mass is given by, $m_b = \int_{eR}^{R} m_0 dr_b$,

the blade moment of mass is given by, $M_\beta = \int_{eR}^{R} m_0 r_b dr_b$ and

$\underline{\omega}_x, \underline{\omega}_y, \underline{\omega}_z$ are the angular velocity components of the blade element in their respective axes.

The expansion of the equations contained in C1.22 is completed by including the blade angular velocities and accelerations, and the blade flap angle as functions of azimuth position. The resulting expressions are made non-dimensional by dividing through by the term, $\rho(\Omega R)^2 \pi R^2$ which, for similarity is expressed in multiple angle format up to and including the first harmonic. The non-dimensional blade inertial coefficients are,

$$\begin{aligned} C_{X_I} &= C_{X_{I0}} + C_{X_{I1c}} \cos\psi + C_{X_{I1s}} \sin\psi \\ C_{Y_I} &= C_{Y_{I0}} + C_{Y_{I1c}} \cos\psi + C_{Y_{I1s}} \sin\psi \\ C_{Z_I} &= C_{Z_{I0}} + C_{Z_{I1c}} \cos\psi + C_{Z_{I1s}} \sin\psi \end{aligned} \qquad \text{(C1.23)}$$

C1.2.2 Total Rotor Forces

The total rotor forces can be obtained through the summation of the inertial and aerodynamic components calculated above. For example, the *y* force coefficient is given by, $C_{Y/\mathbf{bl}} = C_{Y_I} + C_{Y_A}$ etc. Obtaining all the equations in the same manner gives in component coefficient form ,

$$\begin{aligned} C_{X/\mathbf{bl}} &= C_{X_0} + C_{X1c/\mathbf{bl}} \cos\psi + C_{X1s/\mathbf{bl}} \sin\psi \\ C_{Y/\mathbf{bl}} &= C_{Y_0} + C_{Y1c/\mathbf{bl}} \cos\psi + C_{Y1s/\mathbf{bl}} \sin\psi \\ C_{Z/\mathbf{bl}} &= C_{Z_0} + C_{Z1c/\mathbf{bl}} \cos\psi + C_{Z1s/\mathbf{bl}} \sin\psi \end{aligned} \qquad \text{(C1.24)}$$

where,

$$C_{X_0} = C_{X_{I0}}, C_{Y_0} = \frac{sa_0}{2b} C_{Y_{A0}} + C_{Y_{I0}} \text{ etc.}$$

As the initial vehicle equations of motion are expressed in body axes, the rotor force must also be referred to this axes set. This is achieved by performing the same transformations as given in Sections C1.2.1.1 and C1.2.1.2 of this Appendix, but in reverse order, that is, using the transpose of the matrices to transform from blade to shaft and from shaft to hub. During the transformation it is assumed that only the steady terms contribute to the overall dynamics of the aircraft and hence the periodic terms that are a function of blade azimuth are neglected. Effectively, only the steady average force around the azimuth travel of the blade is retained. A final transformation, from hub to body axes (through the shaft angle) is performed and the main rotor contribution of forces to the dynamics of the aircraft is given by,

$$\begin{aligned} X_R &= \rho(\Omega R)^2 \pi R^2 \left[C_{X/\mathbf{hub}} \cos\gamma_{sh}\right] - C_{Z/\mathbf{hub}} \sin\gamma_{sh} \\ Y_R &= \rho(\Omega R)^2 \pi R^2 \left[C_{Y/\mathbf{hub}}\right] \\ Z_R &= \rho(\Omega R)^2 \pi R^2 \left[C_{X/\mathbf{hub}} \cos\gamma_{sh}\right] + C_{Z/\mathbf{hub}} \cos\gamma_{sh} \end{aligned} \qquad \text{(C1.25)}$$

C1.2.3 Rotor Moments

The flapping model included in HGS is assumed to have rigid blades, which are hinged at the hub and have a resistance in flap modelled by a spring of torsion stiffness K_β. The total moments acting on a single blade are calculated by obtaining the elemental aerodynamic and inertial moments, summing them along the blade span and equating them to the restoring moment at the hub due to blade flap. Hence, the roll, pitch and yaw hub moments acting at the centre of gravity of the aircraft (i.e. transformed back to body axes) are given by,

$$\begin{aligned} L_R &= \left[L_{\mathbf{hub}} \cos\gamma_{sh} - N_{\mathbf{hub}} \sin\gamma_{sh} + h_r Y_R\right] \\ M_R &= \left[M_{\mathbf{hub}} - h_r X_R + x_{cg} Z_R\right] \\ N_R &= \left[L_{\mathbf{hub}} \sin\gamma_{sh} + N_{\mathbf{hub}} \cos\gamma_{sh} - x_{cg} Y_R\right] \end{aligned} \qquad \text{(C1.26)}$$

C1.2.4 Rotor Blade Flapping Dynamics and the Multiblade Transformation

The flapping equation is written as,

$$\beta_i'' + \left[\lambda_\beta{}^2 + \frac{\overline{M}_\beta R}{I_\beta}(\eta_x \cos\psi_i - \eta_y \sin\psi_i) \right] \beta_i =$$
$$4 n_\beta \int_0^{1-e} (\overline{U}_T{}^2 \theta + \overline{U}_T \overline{U}_P)(\bar{r} + e) d\bar{r}_b \qquad \text{(C1.27)}$$
$$+ \frac{\overline{M}_\beta R}{I_\beta} \eta_z + 2\left[\left(\frac{q'_{\mathbf{hub}}}{2} + \bar{p}_{\mathbf{hub}} \right) \cos\psi_i + \left(\frac{p'_{\mathbf{hub}}}{2} + \bar{q}_{\mathbf{hub}} \right) \sin\psi_i \right]$$

where,

λ_β is the normalised flap frequency,

I_β is the blade flapping moment of inertia and

n_β is the blade inertia number. Expressions for these terms are given below.

$$\lambda_\beta{}^2 = \frac{K_\beta}{I_\beta \Omega^2} + 1 \qquad I_\beta = \int_{eR}^{e} m_0 r_b{}^2 dr_b \qquad n_\beta = \frac{\rho c a_0 R^4}{8 I_\beta}$$

Some other terms in Equation C1.27 are given as,

$$\ddot{\beta}_i = \frac{d^2 \beta_i}{d\psi^2} \qquad q'_{\mathbf{hub}} = \frac{\dot{q}_{\mathbf{hub}}}{\Omega^2} \qquad p'_{\mathbf{hub}} = \frac{\dot{p}_{\mathbf{hub}}}{\Omega^2}$$

This resulting equation can be used to describe the behavioural dynamics of a flapping rotor blade. However, as HGS is a disc representation or multiblade model, the flapping motion must be described in multiblade co-ordinates.

C1.2.4.1 The Multiblade Transformation

The multiblade transform is applied to Equation C1.27 in order to solve it. Effectively this process converts the individual blade angles, β_i (i = 1 to n), into a multiblade co-ordinate representation given as,

β_0 the coning angle,

β_{1c} longitudinal flapping angle,

β_{1s} lateral flapping angle and

β_d differential coning angle.

The application of the multiblade transformation permits, for a four blade rotor, the calculation of the individual blade angles, $\beta_{\mathbf{I}} = (\beta_1 \beta_2 \beta_3 \beta_4)^{\mathrm{T}}$ from,

$$\beta_{\mathbf{I}} = \underline{\mathbf{L}}_{\beta} \beta_{\mathbf{M}} \tag{C1.28}$$

where,

$$\underline{\mathbf{L}}_{\beta} = \begin{bmatrix} 1 & -1 & \cos\psi & \sin\psi \\ 1 & 1 & \sin\psi & -\cos\psi \\ 1 & -1 & -\cos\psi & -\sin\psi \\ 1 & 1 & \sin\psi & \cos\psi \end{bmatrix} \tag{C1.29}$$

and $$\beta_{\mathbf{M}} = (\beta_0 \beta_d \beta_{1s} \beta_{1c})^{\mathrm{T}} \tag{C1.30}$$

By incorporating the multiblade transformation into the flapping equation and expressing the resulting periodic equation in non-periodic form, allows the flapping equation to be written in the form,

$$\ddot{\beta}_{\mathbf{M}} + \mathbf{C}_{\mathbf{M}_0} + \beta'_{\mathbf{M}} + \mathbf{D}_{\mathbf{M}_0} \beta_{\mathbf{M}} = \mathbf{h}_{\mathbf{M}_0} \tag{C1.31}$$

where the matrices $\mathbf{C}_{\mathbf{M}_0}, \mathbf{D}_{\mathbf{M}_0}, \mathbf{h}_{\mathbf{M}_0}$ are obtained by substituting for successive values of ψ_i for each blade from the equation, $\psi_i = \psi - (i-1)\frac{\pi}{2}$. Hence the resulting expressions are lengthy and the reader is referred to *Thomson (1992)* for the full set of equations.

Equation C1.31 can then be solved for the respective multiblade angles for a given set of control angles and hub velocities. However, the solution of Equation C1.31 is often simplified by assuming quasi-steady flapping, that is, the blade flapping dynamics are uncoupled from the body dynamics of the aircraft and have

little effect on the forces and moments applied by the rotor to the vehicle body. This assumption is based on the fact that blade flap modes are much faster than the body modes and it is likely that there will be little influence. The quasi-steady flap equation becomes,

$$\beta_{\mathbf{M}} = \mathbf{D}_{\mathbf{M}_0}^{-1} \mathbf{h}_{\mathbf{M}_0} \tag{C1.32}$$

which can be solved readily due to its algebraic nature to give the blade flap angles at a discrete point in time.

C1.3 HGS Tail Rotor Model

The approach taken to model the tail rotor is the same as the main rotor with the major exception being, the tail rotor hub is assumed to be rigid so that no blade flapping occurs. Due to the overall similarity of the tail rotor with the main rotor model, only brief details of the formulation of the forces and moments will be presented.

C1.3.1 Overview of Tail Rotor Blade Kinematics

The tail rotor, (subscript **TR**) is assumed to be in a position some distance, $l_{\mathbf{TR}}$ behind the fuselage reference point and a height $h_{\mathbf{TR}}$ above it. An axes set is located at the tail rotor with its *x* direction coinciding with that of the body fixed set, the *y*-axis points down and the *z*-axis points through the tail rotor in the direction of the flow. This implies that the tail rotor is a "pusher" type rotor. After transforming to the tail rotor axes and calculating the velocity and angular acceleration of the tail rotor axes set followed by calculating the velocity of a point rotating on the rotor, it is possible to formulate the rotor forces and moments.

C1.3.2 Tail Rotor Forces and Moments

Again the formulation of the force and moment equations is carried out in the same way as the main rotor, thus, neglecting the inertial forces the normalised force

and torque coefficients are respectively determined, in tail rotor blade axes (subscript **trbl)**. The expressions were evaluated using Mathematica and in keeping with previous calculations terms higher than the zeroth and first harmonic terms are ignored to give the periodic forces and moments,

$$\begin{aligned}
C_{Z\mathbf{TR/trbl}} &= -\frac{1}{2} s_{\mathbf{TR}} a_{0\mathbf{TR}} \left(C_{Z_0\mathbf{TR/trbl}} + C_{Z_{1c}\mathbf{TR/trbl}} \cos\psi_{\mathbf{TR}} + C_{Z_{1s}\mathbf{TR/trbl}} \sin\psi_{\mathbf{TR}} \right) \\
C_{Y\mathbf{TR/trbl}} &= \frac{1}{2} s_{\mathbf{TR}} a_{0\mathbf{TR}} \left(C_{Y_0\mathbf{TR/trbl}} + C_{Y_{1c}\mathbf{TR/trbl}} \cos\psi_{\mathbf{TR}} + C_{Y_{1s}\mathbf{TR/trbl}} \sin\psi_{\mathbf{TR}} \right) \\
C_{Q\mathbf{TR/trbl}} &= \frac{1}{2} s_{\mathbf{TR}} a_{0\mathbf{TR}} \left(C_{Q_0\mathbf{TR/trbl}} + C_{Q_{1c}\mathbf{TR/trbl}} \cos\psi_{\mathbf{TR}} + C_{Q_{1s}\mathbf{TR/trbl}} \sin\psi_{\mathbf{TR}} \right)
\end{aligned} \tag{C1.33}$$

Neglecting the periodic terms, transposing to the tail rotor hub axes, (sub-subscript **trh**) denormalising and adding the moment components due to the offset of the tail rotor hub to the tail rotor moments gives the overall tail rotor force contribution in body axes as,

$$\begin{aligned}
X_{\mathbf{TR}} &= \rho \left(\Omega_{\mathbf{TR}} R_{\mathbf{TR}} \right)^2 \pi R_{\mathbf{TR}}^2 C_{X\mathbf{TR/trh}} \\
Y_{\mathbf{TR}} &= -\rho \left(\Omega_{\mathbf{TR}} R_{\mathbf{TR}} \right)^2 \pi R_{\mathbf{TR}}^2 C_{Z\mathbf{TR/trh}} \\
Z_{\mathbf{TR}} &= \rho \left(\Omega_{\mathbf{TR}} R_{\mathbf{TR}} \right)^2 \pi R_{\mathbf{TR}}^2 C_{Y\mathbf{TR/trh}}
\end{aligned} \tag{C1.34}$$

and for the moments,

$$\begin{aligned}
L_{\mathbf{TR}} &= h_{\mathbf{TR}} Y_{\mathbf{TR}} \\
M_{\mathbf{TR}} &= -\rho \left(\Omega_{\mathbf{TR}} R_{\mathbf{TR}} \right)^2 \pi R_{\mathbf{TR}}^3 C_{Q\mathbf{TR/trh}} + (x_{cg} + l_{\mathbf{TR}}) Z_{\mathbf{TR}} - h_{\mathbf{TR}} X_{\mathbf{TR}} \\
N_{\mathbf{TR}} &= -(x_{cg} + l_{\mathbf{TR}}) Y_{\mathbf{TR}}
\end{aligned} \tag{C1.35}$$

C1.4 HGS Fuselage Model

The aerodynamic forces and moments generated by the fuselage (subscript **fus**) are calculated using look-up tables of aerodynamic coefficients, as functions of angle-of-attack or sideslip angle and are derived from wind tunnel tests. The respective force and moment coefficients are denoted,

$$C_{X\mathbf{fus}}, C_{Y\mathbf{fus}}, C_{Z\mathbf{fus}}, C_{L\mathbf{fus}}, C_{M\mathbf{fus}} \text{ and } C_{N\mathbf{fus}}.$$

The force coefficients in the x and z-axis (drag and lift of the fuselage) and the moment coefficient about the y-axis (pitching moment) are functions of the angle-of-attack. The fuselage force coefficient in the y-axis direction (side force), and the moment coefficient about the z-axis (yawing moment) are functions of the sideslip angle. Since the wind tunnel data used in the look-up tables were measured relative to the fuselage reference point, directly below the rotor hub, the moments due to the offset of the forces from the centre of gravity had to be taken into account. The resulting force coefficients are therefore given by,

$$\begin{aligned} X_{\mathbf{fus}} &= \rho(\Omega R)^2 \pi R^2 C_{X\mathbf{fus}} \\ Y_{\mathbf{fus}} &= \rho(\Omega R)^2 \pi R^2 C_{Y\mathbf{fus}} \\ Z_{\mathbf{fus}} &= \rho(\Omega R)^2 \pi R^2 C_{Z\mathbf{fus}} \end{aligned} \tag{C1.36}$$

and the moment coefficients are given by,

$$\begin{aligned} L_{\mathbf{fus}} &= 0 \\ M_{\mathbf{fus}} &= \rho(\Omega R)^2 \pi R^3 C_{M\mathbf{fus}} + x_{cg} Z_{\mathbf{fus}} \\ N_{\mathbf{fus}} &= \rho(\Omega R)^2 \pi R^3 C_{N\mathbf{fus}} - x_{cg} Y_{\mathbf{fus}} \end{aligned} \tag{C1.37}$$

C1.4 HGS Fin and Tailplane Models

The fin and tailplane force coefficients are respectively denoted by, $C_{Y\mathbf{fin}}$ and $C_{Z\mathbf{tp}}$. In a similar way to the fuselage force coefficients the fin and tailplane forces are obtained from look-up tables which are functions of the fin sideslip angle, $\beta_{\mathbf{fin}}$ and the angle-of-incidence of the tailplane, $\alpha_{\mathbf{tp}}$. Hence the contribution of the fin of surface area, $S_{\mathbf{fin}}$ and the tailplane of surface area, $S_{\mathbf{tp}}$ to the overall external forces and moments can be given by,

Fin

$$
\begin{aligned}
X_{\mathbf{fin}} &= 0 \\
Y_{\mathbf{fin}} &= \rho(\Omega R)^2 s_{\mathbf{fin}} C_{Y\mathbf{fin}} \\
Z_{\mathbf{fin}} &= 0 \\
L_{\mathbf{fin}} &= Y_{\mathbf{fin}} h_{\mathbf{fin}} \\
M_{\mathbf{fin}} &= 0 \\
N_{\mathbf{fin}} &= Y_{\mathbf{fin}} \left(x_{cg} + l_{\mathbf{fin}}\right)
\end{aligned}
\qquad \text{(C1.38)}
$$

Tailplane

$$
\begin{aligned}
X_{\mathbf{tp}} &= 0 \\
Y_{\mathbf{tp}} &= 0 \\
Z_{\mathbf{tp}} &= \rho(\Omega R)^2 s_{\mathbf{tp}} C_{Z\mathbf{tp}} \\
L_{\mathbf{tp}} &= 0 \\
M_{\mathbf{tp}} &= Z_{\mathbf{tp}} \left(x_{cg} + l_{\mathbf{tp}}\right) \\
N_{\mathbf{tp}} &= 0
\end{aligned}
\qquad \text{(C1.39)}
$$

where,

$l_{\mathbf{fin}}$ is the distance from the fuselage reference point to the fin centre of pressure,

$h_{\mathbf{fin}}$ is the height of the fin above the fuselage datum,

$l_{\mathbf{tp}}$ is the distance of the tailplane behind the reference point and

$h_{\mathbf{tp}}$ is the height of the tailplane above the fuselage datum.

Appendix D

Glauert and Peters-HaQuang Inflow Models

As stated in Chapter 3, HGS is equipped with two options for modelling inflow through the rotor. *Taylor (1995)* has detailed the effects of varying the method used and indeed was responsible for the inclusion of the Peters-HaQuang method. This Appendix is included to provide a general outline of equation formulation for each method, the reader is referred to *Chen (1990)* for a summary of inflow models developed since Glauert first proposed the momentum theory in the 1920's.

D.1.1 Glauert Momentum Inflow Model

Glauert inflow is a well-established technique of modelling the induced velocity of airflow through a rotor disc. It is essentially presented as the sum of a steady or uniform component and first order harmonic components with radial variation. The resulting model has the form as given in Appendix C, section C1.2.2.1, (C1.52),

$$v_i = v_0 + \frac{r_b}{R}(v_{1s}\sin\psi + v_{1c}\cos\psi) \tag{D1.1}$$

where,

λ_0 and $(\lambda_{1c}, \lambda_{1s})$ are the non-dimensional uniform inflow component and first harmonic components of the main rotor inflow. The other terms in Equation D1.1 are,

r_b radial position from the centre of the rotor disc and

R rotor blade span.

The non-dimensional form of Equation D1.1 is found by dividing by the term ΩR to obtain,

$$\lambda_i = \lambda_0 + \frac{r_b}{R}(\lambda_{1s}\sin\psi + \lambda_{1c}\cos\psi) \tag{D1.2}$$

The uniform component of the inflow is given in non-dimensional form as,

$$\lambda_0 = \frac{C_T}{2\sqrt{\mu^2 + (\mu_z - \lambda_0)^2}} \tag{D1.3}$$

where,

μ is the in-plane normalised velocity vector of the rotor hub and

μ_z is the normalised velocity vector perpendicular to the rotor hub plane.

The harmonic components of the inflow are evaluated by the introduction of additional, so-called wind axes (subscript **wind**). The axis set is positioned so that its $\underline{\mathbf{i}}_{\mathbf{wind}}$ component is in alignment with the resultant velocity vector of the rotor hub and is obtained by rotation about $\underline{\mathbf{k}}_{\mathbf{wind}}$ through the rotor sideslip angle ψ_{wind}. As a result the harmonic components can be obtained from,

$$\begin{bmatrix} \lambda_{1c} \\ \lambda_{1s} \end{bmatrix} = \begin{bmatrix} \cos\psi_{wind} & -\sin\psi_{wind} \\ \sin\psi_{wind} & \cos\psi_{wind} \end{bmatrix} \begin{bmatrix} \lambda_{1c/\mathbf{wind}} \\ \lambda_{1s/\mathbf{wind}} \end{bmatrix} \tag{D1.4}$$

where the rotor sideslip angle is given by $\psi_{wind} = \tan^{-1}\left[\frac{\mu_y}{\mu_x}\right]$, μ_y and μ_x being the non-dimensional components of rotor hub velocity. The transformation to wind axes yields the lateral component of inflow in wind axes to be zero, i.e., $\lambda_{1s/\mathbf{wind}} = 0$ and *Bramwell (1976)* proposes a method whereby the lateral component can be found from,

$$\lambda_{1c/\mathbf{wind}} = \lambda_0 \tan\left(\frac{\chi}{2}\right) \quad \text{if } \chi < \frac{\pi}{2}$$

$$\lambda_{1c/\mathbf{wind}} = \lambda_0 \cot\left(\frac{\chi}{2}\right) \quad \text{if } \chi > \frac{\pi}{2}$$

where,

χ is the rotor wake angle.

D.1.2 Peters-HaQuang Dynamic Inflow Model

The momentum inflow model of Glauert suffers from the drawbacks of assuming that the airflow accelerates instantaneously through the plane of the disc, whilst also ignoring the effects of pitching and rolling due to the same airflow. Essentially this means that the induced velocity will react instantaneously to changes in the pitch angle of the blades or indeed the flight state of the vehicle. Clearly this is not the case with reference to real aircraft as there is a specific time lag to allow for the build-up of the induced velocity. Furthermore *Gaonkar and Peters (1980)* identify the importance of including the effects of the aerodynamic pitching and rolling moments, which the Glauert model fails to do.

In an attempt to attenuate these limitations dynamic inflow models have been developed in first order matrix form which introduce components to deal with these problems. The form of the dynamic inflow model as given by Peters and Haquang is,

$$[\underline{\mathbf{M}}]\begin{bmatrix}\dot{\lambda}_{0/\mathbf{wind}}\\ \dot{\lambda}_{1s/\mathbf{wind}}\\ \dot{\lambda}_{1c/\mathbf{wind}}\end{bmatrix} + [\underline{\mathbf{L}}]_{nl}^{-1}\begin{bmatrix}\lambda_{0/\mathbf{wind}}\\ \lambda_{1s/\mathbf{wind}}\\ \lambda_{1c/\mathbf{wind}}\end{bmatrix} = \begin{bmatrix}C_{T/\mathbf{wind}}\\ -C_{L/\mathbf{wind}}\\ -C_{M/\mathbf{wind}}\end{bmatrix}_{\mathbf{aero}} \tag{D1.5}$$

where,

$[\underline{\mathbf{M}}]$ is the apparent mass matrix which models the dynamic lag, or takes account of the lag time between pitch changes being applied at the rotor disc and the resulting thrust variations occurring,

$[\underline{\mathbf{L}}]_{nl}$ is the non-linear inflow gains matrix in the wind axes set relating the inflow velocities with the aerodynamic rolling and pitching moment coefficients, $C_{L/\mathbf{wind}}$ and $C_{M/\mathbf{wind}}$ respectively,

$\lambda_{0/\mathbf{wind}}$, $\lambda_{1s/\mathbf{wind}}$, $\lambda_{1c/\mathbf{wind}}$ are the non dimensional uniform, lateral and longitudinal inflow velocities respectively in wind axes.

The apparent mass matrix is defined as,

$$[\underline{\mathbf{M}}] = \begin{bmatrix} \frac{128}{75\pi} & 0 & 0 \\ 0 & -\frac{16}{45\pi} & 0 \\ 0 & 0 & -\frac{16}{45\pi} \end{bmatrix}$$

while the non-linear inflow gains matrix is given by,

$$[\underline{\mathbf{L}}]_{nl} = [\underline{\mathbf{L}}][\underline{\mathbf{V}}]^{-1}$$

where,

$$[\underline{\mathbf{L}}] = \begin{bmatrix} \frac{1}{2} & 0 & \frac{15\pi}{64}\sqrt{\frac{1-\sin\chi}{1+\sin\chi}} \\ 0 & -\frac{4}{1+\sin\chi} & 0 \\ \frac{15\pi}{64}\sqrt{\frac{1-\sin\chi}{1+\sin\chi}} & 0 & -\frac{4\sin\chi}{1+\sin\chi} \end{bmatrix}$$

and

$$[\underline{\mathbf{V}}] = \begin{bmatrix} \lambda_{Tot} & 0 & 0 \\ 0 & \lambda_{Cyc} & 0 \\ 0 & 0 & \lambda_{Cyc} \end{bmatrix}$$

The mass flow parameter matrix, $[\underline{\mathbf{V}}]$ contains the resultant flow through the rotor disc, λ_{Tot} and the mass flow parameter due to cyclic disturbances, λ_{Cyc}. These

parameters are defined by the equations,

$$\lambda_{Tot} = \sqrt{\mu^2 + (\mu_z - \lambda_{Mom})^2}$$

and

$$\lambda_{Cyc} = \frac{\mu^2 + (\mu_z - 2\lambda_{Mom})(\mu_z - \lambda_{Mom})}{\lambda_{Tot}}$$

Some other terms not yet identified in the above equation are the non-dimensional momentum theory induced velocity due to rotor thrust, λ_{Mom} and the non-dimensional in-plane and perpendicular component disc velocities, μ and μ_z respectively.

Recall that,

$$\mu = \sqrt{(\mu_x^2 + \mu_y^2)},$$

$$\mu_x = \frac{u_{hub}}{\Omega R},$$

$$\mu_y = \frac{v_{hub}}{\Omega R},$$

$$\mu_z = \frac{w_{hub}}{\Omega R}$$

The rotor wake angle is defined as,

$$\chi = \tan^{-1}\left(\frac{|\mu_z - \lambda_{Mom}|}{\mu}\right)$$

and the wind side-slip angle ψ_{wind} has been defined previously.

The theory developed thus far is in the wind axes set. Hence, several

transformations have to be made to convert the relevant coefficients and non-dimensional parameters into an axes set which is aligned with the rotor disc (recall hub axes). The transformations are as follows,

$$\begin{bmatrix} C_{T/\mathbf{wind}} \\ -C_{L/\mathbf{wind}} \\ -C_{M/\mathbf{wind}} \end{bmatrix}_{\mathbf{aero}} = \begin{bmatrix} 1 & 0 & 0 \\ 0 & \cos\psi_{wind} & \sin\psi_{wind} \\ 0 & -\sin\psi_{wind} & \cos\psi_{wind} \end{bmatrix} \begin{bmatrix} C_{T/\mathbf{hub}} \\ -C_{L/\mathbf{hub}} \\ -C_{M/\mathbf{hub}} \end{bmatrix}_{\mathbf{aero}}$$

and

$$\begin{bmatrix} \lambda_{0/\mathbf{wind}} \\ \lambda_{1s/\mathbf{wind}} \\ \lambda_{1c/\mathbf{wind}} \end{bmatrix} = \begin{bmatrix} 1 & 0 & 0 \\ 0 & \cos\psi_{wind} & \sin\psi_{wind} \\ 0 & -\sin\psi_{wind} & \cos\psi_{wind} \end{bmatrix} \begin{bmatrix} \lambda_{0/\mathbf{hub}} \\ \lambda_{1s/\mathbf{hub}} \\ \lambda_{1c/\mathbf{hub}} \end{bmatrix}$$

If the above transformation matrix is referred to as $[\mathbf{T}_{wind/\mathbf{hub}}]$ then the expanded version of Equation D1.5 can be written as,

$$[\underline{\mathbf{M}}][\mathbf{T}_{wind/\mathbf{hub}}] \begin{bmatrix} \dot{\lambda}_{0/\mathbf{hub}} \\ \dot{\lambda}_{1s/\mathbf{hub}} \\ \dot{\lambda}_{1c/\mathbf{hub}} \end{bmatrix} + [\underline{\mathbf{V}}][\underline{\mathbf{L}}]^{-1}[\mathbf{T}_{wind/\mathbf{hub}}] \begin{bmatrix} \lambda_{0/\mathbf{hub}} \\ \lambda_{1s/\mathbf{hub}} \\ \lambda_{1c/\mathbf{hub}} \end{bmatrix} = [\mathbf{T}_{wind/\mathbf{hub}}] \begin{bmatrix} C_{T/\mathbf{hub}} \\ -C_{L/\mathbf{hub}} \\ -C_{M/\mathbf{hub}} \end{bmatrix}_{\mathbf{aero}} \qquad \text{(D1.6)}$$

To enable the removal of the transformation matrix, $[\mathbf{T}_{wind/\mathbf{hub}}]$ Equation D1.6 is multiplied by its transpose, i.e.,

$$[\mathbf{T}_{wind/\mathbf{hub}}]^T[\underline{\mathbf{M}}][\mathbf{T}_{wind/\mathbf{hub}}] \begin{bmatrix} \dot{\lambda}_{0/\mathbf{hub}} \\ \dot{\lambda}_{1s/\mathbf{hub}} \\ \dot{\lambda}_{1c/\mathbf{hub}} \end{bmatrix} + [\underline{\mathbf{V}}][\underline{\mathbf{L}}]^{-1}[\mathbf{T}_{wind/\mathbf{hub}}] \begin{bmatrix} \lambda_{0/\mathbf{hub}} \\ \lambda_{1s/\mathbf{hub}} \\ \lambda_{1c/\mathbf{hub}} \end{bmatrix} = [\mathbf{T}_{wind/\mathbf{hub}}] \begin{bmatrix} C_{T/\mathbf{hub}} \\ -C_{L/\mathbf{hub}} \\ -C_{M/\mathbf{hub}} \end{bmatrix}_{\mathbf{aero}}$$

The order of the matrix multiplication can be reversed since the first element of $[\mathbf{T}_{wind/\mathbf{hub}}]$ is unity and $[\underline{\mathbf{V}}]$ and $[\underline{\mathbf{M}}]$ are diagonal. The result is a first order differential equation which represents the non-linear dynamic flow theory of a rotor disc and is given as,

$$\left[\underline{\mathbf{M}}\right]\begin{bmatrix}\dot{\lambda}_{0/\mathbf{hub}}\\ \dot{\lambda}_{1s/\mathbf{hub}}\\ \dot{\lambda}_{1c/\mathbf{hub}}\end{bmatrix}+\left[\hat{\underline{\mathbf{L}}}\right]_{nl}^{-1}\begin{bmatrix}\lambda_{0/\mathbf{hub}}\\ \lambda_{1s/\mathbf{hub}}\\ \lambda_{1c/\mathbf{hub}}\end{bmatrix}=\begin{bmatrix}C_{T/\mathbf{hub}}\\ -C_{L/\mathbf{hub}}\\ -C_{M/\mathbf{hub}}\end{bmatrix}_{\mathbf{aero}} \tag{D1.7}$$

where,

$$\left[\hat{\underline{\mathbf{L}}}\right]^{-1}=\left[\underline{\mathbf{V}}\right]\left[\mathbf{T}_{wind/\mathbf{hub}}\right]^{T}\left[\underline{\mathbf{L}}\right]^{-1}\left[\mathbf{T}_{wind/\mathbf{hub}}\right]$$

Appendix E

Mathematical Model of a Stability and Control Augmentation System (SCAS)

The mathematical description of the SCAS that follows relates to a relatively simple approximation of the Lynx helicopter, and was first presented by *Padfield (1981)*. Each of the separate channels or controls is discussed in turn in terms of the primary control linkage and, in addition, the control interlinks between main rotor collective, longitudinal cyclic and tail rotor collective are included. The system possesses the ability to perform cyclic pitch mixing before transmission to the rotor blades and subsequent actuation.

i) *Pitch Channel*

The collective lever and longitudinal cyclic control channels are responsible for the longitudinal cyclic pitch achieved prior to mixing, given the notation, $\theta_{1s_p}{}^*$. The collective lever position is included to attenuate undesirable coupling characteristics between longitudinal cyclic and collective lever control inputs that occur with changes in forward airspeed. The longitudinal cyclic channel contribution from the pilot can be written in the form,

$$\theta_{1s_p}{}^* = g_{1s0} + g_{1s1}\eta_{1s} + \left(g_{sco} + g_{sc1}\eta_{1s}\right)\eta_c \qquad \text{(E1.1)}$$

where,

$g_{1s0}, g_{1s1}, g_{sc0}, g_{sc1}$ are representative of gains and offsets in the longitudinal and collective channels and

η_{1s}, η_c are the longitudinal cyclic and collective lever inputs respectively.

The autostabiliser contribution to the longitudinal cyclic channel, $\theta_{1s_a}{}^*$ is obtained from simple proportional and derivative feedback of the pitch attitude, θ and pitch rate, q and is realised via limited authority series actuators. The short and long term longitudinal modal responses are controlled in this way. A further term in the form of a feedforward of the current cyclic stick and trim position is included which permits improved vehicle response in the longitudinal sense to a given control input. The longitudinal autostabiliser contribution before mixing can be written in the form,

$$\theta_{1s_a}{}^* = k_\theta \theta + k_q q + k_{1s}\left(\eta_{1s} - \eta_{1s0}\right) \tag{E1.2}$$

where,

k_θ, k_q, k_{1s} are the proportional feedback, derivative feedback and feedforward gains respectively and

η_{1s0} is the reference longitudinal trim position or datum, $\left(0 \le \eta_{1s0} \le 1\right)$.

The combined signal of the autostabiliser and pilot contributions to longitudinal cyclic is passed through an actuation element. It is assumed that this can be modelled by a first order lag, although this is a relatively crude method to do so as the servo-elastic actuation system is complex. Nevertheless, the transfer function is given as,

$$\frac{\theta_{1s}{}^*}{\theta_{1s_p}{}^* + \theta_{1s_a}{}^*} = \frac{1}{1 + \tau_{c1} s} \tag{E1.3}$$

where,

τ_{c1} is the longitudinal cyclic actuator time constant.

A mixing unit is located at the swashplate to ameliorate coupling effects. Essentially, these units combine the actuation outputs from the two cyclic channels with a cyclic mixing or phase angle (typically between 8 and 12 degrees). If, for example, a pilot wished to achieve a manoeuvre in pure pitch or roll, (since the phase lag between cyclic pitch and blade flap is less than 90 degrees), then coupled control

inputs are required. Although the phase lag varies from the hover to low speed and forward flight regimes, a single mixing is usually selected to be a compromise of all flight conditions and is modelled by,

$$\begin{bmatrix} \theta_{1s} \\ \theta_{1c} \end{bmatrix} = \begin{bmatrix} \cos\psi_f & \sin\psi_f \\ -\sin\psi_f & \cos\psi_f \end{bmatrix} \begin{bmatrix} \theta_{1s}^{*} \\ \theta_{1c}^{*} \end{bmatrix} \tag{E1.4}$$

where,

θ_{1s} and θ_{1c} are the respective longitudinal and lateral cyclic pitch displacements at the swashplate after mixing,

θ_{1s}^{*} and θ_{1c}^{*} represent the same displacements but are prior to mixing and

ψ_f is the cyclic mixing or phasing angle.

ii) *Roll Channel*

The development of the theory for the lateral cyclic channel is fundamentally the same as that stated previously for the longitudinal channel without collective channel coupling effects. The lateral cyclic pitch displacement at the rotor due to inputs from the pilot alone, $\theta_{1c_p}^{*}$ is given by,

$$\theta_{1c_p}^{*} = g_{1c0} + g_{1c1}\eta_{1c} \tag{E1.5}$$

where,

g_{1c0}, g_{1c1} are representative of gains and offsets in the lateral cyclic channel and

η_{1c} is the lateral cyclic stick displacement $(0 \le \eta_{1c} \le 1)$.

The autostabiliser contribution to the lateral cyclic channel is again derived using proportional and derivative feedback control, this time in roll attitude, ϕ and roll rate, p respectively. The additional feedforward term based on lateral stick position with respect to a pre-set datum position is also included and for the same

reasons as in the longitudinal channel. So, the lateral cyclic channel contribution from the autostabiliser, $\theta_{1c_a}{}^*$ can be written as,

$$\theta_{1c_a}{}^* = k_\phi \phi + k_p p + k_{1c}\left(\eta_{1c} - \eta_{1c0}\right) \tag{E1.6}$$

where,

k_ϕ, k_p, k_{1c} are the proportional feedback, derivative feedback and feedforward gains respectively and

η_{1c0} is the reference longitudinal trim position or datum, $\left(0 \le \eta_{1c0} \le 1\right)$.

The lateral cyclic actuator output is therefore the sum of the pilot and autostabiliser contributions and can be written as,

$$\frac{\theta_{1c}{}^*}{\theta_{1c_p}{}^* + \theta_{1c_a}{}^*} = \frac{1}{1 + \tau_{c2} s} \tag{E1.7}$$

where,

τ_{c2} is the lateral cyclic actuator time constant.

iii) *Heave Channel*

Starting with the pilot contribution alone to the collective channel, we have,

$$\theta_{0_p} = g_{c0} + g_{c1}\eta_c \tag{E1.8}$$

where,

g_{c0}, g_{c1} are representative of gains and offsets in the collective channel and

η_c is the collective cyclic lever displacement $\left(0 \le \eta_c \le 1\right)$.

The autostabiliser contribution to the collective channel is given by,

$$\theta_{0_a} = k_g \Delta n \tag{E1.8}$$

where,

$$\Delta n = 1 + \frac{a_z}{g},$$

k_g is the accelerometer feedback gain,

a_z is the heave axis acceleration measured by the accelerometer and

g is the acceleration due to gravity.

The sum of the pilot and autostabiliser contributions are passed through the actuator, as discussed, and modelled via a transfer function, given as,

$$\frac{\theta_0}{\theta_{0_p} + \theta_{0_a}} = \frac{1}{1 + \tau_{c4} s} \tag{E1.9}$$

where,

τ_{c4} is the collective actuator time constant.

iv) *Yaw Channel*

The yaw channel is understandably modelled using a coupling of the main rotor collective and the tail rotor collective. The theory is as follows. A linear relationship is used to combine the inputs from both pedals and collective into an equivalent term known as cable length, η_{ct}, which is expressed as,

$$\eta_{ct} = g_{ct0}\left(1 - \eta_p\right) + \left(1 - 2g_{ct0}\right)\eta_c \tag{E1.10}$$

where,

g_{ct0} is representative of the gearing constant used in the combination of collective lever and pedal displacements and

η_p is the pedal displacement made by the pilot, $\left(0 \le \eta_p \le 1\right)$.

The pilot contribution alone to tail rotor collective, θ_{0tr_p} is then given by,

$$\theta_{0tr_p} = g_{tr0} + g_{tr1}\eta_{ct} \tag{E1.11}$$

where,

g_{tr0}, g_{tr1} are gearing constants.

The contribution of the autostabiliser alone is given by,

$$\theta_{0tr_a} = k_\psi \psi(\psi - \psi_h) + k_r r \tag{E1.12}$$

where,

k_ψ, k_r are the proportional and derivative feedback in the heading angle, ψ and yaw rate, r of the aircraft respectively and

ψ_h is a heading hold term which is pilot adjustable.

Combining the pilot and autostabiliser outputs through the actuation system then gives in transfer function format,

$$\frac{\theta_{0tr}}{\theta_{0tr_p} + \theta_{0tr_a}} = \frac{1}{1 + \tau_{c3}s} \tag{E1.13}$$

where,

τ_{c3} is the tail rotor collective actuator time constant.

Appendix F

Wavelet Based Charts and Rule Induction Techniques

The purpose of this Appendix is to summarise, briefly, work conducted at DERA and Glasgow Caledonian University concerning the development of the wavelet based method of calculating the attitude quickness and pilot attack charts similar those presented in Chapter 5 of the dissertation. Additional discussion is given to the rule induction technique of deriving a Workload Rating (WR) from the resulting attack charts. The work is extremely relevant in the field of rotorcraft handling qualities and represents a novel method of approach in this field. Each topic will be discussed in turn with the main sources of reference being, *Jones and Padfield et al (1996)* and *MacDonald and Bradley (1997)*.

F1.1 The Wavelet Analysis Method

Padfield and Charlton et al (1994) made the assumption that when pilots fly tightly constrained manoeuvres in the nap-of-the-earth region of the flight envelope, the tasks of the pilot are divided between guidance and stabilisation of the vehicle. It was identified that imposing tighter constraints on the manoeuvre increased task difficulty and continually degraded performance of the rotorcraft. During such missions information can be gathered either from inverse simulation or flight test data on the behaviour of vehicle or pilot in terms of attitude or control displacement time histories. Using the method of wavelet decomposition, this data can be broken down into discrete wavelets in attitude quickness or pilot control activity ('worklets'). The importance of the calculation of the wavelets and indeed the concept of wavelet decomposition is that an association can be made with the underlying guidance and stabilisation tasks that the pilot has to perform. The aim of this section is to analyse

the wavelet decomposition process and make identifications with the appropriate piloting tasks.

F1.1.1 The Wavelet Analysis Method

Wavelet analysis is an alternative method of calculating the quickness or attack parameters mentioned throughout the dissertation and is concerned with the reconstruction of a signal which is based on a number of discrete features that have been extracted from the original signal. The mathematics involved can be lengthy and are beyond the scope of this appendix, however some basics are explained below.

The real wavelet transformation of a given function *g(x)* takes the form:

$$g \rightarrow T(y,L) = L\int_{-\infty}^{\infty} g(x)F\left\{\frac{(x-y)}{L}\right\}dx \qquad \text{(F1.1)}$$

where,

$F\left\{\frac{(x-y)}{L}\right\}$ is the analysing wavelet obtained from a chosen function *F(x)* through the operations of; translation by *y* and dilation by *L* which is the scale or duration of the wavelet and

g(x) can be any function, but in the current context is manoeuvre attitude time history for calculating the quickness parameters and pilot control time history for calculating attack parameters, *Jones and Watson (1992)*.

The outcome of the signal breakdown is to process the function or time-history through varying degrees of magnification revealing smaller transient components that are localised in time with respect to the input time-history. In Equation F1.1, *x* refers to some position in the time-history and is consequently associated with time, *t*. The scale of the wavelet, is taken to be its duration and is given the symbol Δt, thus $L=\Delta t$.

A so-called pre-whitening[1] process which simplifies the wavelet analysis technique is applied to the data and the resulting signal is then assumed to be *g(x)* in Equation F1.1. *Jones and Watson (1992)* have shown that if *F(x)* is taken as the positive pulse then a great deal of the information concerned with the structure of the of the data, *g(x)* is concentrated into local extremes of *T(y,L)*. Since *g(x)* can be represented by a discrete number of positive pulse "coding wavelets", then by matching the position and scale of the wavelets to the local extremes it is possible to create a reconstruction of the data *g(x)*. The shape of the pulse is selected to yield the lowest mean square error for any set number of describing wavelets, which are representative of the data in "whitened space". An inverse "de-whitening" process is then required to express the data in its original format. To perform this operation the pulse used in whitened space is decoded and transformed into a de-whitened pulse which can take several forms, depending on the method used to whiten the data in the first instance.

The result from the adaptive wavelet analysis technique is to decompose the data *g(x)* into a number of discrete evens which can be plotted on a quickness or attack chart depending upon whether it is aircraft attitude or pilot stick activity that is being analysed.

F1.2 The Rule Induction Method

The rule induction method has been applied to attack charts created from associated pilot control displacement time histories and the approach is based on the particular distribution of worklets on the chart. It is assumed that the Workload Rating[2] (WR) is a function of worklets in specific regions of the chart, thus identification and partitioning of the chart is of considerable importance. In effect the input variables are the number of worklets or events in each region of the chart (depending upon partition method) and the output is a WR in the form of a decision tree capable of replication to existing data or analysing and predicting a rating for new

[1] Pre-whitening is a filtering type process whereby the resulting data has a Power Spectral Density (PSD) approximately the same as white noise, i.e. constant over all frequencies.

[2] The Workload Rating is based upon the DERA, Bedford Pilot Workload rating Scale

data. The method has found considerable success in this application with reasonably good correlation with pilot awarded subjective HQRs, as reported in *MacDonald and Bradley (1997)*. Further discussion of the method follows.

F1.2.1 Rule Induction Techniques

The rule induction technique is a type of Machine Leaning (ML) algorithm. The workload ratings used to train the algorithm have been acquired from flight or ground-based simulation trials and are founded on qualitative assessment techniques. Providing a sufficient number of examples are used to 'train' the decision tree, the algorithm can then replicate the workload classification of the data supplied to it and will be able to offer predictions of workload ratings for new input data. The comparison of the two techniques can be written as experimental and theoretical processes:

Experimental

1. Simulator Trial ⇒ Pilot's HQR - Qualitative Assessment ⇒ Workload Rating

Theoretical

2. Stick Displacement Signal ⇒ Attack Chart ⇒ Workload Rating

The approach taken is to divide the attack chart, into a number of regions containing a significant amount of attack parameters. Either the adaptive wavelet or direct processing techniques can be used to calculate the attack parameters. Since the attack parameters are discrete representations of pilot workload in terms of guidance and control, it is assumed that the workload rating is a function of the number of attack parameters in each region of the chart.

In light of the fact that the method has found recent application in helicopter handling qualities studies, it is obvious that one of the main problems will lie in deciding the correct partitions of the attack chart. *MacDonald and Bradley (1997)* have conducted such an investigation using straight partition lines of constant pilot

attack, rectangular partitions, rectangular and orthogonal hyperbolic partitions, and various combinations of these partitions. One of the conclusions of the work seemed to support a similar study carried out by *Jones and Padfield et al (1996)* who suggested a partitioning into four rectangular areas, corresponding to areas of workload associated with guidance and stabilisation. Using this method of partitioning achieved improved correlation with pilot subjective ratings.

References

Anon., “Aeronautical Design Standard ADS-33C Handling Qualities Specifications For Military Rotorcraft”, United States Army Aviation and Troop Command, St. Louis, Mo., Directorate for Engineering, August 1989.

Anon., “Aeronautical Design Standard ADS-33D Handling Qualities Specifications for Military Rotorcraft”, United States Army Aviation and Troop Command, St. Louis, Mo., Directorate for Engineering, July 1994.

Anon., “Helicopter Flying and Ground Handling Qualities; General Requirements for: Mil-H-8501A”, 1961.

Anon., Military Specification, “Flying Qualities Of Piloted Airplanes”, MIL-F-8785B (ASG), 1969.

Anon., UK Def Stan 00-970, “Design and Airworthiness Requirements for Service Rotorcraft”, Vol. 2, Rotorcraft, Book 1, 1984.

Atencio, A., Jr., “Fidelity Assessment of a UH-60A Simulation on the NASA Ames Vertical Motion Simulator”, NASA TM 104016, September 1993.

Blanken, C. L. and Ockier, C. J., “An Analysis of Pilotage Task Manoeuvre Metrics”, Paper 44, 23rd European Rotorcraft Forum, Dresden, 1997.

Bradley, R. and Thomson, D. G., “Handling Qualities and Performance Aspects of the Simulation of Helicopters Flying Mission Task Elements”, Paper 139, 18th European Rotorcraft Forum, Avignon, September 1992.

Bradley, R. and Thomson, D. G., “The Development and Potential of Inverse Simulation for the Quantitative Assessment of Helicopter Handling Qualities”, Piloting Vertical Flight Aircraft: Flying Qualities and Human Factors, AHS/NASA Conference, San Francisco, January 1993.

Bramwell, A. R. S., “Helicopter Dynamics”, Arnold, 1976.

Cao, Y. and Gao, C., “A Method for Calculating Kinematic Parameters of Helicopter in Loop and Roll Manoeuvres”, Transactions of Nanjing University of Aeronautics and Astronautics, Vol. 11, No. 1, May 1994.

Cerbe, T. and Reichert, G., “Influence of Ground Effect on Helicopter Takeoff and Landing Performance”, Paper 70, 14th European Rotorcraft Forum, Milano, September 1988.

Charlton, M. T., Howell, S. E., Padfield, G. D., Jones, J. G., Bradley, R., MacDonald, C., Thomson, D. G. and Leacock, G. R., “A Methodology for the Prediction of Pilot Workload and the Influence on Effectiveness in Rotorcraft Mission Tasks”, Paper 05, 24th European Rotorcraft Forum, Marseilles, September 1998.

Charlton, M. T., Jones, J. G., Padfield, G. D., “The Development Of A Methodology For Prediction Of Pilot Workload And The Influence On Effectiveness In Rotorcraft Mission Tasks: A Progress Review”, Flight Management and Control Department, Defence Evaluation and Research Agency, October 1997.

Chen, R. T. N., “A Survey of Non-uniform Inflow Models for Rotorcraft Flight Dynamics and Control Applications”, Paper 64, 15th European Rotorcraft Forum, Amsterdam, September 1989.

Cheney, W. and Kincaid, D., “Numerical Mathematics and Computing. Second Edition"” Brooks/Cole Publishing, 1985.

Cheeseman, I. C. and Bennett, W. E., “The Effect of the Ground on a Helicopter Rotor in Forward Flight”, A.A.E.E. Report Res/288, Reports and Memoranda No. 3021, September 1955.

Cooper, G. E. and Harper, R. P. “The Use of Pilot Rating in the Evaluation of Aircraft Handling Qualities”, NASA TN D-5153, April 1969.

Gaonkar, G. H. and Peters, D. A., "Use of Multiblade Coordinates for Helicopter Flap-lag Stability with Dynamic Inflow", Journal of Aircraft, Vol. 17, No. 2, February 1980.

Gerlach, O. H., "Developments in Mathematical Models of Human Pilot Behaviour", The Aeronautical Journal, July 1977.

Glauert, H., "A General Theory of the Autogyro", R&M No. 1111, British A. R. C., 1926.

Grace, A., "Optimisation Toolbox for use with MATLAB", The Math Works Inc., November 1992.

Gray, G. and von Grünhagen, W., "An Investigation of Open Loop and Inverse Simulation as Non-linear Model Validation Tools for Helicopter Flight Mechanics", Paper 6, 20th European Rotorcraft Forum, October 1994.

Hoblit, F. M., "Gust Loads On Aircraft: Concepts And Applications", American Institute of Aeronautics and Astronautics, 1988.

Howell, S. E., "Preliminary Results From Flight And Simulation Trials To Investigate Pilot Control Workload In Slalom Manoeuvres", Flight Management and Control Department, Defence Evaluation and Research Agency, December 1995.

Howell, S. E. and Charlton, M. E., "Trial Specification For AFS Simulation Trial TWIN3", Draft Version, Flight Management and Control Department, Defence Evaluation and Research Agency (DERA), November 1997.

Jacobs, O. L. R., "Introduction to Control Theory", Second Edition, Oxford Science Publications, 1993.

Jones, J. G., Padfield, G. D. and Charlton, M. T., "Identification of Components of Pilot Workload in Helicopter Low Level Flying Tasks Using Adaptive Wavelet Analysis", Paper 76, 2nd European Rotorcraft Forum, Brighton, September 1996.

Jones, J. G. and Watson, G. H., "Positive Wavelet Representation of Fractal Signals and Images", 1991, Prepared for International Conference, Applications of Fractals and Chaos, London, February 1992.

Lane, S. H. and Stengel, R. F., "Flight Control Design using Non-linear Inverse Dynamics", Automatica, Vol. 24, No. 4, July 1988.

MacDonald, C. and Bradley, R., "An Initial Investigation of Helicopter Pilot Workload Rating Prediction Using Rule Induction Techniques", Technical Report TR/MAT/CmacD/RB/97-65, Department of Mathematics, Glasgow Caledonian University, June 1997.

McRuer, D. T. and Jex, H. R., "A Review of Quasi-linear Pilot Models", IEEE Transactions on Human Factors in Electronics, Vol. HFE-8, No. 3, September 1967.

McRuer, D. T. and Krendel, E. S., "Mathematical Models of Human Pilot Behaviour", AGARD-AG-188, January 1974.

Newman, E. M., "A New Approach to the Calculation of the Effect of the Ground on the Performance of Rotary Wing Aircraft", Special Project No. 71-02, Naval Air Systems Command, Washington D.C., February 1972.

O'Hara, F., "Handling Criteria", Journal of the Royal Aeronautical Society, Vol. 71, April 1967.

Ockier, C. J. and Gollnick, V., "ADS-33 Flight Testing – Lessons Learned", Proceedings of the FVP Symposium on Advances in Rotorcraft Technology, Ottawa, Canada, May 1996.

Padfield, G. D., "A Theoretical Model of Helicopter Flight Mechanics for Application to Piloted Simulation", RAE Technical Report 81048, 1981.

Padfield, G. D., "Helicopter Flight Dynamics", Blackwell Science Ltd., 1996.

Padfield, G. D., Charlton, M. T., Houston, S. S., Pausder, H. J. and Hummes, D., "Observations Of Pilot Control Strategy In Low Level Helicopter Flying Tasks", Vertica, Vol. 12, No. 3, 1988.

Padfield, G. D., Jones, J. P., Charlton, M. T., Howell, S. E. and Bradley, R., "Where Does the Workload Go when Pilots Attack Manoeuvres? An Analysis of Results from Flying Qualities Theory and Experiment", Paper 83, 20th European Rotorcraft Forum, October 1994.

Pausder, H. J., and Blanken, C. L., "Investigation Of The Effects Of Bandwidth And Time Delay On Helicopter Roll Axis Handling Qualities", Paper 80, 18th European Rotorcraft Forum, Avignon, France, September 1992.

Pausder, H. J. and Jordan, D., "Handling Qualities Evaluation of Helicopters with Different Stability and Control Characteristics", Vertica, Vol. 1, 1976, pp. 125-134.

Pausder, H. J. and von Grünhagen, W., "Handling Qualities Evaluation for Highly Augmented Helicopters", Unknown Source.

Peters, D. A. and HaQuang, N., "Dynamic Inflow for Practical Applications", Journal of the American Helicopter Society, Technical Note, pp. 64-68, October 1988.

Prouty, R., "Helicopter Performance, Stability and Control", Krieger, 1990.

Rutherford, S. and Thomson, D. G., "Improved Methodology for Inverse Simulation", The Aeronautical Journal, March 1996.

Rutherford, S. and Thomson, D. G., "Helicopter Inverse Simulation Incorporating an Individual Blade Rotor Model", Journal of Aircraft, Vol. 34, No. 5, October 1997.

Sutton, R., "Modelling Human Operators in Control System Design", John Wiley and Sons Inc. 1990.

Taylor, C., "The Development of a Simulation Technique for the Analysis of Helicopter Offshore Operations", PhD Thesis, University of Glasgow, 1995.

Thomson, D. G. "An Analytical Method of Quantifying Helicopter Agility", Paper 45, 12th European Rotorcraft Forum, Garmisch-Partenkirchen, September 1986.

Thomson, D. G., "Development of a Generic Helicopter Mathematical Model for Application to Inverse Simulation", University of Glasgow, Department of Aerospace Engineering, Internal Report No. 9216, June 1992.

Thomson, D. G. and Bradley, R., "Inverse Simulation of Helicopter Manoeuvres Subject to a Prevailing Wind", Internal Report No. 9305, Department of Aerospace Engineering, University of Glasgow, March 1993.

Thomson, D. G. and Bradley, R., "Development and Verification of an Algorithm for Helicopter Inverse Simulation", Vertica, Vol. 14, No. 2, May 1990a.

Thomson, D. G. and Bradley, R., "Mathematical Definition of Helicopter Manoeuvres", Journal of the American Helicopter Society, October 1997.

Thomson, D. G. and Bradley, R., "Prediction of the Dynamic Characteristics of Helicopters in Constrained Flight", The Aeronautical Journal, December 1990b.

Thomson, D. G. and Bradley, R., "The Principles and Practical Application of Helicopter Inverse Simulation", Simulation Practice and theory, International Journal of the Federation of European Simulation Societies pp. 47-70, 1998.

Thomson, D.G., Talbot, N., Taylor, C., Bradley, R., and Ablett, R., "An Investigation of Piloting Strategies for Engine Failures during Take-off from Offshore Platforms", The Aeronautical Journal, January 1995.

Tischler, M. B., Fletcher, J. W., Morris, P. M. and Tucker, G. E, "Flying Quality Analysis And Flight Evaluation Of A Highly Augmented Combat Rotorcraft", Journal of Guidance, Vol. 14, October 1991.

Tustin, A, “An Investigation of the Operator’s Response in Manual Control and its Implications for Controller Design”, Journal of the Institute of Electronic Engineers, 94, 1947.

Whalley, M. S., “Development and Evaluation of an Inverse Solution Techniques for Studying Helicopter Manoeuvrability and Agility”, NASA TM 102889, 1991.

Wolfram, S., “Mathematica : A System for doing Mathematics by Computer”, Redwood City, Addison-Wesley Publishing Co., 1988.